UNIVERSITY OF LEEDS

syngenta

AstraZeneca

Electrochemical Activation of Catalytic Species in Metallic and Non-Metallic Catalysis

Name: Rosalie Hamill

Student ID: 200755739

Supervisors: Dr Bao N. Nguyen, Professor A. John Blacker

Industrial Supervisors: Dr Niall McCreanor (AZ), Dr Stanley Lai (Syngenta)

Submission Date: 22.02.2022

Submitted in accordance with the requirements for the degree PhD in Chemistry at the University of Leeds.

The candidate confirms that the work submitted is her own and that appropriate credit has been given where reference has been made to the work of others.

This copy has been supplied on the understanding that it is copyright material and that no quotation from the thesis may be published without proper acknowledgement.

My Chemistry Girls, Hazel, Sammie, and Miriam, where would I be without you? All those days spent in the library and the nights wondering why we subjected ourselves to this were worth it for the friendship we have. You've been my rock throughout these past 8 years, and you have changed my life for the better. I feel honoured to call you best friends.

Finally, I would like to thank my family for their love and support since, well since birth. To Rose, my child, I wish you could have been here to celebrate this with me. You always saw something in me and reminded me of that when I felt lost. To Grandad, thank you for your motivational speeches and your Baileys-fuelled conversations. To my Mum and Dad, you have always been there with love and support, this would not have been possible without you, and I can't put into words how much what you have done for me means. I would like to thank Ellie, your weird voices, extensive voice notes, the fun games we play together, impromptu duetting, our inside jokes, and our weird telekinesis have always been able to cheer me up no matter what was on my mind. I love you all.

Abstract

In recent years the application of electrochemistry in synthetic organic chemistry has been increasing in popularity as chemists are tasked with finding cleaner synthetic routes for highly complex molecules. It is seen as an auspicious method to solve persistent problems in organic chemistry; however, it is still considered a last resort out of "sheer desperation" by many. Reactions which traditionally require strong oxidants/ reductants or often expensive metal catalysts in stoichiometric quantities can be performed under milder conditions by substituting these harsh reagents with so called "traceless reagents" *i.e.* photons or electrons.(1) However, there are inherent issues which can render it inaccessible for some researchers including technical know-how, lack of access to standardised equipment which leads to reproducibility issues, and the lack of teaching electrochemistry as a synthetic strategy.

In this work, the issues of standardised reactors, reproducibility, and reaction profiling of electrochemical reactions are addressed. Herein, home-made and standardised reactors are utilised for a variety of synthetic protocols; their efficacy is compared in terms of product yield and reproducibility. The different impacts that batch and flow electrochemistry can have on a reaction and how these differences can be used to explore a reaction's kinetic profile is also investigated in Chapter 2. It was found that the reaction was zero order and the electrochemical step was identified as rate determining. This coupled with cyclic voltammetry shed key insights into the mechanism of the reaction with regards to the proposed catalytic species. Studies of electrode material in both batch and flow chemistry highlighted the importance of electrode material and the issue of electrode dissolution and deposition that arise when using metals over inert materials. The profiling

techniques, electrode analysis, and technical know-how achieved in Chapter 2 was applied to the work in Chapter 3 to investigate surface morphology, kinetics, and reactor set-up.

The applications of electrodeposited zinc in known as well as novel case studies to form complex products is described in Chapter 3. We were able to demonstrate the applicability of a simple electrodeposition technique of zinc to form β-ketoesters, β-hydroxyesters, and substituted 2-azetidinones. Using home-made and standardised reactors, we were able to demonstrate the importance of standardised systems and the improvement standardised reactors have in reproducibility, which is a key issue in zinc chemistry. Using electrodeposited zinc presents an elegant, cost-efficient method of metal activation, obviating expensive and toxic precious metals.

Table of Contents

Table of Figures

Table of Tables

Table of Schemes

Abbreviations List

Å	Angstroms
A	Amperes
AAS	Atomic Absorption Spectroscopy
AcOH	Acetic Acid
BDD	Boron Doped Diamond
BET	Brunauer Emmett Teller (analysis)
C	Coulombsa
CV	Cyclic Voltammetry
DBNE	*N,N*-Dibutylaminonorephedrine
DCM	Dichloromethane
DFT	Density Functional Theory
DMC	Dimethyl carbonate
DMF	*N,N*-dimethylformamide
DoE	Design of Experiments
ε	Dielectric constant
e.e.	Enantiomeric Excess
e.g.	exempli gratie (for the sake of example)
EDX	Energy Dispersive X-ray (analysis)
EFR	Electrochemical Flow Reactor
Eq.	Equivalents

et al.	et alia (and others)
ECW	Electrochemical Window
GC	Gas Chromatography
GCMS	Gas Chromatography-Mass Spectrometry
HAT	Hydrogen Atom Transfer
HFIP	Hexafluoroisopropanol
HPLC	High Performance Liquid Chromatography
IR	Infrared (spectroscopy)
LCMS	Liquid Chromatography-Mass Spectrometry
mA	milli Amperes
M	Molar
MeCN	Acetonitrile
mL	milli Litre
NMR	Nuclear Magnetic Resonance (spectroscopy)
OVAT	One Variable at a Time
PC	Photocatalyst
PCA	Principal Component Analysis
PTFE	Polytetrafluoroethylene
r.t.	Room Temperature
RVC	Reticulated Vitreous Carbon
SCE	Saturated Calomel Electrode

SEM   Scanning Electron Microscopy

SET   Single Electron Transfer

SHE   Standard Hydrogen Electrode

TBAI   Tetrabutylammonium iodide

TBATBF Tetrabutylammonium tetrafluoroborate

THF   Tetrahydrofuran

TLC   Thin Layer Chromatography

UPLC   Ultra-Performance Liquid Chromatography

UV   Ultraviolet

V   Volts

vs.   versus (compared to/against)

1   Introduction to Electrochemistry

An electrochemical reaction is a heterogeneous exchange of electrons between the cell's electrodes, a conductive substance (carbon, metal, boron doped diamond [BDD] *etc.*), and the bulk reaction mixture.(2) For example, in Daniell cells electrons flow by oxidation at the zinc anode and reduction at the copper cathode, with a salt bridge connecting the two separate chambers (Figure 1.1). To avoid charge build-up at the anode or cathode this exchange must occur to equal extents, facilitated by a conductive reaction mixture of ions in a liquid medium (in this example aqueous solutions of $ZnSO_4$ and $CuSO_4$ are used). These ions can be the reaction substrates, additives, or electrolytes (or all three). Electrolytes are typically inert, low charge density species made up of a cation and anion, which can be reduced and oxidised accordingly to prevent net charge build-up within the reaction (See 1.3.5).
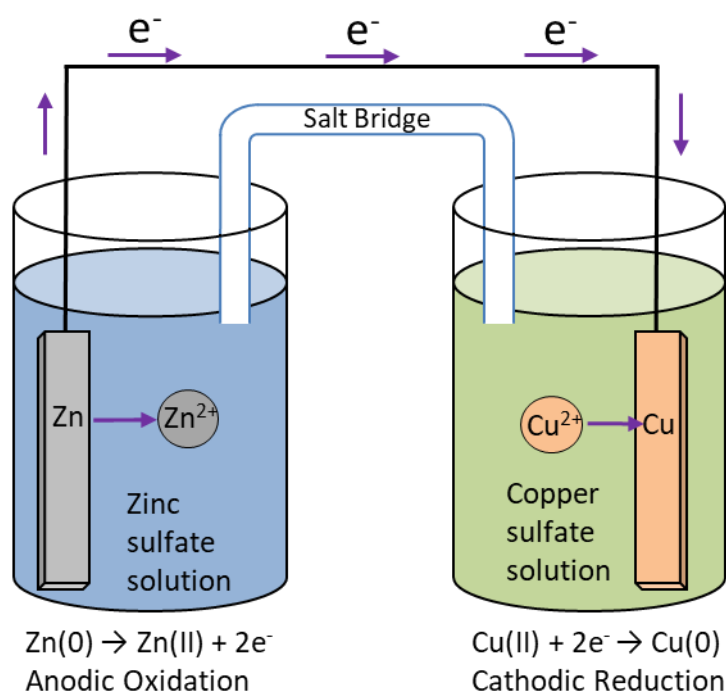
Figure 1.1 Diagram of a Standard Daniell cell showing spontaneous electron movement in a copper-zinc cell with anodic oxidation (left) and cathodic reduction (right).

1.1   Electrochemistry in Synthesis

Electrochemistry has been used by synthetic chemists since the late 19th century to prepare substances in bulk;(3) such as the Hall-Héroult process of aluminium production which was first run in 1886(4) and the chlor-alkali process of sodium chloride electrolysis to generate Cl_2 and NaOH, first run on an industrial scale in 1892.(5) Recent examples of electrosynthesis in literature can be seen in Figure 1.2: electrochemical C-C bond formation in salutaridine in the total synthesis of (-)-oxycodone,(6) direct oxidative *N-N* dimerization to produce the natural product dixiamycin B,(7) decarboxylative dimerization in the preparation of β-onoceradiene,(8) and electrochemical oxidative coupling of two nucleophilic groups in the synthesis of Alliacol A.(9)
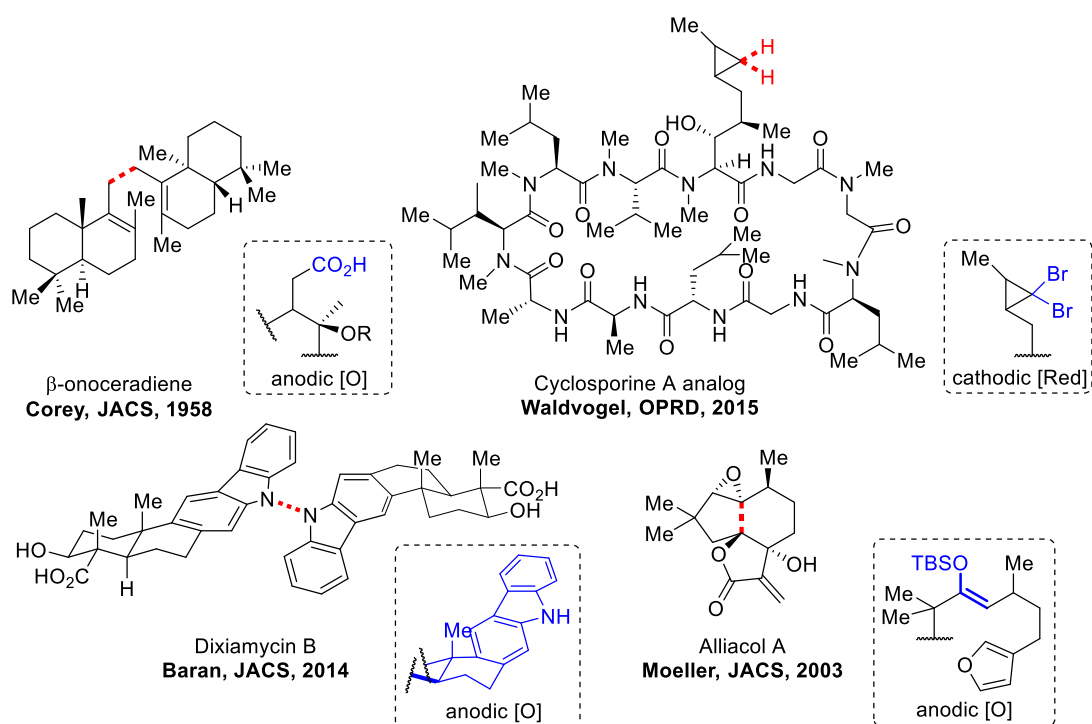
Figure 1.2. Recent molecules synthesised using electrochemistry. Bonds formed are highlighted by red, dashed lines. The prefunctionalised portion of the structure highlighted in blue in a box with dashed lines with the reaction type underneath. * indicates the two carbons which are joined by anodic oxidation.

In conventional chemical reactions substrates rarely spontaneously react upon initial mixing; a push to reach the activation energy is introduced, *e.g.* in the form of heating, for the reaction to proceed. In a similar way, electrochemical reactions begin with an unreactive starting material [R] which then reacts, either directly with the electrodes or indirectly by way of a redox mediator, to form the desired product or a reactive intermediate which then reacts further.
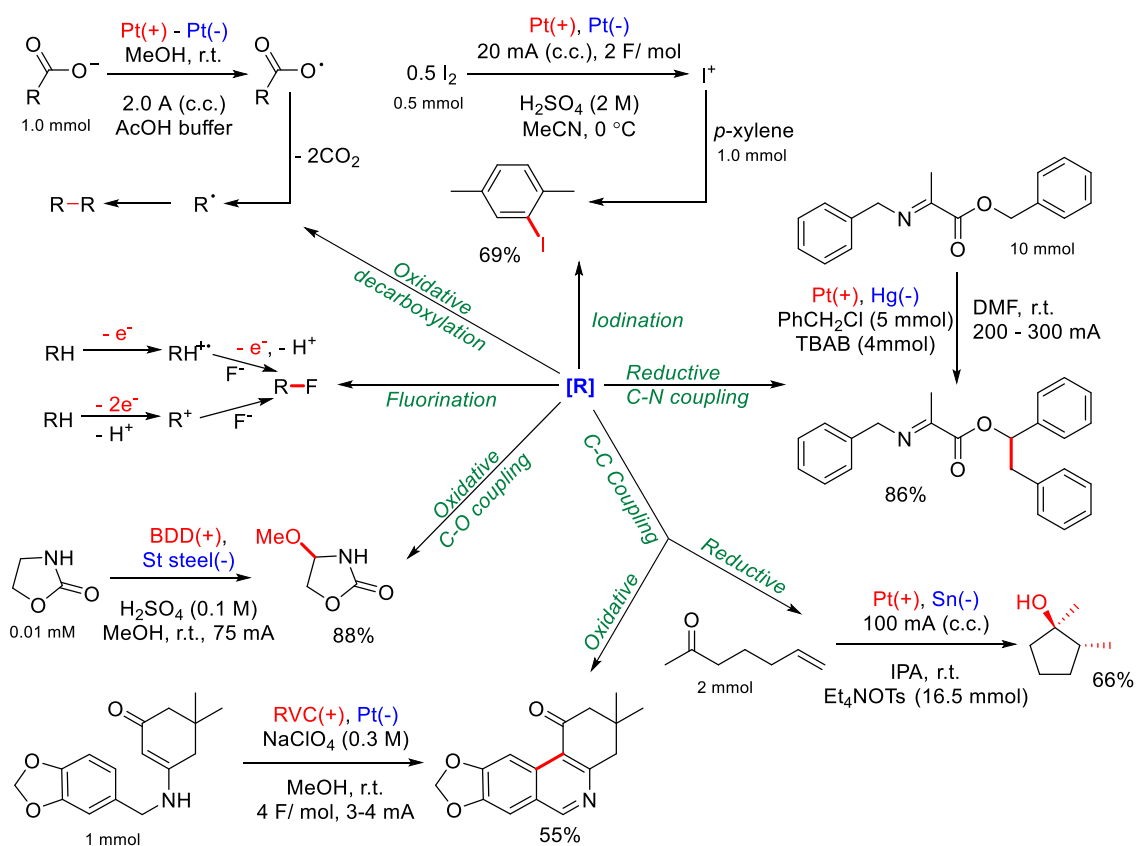
Figure 1.3. Examples of organic reactions in an electrochemist's synthetic toolbox.

Figure 1.3 depicts some of the numerous organic reactions available to an electrochemist:

- Halogenation of organic compounds with iodine (10) or fluorine (11) is a highly useful tool in the generation of valuable and versatile intermediates

for medicinal chemists, and electrochemical generation subverts the use of oxidants and reduces the associated waste

- C–N,(12) C–C,(13,14) and C–O(15) couplings are accessible *via* reduction/oxidation and allow for late-stage coupling of highly functionalised substrates, a vital tool in natural product synthesis, without the transition metal catalysts required in traditional synthetic methods and their subsequent removal upon work-up

- Oxidative decarboxylations such as the Kolbe electrolysis are powerful processes to create symmetrical dimers(16) from simple carboxylic acids

1.2 Industrial Applications of Organic Electrochemistry

Electrochemistry is becoming a much more popular synthetic option for organic and inorganic chemists, with numerous tutorials and informative papers explaining solvents, electrolytes, set up, and other parameters to be considered for a beginner.(3,11,25–31,17–24) In industry, many household names (BASF, Monsanto, and Hoffman - La Roche *etc.*) use electrochemistry from relatively basic starting materials on a commercial and pilot plant scale (Table 1.1).(11,21)

Table 1.1. Electrochemical Processes in industry. P = pilot scale, C = commercial scale. Adapted from references (11,21)**.**

Product	Starting material	Company	Scale
Adiponitrile	Acrylonitrile	Monsanto (Solutia), BASF, Asahi Chemical	C
Ceftibuten	Cephalosporin C	Electrosynthesis Co., Schering Plough	P
Ethylene Glycol	Formaldehyde	Electrosynthesis Co.	P

4

p-methoxybenzaldehyde	p-methoxytoluene	BASF	C
Pinacol	Acetone	BASF, Diamond Shamrock	P
Polysilanes	Chlorosilanes	Osaka Gas	C
Substituted benzaldehydes	Substituted toluenes	Hydro Quebec	P

1.3   Electrochemical Cells

1.3.1   Galvanic vs. Electrolytic Cells

Electrochemical cells can be divided into two different categories: Galvanic and Electrolytic (Figure 1.4).
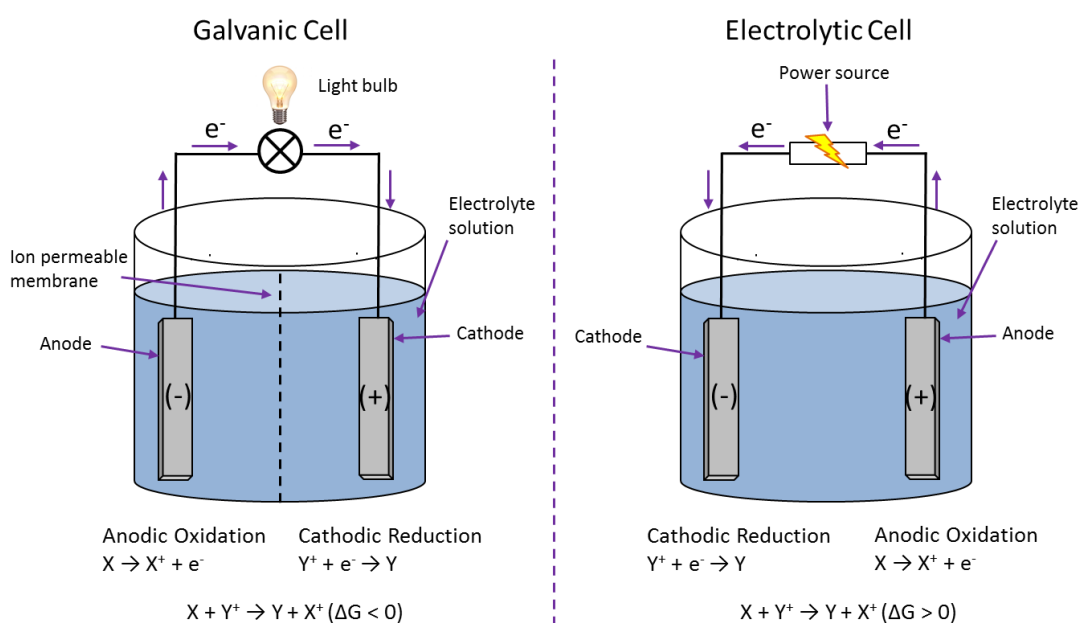
Figure 1.4. A diagram comparing a standard Galvanic with an Electrolytic cell.

Galvanic cells produce energy from spontaneous redox reactions which occur within the cell, where reactants of high energy are converted to lower energy products. The general setup is either two metal electrodes submerged in a solution of electrolyte, or

two individual half cells connected by either a semi-permeable membrane (*e.g.* Nafion) to allow selective ion transfer or a salt bridge as seen in the Daniell cell from Figure 1.1. Although one such cell can be termed a battery, batteries normally consist of multiple cells in series.

Electrolytic cells use electrical energy from an external source (*e.g.* batteries, power packs) to instigate a non-spontaneous redox reaction. The setup is similar to the Galvanic cell; two electrodes are submerged in a solution of electrolyte or two individual half cells with their own solutions (catholyte for the cathode, anolyte for the anode). The key difference is the external power supply connecting the anode and cathode. Electrolytic cells are the system of choice for electroorganic chemistry as they can explore non-spontaneous reactions such as generating high energy intermediates. Due to the multitude of reactions which are possible in an electrochemical cell, standard reduction potential is a vital consideration, as is electrode selection, as both factors can influence whether your cell preferentially facilitates one or two electron transfer. An example of this is the use of platinum metal as an electrode in Kolbe electrolysis; platinum electrodes have been found to stabilise the single electron transfer alkyl radicals produced in this reaction by chemisorption, whereas carbon-based electrodes have been found to undergo oxidative desorption and prevent the formation of the desired product.(16)

1.3.2 Reactor Types in Synthetic Electrochemistry

1.3.2.1 Electrochemical Batch Cells

As previously mentioned, there are certain factors to consider when selecting an electrode for electrochemical processes; in batch there is a third factor to consider: the number of electrodes to use. Analytical chemistry typically employs a three-electrode system (working electrode, auxiliary electrode, and reference electrode),

whereas batch electrochemistry typically uses two (anode and cathode) (Figure 1.5). The working electrode is a term used to define the electrode that the intended reaction will occur at *e.g.* for an anodic oxidation reaction the anode would be considered the working electrode. The auxiliary electrode is the electrode where the intended reaction does not occur but is still involved in the electrical circuit. The reference electrode is a system which has a known and stable standard electrode potential such as the Standard Hydrogen Electrode (SHE).
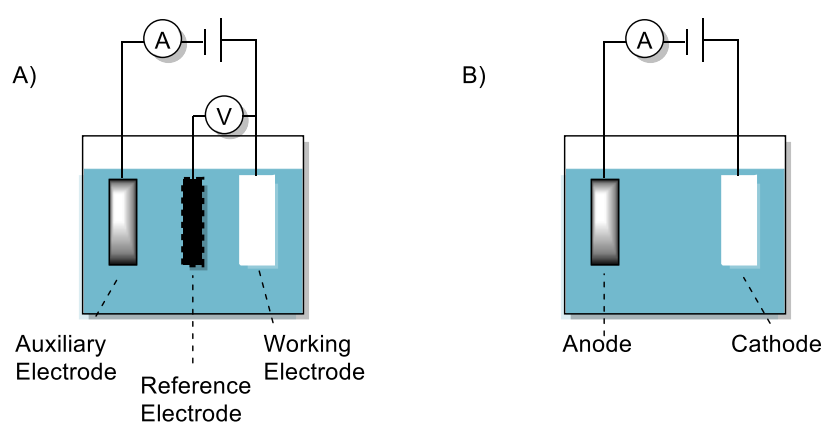
Figure 1.5. Diagram depicting typical batch electrochemistry cells using a 3-electrode system (A) and a 2-electrode system (B).

Synthetic electrochemists tend to use two-electrode systems with no reference electrode, as evidenced by the absence of three-electrode systems in the literature. This may be linked to the difficulty of scaling up a three-electrode system, but it is more likely to be due to it not being particularly necessary to have a reference electrode in most cases. Unless there is evidence of a discrepancy between the electrons used and the potential/current output for example, or for testing the energy efficiency of a particular system most researchers will avoid a reference electrode.

Batch reactors are generally the go-to option for synthetic organic chemists when testing a reaction. Once it has been established that the new reaction does in fact

occur, the conditions can then be modified to optimise the reaction *e.g.* using Design of Experiments (DoE) or One Variable At a Time (OVAT) methods. These optimised reaction conditions generate new process understanding which allows for translating batch processes into flow.

1.3.2.2   Electrochemical Flow Cells

Electrochemical flow cells have recently seen a boom in publication,(25,32,41,33–40) due to their inherent advantages of lower electricity requirements (smaller interelectrode distance and improved surface area to electrode ratio) and facile temperature and pressure modulation.

Owing to the decreased interelectrode distance and increased interfacial ratio of electrode to reaction stream within an electrochemical flow system, the efficiency of mass, heat, and electron transfer is significantly enhanced. These improvements can resolve these problems found in batch reactors upon scale-up. Furthermore, flow reactors can be made with specific dimensions (reactor volume, electrode size, *etc.*) meaning they are easier to replicate for other researchers.

Although flow reactions require initial data on reaction progression, solubility of starting materials, and a basic idea of how the reaction proceeds, this does not always require exhaustive batch testing. The basic flow set-up consists of an inlet and outlet plate with alternating positive and negative electrodes separated by PTFE (or another inert, non-conductive substance) dividers with the flow-path cut out. Flow is achieved using a pump, often supported by a backpressure regulator when dealing with gas evolution or high temperatures. Numerous in-line, on-line, or off-line analytical processes (*e.g.* HPLC, mass spec) can be added to the set-up to monitor the reaction. The number of electrode plates used and total volume of the reactor is

often reaction dependent, and requires some optimising when dealing with new reactions and reaction systems.

1.3.3   Batch *vs.* Flow Cells

Batch is an excellent reactor choice for multiphasic systems as they are largely unaffected by unexpected precipitation or gas formation during the reaction. Surprise precipitation or increases in viscosity can block up a flow reactor, rendering it useless until it can be taken apart and cleaned. Furthermore, production must also be halted until the cause is identified. Blockages can also easily occur when using metal electrodes in flow, as electrodeposition of metal can "bridge" the gap between anode and cathode causing a short circuit. This is not impossible in batch, however it is much less likely due to the larger interelectrode distances.
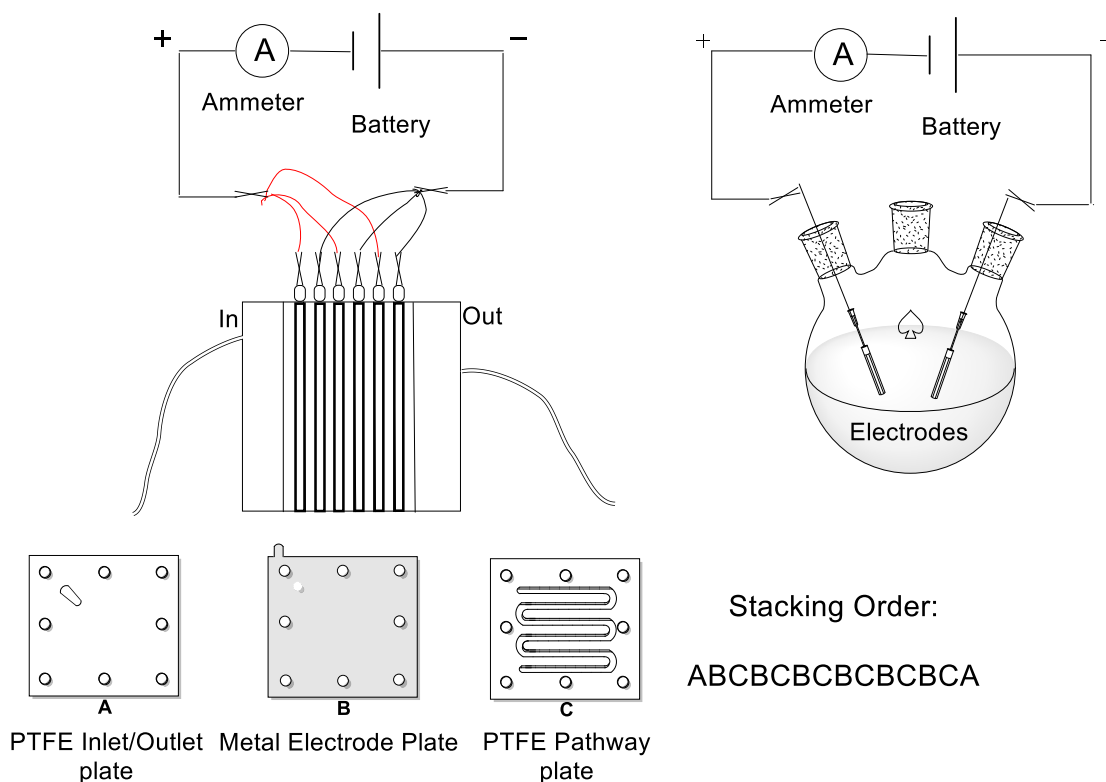
Figure 1.6. A diagram of the basic skeleton of an electrochemical flow reactor and its components (left) and round bottom flask batch reactor (right). Electrochemical plates arranged $A(BC)_nBA$, where $n \geq 1$ depending on desired flow cell size.

While organic electrosynthesis in batch represents a useful approach for small scale reactions, it can be difficult to efficiently scale up to the quantities required in industry. This is predominantly due to poor mass and electron transfer: the electrode surface area to electrolyte volume ratio decreases upon scale-up, and greater interelectrode distances for the substrates to cross requires higher amounts of electricity to compensate.

Furthermore, batch systems can have problems with reaction reproducibility; currently each synthetic group will tend to have their own, idiosyncratic, set-up. While the idea of home-made reactors is appealing in a cost-effective sense, its drawback is that whatever results are achieved can be difficult to replicate by others.

However, this is changing with companies such as IKA selling electrochemical reactors (both batch and flow) indicating that soon this may no longer be an issue.

To conclude, electrochemical reactor selection usually begins with traditional batch chemistry; once the reaction behaviour has been observed and its process better understood it can be moved into flow, however some reactions do not effectively proceed in continuous flow.

1.3.3.1   Divided vs. Undivided Cells

In electrochemical processes, one has the choice between an undivided (Figure 1.7A) and a divided (Figure 1.7B) configuration.
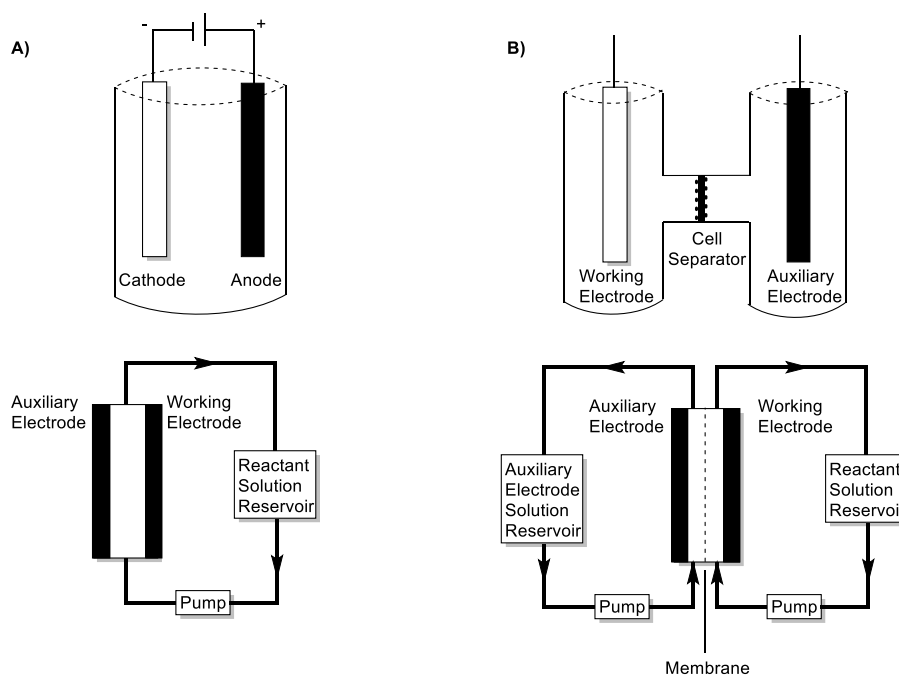
Figure 1.7. Batch (top) and continuous flow (bottom) process example of an undivided electrochemical cell (A) and a divided electrochemical cell (B).(16)

In an undivided cell, the anode and cathode are immersed in the solution containing the electrolytes and substrates and are not separated by anything other than distance. Undivided cells have been favoured by many synthetic electrochemists due to their

relative ease of assembly, lower internal resistance, and longer lifetime than its divided counterpart.

Divided cells consist of a working electrode and an auxiliary electrode in a solution of electrolytes and substrates (anolyte and catholyte solutions for the anode and cathode respectively), separated by a porous semipermeable membrane which selectively allows certain ions across. This division is favourable when ions or intermediates formed at one electrode can interfere with the reaction at the other electrode, leading to better yield and selectivity. However, it also increases the resistance of the cell as it widens the interelectrode distance, and also the membrane itself can slow the reaction down. Furthermore, the lifetime of the electrochemical cell is limited by the mechanical properties of this membrane.(16) It can therefore be more practical to perform electrochemistry using an undivided cell.

1.3.4   Electrode Selection for Synthetic Electrochemistry

Electrode material selection is crucial to the success of any electrochemical experiment; each electrode material will have its own surface properties, conductivity, and electron transfer kinetics *etc.* which are vital to consider. Though electrodes can be in liquid, solid, or even gaseous form synthetic chemistry has historically always opted for solid forms. Solid electrodes can be metallic, such as nickel, or non-metallic, such as graphite; electrode pairings are dependent on the desired chemistry, as the electrodes themselves can facilitate chemical reactions. Chemically inert electrodes such as reticulated vitreous carbon (RVC) can be used to ensure no electrode material interference and have been successfully used in metal free electrochemical reactions.(42) Knowledge of standard redox potential (E^o) is also vital when selecting electrodes for an electrochemical cell, as the values will dictate whether a material is better suited as the cathode or the anode. Values

are measured relative to a reference electrode with its own intrinsic standard reduction potential such as the saturated calomel electrode (SCE) [$E^o = +0.241$ V], the standard hydrogen electrode (SHE) [$E^o = 0.000$ V], or a silver chloride electrode [$E^o = +0.197$ V]. For example, in an electrolytic system with one iron electrode and one copper electrode: $E^o(Fe_{(s)}) = -0.440$ V, $E^o(Cu_{(s)}) = +0.337$ V. Here, Cu is more readily reduced and would therefore act as the anode. Iron is comparatively more readily oxidised, so would suit the cathode (Table 1.2).

Table 1.2. Common electrode materials and their associated standard potential, V, in descending order from most anodic (platinum) to most cathodic (lithium) *vs*. SHE.(43)

½ Equation	E^o/ V	½ Equation	E^o/ V
$Pt^{2+} + 2e^- \leftrightarrow Pt$	1.180	$Fe^{3+} + 3e^- \leftrightarrow Fe$	-0.037
$Ag^+ + e^- \leftrightarrow Ag$	0.800	$Pb^{2+} + 2e^- \leftrightarrow Pb$	-0.126
Calomel Electrode (SCE)	0.241	$Ni^{2+} + 2e^- \leftrightarrow Ni$	-0.257
$Cu^{2+} + 2e^- \leftrightarrow Cu(s)$	0.337	$Fe^{2+} + 2e^- \leftrightarrow Fe$	-0.447
$2H^+ + 2e^- \leftrightarrow H_2$ (SHE)	0.000	$Li^+ + e^- \leftrightarrow Li$	-3.04

When selecting electrode materials, one must also consider the possibility of cathodic electrodeposition and electrode dissolution. The former describes the process by which metal ions are reduced at the cathode and either deposit on to the cathode itself or in the reactor; the latter describes the movement of the electrode metal particles into the bulk solution thereby degrading the electrode which will in

time have to be replaced. Electrodeposition and electrode dissolution is the principle behind electroplating: the anode metal dissolves into solution and is reduced at the cathode, coating the cathode in the anode metal. It is therefore often preferable to use more inert materials such as carbon (graphite, reticulated vitreous carbon [RVC]) or platinum at higher potentials. Selection of the wrong electrode can drastically reduce the yield of the reaction or can result in unwanted side reactions sometimes overwhelming the desired reaction itself.

1.3.5 Solvent Selection for Electrochemistry

Solvents are not immune to electricity and have an Electrochemical Window (ECW) between anodic and cathodic decomposition. The range varies from solvent to solvent and is why certain solvents are or are not suitable for certain types of electrochemistry, for example hexafluoroisopropanol (HFIP) has an ECW of +0.4 V to +2.1 V and would therefore be unsuitable for any cathodic reactions whereas *N,N*-dimethylformamide (DMF) has an ECW of -3.5 V to +1.5 V and therefore is very suited to cathodic reactions.(44) For non-aqueous electrochemistry common solvents include acetonitrile, THF, DMF, and DCM. Common protic electrochemical solvents are water, short chain alcohols (MeOH, EtOH), and HFIP. Solvent mixtures are also common and have shown to be able to direct synthesis, however this research is in its infancy with only a few papers mentioning it.(45–47)

The intrinsic characteristics of certain solvents can also affect the type of chemistry they are used in; for example MeCN has been suggested to stabilise activated zinc,(48) and DMF has been reported to react with cation radicals.(49)

1.3.6   Electrolyte Selection

The function of an electrolyte is to, when dissolved, create an electrochemically conductive solution. Once electricity is applied to the circuit, it causes a negative charge cloud around the cathode, and a positive cloud around the anode. The charged electrolyte neutralises these clouds and allows electron flow to continue; electron density at the cathode reduces an electrolyte ion, which moves into the bulk solution to the anode where it is oxidised.

There are a wide variety of known electrolytes that have been used over the years; they are chosen depending on the type of chemistry performed and the solubility of the electrolyte in the chosen solvent. They can be inorganic, such as lithium perchlorate, or organic, such as tetrabutylammonium iodide (TBAI), but are always an ionic salt which dissociates into its constituent ions in solution. Though electrolytes of the same class will not perform better than each other, the solubility of the salt and its intrinsic resistance in the solvent of choice will greatly impact the efficacy of the reaction. Care must be taken when selecting an electrolyte to avoid any possible interference from the constituent ions such as with I^- (in TBAI) which has been reported to form hypervalent iodine, a reasonably good oxidant.(50,51)

1.4   Electrochemical Catalysis

Electrocatalysis has found applications spanning science: from nanoscale reactors used in diagnostics and therapeutics,(52) to biohydrogen production using microbial electrolysis cells,(53) to the ever expanding universe of batteries and energy storage.(54)

There are numerous ways in which an electrochemical reaction may proceed depending on how each species interacts with the electrodes. A substrate's E^o,

determined using cyclic voltammetry, can help decide whether the reaction should use direct electrolysis (if E^o is within the solvent's ECW) or indirect electrolysis (if E^o is outside the ECW). A direct process is where the electrons put in the reaction mixture directly affect chemical change of the substrate, and the potential applied is equal to or larger than the electrochemical redox potential of said substrate. Indirect electrochemistry utilises a separate chemical species to elicit a chemical reaction; this second species is referred to as a redox mediator. The redox mediator has an E^o value lower than that of the substrate but once activated electrochemically it forms a reactive intermediate which goes on to facilitate the desired chemical reaction (Figure 1.8).
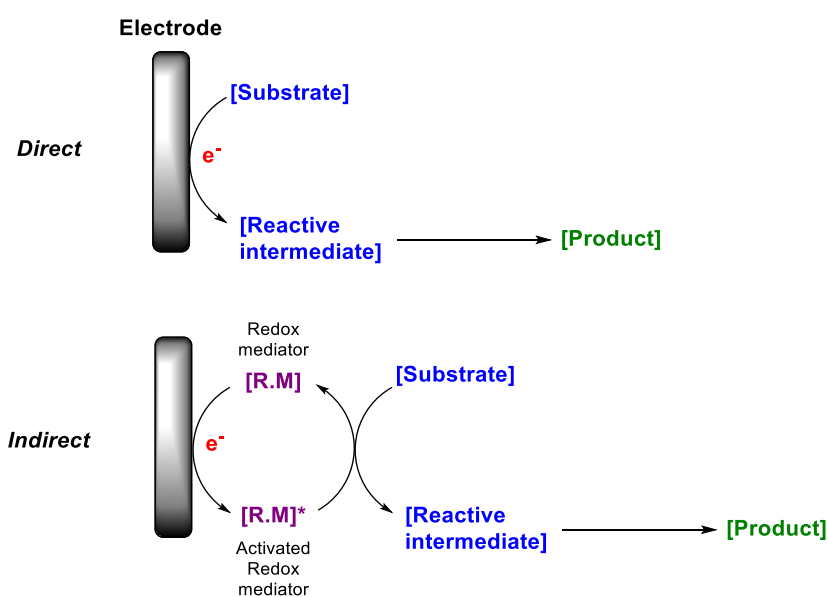
Figure 1.8. A comparison of direct and indirect electrochemical processes.

Some reactions have one "active" electrode which is actively involved in facilitating the desired reaction and a "passive" (or auxiliary) electrode to complete the circuit; electrolysis reactions where both electrodes are "active" proceed (paired electrolysis) by one of the four methods seen below (Figure 1.9):

16

- Standard paired electrolysis - two substrates (A + B) which react with opposite electrodes to each make a product (C + D)

- Convergent electrolysis - two substrates (A + B) which react with an electrode each to form reactive intermediates (A* + B*) which combine together to make a product (C)

- Domino electrolysis - one active substrate (A) reacts with one electrode to form another electroactive substance (B) which reacts with the second electrode to form a product (C)

- Convergent electrosynthesis – one substrate (A) can react with both electrodes and form 2 different products (B + C)
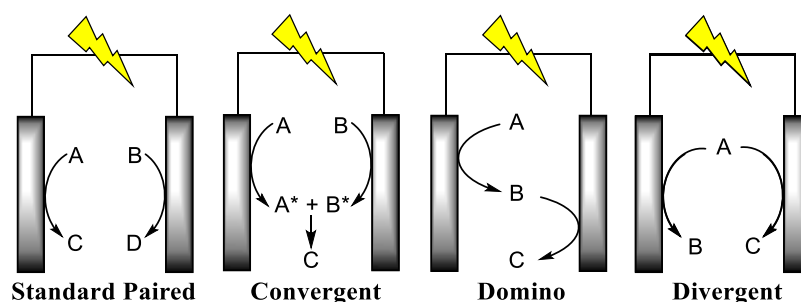
Figure 1.9. A depiction of different types of paired electrolysis.(55,56)

Paired electrolysis allows for minimisation of waste and improvement in green metrics as the reactions at both electrodes produce a valuable product,(57) however as there is no standard for pairing species together it can be difficult to find a good substrate pairing. Due to the difficulty in predicting the behaviour of the starting material under electrolysis, standard paired is usually the starting point for new substrate pairings with convergent and domino systems emerging later to optimise the reactions.

1.5   Applications of Electrochemistry in This Work

Electrochemistry can offer a wide range of possibilities for synthesis in terms of reaction mechanism, materials, and reactor types to access a plethora of novel and known molecules. Numerous recent reviews on electrosynthesis have remarked upon this, demonstrating the shift towards its implementation into standard lab practice.(18,33,34,37,39–41,58,59)

However, due to its relative infancy there is little in the way of available process understanding (kinetics, scale up factors, *etc.*) and standardisation which detrimentally affects reproducibility and how easy it is for novice electrochemists to get into the field. Furthermore, processes are generally limited to one reaction type/one substrate type (C-H activation, hydrolysis, dimerization, *etc.*), with each redox mediator preferentially reacting with certain functional groups.

My work has focussed on the investigation of electrocatalytic systems, both metallic and non-metallic, to synthesise industrially relevant substrates. The research described in this thesis focuses on two main aspects:

a. C-H activation-amination of benzoxazole with morpholine using flow chemistry (Chapter 2)

b. Utilisation and manipulation of highly reactive zinc particles in a number of known zinc mediated reactions (Chapter 3).

The specific aims are described in the following sections.

1.5.1   C-H Activation using Flow Electrochemistry

C-H activation traditionally require a transition metal; unfortunately, this also means there is transition metal waste produced. Once these catalysts have served their purpose the mixture needs expensive and arduous metal-removal processes to adhere

to the minimum amount of metal guidelines. Therefore, research into metal-free C-H activation is of considerable fiscal and environmental interest in synthesis.

The work in this thesis explores a published electrochemical C-H activation/amination coupling morpholine with benzoxazole(42) and its adaptation from batch into flow, analysing the reaction with regards to kinetic profiles, alternative electrodes, and the effect of constant potential at varying voltages. The aim of this work was to generate new process understanding and develop protocols for translating batch to flow reaction set-up with the intention of improving substrate scope and yield of reaction. Additionally, metal-free electrocatalytic C-H activation presents a greener, more environmentally friendly, and safer alternative to transition metal catalysis, which suffers from the high cost of transition metals and extensive purification requirements.

1.5.2   Utilisation of Electrodeposited Zinc Particles

Organozinc reagents have a broad synthetic scope in organic chemistry, however they are rarely used in an industrial setting due to its issues with inherent instability and handling difficulties, pyrophoricity, and reproducibility. In fact, large scale synthetic protocols will tend to avoid zinc altogether as organozinc reactions "occasionally (and unpredictably) fail completely".(60–62)

Herein, electrochemically deposited zinc particles formed using a published methodology(63) were used to (1) replicate literature results, (2) investigate the Blaise reaction dynamics for process understanding, (3) investigate the synthetic applications of this highly reactive zinc to form substituted β-lactams. Previous tried and tested methods of reactive zinc particle generation often require highly specific starting materials (Staudinger reaction – ketenes, Kinugasa reaction - nitrones)(64,65), high temperatures (refluxing for metallic zinc),(66,67) specialised

ligands for metal catalysts (Mannich reactions),(68) or highly flammable commercially available products. The formation of these particles is non-pyrophoric and, when compared to standard procedure in particular, simple and highly cost-effective Our results prove that this method is versatile in terms of reaction type, has good functional group tolerance, and gives yields up to 99% (Reformatsky reaction, Section 3.4.2). This work proved that zinc is a viable electrocatalyst with greatly improved process safety and more reliable method of zinc activation, which opens new opportunities for organic synthesis.

2 C-H Activation/Amination of Benzoxazoles

2.1 C-H Activation

C-H activation is an extremely valuable reaction in a synthetic chemist's toolbox as it removes the need for pre-functionalised molecules (necessary for many popular C-C forming reactions such as Suzuki-Miayura and Heck reactions) and can be more time and material-efficient because of this. The primary difficulty is in "activating" the thermodynamically stable C-H bond. For example, the bond enthalpy ΔH_{298K}(C-H) for ethane is 101 kcal.mol^{-1}, comparatively the bond enthalpy ΔH_{298K}(C-Br) in bromoethane is 72 kcal.mol^{-1}.[69] This aligns with what we already know about carbon-halogen bonds: halogens are excellent leaving groups as the bond is relatively easily broken.

There is a second more obvious issue: most molecules targeted by this reaction type will have more than one C-H bond, so how do you target one specific bond? Current solutions include using highly specialised catalysts (usually a transition metal *e.g.* Ru), highly complex ligands (such as substituted catechols), or precise prefunctionalisation. Novel solutions include electrochemistry and photochemistry, which can allow for more selective C-H activation reactions.[70–72]

Electrochemistry and photochemistry are becoming more popular for capricious reactions; electrochemistry is discussed in length in Chapter 1. Photochemistry uses a catalyst or redox mediator which is activated by light in the ultraviolet [UV] (100-400 nm), visible (400-750 nm), infrared [IR] (750-2000 nm) region and goes on to initiate a catalytic cycle to form the desired product. This redox mediator is often metallic (*e.g.* iridium)[73] but this is not always case (*e.g.* TEMPO).[74] The main function of a redox mediator is to overcome high activation energy barriers, which

would be inaccessible by traditional thermal routes. It is used industrially to synthesise benzyl chloride (approximately 100,000 tonnes per year) by gas phase photochemistry of toluene and chlorine *via* radical pathways with HCl as a by-product.(75) The further literature review will focus on metal catalysed C-H activation, Hydrogen Atom Transfer (HAT), and use of highly specific directing groups.

2.1.1 Metal Catalysed C-H Activation

Mechanisms of metal catalysed C-H activation fall into one of three groups: electrophilic activation (Figure 2.1A), oxidative additions (Figure 2.1B), and sigma bond metathesis (Figure 2.1C). In electrophilic activation an electrophilic metal attacks the hydrocarbon to displace a proton, and is a popular choice for alkenes, allenes, and allynes.(76) Oxidative additions occur when a low valency metal oxidises the C-H bond.(77,78) Sigma bond metathesis proceeds *via* a four-membered ring transition state where all bonds are formed and broken in a single step and is common in metals with d^0 electronic configurations.(79)

A - Electrophilic Activation

$$L_nM^+ + RH \longrightarrow L_nMR + H^+$$
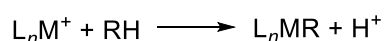
B - Oxidative Addition

$$L_nM + RH \longrightarrow L_nMR + H^+$$
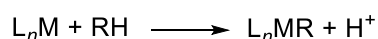
M = Metal centre
L_n = Ligand
R/R' = Organic group

C - σ-Bond Metathesis
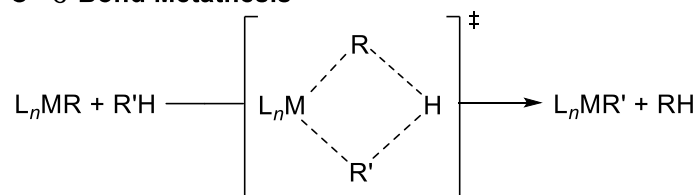
Figure 2.1. Three mechanistic pathways of C-H bond Activation.

Typical metals for C-H activation are palladium, rhodium,(80) iridium,(81) and platinum.(82) Palladium is a powerhouse of C-H activation chemistry, with numerous papers and reviews detailing its versatility and reproducibility, making it often a chemist's first port of call when attempting C-H activation.(83–87) Other transition metals such as cobalt,(88–90) iron,(91–95) and manganese,(96–98) are becoming more commonplace in C-H activation chemistry in an attempt to reduce costs by using more abundant metals.

2.1.2 Hydrogen Atom Transfer

Hydrogen atom transfer, also known as hydrogen atom extraction, involves the movement of an electron and a proton and follows the general equation $XH + Y^{\cdot} \rightarrow X^{\cdot} + YH$. It is a key methodology in photochemistry and traditional chemistry (*e.g.* the action of cytochrome P450 in the body), and can be either direct or indirect (Figure 2.2).(99)

HAT = Hydrogen Atom Transfer; SET = Single Electron Transfer
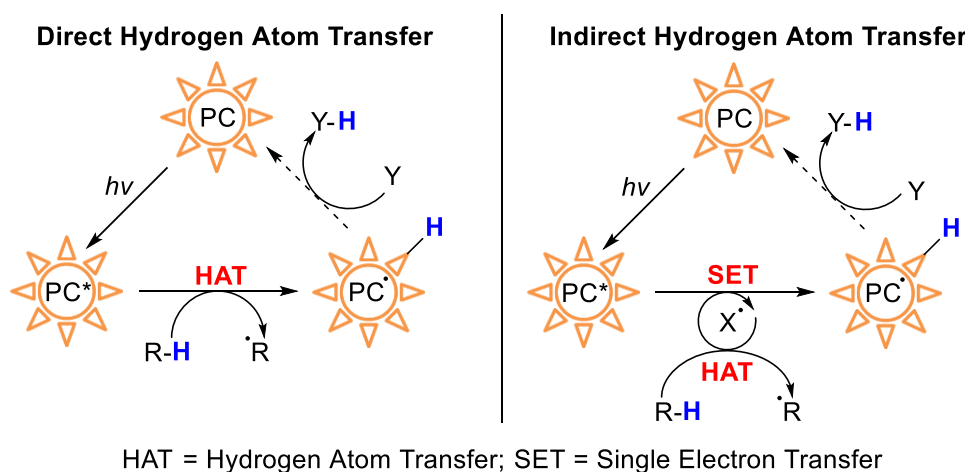
Figure 2.2. Diagram of a standard direct (left) and indirect (right) photocatalytic Hydrogen Atom Transfer. PC = photocatalyst, Y = proton acceptor, X = co-catalyst/hydrogen abstractor.

Traditional HAT (*i.e.* non-photocatalytic HAT) proceeds in a similar way to that seen in Figure 2.2, the key difference is that the catalyst is not activated by light but

23

a chemical hydrogen extractor. Direct HAT proceeds by light activation of a photocatalyst (PC) to form PC*, this acts as a H-atom extractor and HAT occurs with a given molecule (R-H) to form R⋅ and ⋅PC-H. The PC radical is quenched with a hydrogen acceptor (Y) and the R radical goes on to react. Indirect HAT proceeds in a similar way except the photocatalyst is not the hydrogen extractor; once activated it undergoes a single electron transfer with a co-catalyst (X) to form the hydrogen extracting species.

This process can be extremely selective and, when done photocatalytically with an organic catalyst, greatly improve a reaction's green metrics by obviating the need for transition metal catalysts. One interesting example is the anti-Markovnikov hydrothiolation of alkenes using UV light and a benzophenone photocatalyst to give good to excellent yields.
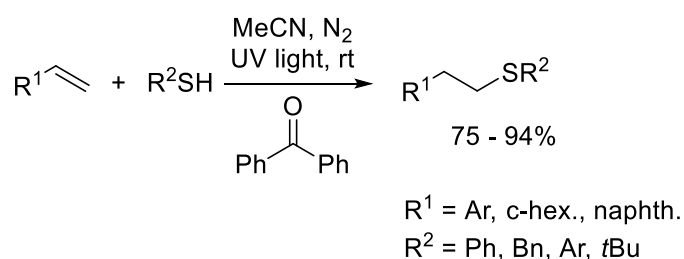
Scheme 2.1 A literature example of photochemically catalysed thiolation of alkenes using a benzophenone redox catalyst.(100)

However, the need for fine-tuning and a lack of catalyst-to-reaction pairing means that when applied to a novel reaction it may not work entirely. Therefore, it can be time and resource consuming to attempt this with unknown substrates. This also applies to "traditional" HAT, where the hydrogen abstractor may need to be fine-tuned sterically/electronically until the desired reaction predominates.

2.1.3 Directed C-H Activation

Specific C-H bonds can be activated or deactivated by changing a molecule's functional groups to selectively direct regio- and stereochemistry; it can be either "innate" (reactivity already present within the molecule) or "guided" (reactivity induced by external interference). Examples of innate and guided activation can be seen below (Scheme 2.2), where the innately activated C-H bonds are highlighted in blue, and the guided activated bonds are highlighted in red. Transformations **A** and **B** use metal complexation with the carboxylic acid and methoxy groups to alter the reactivity of the ring C-H bonds to give the desired substitutions. The use of a bulky iridium catalyst in transformation **C** induces a steric bias of the reagent for the *meta* hydrogen over the *ortho/para*.(101–103) 2-methoxybenzoic acid can undergo the electrophilic substitutions described in **D** and **E** as the combination of functional groups selectively activates the 5-position C-H. Similar reasoning is behind process **F**.(104,105)
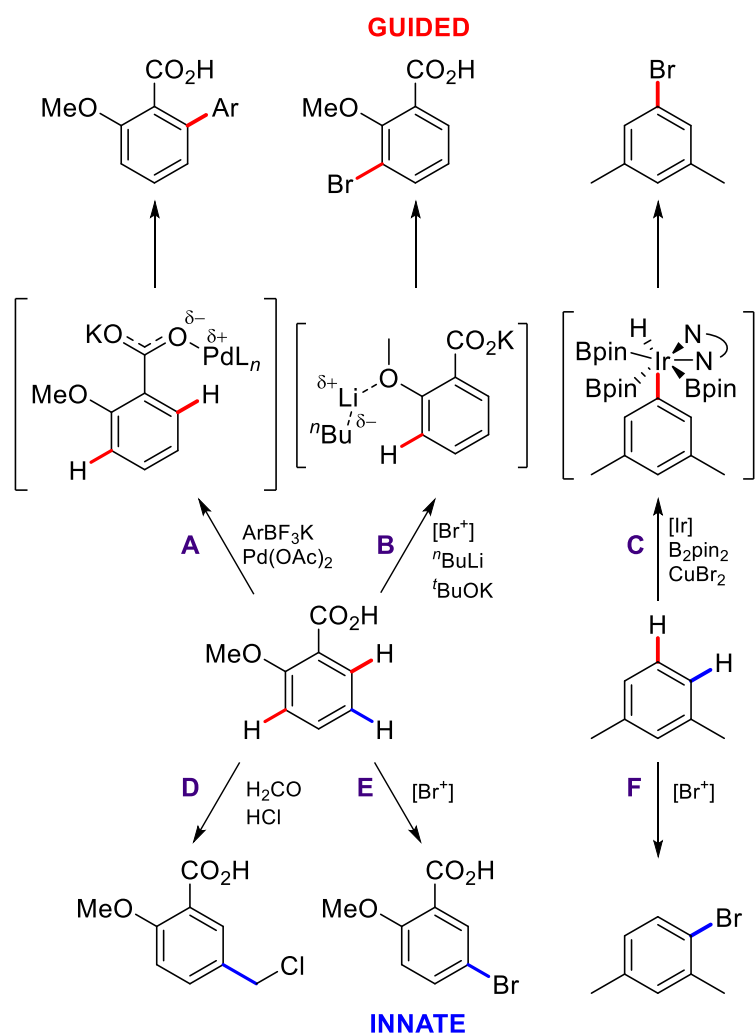
Scheme 2.2 Examples of innate(104,105) (blue) *vs.* guided(101–103) (red) C-H

functionalisation. Image adapted from reference (106).

Despite the positive reviews given to this retrosynthesis method by Baran *et al.*, it does not change the fact that more complex molecules will need more convoluted strategies to either prefunctionalise a molecule or combine the correct additives and catalysts to ensure good selectivity.

2.2   C-H Activation/Amination of Benzoxazole

A good example of industrially applicable direct C-H activation is amination of benzoxazole, which is biologically relevant moiety observed in both receptors and enzymes in the body;(107) 2-amino benzoxazole alone has over 6400 potential

ligand investigations to its name,(108) with its uses spanning a wide medicinal research range such as antibacterial(109) and antiproliferative(110) agents. Currently used functionalisation methods require precious metal catalysts such as palladium, and high temperatures.(83) This negatively effects the green metrics for large scale production such as E-factor (mass ratio of waste to desired product including solvent waste, catalysts, and product yield) and atom economy (efficiency of the reaction's principal components).(111,112)

Greener methodologies using hypervalent iodine catalysis have emerged as promising alternatives to this, however, the iodine requires a co-oxidant in stoichiometric quantities to form the catalytic species. Electrochemical oxidation of iodine is a cleaner, and more efficient method as it leaves no waste and requires no removal post synthesis. It has been reported previously in the literature,(42,107,113) but at the time of this research (2018) only the work by Gao *et al.* was available.

Further work by the Francke group investigated the mechanism using DFT and radical-based reaction studies, disproving the original idea of an iodine cation catalytic species.(113) Their work confirmed what was found below regarding the rate determining step. They also attempted to optimise reaction yield by changing electrolyte, reaction time, and solvent medium. Electrode material was also investigated and it was found that using aluminium was beneficial. Using an anilide starting material without an additive was demonstrated by the Waldvogel group using single electron transfer electrochemistry.(114) However, the publications listed above were all performed using their own batch reactors with no attempts made to move to electrochemical flow.

This work was based off a paper from Gao *et al*. which described a C-H activation amination of benzoxazole catalysed by hypervalent iodine (Scheme 2.3). (42) It has

advantage over common functionalisation techniques as it is metal-free and therefore would allow for much simpler purification techniques and uses a cheap and readily available redox mediator. Iodine has been shown to effectively catalyse this reaction with an oxidising additive such as hydrogen peroxide,(115,116) but this was the first use of iodine as a redox catalyst to catalyse this reaction. Their work was repeated and then moved from a batch reactor system to an electrochemical flow reactor to determine the underpinning kinetic processes for the reaction and use this knowledge for optimised scale-up. The reaction between morpholine and benzoxazole was chosen as a model reaction for its high reported yield (91 %) and availability.
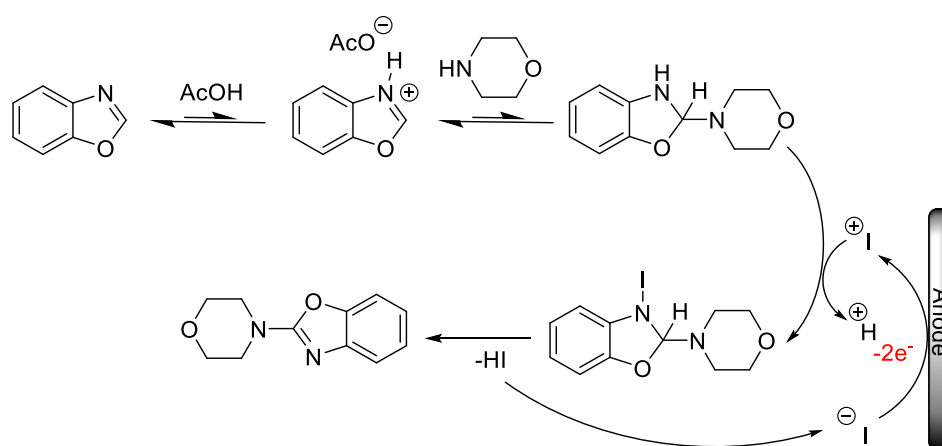
Scheme 2.3 Proposed reaction scheme for electrochemical oxidation amination of benzoxazole with morpholine mediated by I$^+$.

2.2.1 Reaction Monitoring

Herein we describe investigations into the amination of benzoxazole as a function of electrode material, additive concentration, constant current *vs.* constant potential, varying potential and current, and flow rate. The batch reaction described by Gao *et al.*(42) was reported to have been monitored by thin layer chromatography (TLC) until the starting material disappeared. Unfortunately, the protocol gave no indication of reaction time other than "until TLC showed no starting material remained" which

is not especially quantitative, therefore alternative reaction analysis techniques were used. Furthermore, while benzoxazole is UV active, morpholine is not, therefore TLC can only be used to observe benzoxazole depletion. The reaction was monitored using Gas Chromatography (GC) which was calibrated for benzoxazole and the product; this allowed facile kinetic testing and easily quantifiable yield calculation. Once the reaction had been studied and its rate determining step identified it can be more easily moved into a flow reactor; if successful, this would allow for more complex structures to be used as substrates. It was hoped that effective transfer of this reaction from batch to flow would allow design of a standard protocol for reactions of this ilk to be easily transferred from batch to flow.

2.2.2 C-H Activation/Amination in a Batch Electrochemical Reactor

Figure 2.3 Left: an image of the batch reactor set-up (L-R: potentiostat, ammeter, reactor). Right: close-up image of the reaction vessel.

For the initial batch process, the conditions used were those described in the literature: 0.05 M concentration of starting material and iron cathode RVC anode electrode system. This was to observe the reaction and to acquire sufficient product for a GC calibration. Once this was completed the reaction was scaled up by a factor of 5 (5 mmol in 100 mL MeCN) to increase product yield. The power supply was

capable of constant potential; constant current was achieved by manually changing the applied potential while reading the current on the multimeter.

2.2.3   Kinetic Analysis

To understand the reaction itself, certain variables needed to be changed to ascertain what the rate determining step is and to investigate whether the reaction mechanism described in Scheme 2.3 is correct. The hypothesised mechanism appeared to be zero-order with respect to the substrates involved in the reaction and determined by the amount of charge passed through the reaction. Therefore, doubling the applied current should in turn double the rate of product formation.

To confirm this we ran two reactions under identical conditions other than the applied current, one at 12 mA and the other at 24 mA. The rate of product formation at 12 mA was almost half that of the reaction run at 24 mA (Figure 2.4); this was also reflected in percentage conversion and percentage yield, confirming that the amount of charge applied is indeed the limiting factor for this reaction.

y = 0.099x + 7.54E-04

y = 0.045x + 4.42E-04
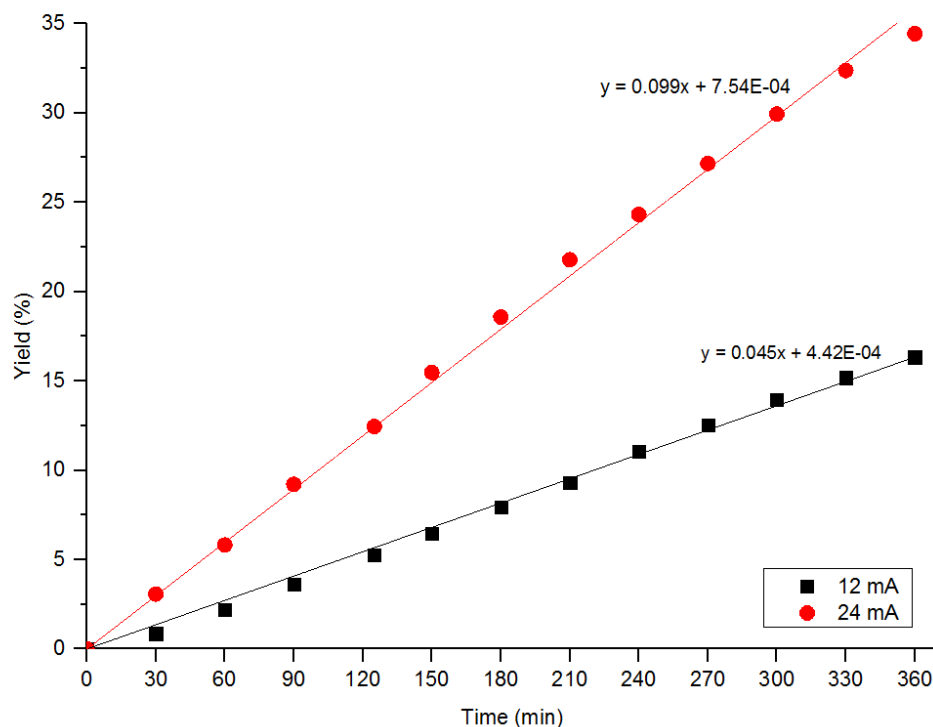
■ 12 mA
● 24 mA

Figure 2.4. Graph depicting reaction progress at 12 mA and 24 mA.

Once the reaction's limiting factor had been ascertained we moved on to investigate the impact of factors not covered by Gao *et al.* such as electrode material and pairing.

2.2.4 Electrode Selection

In total, seven different variations of the C-H amination/activation of benzoxazole with morpholine reaction were run (Table 2.1). It was discovered early on that using silica to remove trace metal from GC samples affected the results significantly, as far greater starting material depreciation rates were observed compared to Celite-filtered samples. Therefore, the reactions were repeated using Celite filtration which rectified these anomalous rates, the results of which can be seen in Table 2.1.

Table 2.1. Reaction performance of electrochemical C-H amination/activation of benzoxazole with morpholine in batch. RVC = reticulated vitreous carbon.[a]

	Anode	Cathode	Current/ mA	Potential/ V	Time/ h	% Yield	% Mass Balance	Total Charge/ C
1	RVC	Fe	12	6.4 – 6.9	3	8	118	129.6
2	RVC	Fe	12	6.8 – 7.2	6	16	99	259.2
3	RVC	Fe	24	13.0 – 13.7	6	34	95	518.4
4	RVC	St. Steel	12	6.1 – 6.5	6	13	105	259.2
5	St. Steel	Fe	12	N/A[b]	6	8	107	259.2
6	RVC	RVC	12	7.3 – 7.8	6	20	101	259.2
7	RVC	RVC	24	9.5 – 10.6	6	35	105	518.4

a. Benzoxazole (5.04 mmol), morpholine (10.08 mmol), TBAI (0.504 mmol), AcOH (25.2 mmol), MeCN (40 mL). b. Current reading was not possible due to constant jumping of the meter.

The higher yields in entries **3** and **7** appear to be mostly electrode independent, as both the RVC-RVC and RVC-Fe system yielded similar results (34% and 35% respectively), however, none of the batch scale reactions gave results that were comparable with the literature yield (91%). It was unclear why the literature yields were not able to be replicated; the yield disparity could be due to a number of reasons: time, equipment differences, definition of room temperature, or electrode size. However, without a detailed kinetic analysis it would be impossible to pinpoint a reason for the lower than expected yields.

It was hypothesised that the reaction in an electrochemical flow reactor would be much more efficient, as the interelectrode distance would be much smaller, the area

of electrode in contact with the reaction solution would be larger, and the overall amount of electricity required would also be greatly reduced as the applied current would be lowered. This has been shown in the literature and is one of the major advantages of electrochemical flow.(33,58,117) Therefore, our next step was to attempt to use flow electrochemistry to improve yields and electrical efficiency.

2.2.5   C-H Activation/Amination in a Flow Electrochemical Reactor

Figure 2.5. The equipment used for flow electrochemistry (L-R): battery, syringe pump, multimeter, flow reactor, outlet.

For the electrochemical flow reactor (EFR) the concentrations used were identical to the batch results. A syringe pump was used to push the reaction mixture through the flow cell, a battery pack provided the power, and the current and potential were monitored *via* a benchtop multimeter. The flow cell used alternating plates of electrode and PTFE pathways.

2.2.6   Electrochemical Flow Results

Table 2.3 details the results of C-H activation/amination of benzoxazole in continuous flow using the reaction set-up described previously in the same quantities as in batch. Due to equipment limitations, constant current was maintained by manually increasing/decreasing applied potential to maintain multimeter reading at the desired current. Entry 1 was run at pseudo-constant current as the power base did

not have the capabilities to maintain current (only potential); it was found that, unlike with the batch reactor, the current could not be effectively maintained and would jump (±4 mA) and the results would not be reproducible. Despite RVC's success in batch it is not feasible to use in this flow system due to its inherent brittleness; to avoid leakage from the reactor the base and plates are screwed tightly together, if this were attempted using RVC it would lead to either leakage or shattering of the electrode.

Table 2.2. Results of the continuous flow process C-H activation/amination.

	Electrode	Flow Rate/ mL min^{-1}	Potential/ V	Current / mA	t_R/ min	AcOH Eq.	% Conv.	% Mass Balance	Total Energy/ C[f]
1[a,c]	St. Steel	5	1.2-1.8	12	2.4	5	3	400	14.4
2[b,d]	St. Steel	0.25	2.0	57.6-106.1	48	5	26	64	235.7
3[b,d]	St. Steel	0.25	1.8	43.0-70.4	48	5	6	64	163.3
4[b,d]	St. Steel	0.25	2.0	9.8-20.4	48	2.5	12	51	43.5
5[b,d]	Fe	0.25	2.0	133-164	48	5.0	2	69	427.7
6[b,e]	Cu	0.25	2.0	-	48	5.0	-	-	-

a. Constant current conditions. *b*. Constant potential conditions. *c*. Sampled at regular time intervals. *d*. Sampled every half-reactor volume. *e*. No results possibly due to immediate short circuit. t_R = residence time. *f*. Energy per residence time.

Unfortunately, both the yield and the mass balance significantly worsened upon moving to continuous flow; the maximum yield achieved (26%) is substantially lower than was achieved in batch (35%). Because of the issues with constant current

34

discussed above, constant potential was used. Using a potential of 2.0 V increased yield from 6 to 26 % which was in agreement with what was found in batch (*i.e.* increase in electricity increases yield). However, a further increase was not used as it was thought that it would further increase the electrode dissolution and cause blockages as the reaction progressed. Stainless steel electrodes performed better than iron electrodes, and the current significantly increased in the iron electrode pairing. At 2.0 V constant potential using iron electrodes (Entry 5) a very poor yield was observed (2%); during the reaction the current reading would jump to 200 mA frequently and the reactor was observed to leak after 0.5 reactor volumes. It was suspected that a blockage in the system caused these jumps in current which is accompanied by the presence of a brown substance upon cleaning post-reaction (Section 2.7). Therefore, it was concluded that iron electrodes were not sufficiently stable to use in this reaction system.

Post-reaction, the electrodes had visibly undergone structural change as the reaction pathways from the PTFE plates had been etched into each side. This suggested that both electrodissolution and electrodeposition occurred in this system; we investigated the surface using EDX and SEM techniques, the results of which can be found in Section 2.7.

When copper electrodes were used (Table 2.2, entry 6) the system appeared to short-circuit straight away as the current reading dropped to 0 mA, therefore, the reaction was stopped immediately. Interestingly, the outlet flow turned bright blue almost immediately. Upon evaporation of the reaction mixture, copper acetate monohydrate crystals were identified; this confirmed our suspicions that electrodissolution of the copper electrodes occurred, and that copper is not a suitable electrode material for this reaction.

For this reaction it became apparent that the parameters used were not ideal for the flow set-up. The currents and potentials used resulted in numerous side-reactions due to electrodissolution of the metal electrodes, and we were unable to reduce the stoichiometric amount of AcOH as it more than halved the yield. The batch results had a more consistent "constant" current and better yields a more reliable constant current set-up was found, the results of which can be seen below.

2.3   Electrasyn2.0 Reactor Results

Figure 2.6 Images of the Electrasyn and how it is set up for electrochemistry; L: the Electrasyn2.0 and its components, M: Set-up in use with electrochemical reactor vessel attached to base. R: Set-up with home-made adaptor attached.

A second type of batch reactor was also used once it became clear that constant current was a better option than constant potential and a more precise method of achieving this was necessary. An Electrasyn2.0 was purchased as it has constant current and potential capabilities (Figure 2.6), however it does not have a particularly good seal and is therefore not suitable for reactions which are air and moisture sensitive. Furthermore, there is no capability for thermal control and reactions can only be run at room temperature.

To use the powerbase as much as possible an adaptor was created which allowed us to use its programmable functions on other reactor types and not limiting its use to the supplied reactor. This PTFE attachment can be seen above. With this extra appendage we were able to reliably attain constant current conditions and maintain this over a long period of time for our own reactor. The "Create experiment" function was used to set the current and total charge applied to the desired values, the black "arm" was screwed in place and the adaptor fastened using an elastic band. The anode and cathode wires were then attached to the appropriate electrodes of the reactor using crocodile clips.

Table 2.3 shows the results of using the IKA reaction vessel (entries 1 and 2) and using the base with the adaptor seen in Figure 2.6 as a powerpack for the round bottom flask seen in Figure 2.3 (entries 3 and 4).

Table 2.3. Reaction performance of C-H activation/amination of benzoxazole with morpholine using the Electrasyn2.0 reaction vessel.

	Current/ mA	Electrode Material	Observed Voltage/ V	Run time/ h	% Yield	% Mass Balance	Total Charge/ C
1^a	24	Graphite	11.5 – 17.8	14	13	104	1209.6
2^a	1.2	Graphite	1.5 – 2.0	14	42	93	60.5

a. Electrasyn2.0 reaction vessel used. Benzoxazole (0.256 mmol), morpholine (0.502 mmol), TBAI (0.026 mmol), AcOH (5.02 mmol), MeCN (5 mL).

Entry 1 was run at 24 mA and gave a low yield of 13%; the mass balance of 104% was likely due to a sampling error. Using the constant current set-up the maximum yield achieved was 42% (entry 2): a marked improvement on our previous results. It is possible that the Electrasyn set-up performed better than our previous batch set-up

due to the smaller scale of reaction, the decreased interelectrode distance, or the consistent interelectrode distance. Furthermore, a lower current of 1.2 mA drastically improved the yield when compared to entry 1, suggesting that too much electricity is a hindrance to the system rather than helpful.

The Electrasyn2.0 set-up was found to be a marked improvement on previous batch results. Using the power base and adaptor, we were able to investigate alternating electrode polarity at specified intervals which can reduce electrode surface fouling and improve mass transfer of active ingredients from the electrode surface to bulk solution.

Table 2.4 Results of the C-H activation/amination reaction of benzoxazole with morpholine using the Electrasyn2.0 power base and home-made adaptor to alternate electrode polarity.

	Current/ mA	Electrode Material	Observed Voltage/ V	Run time/ h	% Yield	% Mass Balance	Total Charge/ C
1^a	12	RVC	$\pm 9.8 - 10.0^b$	21	35	82	907.2
2^a	24	RVC	$\pm 15\text{-}0 - 15.5$	21	31	52	1814.4

a. Electrasyn power base and adaptor used with round bottom flask reactor. Benzoxazole (5.04 mmol), morpholine (10.04 mmol), TBAI (0.504 mmol), AcOH (25.20 mmol). Electrode polarity reversed every 60 seconds. b. Voltage limit on powerbase was set to 10 V.

It was found that alternating polarity every 60 seconds at 12 mA for 21 h gave a reasonable yield of 35% (entry 1); however, this was only slightly better than no polarity inversion with the same electrodes using RVC cathodes (Table 2.1, entry 7). Further increasing the current to 24 mA at the same alternating frequency decreased the yield to 31%.

Neither reactions using alternating polarity improved the reactions yield or mass balance in the round bottom flask reactor, therefore it was not investigated further.

2.4   Cyclic Voltammetry Analysis of Reaction Components

Cyclic voltammetry (CV) was utilised as a tool to validate the proposed reaction mechanism: if there were unidentified peaks in the voltammogram this could be the purported I^+ species. Three different samples were analysed for electrochemical activity: TBAI (source of hypervalent iodine), benzoxazole (starting material), and benzoxazole with AcOH (starting material, conductivity promoter). These were chosen for three main reasons: to identify the iodine redox peaks, to ascertain if benzoxazole has its own electroactivity within the applied electrochemical window (ECW), and whether the use of 5 eq. acetic acid alters the electroactivity of the starting material. We chose to apply a potential window of -1.5 – +2.5 V, as it is well within the ECW of acetonitrile (-1.8 – +2.8 V, Pt electrode *vs.* SCE) with tetrabutylammonium tetrafluoroborate (TBATBF) as a supporting electrolyte, therefore we would not need to take solvent decomposition into account. The substrate concentration in dry, degassed MeCN was 5×10^{-3} M for each solution, the electrolyte concentration was 0.1 M in each solution, and the reference electrode was a silver/silver chloride system. Each solution was run at 3 different speeds (0.1 V/s, 1.0 V/s, and 10 V/s) in an attempt to observe long, medium, and short lifetime intermediate species. All voltammograms can be found in Section 8.1.1.
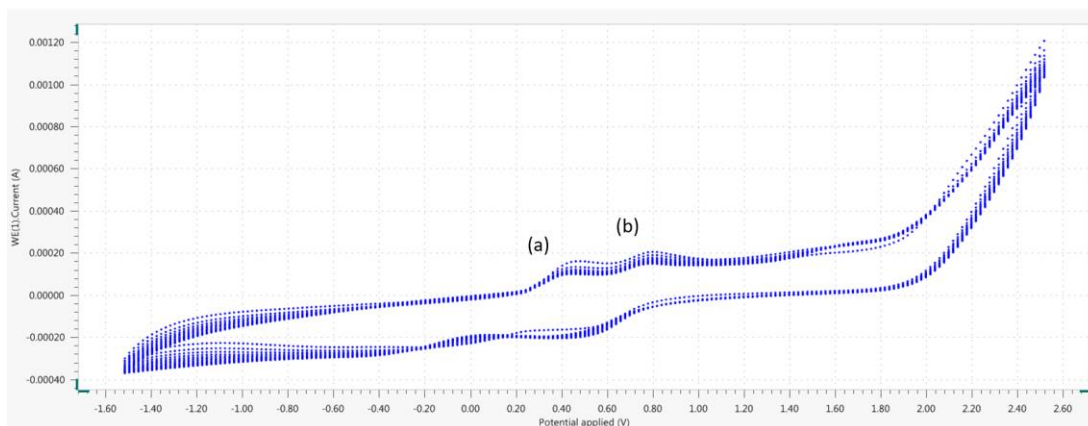
Figure 2.7. Cyclic voltammogram of TBAI, 20 scans run at 10 V/s. (a) and (b) denote significant reduction events.

$$I_3^- + 2e^- \leftrightarrows 3I^- \qquad E^o = 0.53\,V$$

$$I_2(s) + 2e^- \rightleftarrows 2I^- \qquad E^o = 0.54\,V$$
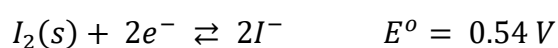
Equation 2.1 Standard Reduction Potentials of iodide species

The CV results for TBAI showed 2 distinct reduction and 2 corresponding oxidation peaks (Figure 2.7). This is in agreement with literature diagrams for the activity of iodide (I^-) and tri-iodide (I_3^-).[118,119] As the shape of the voltammogram does not show any abnormal peaks, it is unlikely that the suggested I^+ species is formed electrochemically.
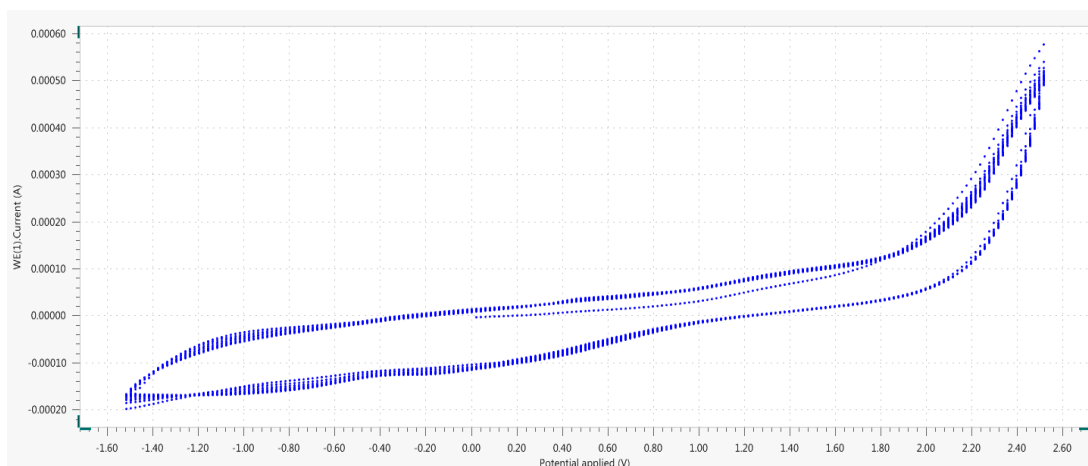
Figure 2.8 Cyclic voltammogram of benzoxazole, 20 scans run at 10 V/s.

The cyclic voltammogram of benzoxazole did not show any significant oxidation or reduction events at the three scan rates used (Figure 2.8). This confirms that it was not involved in the electrochemical step or electroactive within this electrochemical window.
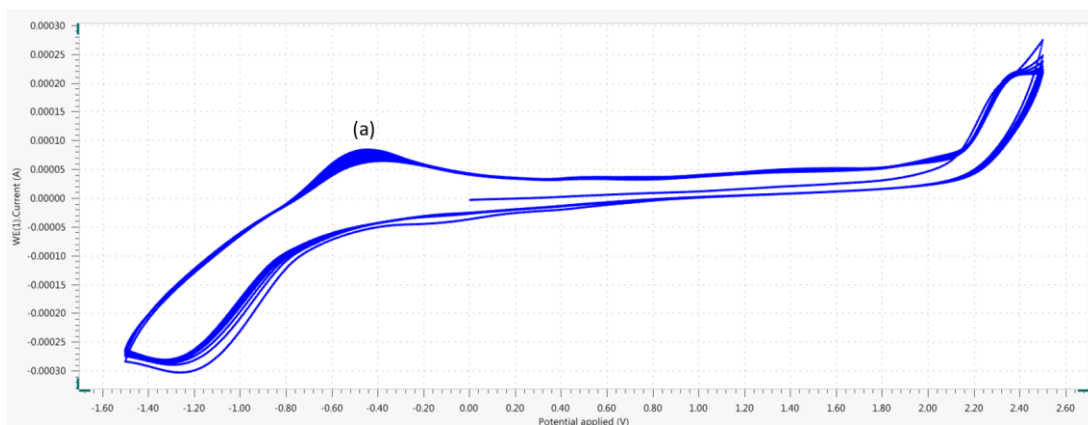
Figure 2.9 Cyclic voltammogram of benzoxazole (1 eq.) and acetic actid (5 eq.).10 scants at 1.0 V/s.

A sample of benzoxazole and acetic acid (Figure 2.9) showed a significant reduction event (a) and a corresponding oxidation event which is likely to be the oxidation of acetic acid into carbon dioxide:

$$CO_2 + 8e^- + 8H^+ \rightleftarrows C_2H_4O_2 + 2H_2O \qquad E^o = -0.32\,V$$
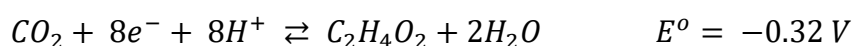
The analysis described above confirmed that neither the benzoxazole, nor a combination of the benzoxazole with the acetic acid are electroactive.

2.5 Electrode Surface Analysis in Batch and Flow Systems

From the results seen above, batch process C-H activation/amination demonstrates excellent mass balance using an RVC anode and an RVC cathode. This is likely to be due to the low reactivity of RVC and relative inertness; iron and stainless steel electrodes both exhibited signs of electrodeposition and electrodissolution in all systems they were used in (Figure 2.10).
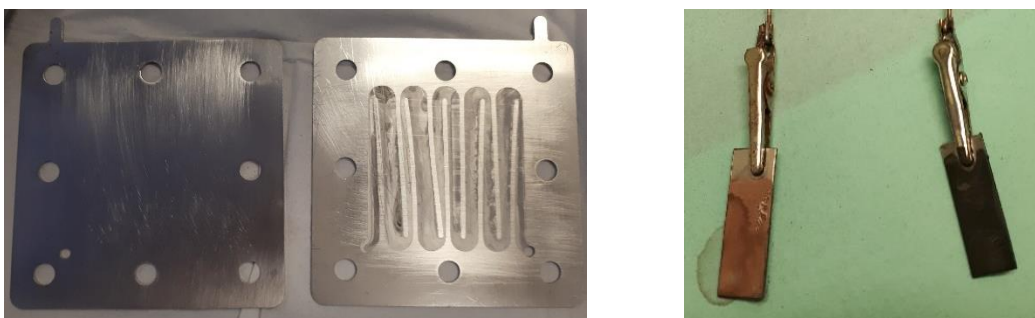
Figure 2.10. Left: Image of the stainless steel electrodes before (left) and after (right) electrochemical process. Right: Image of the stainless steel (left) and iron (right) electrodes after a batch electrochemical process.

When stainless steel electrodes were used in batch for a six-hour reaction the surface became visibly altered, in some cases an orange-brown powder appeared suggesting a metal oxide formation. Similarly, when iron electrodes were used in batch there was also a physical change in the surface obvious to the naked eye. For the electrochemical flow reactor electrodes there was also a stark difference observed before and after the reaction; on both anode and cathode plates the reaction pathway had been etched into the electrode.
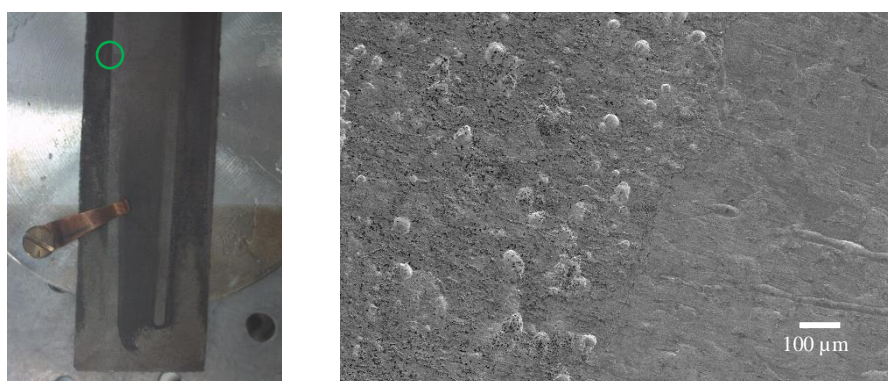
Figure 2.11. Image of a section of the cathode from an electrochemical reaction with section highlighted in green (left) and SEM image of the highlighted section.

Scanning Electron Microscopy (SEM) was used to further investigate the extent of the etching undergone by the electrodes in the EFR system. An iron cathode was

used as a sample, as it could be used to establish electrodeposition from the steel anode and also the effect the electrochemical reaction has on the metal surface. The flow reactor electrode seen in

Figure 2.11 highlights the difference pre- and post-reaction; very clear etchings of the reaction pathway can be seen in the right electrode compared to the smooth surface on the left. It is unclear whether this is due to the electricity itself or the reaction mixture producing an active intermediate after electricity is introduced which affects the surface. However, due to the CV investigation results showing no obvious intermediate (Section 2.4) we have concluded that electrodissolution/deposition due to the electricity is much more likely. SEM images for the iron and stainless steel electrodes in both batch and flow can be found in Section 2.7.1.

Using Energy-Dispersive X-ray Spectroscopy (EDX) analysis techniques we were able to observe electroplating and electrodissolution in batch process from the stainless steel-iron electrode pairing. The EDX map of stainless steel and iron which did not come into contact with the solution compared to that which was involved in the electrochemical reaction showed resounding evidence for electrodissolution of the stainless steel electrode and electrodeposition of metals from the steel electrode onto the iron electrode (Table 2.5).

Table 2.5. Observed elemental weight from EDX analysis electrodes after a batch electrochemical reaction.

	Element weight % (± error%)									
	Mo		Cr		Fe		Ni		I	
	T	B	T	B	T	B	T	B	T	B
a	1.63 ±34.90	1.48 ±35.87	15.36 ±5.40	17.76 ±5.71	72.69 ±3.52	70.15 ±3.45	10.32 ±11.83	9.60 ±12.83	0.00	0.37 ±58.34

43

| b | 0.00 | 2.28 ±17.60 | 0.00 | 0.00 | 97.55 ±2.80 | 76.74 ±3.34 | 0.00 | 10.81 ±8.75 | 0.00 | 0.75 ±57.48 |

a. Stainless steel anode. b. Iron cathode. T = top of electrode, not submerged. B = bottom of electrode, submerged in solution.

The table above shows results from a batch system using a stainless steel anode (a) and an iron cathode (b); the top of the electrode which was not exposed to the electrochemical system is denoted by T, and the exposed section by B. The stainless steel shows typical metals used in stainless steel (chromium [Cr], iron [Fe], nickel [Ni], molybdenum [Mo]) and the iron was found to have no other metals on the surface. The stainless steel B section shows a decrease in Elemental weight % in Mo, Fe, and Ni, but an increase in Cr and I. This coincides with the appearance of Mo, I, and Ni on the iron surface confirming electrodeposition; the cathode also appears to lose weight % of Fe suggesting the cathode also undergoes electrodissolution.

The red error % values in the table were also of interest, as there are errors significantly larger than the reported values themselves (Mo, Ni, I). These were left in the table as it was felt that just because it appears to be anomaly to us, future replications of this experiment may find the same results. Furthermore, researchers with better knowledge of this technique may be able to rationalise it.

Unexpected electrode erosion also occurred when the protocol was moved into continuous flow in both stainless steel and iron systems, where post-reaction the electrode surfaces were visually and physically different to the unreacted metal plates. It is highly likely that the metal electrodes also underwent electrodissolution and electrodeposition in the electrochemical flow system. Furthermore, the orange/brown deposit seen in Figure 2.11 was also found in the EFR system (Figure 2.12).

Figure 2.12. Images showing the brown substance formed during electrochemical flow reaction on the pathway plates (left) and once dry in a sample vial (right).

In particular the iron electrode system produced significantly more than the stainless steel system. This substance was analysed using AAS and confirmed to be an iron complex, further proving that the potentials used were affecting the metal surface.

Despite the strides made in identification of key parameters of this reaction, once it was confirmed that electrodissolution of the electrodes had occurred coupled with the low yields, further investigations into this process were stopped.

2.5.1   SEM Images

2.5.1.1 Batch Iron Cathode
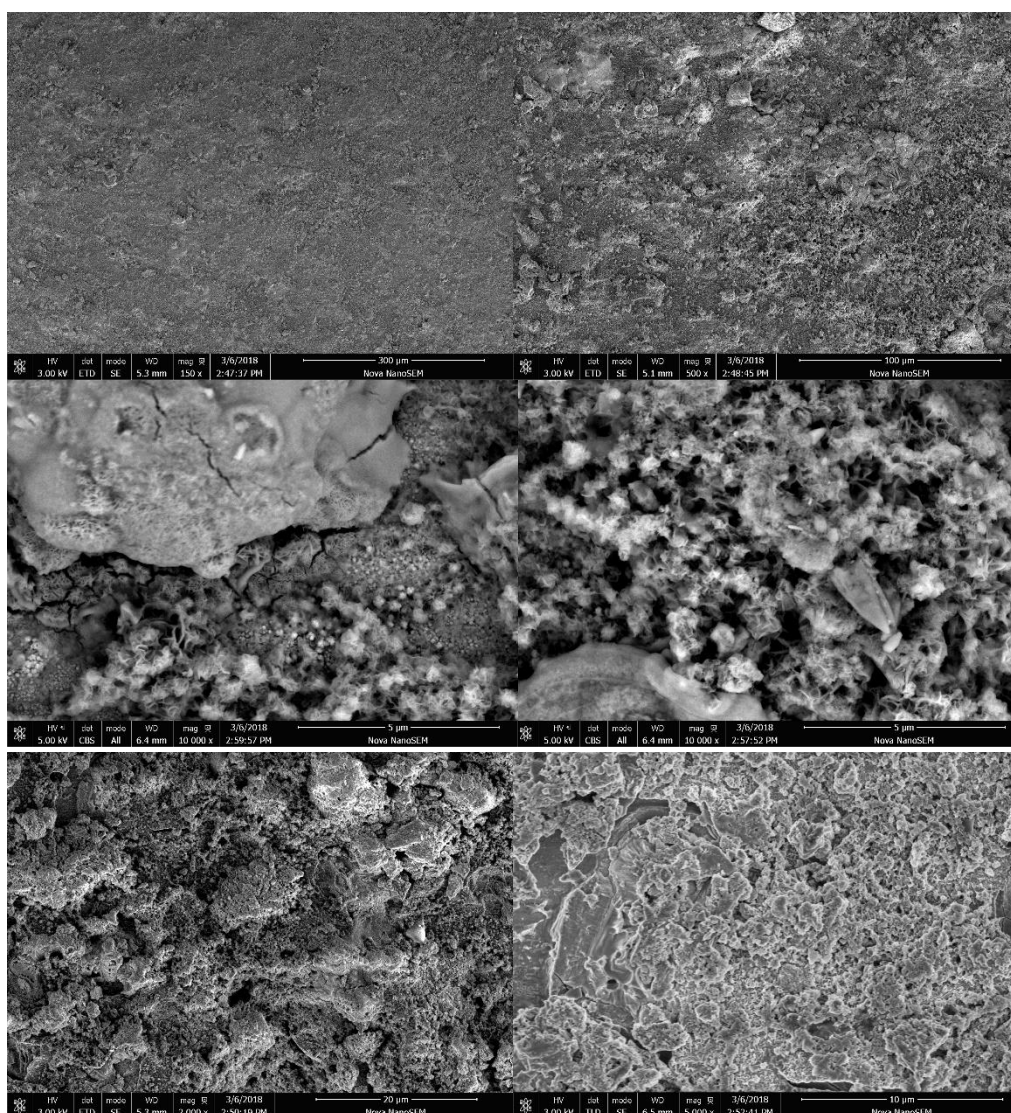
As magnification increases in this sample there is clear evidence for deposition of a conductive substance on the surface. It appears in the form of clusters which could indicate a form of seeding similar to what is observed in crystallisation, or that due to mixing those electrode sections were the most likely to come into contact with labile metal ions.

2.5.1.2   Batch Stainless Steel Anode
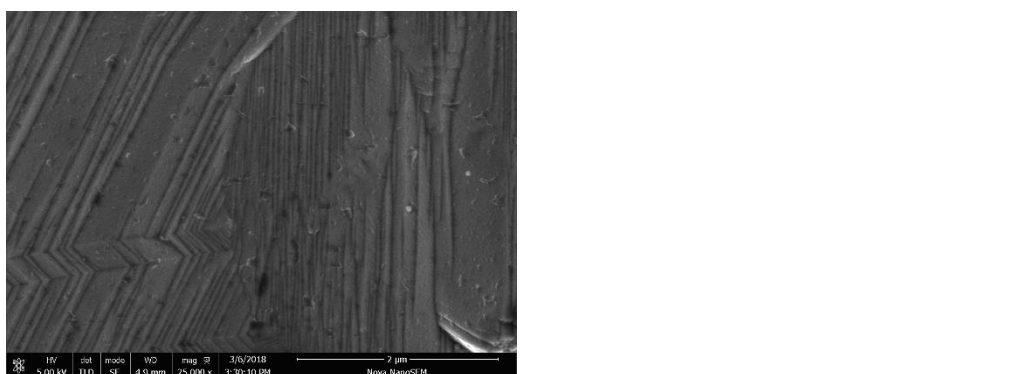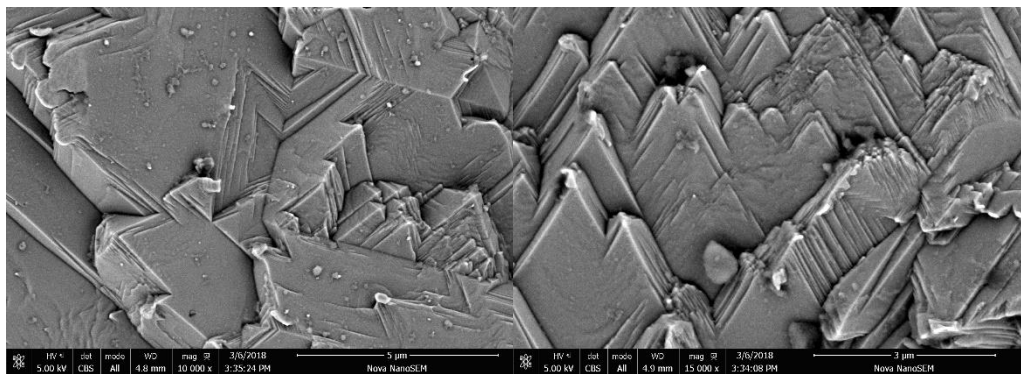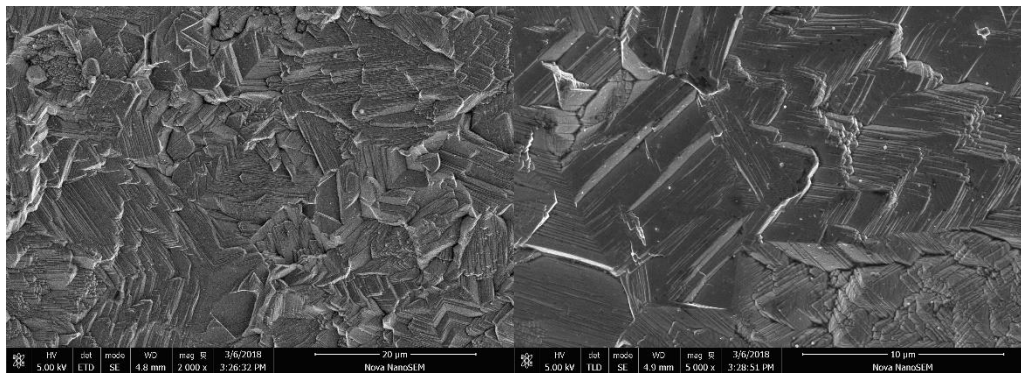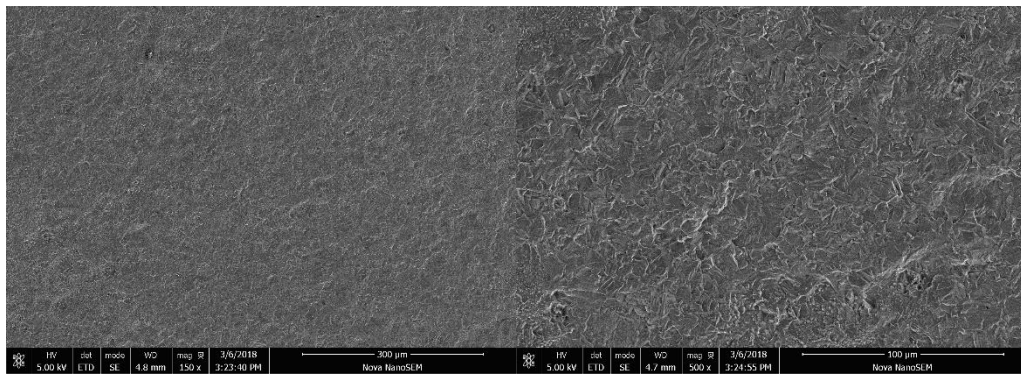
As magnification increases there are clear layers visible which suggests that material was removed from the surface during the electrosynthesis. There is a clear

distinction between the anode surface and the cathode surface (4.1.3.2), and both are noticeably different than the surface before the reaction. There is an interesting surface shape of triangular layers, and the topography also supports the electrode leeching hypothesis from the anode to the cathode.

2.5.1.3 Flow Iron Electrodes
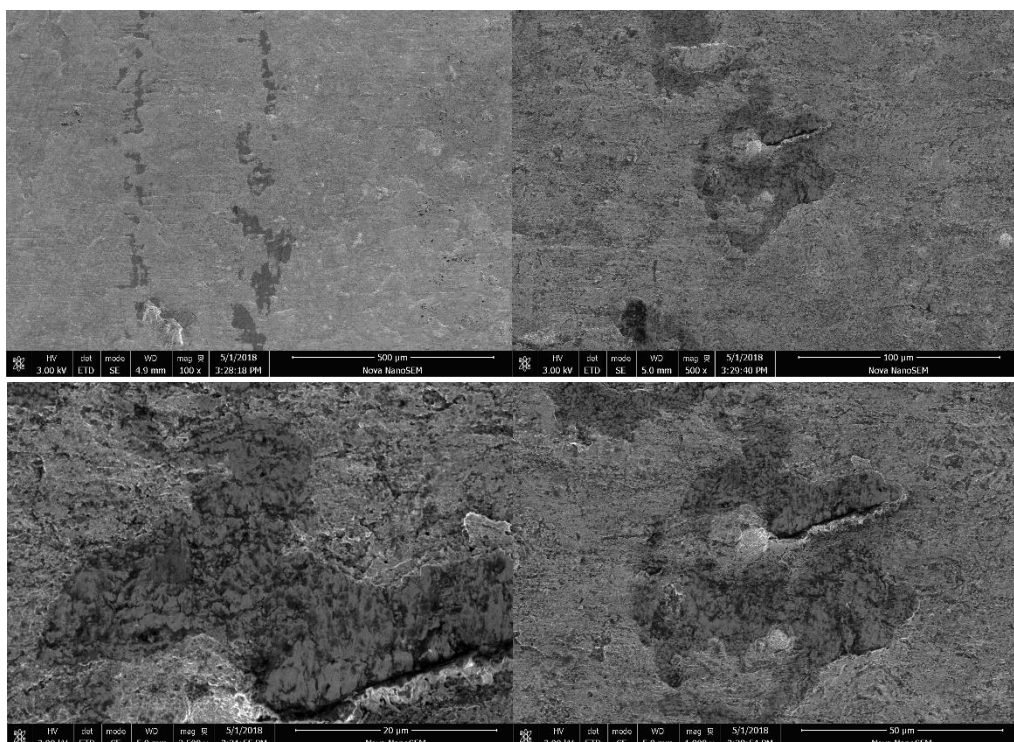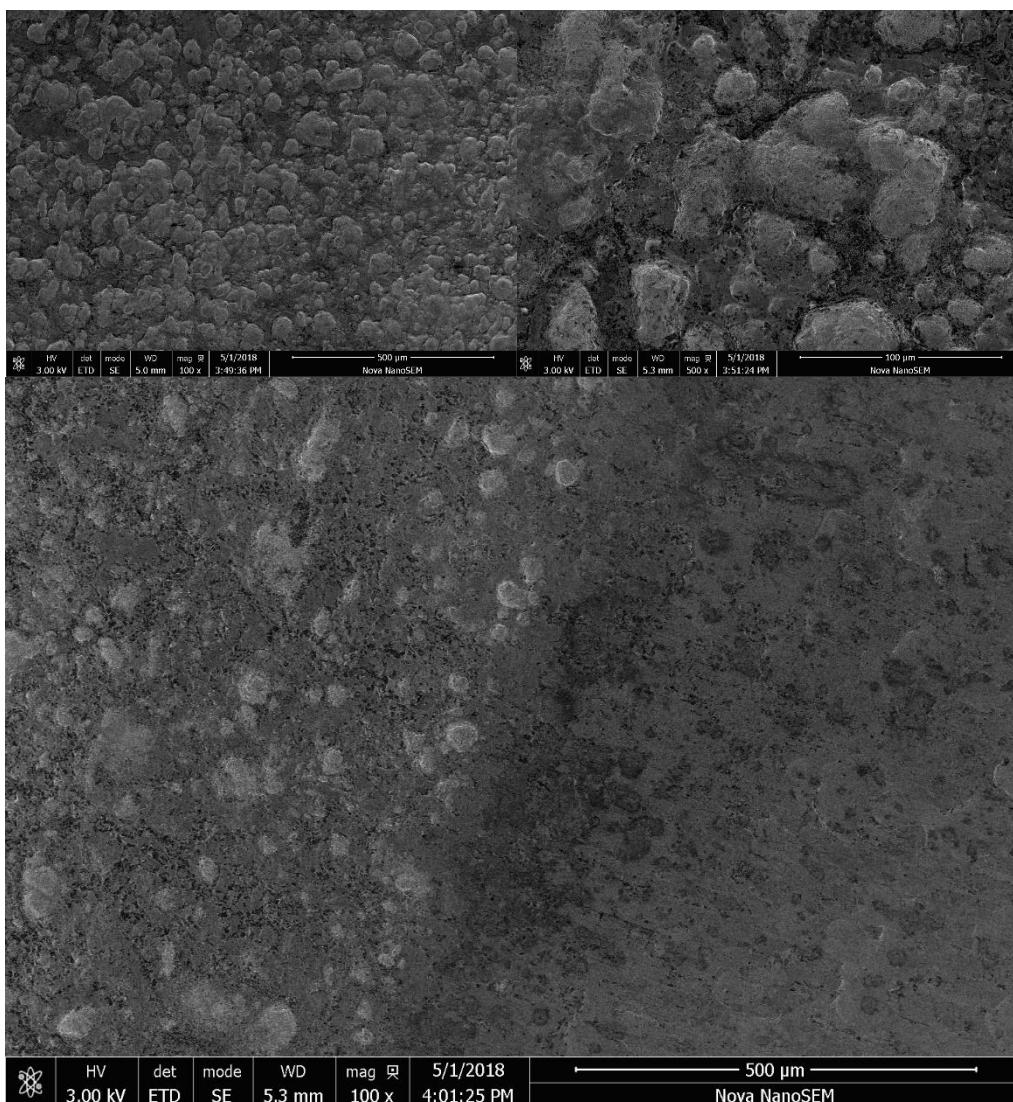
The SEM analysis in this section can be used to show a direct comparison between electrode sections which were exposed to electrosynthesis and sections where it was not. The difference is obvious as on the right hand side the electrode is smooth, the left hand side shows clear electrodeposition on the surface.

2.6   Conclusion to C-H Activation Work

This work shows attempts to understand the process behind the C-H activation/amination of benzoxazole with morpholine. This work was concluded when it was realised that this reaction was reasonably capricious in batch and even more so in continuous flow. Initially, it was assumed that the relatively simple published reaction will be a good model study for learning practical

electrochemistry. However, electrodeposition and electrodissolution issues, which were not mentioned in the literature, significantly constrained planned research into flow electrochemistry.

Kinetic analysis of the reaction in batch successfully confirmed the rate determining step as the electrochemical step, as doubling the applied current appeared to double the reaction rate and overall yield. Unfortunately, the yields described by Gao *et al.* were not replicated and a maximum yield of 42% was achieved in batch. Attempts to move this reaction into continuous flow were not successful, as the reaction mixture under electrochemical conditions was not compatible with the three metal electrodes tried.

In the subsequent years after this research was completed, other groups have reported this electrochemical reaction such as Ghoshal *et al.* who used a 5 V phone charger as a power source and report high yields of up to 93%.(107) Interestingly, they found a carbon-aluminium electrode pairing to give optimal results, and a carbon-iron pairing gave less than 5% yield after 3 h which contrasts with previous reports and our own research. Unfortunately, this further highlights the issues with electrochemistry in research previously described; because each group will have their own home-made reactor, result reproducibility can be extremely difficult. Furthermore, many of these papers have insufficiently reported or have not investigated the electrical parameters of the experiment (*e.g.* electrode surface area or total charge applied) which only adds to the issue.

Cyclic voltammetry of the reaction components was performed to better understand the electroactivity of the reaction components and give a better insight into the reaction mechanism. The proposed literature mechanism claims an I^+ species formed by anodic oxidation is the driving force for this reaction, however there was no

spectroscopic evidence (CV, cation trapping experiments, *etc.*) provided to validate these claims. Three years after Gao *et al.* published their findings, Koleda *et al.* published an investigation into the synthesis of substituted benzoxazoles using "hypervalent iodine" which they proposed to be an I(III) species.(113)
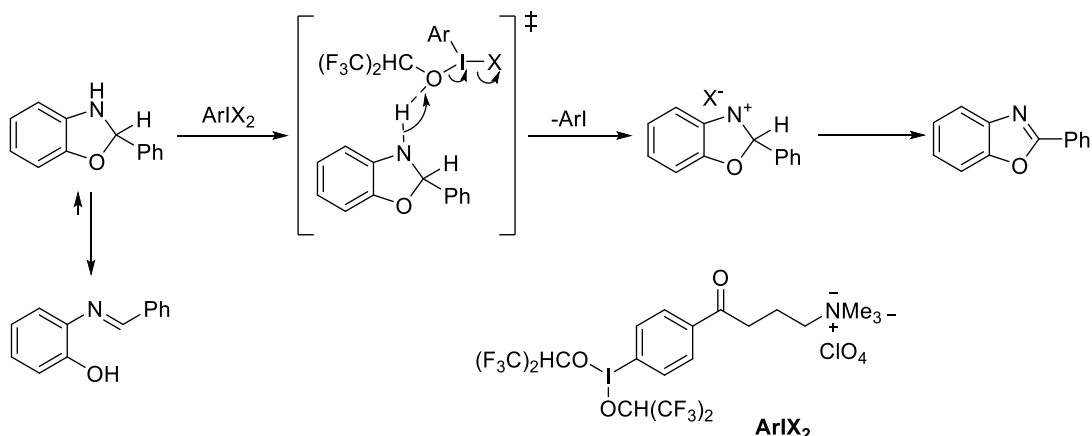
Scheme 2.4 Proposed mechanism for I(III) mediated C-H activation of benzoxazole.(113)

Through mechanistic studies and calculations of the proposed transition state reaction barriers they provide reasonable evidence to support their mechanism after narrowing down from three possibilities. This in combination with the lack of I^+ signal and presence of I(III) signal seen in the cyclic voltammetry shown in section 2.6 of this work, it is highly likely that I(III) is the catalytic species in this reaction, however it is not clear what the equivalent of $ArIX_2$ is in this reaction.

In 2018 Qui *et al.* published a catalyst and electrolyte-free C-H activation/amination of benzoxazoles with secondary amines which, contrary to the work done previously by Gao *et al.* and Koleda *et al.*, described a "catalyst- and reagent-free" synthesis in yields of up to 94%. Using numerous techniques including kinetic analysis, computational studies, and *in operando* IR reaction monitoring they proposed an alternative mechanism of Single Electron Transfer (SET) based anodic oxidation.(120) However, as there was no investigation into residual metal content of

their glassware, stirrer bars, *etc.* therefore it is unclear whether this truly is reagent free or due to residual amounts of transition metals such as palladium or rhodium.
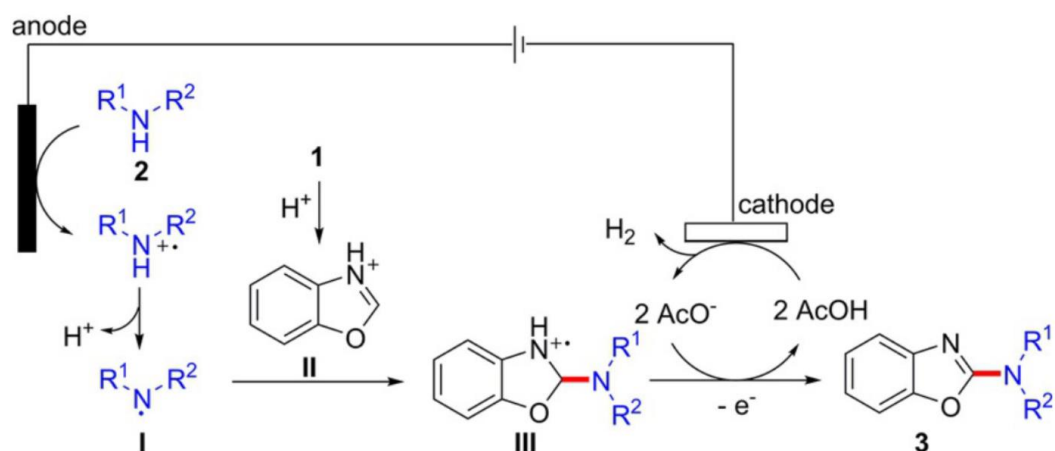
Scheme 2.5 Mechanism of reagent-free C-H Activation/Amination proposed by Qui *et al.* where **1** = benzoxazole.. Image from reference (120).

As the work in this chapter contained both acetic acid and an iodide source it is likely that both mechanisms are occurring during the reaction. However, we cannot be certain whether the two interfere with each other and consequently inhibit each other, resulting in the lower than reported yields.

2.7   Future Work

When this work was originally concluded the ideas for future work were to use DoE (Design of Experiments) of the reaction in flow by initially identifying the critical parameters and then moving on to a yield optimisation using software such as MODDE. Once the optimised reaction parameters were identified, the next step would be a scale-up investigations and substrate scope to investigate for example other nucleophiles we could use to couple with the benzoxazole and primary, secondary, and tertiary amines. The literature published in proceeding years provided more understanding of the reaction by investigating the reaction's mechanism(113)

and its scale-up.(107) Computational and kinetic studies of the reaction mechanism described in reference 44 put together a very convincing reaction mechanism which is useful for future rationalisations of reaction behaviour, and the successful scale-up process shows that this reaction does in fact perform well when scale is increased. Future work could be focused on further optimisation using DoE which could support scale-up investigations. Additionally, substrate scope could be extended to include different nucleophiles and possibly less electron-dense amines *e.g.* amides.

3 Electrodeposition and Utilisation of Highly Reactive Metallic Zinc

3.1 Introduction to Organozinc Chemistry

The first recorded organozinc compound was discovered by Edward Frankland in 1848; diethylzinc was prepared by heating ethyl iodide in the presence of zinc metal, creating a volatile, colourless liquid which spontaneously combusted upon exposure to air.(121) As some diorganozinc reagents are pyrophoric, this requires preparation using air-free techniques and are often made and used *in situ* due to their instability.

Zinc metal as a mediator in synthesis as it can be effective, selective, and have a wide application. They can be used to form functional groups such amines, epoxides, disulphides, and alcohols (Figure 3.1) and have remarkable functional group tolerance.
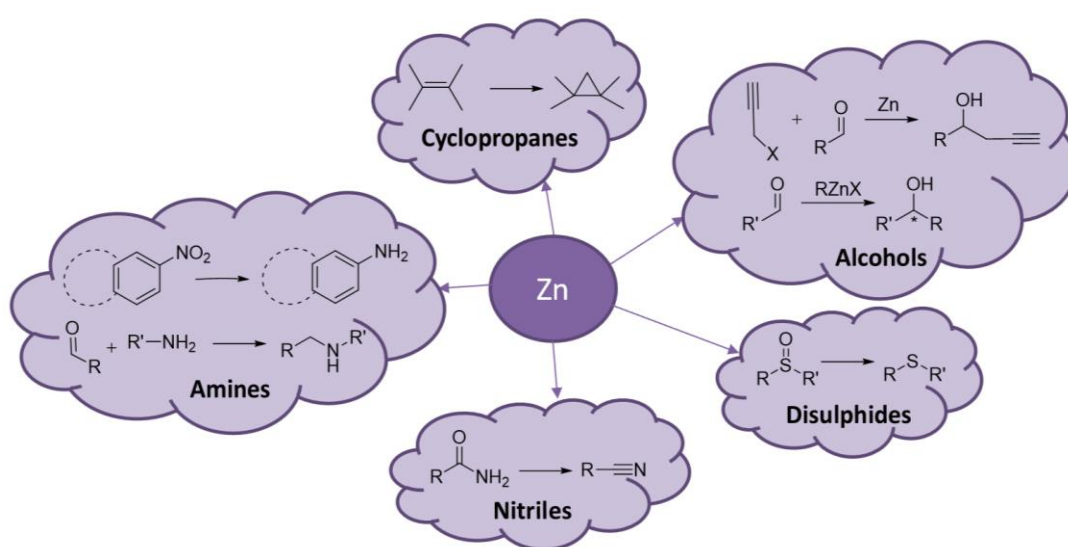
Figure 3.1. Diagram of possible functional groups that can be formed using various zinc catalysts.(122)

Some of the most well-known applications of zinc chemistry are the Reformatsky,(123,124) Blaise,(125) Simmons-Smith,(126) and the Nobel prize winning Negishi reactions(127) (Figure 3.2). These can be used to form complex

structures from simple starting materials and are relevant in all aspects of synthetic chemistry.

Reformatsky Reaction

X = Br, I, Cl, F; R = allyl, alkyl, aryl

Blaise Reaction

R = allyl, alkyl, aryl, *etc.*

Simmons-Smith Reaction

R = allyl, alkyl, aryl, *etc.*

Negishi Coupling

R-X + R^1-ZnX $\xrightarrow[\text{NiL}_n]{\text{PdL}_n \text{ or}}$ R^1-R

X = Br, I, F, OTf
R, R^1 = alkenyl, allyl, aryl, propargyl
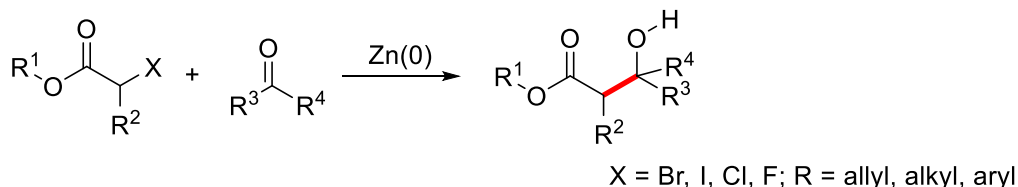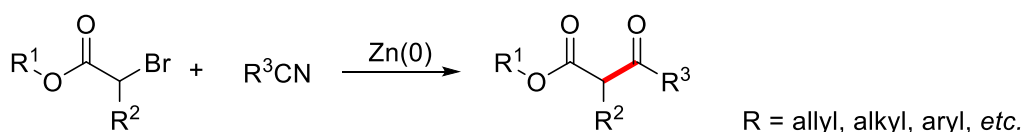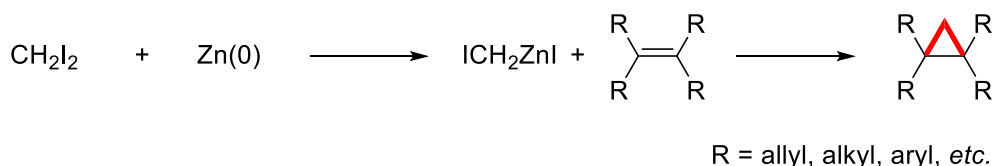
Figure 3.2. Three different applications of Zn(0): Reformatsky, Blaise, Simmons-Smith, and Negishi coupling reactions.

Despite its advantages, zinc chemistry is rarely found in industrial scale synthesis. Its scarcity can be partially accredited to its issues with reproducibility,[61] reliability,[60] and unpredictable induction periods.[62] Furthermore, many organozinc reagents such as diethyl-, dimethyl-, and diphenylzinc are pyrophoric and react exothermically with air and moisture. This can discount solvents other than aprotic solvents, however, work by Lipshutz *et al*. and Jackson *et al*. have published methods of organozinc formation in water for zinc mediated palladium catalysed cross-couplings of aryl bromides,[128] and Negishi couplings.[129] The solvent

specificity of pyrophoric zinc reagents often precludes their use in industrial quantities as their handling and use would require lengthy health and safety procedures which can be avoided by choosing a different synthetic route. When zinc chemistry is found in industry it is usually in the form of a less reactive organozinc halide; this can be used with a secondary activating reagent such as a magnesium or copper derivative.(130)

3.1.1 Formation of Organozinc Reagents

Organozinc reagents traditionally fall into one of the following categories: diorganozinc (R_2Zn), heteroleptic ($RZnX$) where X denotes an electronegative ligand, and ionic (R_nZn^- and $RZnL_n^+$). Synthesis of these reagents can be achieved *via* several routes; three popular methods are: directly from zinc metal, functional group exchange,(131) and transmetalation. (132,133)

A. $ZnX_2 + [H] \longrightarrow Zn^0 + R\text{-}X \longrightarrow R\text{-}Zn\text{-}X$

B.
$$R^1 \diagdown \diagup_I + Et_2Zn \xrightarrow{\text{cat. CuI}} R^1 \diagdown \diagup Zn \diagdown \diagup R^1$$

C. $MR_2 + Zn \longrightarrow ZnR_2 + M$; $MR_2 + ZnX_2 \longrightarrow RZnX + MRX$
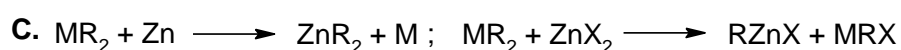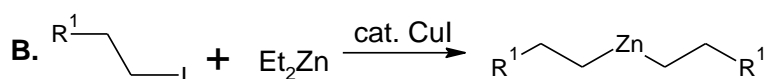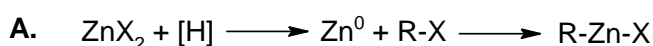
Figure 3.3. Three different methods of organozinc reagent generation: from zinc metal (A), functional group exchange (B), and transmetalation (C).

Activation of zinc metal to remove the highly stable oxide layer can be achieved *via* many different routes: acid or base, sonication,(134) naphthalene and lithium (Rieke method),(135) electrochemical,(136) and mechanochemical methods(137) (Figure 3.3A). These methods can be challenging to perform and can also have issues with reproducibility and impurity removal. Commercially available diorganozinc reagents can be used as a more direct route to unsymmetrical zinc reagents such as MeZnPh

(Figure 3.3B). However, these can be expensive, are limited in what can be bought, and are typically suspensions which can be difficult to quantify. Once formed, the asymmetric diorganozinc reagents are typically purified by distillation. This can be capricious on a small scale, let alone when applied to industrial scales. Transmetalation strategies using a zinc salt and an organomagnesium or organolithium compound is a straightforward way to form simple organozinc reagents (Figure 3.3C); however, this method is not functional group tolerant and would not be useful in the formation of more complex organozinc reagents containing an alcohol group for example.

When diorganic zinc reagents are formed in the presence of a zinc halide salt, expedient separation of the reagent from zinc salts must be done in order to prevent the reversible formation of organozinc halides (heteroleptic zinc reagents), also known as the Schlenk Equilibrium.

3.1.1.1 The Schlenk Equilibrium

The Schlenk equilibrium was first put forward by Wilhelm Schlenk in 1929, and describes an equilibrium between heteroleptic and diorganometallic species.(138) First described in Grignard reagents, the equilibrium is also found in all metal halides with Lewis acid character, and can therefore also be applied to zinc (Equation 3.1). It has been previously shown that in tetrahydrofuran (THF), the Schlenk equilibrium for methyl- and ethylzinc iodides (and the corresponding dimethyl- and diethylzinc) lies far to the left.(139,140) Unlike magnesium, there is little to no literature on quantitative study of the zinc-based Schlenk equilibria so in house techniques must be used to monitor the effect in each individual reaction.(141)

$$2\ RZnX\ \rightleftarrows R_2Zn + ZnX_2$$
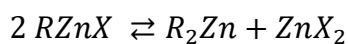
Equation 3.1. The Schlenk equilibrium of zinc.

Most synthetic protocols for diorganozinc reagents form zinc halide (ZnX_2) as a by-product which means that considerations to minimise the effect of the Schlenk equilibrium on the yield of the diorganozinc used must be taken. Equilibrium can be shifted by manipulating concentration of either side. One method is to distil and collect the diorganozinc as it forms. A second, slightly trickier alternative is using a solvent that the zinc salt is either insoluble or sparingly soluble, causing it to immediately precipitate upon formation. Both methods work by shifting equilibrium to the right to reduce the backwards reaction. As organozinc reagents can be exothermic in air and moisture distillation is not always a favourable choice. Furthermore, most zinc salts are highly hygroscopic and to avoid a pyrophoric incident the method must be run under extreme dry conditions.

3.1.2 Direct Activation of Zinc Metal

Activation of zinc metal can be achieved through numerous different methods which cover organic, inorganic, and engineering backgrounds. Arguably the most famous method of activation forms what is known as "Rieke Zinc"; first published by Reuben D. Rieke in 1972, Rieke metals are highly reactive metal powders which are generated by the reduction of an anhydrous metal salt with an alkali metal in a suitable solvent, usually THF.(135) This method was successfully applied to zinc,(135,142–144) obviating the need for specialist equipment required for previously discovered activation techniques such as ultrasonic irradiation.(134) Despite its commercial success, purchased Rieke zinc is a suspension of the active particles in an aprotic solvent (*e.g.* THF, toluene) which poses reproducibility issues as it is difficult to quantify exactly how much zinc you are adding each time.

Furthermore, Rieke zinc is difficult to prepare consistently due to the nature of the material and the number of variables involved in making it. Further chemical methods of surface activation include iodine, potassium, and trimethylsilyl chloride (TMSCl).(145) While they can be advantageous, as with HCl activation the removal of the activating agent can be time and material consuming.

Mechanochemical activation of the zinc surface has been shown by the Browne group to be highly effective in the Reformatsky,(146) Barbier,(147) and Negishi coupling reactions.(137) Its energy efficiency and the ability to run solvent free greatly improves the green metrics of the reactions run. However, as with sonication and irradiation of the surface metal the equipment required to run these reactions are highly specific and, though they can be run on gram scale, excess quantities of zinc are required (up to 2 equivalents) to achieve good yields.

Electrochemical activation of metal surfaces has seen success in transition group metals such as copper and iron and is derived from the concept of electroplating where electricity is used to deposit small metal particles onto a surface. This method has been shown to eliminate the issues often found in commercial zinc powder products, namely the small but significant lead content(148) which has been proven to affect known zinc reactions such as the Simmons-Smith cyclopropanation.(149) However, as with mechanochemistry, the required equipment and knowledge of the basics can be a barrier to its implementation, although standardised reactors are available for purchase. Unlike mechanochemistry, reactors can be easily assembled from commonly found lab materials. This then makes results difficult to reproduce because of each individual reactor's idiosyncrasies and dynamics.

3.1.3 Electrodeposition of Metallic Zinc Particles

Electrochemical activation of zinc typically involves electroreduction of a zinc salt at between -0.8 and -1.4 V *vs.* a standard calomel electrode (depending on solvent) to produce active metallic Zn(0).(136) This reduction requires a counter-reaction; this is usually the oxidation of a sacrificial anode using an easily oxidised metal such as magnesium, aluminium, or zinc. The electrodeposited Zn^0 can react with an organohalide (RX) to form an organozinc halide (RZnX). When a sacrificial zinc anode is used, the oxidation creates Zn^{2+} which can then be reduced at the cathode to create further zinc deposits or, in the presence or organohalides and further electron addition, can form heteroleptic organozinc reagents. Furthermore, zinc anodes can become activated *via* electroscoring of the surface (Figure 3.4).
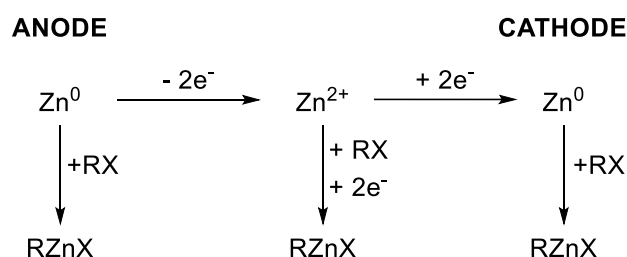
Figure 3.4. Possible reaction pathways of active zinc and organohalides to form organozinc halide complexes.

Tokuda *et al.* reported that electrogenerated zinc was not only purer than the commercially available zinc powder (which contained impurities such as lead), but also had a significantly smaller particle size and larger surface area (Table 3.1). Here, the reactive metal was prepared by electroreduction under nitrogen of a sacrificial zinc anode in a 0.1 M solution of Et_4NClO_4 in DMF using a platinum cathode at 25 mA constant current for 200 C. This method was adapted from work done by Perichon *et al.* on the use of electrogenerated zinc as a catalyst for the Blaise reaction.(48) The electrodeposited zinc was also shown to have better reactivity than

60

commercial zinc through isoprenylation of various carbonyls (85% *vs.* 38% using zinc powder),(150) which was thought to be due to the larger surface area.

Table 3.1. Characterisation of zinc metals by Tokuda *et al.* from Reference (148).

Zinc Metal	Particle Size[a] (μm)	Specific Surface Area[b] (m^2/g)
Electrodeposited Zn	< 0.1	23.8
E. Merck	5 - 15	1.9
Aldrich Chemical	50 - 150	0.4
Rare Metallic	100 - 400	0.5
Wako Pure Chemical	2 - 8	2.5
Nacalai Tesque	3 - 9	1.3
Kanto Chemical	3 - 10	0.8

a. Estimated by FE-SEM photographs. b. Measured by BET surface area analysis.

3.2   Objectives of Electrodeposition Research

In this section the reactivity of the electrochemically activated zinc will be tested on three case studies:

1) Blaise reaction to form β-ketoesters

2) Reformatsky reaction to form β -hydroxyesters

3) Formation of 2-azetidinones.

Case studies 1 and 2 were chosen as they have been reported using electrodeposited zinc.(48,63) However, both reactions have not been investigated in terms of surface morphology, the importance of each electrode, and the reproducibility of the zinc deposits.
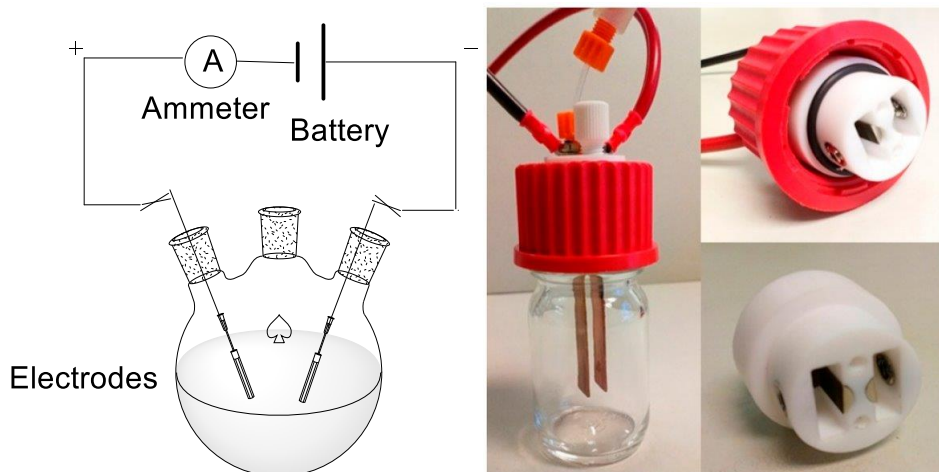
Figure 3.5. Left: Diagram of an electrochemical round bottom flask reactor. Right: Image of bottle reactor from reference (151) showing the assembled reactor, the full lid, and the PTFE electrode holders.

Initially, a standard 3-necked round bottom flask was used as the electrochemical reactor; the reactions were later run using a bottle reactor from the Willans group at the University of Leeds (Figure 3.5).(151) The above case studies were chosen as they were known to have success using traditional zinc metal techniques; both Blaise and Reformatsky reactions have been published using electrodeposited zinc. Furthermore, all reactions have documented issues with stereoselectivity and enantioselectivity which would be interesting to investigate to what extent this electrodeposited zinc would have an effect on these.

3.2.1 Reformatsky Reaction

The Reformatsky reaction was discovered in 1887 by Sergey Reformatsky and is the condensation of aldehydes or ketones with α-haloesters using zinc as a mediator to form β-hydroxyesters. The reaction proceeds *via* formation of a Reformatsky enolate, where after oxidative addition of the zinc into the carbon-halogen bond a dimer forms (Figure 3.6) which rearranges to give two zinc enolates.
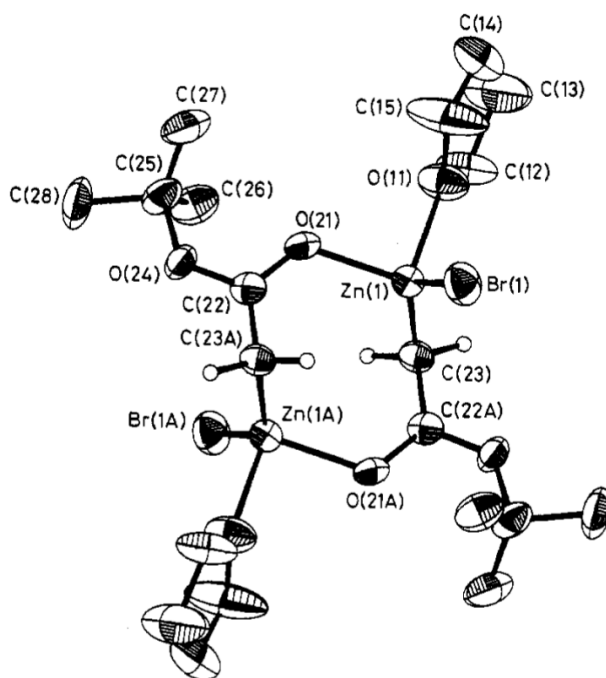
Figure 3.6 Image of the crystal structure of the Reformatsky dimer from reference (152).

The enolate co-ordinates to the carbonyl and forms a pseudo-six membered ring transition state which is then hydrolysed to give the hydroxyester product.

X = Br, I, Cl, F; R = allyl, alkyl, aryl
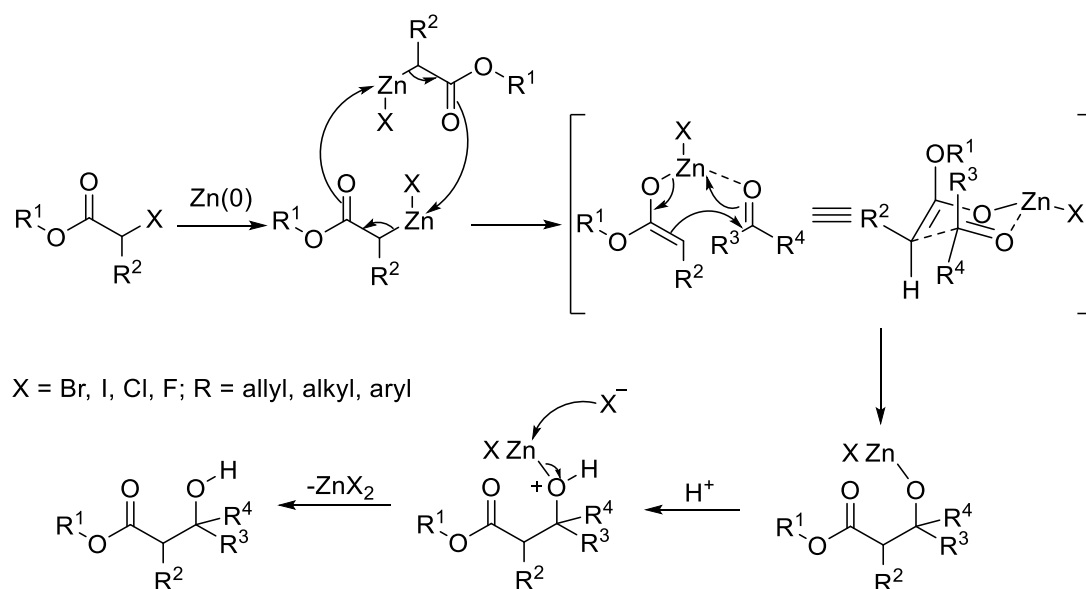
Scheme 3.1 The Reformatsky reaction mechanism.

Reformatsky enolates are relatively stable and slightly less reactive *e.g.* will not react with esters.(124) This allows it to be used to selectively target aldehydes and ketones without the need to protect the ester groups.

Reformatsky reactions using electrodeposited zinc has been reported by Rollin *et al.* in yields of up to 92%.(48) Despite its apparent efficacy, further work on electrodeposited zinc's use in Reformatsky reactions has had few publications outside of the Perichon group. This may be due to the sparse descriptions given of the electrochemical process in the papers which makes replication difficult.

3.2.2   Blaise Reaction

Similar to the Reformatsky reaction, the Blaise reaction also exploits the reactivity of metallic zinc towards α-haloesters but swaps the electrophile to a nitrile group. It was discovered in 1901 by Edmond Blaise,(153) and proceeds by insertion of the

zinc into the carbon-halogen bond, reaction with the nitrile to form an imine intermediate, which is then hydrolysed to form a β-ketoester (Scheme 3.2).
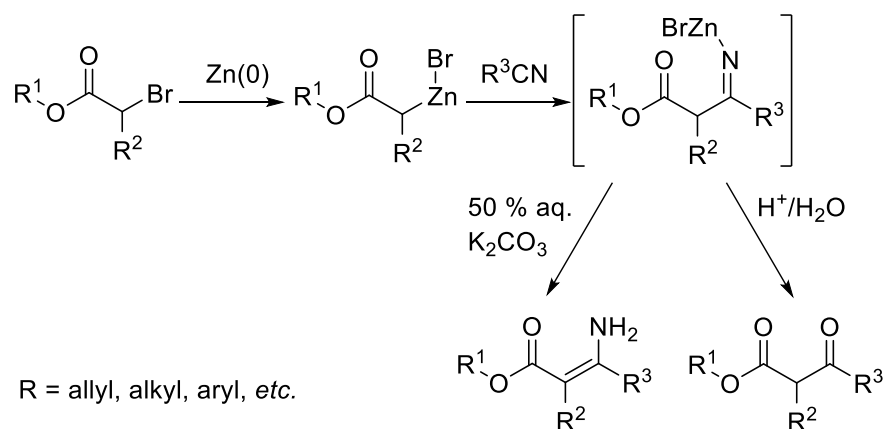
Scheme 3.2 Mechanism of the Blaise reaction with its two possible products and their work-up.

This reaction is tolerant of unprotected alcohol groups, allowing for carbon-carbon bond formation without lengthy protection and deprotection steps.(154) Functional group tolerance is a highly desirable trait for organometallic reactions, as it obviates the need for more extensive guided synthesis and can in turn greatly improve process efficiency. Furthermore, a simple change to the reaction work-up from acidic to basic (50% $K_2CO_{3(aq.)}$) allows access to the enamine intermediate.(48)

Similar to the Reformatsky reaction, the sub-stoichiometric electrochemical activation of zinc electrodes in the Blaise reaction has been reported by the Perichon group with moderate to good results up to 95%.(48) Since this was also published by the same group, there are similar issues with its replication by other researchers.

3.2.3 2-Azetidinone Ring Formation

2-azetidinone is, arguably, one of the most important in antibiotics as they are found in all β-lactam antibiotics. These are globally the drug of choice for bacterial diseases due to their efficacy and the sheer variety from the plethora of core

structures available (Figure 3.7).(155) Industrially, penicillin derivative drugs are produced *via* fed-batch fermentation of genetically engineered bacteria.(156) However, 2-azetidinone is not limited to antibacterial activity, and has been found to be of interest across medicinal chemistry for anti-cancer, analgesic, and anti-inflammatory properties.(157,158)
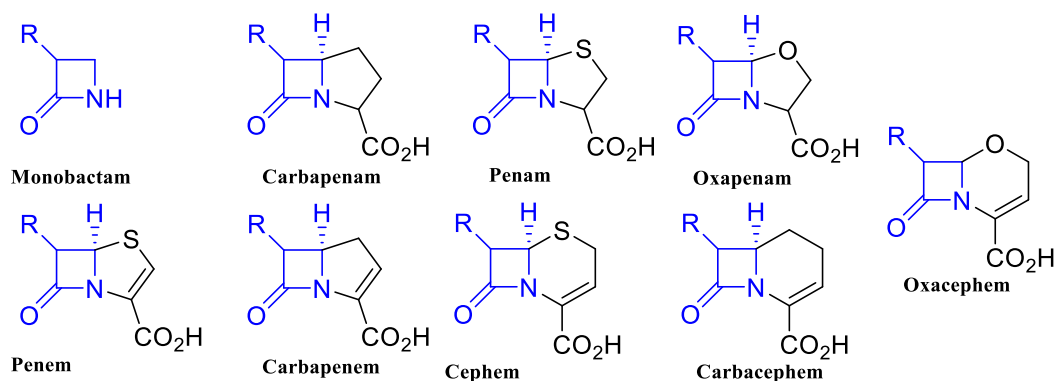
Figure 3.7. The core structures of β-lactam antibiotics and their nomenclature.

For smaller scale production, these structures can be made using a variety of techniques *e.g.* enolate-imine condensation, intramolecular cyclisation, ring-opening/closure, and named reactions. Substituted 2-azetidinone formation has issues with *cis-trans* diastereoselectivity at the C-3 and C-4 position as the *trans*-lactam is usually the more sterically stable isomer, leading to isomerisation of the *cis*-lactam.(159)

66

Intramolecular Cyclisation
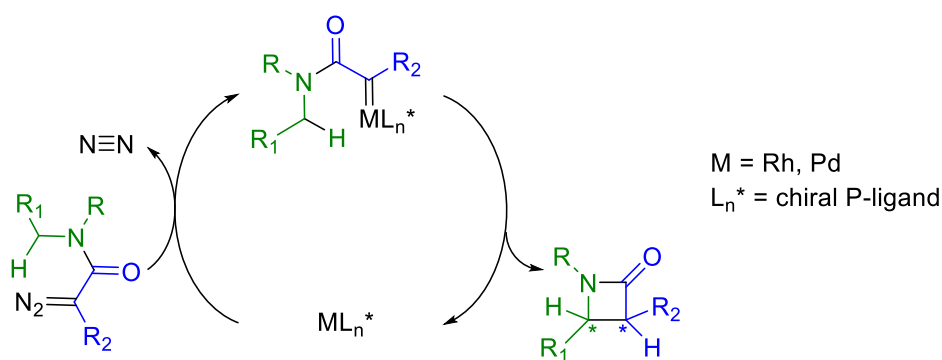
Scheme 3.3 Mechanism of forming substituted 2-azetidinones *via* Intramolecular cyclisation.

Intramolecular cyclisation techniques (Scheme 3.3) proceed *via* metal co-ordination from an azo compound which facilitates C-H insertion to form the azetidinone. First reported in 1965,(160) it was developed into an enantioselective system using a dirhodium(II) catalyst with chiral ligands with up to 80% e.e. but this promoted the formation of the pyrrolidinone (91%) over the azetidinone product (9%).(161) Further research brought the yield of the 4-membered ring up to 81% yield and 93% e.e. using different chiral ligands and a ring system locking the N1 and C4 position which is not always possible in synthesis.(162) Despite these successes, it is apparent from the literature that this system has a variety of issues: catalyst pairing, substrate design, and catalyst synthesis. Chiral catalysts such as oxazolidinone or pyrridones to form the desired dirhodium catalyst can be complex and time-consuming to prepare. Specific catalyst and substrate design can lead to discounting intramolecular cyclisation due to time and financial constraints.

Staudinger Cyclisation
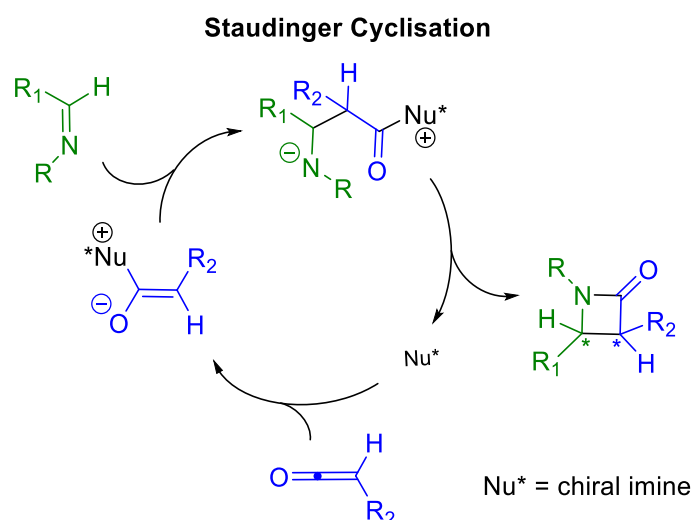
Scheme 3.4 Staudinger cyclisation mechanism to form a substituted 2-azetidinone ring.

The Staudinger reaction (Scheme 3.4) was published in 1907,(163) and is a [2+2] cycloaddition between an imine and ketene followed by a conrotatory cyclisation. In recent years, success has been found in using an electron-deficient imine and a ketene-enolate rather than a ketene in an example of Umpolung chemistry. This method used a benzoquinone photocatalyst catalyst (10 mol%) and gave impressive e.e. of 95-99% but average yields of 36-65%.(164) Further applications using Wang resin peptide mesh(165) and flow photochemistry(166) display the applicability of this reaction to a wide variety of chemistry techniques. As with intramolecular cyclisation, the ketene and ketene-enolate starting materials required for this synthesis can be capricious to form due to their inherent reactivity, and the complex chiral catalysts required are also time and cost-consuming to prepare.

Enolate-Imine Coupling
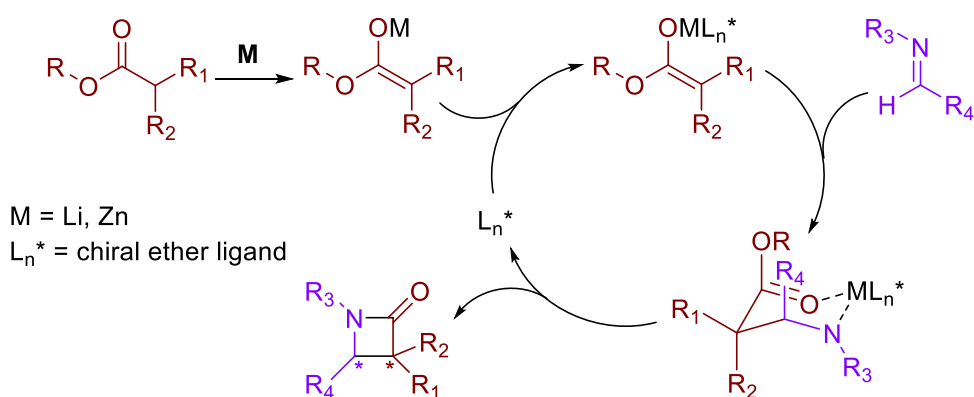
Scheme 3.5 Enolate-Imine Coupling mechanism to form a substituted 2-azetidinone ring.

Enolate-Imine coupling (Scheme 3.5) is similar to the Umpolung Staudinger reaction as it also couples an imine and an enolate; however, this is done *via* metal catalysis with chiral ligands. The original methodology proceeded *via* formation of a Reformatsky enolate using zinc and iodine known as a Gilman-Speeter reaction,(167) but many variations have now been reported: silyl ether instead of metal,(168) rhodium catalysis,(169) and high intensity ultrasound.(170) Enolate-imine couplings require relatively more commonplace starting materials than some of the other processes, as enolates are relatively easy to produce. The primary issue with this process is the formation of a non-cyclised aminoester by-product; according to a review by Brandi *et al.*, this is an issue that has been frequently reported in enolate-imine coupling reactions.(159)

Kinugasa Reaction
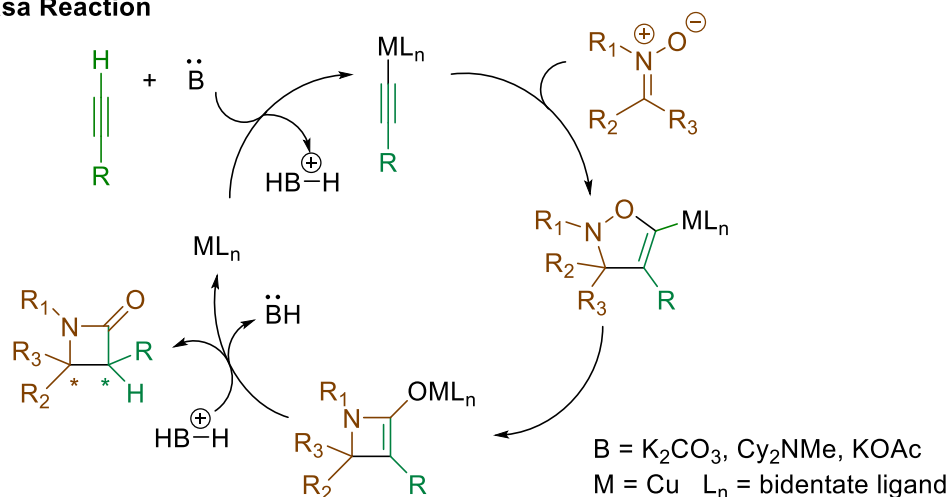
Scheme 3.6 Kinugasa Reaction mechanism to form a substituted 2-azetidinone.

The eponymous Kinugasa reaction (Scheme 3.6) was first published in 1972,(171) and has since seen applications in the enantioselective synthesis of natural products such as (+)-lupinine,(172) hydroxycotinine,(173) and (+)-porantheridine.(174) The protocol boasts a high atom economy, and accessible and stable starting materials.(175) It couples a metal alkyne with a nitrone to form a 5-membered isooxazoline intermediate which rearranges into an azetidine, and a base is added to form the azetidinone. Unfortunately, using an alkyne presents issues with diastereoselectivity in addition to the enantiomeric selectivity. Therefore, although it's not necessary to use chiral ligands for good conversion, they are required when a specific enantiomer is required or chiral resolution is too difficult.

Ring Expansion
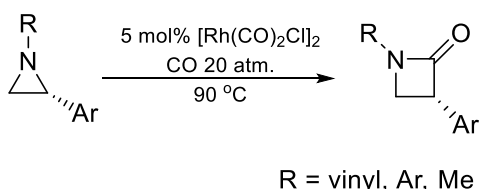
Scheme 3.7 An example of ring expansion of an azirane to form a substituted 2-azetidinone.

Ring expansion methods using carbon monoxide (Scheme 3.7) is an attractive synthetic route because it gives regiospecific and enantiospecific control of the reaction without requiring a complex chiral catalyst (though an enantiopure starting material is required) in good to high yields of above 81%.(176) Furthermore, kinetic resolution studies found that using stoichiometric quantities of chiral additive *l*-menthol (3 eq.) the optical yield could be optimised to 96% and above.(177) Despite its impressive yield and resolution capabilities, this reaction is less practical than other methods listed. The chiral aziridine starting material is "not straightforward" to make and it is more preferable to go *via* the more easily accessible epoxides. Thus, enantiomeric purity is achieved earlier in the synthesis.

Ring Contraction

$R_1 = C{\equiv}C{-}CH_3$ $R_2 = CO_2Et$
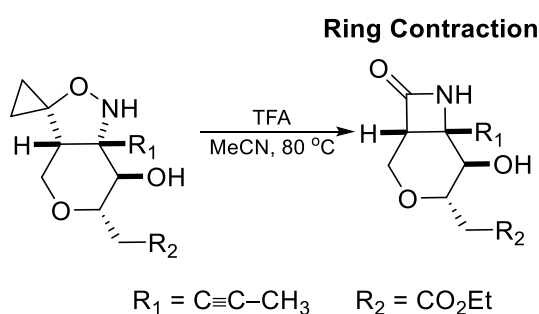
Scheme 3.8 An example of ring contraction to form a substituted 2-azetidinone ring.

Ring closure (Scheme 3.8) of a ≥5-membered ring is an interesting approach that has been applied in the total synthesis of (+)-Gelsemoxonine.(178) Closing a larger heterocycle had previously seen success in forming azetidines from oxazinones,(159) and was then adapted for the natural product formation. This begins with a step similar to that seen in the Kinugasa reaction where the 5-membered heterocycle collapses into a 4-membered ring. While this is an interesting reaction technique, it is not always feasible to plan a synthesis around creating then contracting this ring system.

Of the presented routes of substituted azetidinones which are mediated by zinc, the three most commonly used zinc sources are diorganozinc reagents and zinc powder suspensions. Using diorganozinc reagents can cause issues with reproducibility, while also adding issues with safety and stability as diorganozincs are inherently pyrophoric and air/water unstable. Use of zinc powder in THF at reflux can also discount more volatile compounds as the boiling point of THF is 66 $^{\circ}$C. In this work, the main focus is on electrochemically activated zinc to avoid issues with pyrophoric and unstable compounds.

3.3   Surface Characterisation of Zinc Electrodes

In heterogeneous catalysis, knowledge of surface morphology is vital as it gives an insight into the nature of the active metal and is typically achieved using electron microscopy for imaging, BET for surface area, EDX for elemental analysis, and XPS to identify the chemical state of the elements. Electrogenerated zinc for catalysis has previously been analysed using BET and SEM to analyse particle size and surface area (see section 3.1.3).

For electrodeposition and electroscoring reactions, it is important to ensure that the surface morphology is similar when changing reaction types as this has the potential to affect reactivity. Therefore, when work using the Bottle reactor began the electrode surfaces were also characterised in the same way as the round bottom flask reactor in order to ensure that there were no significant differences in morphology between methods. This was determined using SEM and EDX technology and is summarised in the table below.

Table 3.2. Comparison of electrode surface between the reactor types used.

	RBF	Bottle Reactor
ANODE		
Pre-Blaise	A	B
Post-Blaise	C	D
CATHODE		
Pre-Blaise	E	F
Post-Blaise	G	H
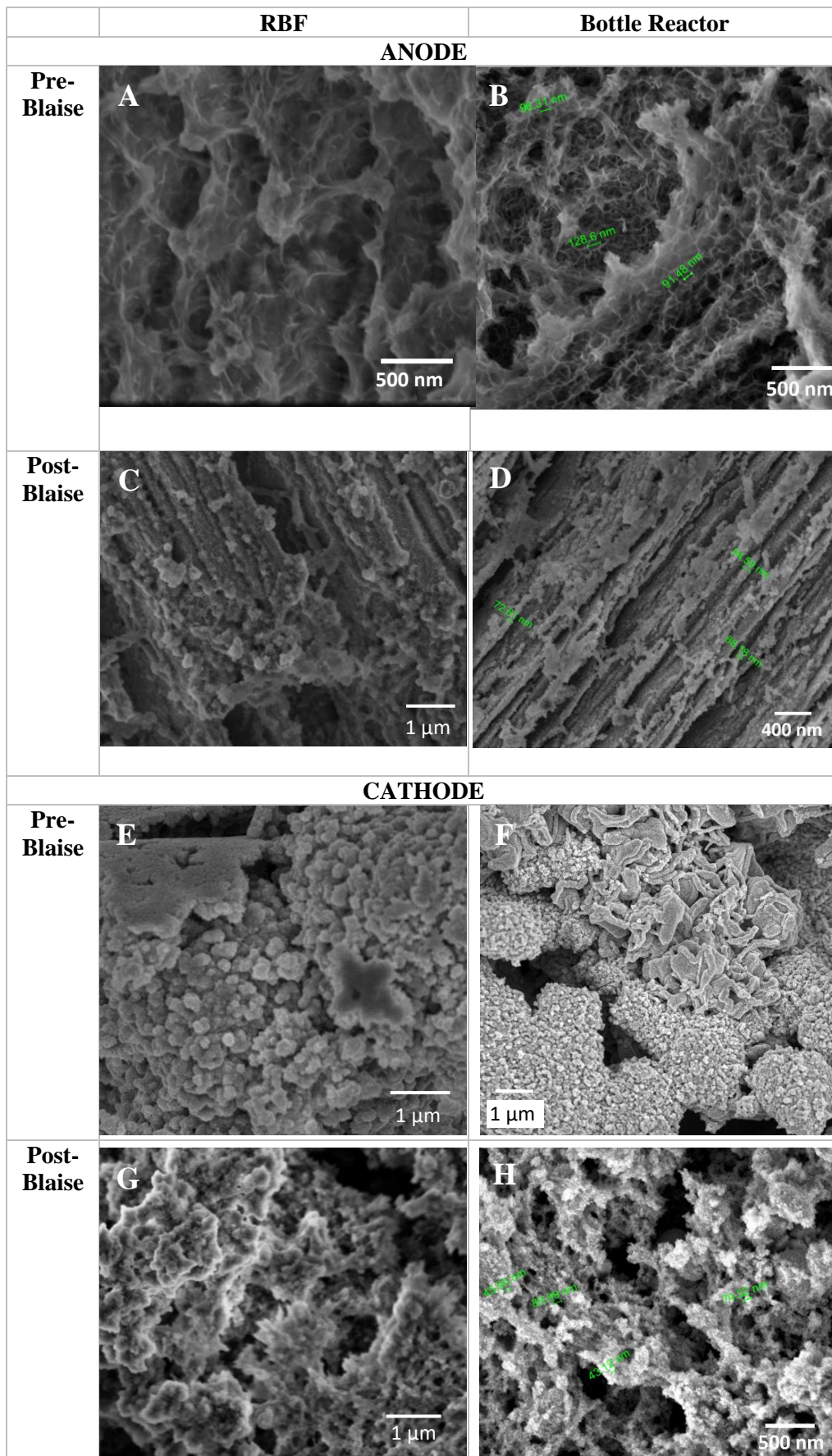
All images taken of the zinc surface electrodes using SEM analysis can be found in section 4.2.2 and 4.2.3 in the Appendix.

The pre Blaise reaction anode for both reactor types (**A** + **B**) shows very fine structures. The surface looks like a solid foam or that bubbles have been removed from surface; these craters are approximately 100-150 nm in size; this is likely due to electrodissolution of the zinc into the bulk solution. The post Blaise anode in both RBF and bottle reactors (**C** + **D**) shows large cracks visible on the surface; upon magnification we see under those cracked plates are dendrous looking structures, or possibly stacked metal plates. This is visibly different than **A** + **B** where no chasms were observed, which is thought to be due to further reaction of the anode surface with the substrates.

The pre Blaise cathode (**E** + **F**) showed obvious metal deposits on the surface, which is almost certainly due to electrodeposition of zinc metal from the bulk solution. There are large chasms/holes on the surface as the deposits appear to cluster together into macrostructures of <100 nm particles. The macrostructures are similar in size to the craters seen in the anode (100-150 nm). It is uncertain why the nanodeposits cluster together, however, as with crystallisation, there may be a seeding effect which causes clusters to form. Measurements of all of the fine structures found them to be nanoscale. The post Blaise cathode (**G** + **H**) shows big cracks and chasms for both reactors. Almost crystalline deposits were found with increasing frequency at the edges; these were found to also be zinc. There are no bubble type macrostructures seen as in the pre Blaise cathode. There are chasms, but they are very different to previous electrodes and a particle size of ≤50 nm. These chasms are thought to be where the electrodeposited zinc had reacted, exposing the active zinc metal of the electrode below. Reaction of this zinc with the bromoester substrate

could cause the metal to be removed in a way which would result in the observed topography.

The images in Table 3.2 clearly show that the electrode surface morphology between reactors is very similar, therefore the bottle reactor should demonstrate similar reactivity to the round bottom reactor. Furthermore, EDX showed no significant element presence other than zinc and carbon which is consistent with our previous results.

Once the surface morphology of the zinc had been characterised its application in synthesis was investigated.

3.4   Electrochemical Reactions in Round Bottom Flasks

The batch reactor used was similar to that described in Chapter 2, The electrodeposition was achieved by passing 202 C of electricity at 50 mA constant current through a solution of MeCN with zinc bromide, TBATBF, and submerged zinc electrodes under an inert atmosphere. The amount of electricity used would electrolyse 50% of the zinc bromide in solution as it was reported by Zylber *et al.* that this gave the highest yield.(48) The applied current in the literature was 100 mA, but there were concerns that the electrodeposition would form a bridge between the two electrodes and cause a short-circuit as larger currents have a tendency to produce larger deposited particles.

3.4.1   β-Ketoester formation - The Blaise Reaction

According to the literature, this method of electrodeposition and utilisation of metallic zinc applied to the Blaise reaction gave yields up to 95%. Here, a variety of substrates were used in an attempt to reproduce the literature data for the Blaise reaction (Table 3.3).
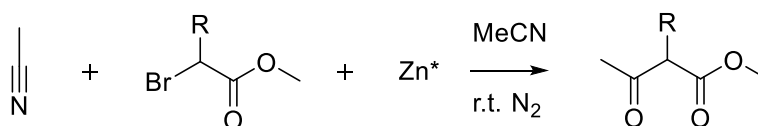
Table 3.3. Results of the Electrochemical Blaise reaction using different bromoesters.[a]

Entry	R	Product	Yield (%)[b]
1	Me	**2a**	70
2[c]	Me	**2a**	59
3[d]	Me	**2a**	58
4	Ph	**2b:** 37% **2c:** 25%	59 (86)[e,f]

Electrodeposition: MeCN (40 mL), ZnBr$_2$ (2 mmol), TBATBF (0.1 M), 50 mA constant current, 202 C. *a.* β-bromoester (10 mmol), MeCN (40 mL) stirred at r.t. for 18 h. *b.* %yield calculated using calibrated HPLC integration *vs.* an internal standard. *c.* One-pot reaction where ester was present during electroformation of Zn(0) *d.* ZnBr$_2$ was dried by vacuum and N$_2$ backfill (x3). *e.* %yield calculated using ^{1}H NMR against a dodecane internal standard. *f.* Total yield including amine by-product.

Entry 1 is a mimic of the published step-wise protocol and gave 70% which is within the bounds of reported yields (70-90%). A one-pot reaction was also run in an attempt to make the reaction more streamlined (entry 2); unfortunately, this gave a lower yield of 58%. To establish the sensitivity of the reaction to air and moisture, the thorough drying of zinc bromide was replaced with a vacuum-refill in triplicate;

this also reduced the yield to 59% (entry 3). It became clear that our initial method was the highest yielding and therefore was used for the substrate screening reactions. Due to the equipment limitations, analytical method was changed to analysis using NMR spectroscopy.

Entry 4 using methyl α-bromophenylacetate gave an excellent yield of 86%, which is comparable to those reported (95%). Interestingly, keto-enol tautomerism was observed with the phenylester, which was not reported by Zylber, but it is a well-known occurrence.(179,180) It was likely not identified in previous reactions as standard HPLC columns do not separate tautomers, however upon NMR analysis the enol ester product was found to be present in low yields ($< 5\%$) for **2a**. Furthermore, a third substance other than the ketoester tautomers was identified; this was found to be an amine version of the imine Blaise intermediate. The amine by-product was found in a low yield of 27%, in between the yields of the ketoester and enol ester (Section 3.6). However, this was not identified for product **2a**. Analysis and identification of this amine, which was identified as the unhydrolyzed Blaise reaction intermediate is described in section 3.6. As the reactions described in Table 3.3 were run visible changes to the electrodes were noted at each reaction stage.
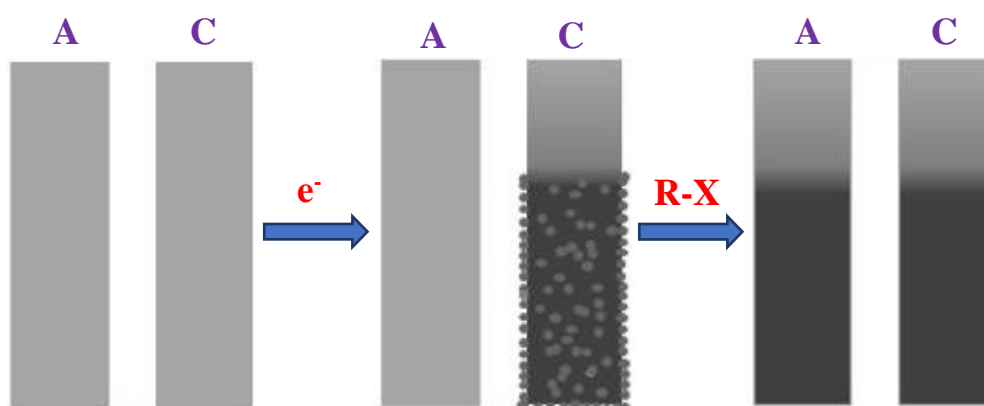
Figure 3.8. Diagram of visual changes in the electrodes as the reaction proceeds. A = anode, C = cathode. Left – before use, middle – after electrodeposition, right – after Blaise reaction.

The above diagram illustrates the difference seen in the zinc electrode surface before use, after electrodeposition, and after the Blaise reaction was run (Figure 3.8):

- initially, both electrodes are identical (reflective and sandpapered)

- during the electrochemical process the zinc cathode blackens within the first 5 minutes, then zinc clusters form on the face of the electrode and along the edges under the solvent line

- after addition of the bromoester the electrodeposited zinc quickly "dissolves" leaving a black cathode. The anode then also slowly turns black.

In particular, the anode appeared to shrink in size, indicating that not only was the zinc bromide salt involved in electrodeposition but also the zinc anode. Between the two electrodes an average of 1 g in weight was lost between starting the reaction and after the Blaise reaction was run. Furthermore, post-electrodeposition the anode was silver but after addition of the bromoester it slowly turned black to match the cathode. It was therefore important to clarify the role of each zinc electrode: are both surfaces electroactivated and if so to what extent is the active zinc involved in the Blaise reaction?
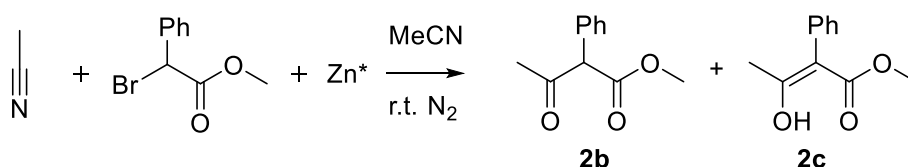
Table 3.4. Electrode removal reactions.[a]

Entry	Total Charge/ C	Electrode Removal	2b (%)[b]	2c (%)[b]	Amine (%)[b]
1	202	Anode	15	12	27
2	202	Cathode	16	13	27
3	202	None	37	25	27

Electrodeposition: MeCN (40 mL), ZnBr$_2$ (2 mmol), TBATBF (0.1 M), 50 mA constant current, 202 C. *a.* Stepwise reaction. β-bromoester (10 mmol), MeCN (40 mL) stirred at r.t. for 18 h. *b.* %yield calculated using ^{1}H NMR against a dodecane internal standard added post-quench.

This involved removing 1 electrode post-electrodeposition before addition of starting material; images of electrodes from these reactions can be seen in Figure 3.9. It had previously been noted that both anode and cathode change visually as the reaction progresses. Interestingly, both anode and cathode behaved similarly in terms of yield, which was considerably less than when both electrodes are present. The main difference was in the yield of the amine intermediate (see section 3.6) which was higher than previously seen in this reaction. For both reactions described in the above table, the remaining electrode was considerably more eaten away than in previous reactions, this suggests the reaction compensates for the lack of secondary electrode and the remainder acts somewhat sacrificially.
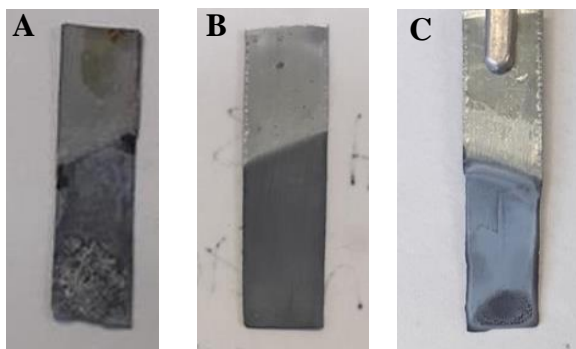
Figure 3.9. A - Image of cathode post anode removal reaction (Table 3.4, entry 1). B - Image of anode post anode removal (Table 3.4, entry 1). C - Image of anode post cathode removal (Table 3.4, entry 2).

It was deduced from this work that both electrodes are significant in the reaction; therefore, we concluded that both electrodes are activated during this process. It is thought that the electrodeposited zinc reacts first as it quickly disappears upon

addition of the starting material, however, it is unclear if both activated anode and cathode react to the same degree. All reactions were continued using the two-electrode system.

3.4.2 β-Hydroxyester Formation – The Reformatsky Reaction

After investigating the Blaise reaction we then decided to explore other electrophiles to broaden the substrate scope. It was decided that benzaldehyde would be an appropriate alternative, and this could be achieved by removing the MeCN solution from the reaction and adding a THF solution of the α-bromoester and benzaldehyde. Electrochemically activated zinc(0) was successful in coupling benzaldehyde with the bromoester to give the hydroxyester **3a** in excellent yields up to 99%.
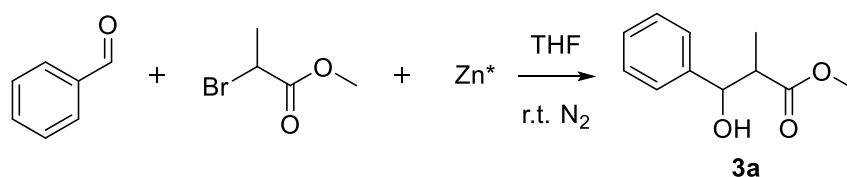
Table 3.5. Results of Electrochemical Reformatsky reaction with benzaldehyde.

Entry	Electrophile	Product	Yield (*syn:anti*) (%)[b]
1[a]			77 (61 : 39)[c]
2[b]			>99 (70 : 30)[d]
2[b]			63 (37:26)[d,e]
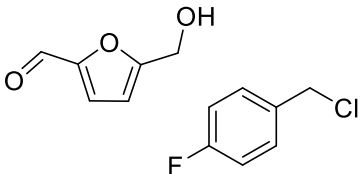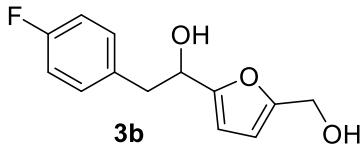
Electrodeposition: MeCN (40 mL), $ZnBr_2$ (2 mmol), 50 mA constant current, 202 C. $ZnBr_2$ dried for 3 h under vacuum at 180 °C prior to use. a. β-bromoester (10 mmol), benzaldehyde (10 mmol), THF (40 mL) stirred at r.t. for 48 h. b. β-bromoester (10 mmol), benzaldehyde (20 mmol), THF (40 mL) stirred at r.t. for 48 h. c. %yield calculated using ^{1}H NMR against
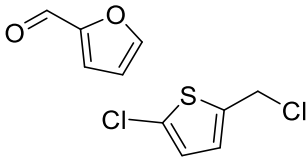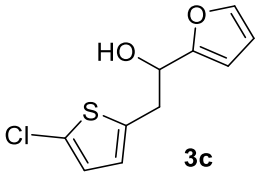
a dodecane internal standard. d. ^{1}H NMR ratio of *syn:anti*, determined by *J* (Hz) values. e. 3.6 mol% D,L-DBNE added.

Interestingly, the *syn* isomer appears to form predominantly over the *anti*; different benzaldehyde:α-bromoester ratios does not appear to influence this. Comparing Entry 1 which used a 1:1 ratio to Entry 2 which used a 2:1 ratio of benzaldehyde to bromoester the *syn:anti* ratio minimally changes from 61:39 to 70:30.

N,N-dibutylamino-D,L-norephedrine (D,L-DBNE), was used to investigate the extent to which a chiral auxiliary would affect the stereochemical ratio of **3a**. This was used in an attempt to control the stereoselectivity of the reaction as DBNE is a known chiral catalyst in zinc chemistry. Though it reduced the yield significantly from 99% to 63%, it did change the *syn:anti* ratio from 70:30 to a more equal 59:41. Considering the structure of DBNE it is possible that there was some zinc complexation with the catalyst which would in turn lower the yield. As the catalyst was racemic it was expected to give an enantiomeric ratio of 50:50; though it was successful in reducing the *syn:anti* disparity the *syn* diastereomer was still prevalent.

Once it was established that this system worked well with bromoesters and benzaldehyde, other carbon-halogen bond containing molecules were used as substrates to investigate this reaction's functional group tolerance.

Table 3.6. Zinc-mediated reactions using heterocyclic substrates.[a]

Entry	Substrates	Product	Yield (%)[b]
1		**3b**	0

| 2 | | 3c | 0 |

Electrodeposition: MeCN (40 mL), $ZnBr_2$ (2 mmol), 50 mA constant current, TBATBF (0.1 M), 202 C. $ZnBr_2$ dried for 3 h under vacuum at 180 °C prior to use. a. organohalide (10 mmol), carbonyl (10 mmol), MeCN (40 mL) stirred at r.t. for 48 h. b. %yield calculated using ^{1}H NMR against a dodecane internal standard.

Unfortunately, neither substrate pairing gave the intended product; both reactions showed only starting material upon work-up. This could be due to the carbon-halogen bonds not sufficiently polarised to allow for zinc insertion; the heteroatom of the ring structure and its carbonyl may co-ordinate with the active zinc constrained the reaction's progress; or the resonance of the ring resulting in a less electrophilic carbonyl (Scheme 3.9).
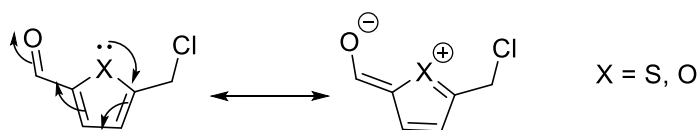
Scheme 3.9 Resonance structure of furan and thiophene aldehydes.

Therefore, as the Reformatsky reaction has been well-researched and we were not able to successfully apply this method to more complex structures, the focus was shifted back to the Blaise reaction. The focus changed to the reproducibility of the results and solvent screening.

3.4.3   Screening for Alternative Solvents

Traditionally, reactions utilising Zn(0) have been run in polar aprotic solvents such as THF or MeCN and the Blaise reaction is no exception.(48,125,181) Both THF and MeCN are widely used as solvents in electrochemistry; the protocol described by Zylber *et al.* utilises the electrolyte tetrabutylammonium tetrafluoroborate

82

(TBATBF) in both dichloromethane (DCM) and MeCN.(48) DCM was not utilised in this research as it is classified as having "major issues" and is to be avoided unless absolutely necessary.(182) It would be highly beneficial if a second solvent with equal suitability for both the electrochemical and Zn(0) reaction was found; ideally this would also comply with industrial solvent requirements. Principle component analysis of solvent properties using data from Murray *et al.*(183) was run by B. Nguyen to make a 3-D solvent map to identify similar solvents to MeCN using DCM as an outer boundary, as this has also been used successfully for the Blaise reaction. The following solvents were chosen: ethyl formate, methyl formate, nitromethane, DMF, methyl acetate, THF, dioxane, and dimethyl carbonate (DMC).

The Nguyen group has previously found TBATBF to be incompatible with THF which is largely due to the large specific resistance of this electrolyte in THF: the specific resistance of a 0.5 M solution of TBATBF in THF is 587 Ω.cm, whereas in MeCN it is 33 Ω.cm.(184) Reported electrochemical reactions in these solvents and their dielectric constants were researched and potential solvents were identified (See Section 3.11.5). DMF has been previously reported as a solvent in electrochemistry as it is a good organic solvent, however it has been reported to have problems with hydrolysis susceptibility and anodic oxidation.(185) Nitromethane has been found to be useful in anodic reactions, with limited capabilities for cathodic reactions which is dependent on the water content of the solvent. Use of dimethyl carbonate has been reported in electrochemistry as a substrate and product;(186) it is likely that, due to its low dielectric constant ($\varepsilon = 3.12$), it has not been successfully used as a solvent. Ethyl formate, dioxane, and methyl acetate all have low dielectric constants ($\varepsilon = 7.10$, 2.20, and 6.80 respectively)(187) and were therefore not considered further. Though methyl formate has a high dielectric constant ($\varepsilon = 39.1$) it has a boiling point

of 34-36 °C and would therefore be unsuitable for a room temperature reaction due to evaporation. Ideal solvents would have a reasonably high boiling point (60 °C $\leq x \leq$ 80 °C), a good dielectric constant ($\varepsilon > 5$), and good solubility and conductivity of a range of electrolytes.

DMC and DMF were used as reaction solvents in the electrochemical and Blaise reaction, where the protocol was identical to previous reactions. The DMC reaction appeared to not form any deposited Zn(0), which was confirmed when the Blaise reaction was analysed to show only starting material. In the DMF electrochemical reaction the solvent turned grey with black deposits which were hypothesised to be small flakes of Zn(0); methyl 2-bromopropionate was added, then after overnight stirring benzaldehyde was also added. The benzaldehyde was used to ascertain whether any active zinc or starting material remained as the Reformatsky product would be seen after work-up. Interestingly, none of the ketoester product was detected by NMR, but high resolution mass spectrometry showed evidence of DMF reacting with the bromoester to form a hydrolysis prone product (Scheme 3.10). The molecular weight of the diamine product and its chemical formula matches that which was identified by the mass spectrometer (Figure 3.10). Unfortunately, due to the inherent instability of this product a yield was not possible to calculate using NMR as with previous experiments.

Chemical Formula: $C_7H_{13}NO_2$
Molecular Weight: 143.19
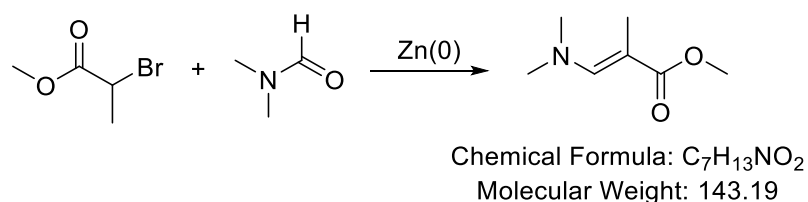
Scheme 3.10 Formation of highly unstable DMF product using zinc.
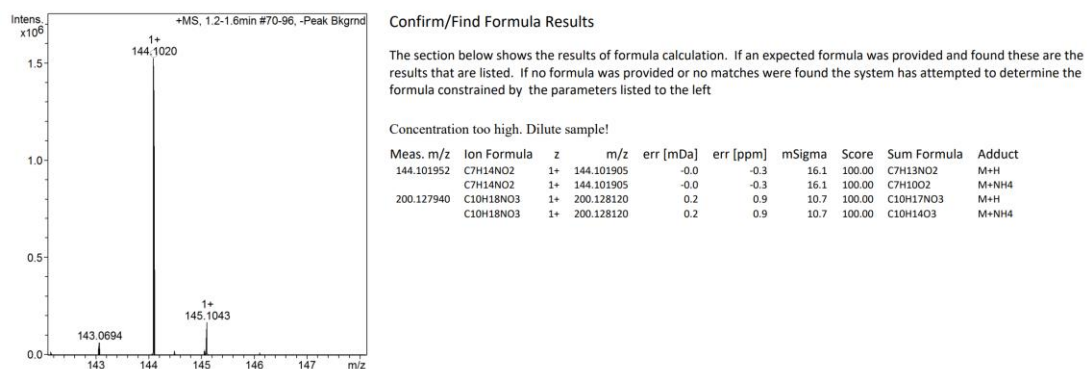
Figure 3.10 Image of High Resolution Mass Spectrometry analysis, M+1 peaks molecular weight aligns with product shown in Scheme 3.10.

The success of MeCN over DMC and DMF is likely due to the stabilisation of the electrodeposited zinc by the nitrile group hypothesised by Zylber *et al.* which was not replicated with the other two solvents.(48) As there were no suitable alternatives to MeCN found, it was used as the solvent for all subsequent reactions.

3.4.4 Reproducibility of the Reactor

As previously mentioned *vide supra*, one of the primary issues with using zinc in synthesis is the unreliable reproducibility. It was therefore important that this was explored in our own reactor system in order to show it is a viable alternative to commercially available methods. For this, timed reactions using the phenyl bromoester were run in triplicate which were halted at 15, 30, and 60 minutes by quenching with saturated NH$_4$Cl solution. This ester was used because it gave us the highest yield (Table 3.3). ^{1}H NMR was used to analyse the ratio of starting material to products, the results of which can be seen in Table 3.7, and all reactions were run using the protocol described in Section 3.10.
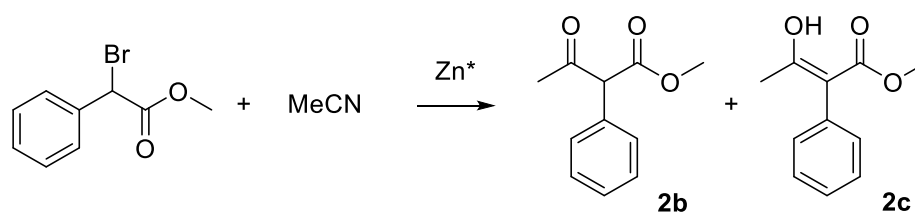
Table 3.7. Results of the reproducibility experiments of methyl-bromophenylacetate and acetonitrile.[a]

Stop time (Min)	SM (%)	2b (%)	2c (%)	Mass Bal. (%)
15	67	49	15	131
15	14	28	5	47
15	17	47	5	69
15[b]	41	5	1	47
30	10	34	14	58
30	35	25	16	76
30[c]	35	6	1	42
30[b]	31	8	2	41
60	16	41	19	76
60	8	26	11	45
60[c]	46	17	3	66

a. ZnBr$_2$ (2 mmol), methyl bromophenylacetate (10 mmol), MeCN (40 mL), TBATBF (0.1 M), 50 mA constant current, 202 C with two zinc electrodes. %yield calculated using HPLC calibrated integration against an internal standard. *b*. Reaction run using high purity zinc (99.9%) electrodes. *c*. Sample was run 24 h after work-up was completed.

The results seen above do not show satisfactory reproducibility. Each column of the table varies significantly with each experiment; the samples which were run 24 h after work-up show that either the quench used is not effective enough or there is a secondary reaction/equilibrium that we are unaware of. To investigate the possibility

of impurity in the electrodes was causing this loss in mass balance high purity zinc (99.9% purity) was used as an electrode material. As they showed no distinct difference to the lower purity electrodes (99%), there was no reason to suspect the electrode purity was influencing product yield. It is highly likely that the variation in results is due to the inconsistency in interelectrode distance from reaction to reaction. Furthermore, the mass balance suggests that there is either degradation of starting material/product or there is a third product that we have not identified. To shed light on this issue, the reaction itself was studied using a variety of techniques.

3.4.5 Attempted Cross-Coupling Reaction

Work by Duncan Browne used ball milling to activate zinc as a catalyst for Negishi style couplings;(137) we attempted to use the electrodeposited zinc in a similar fashion. It was hypothesised that once the imine was formed it could be used in palladium catalysed reactions to form an arylimine (Scheme 3.11).
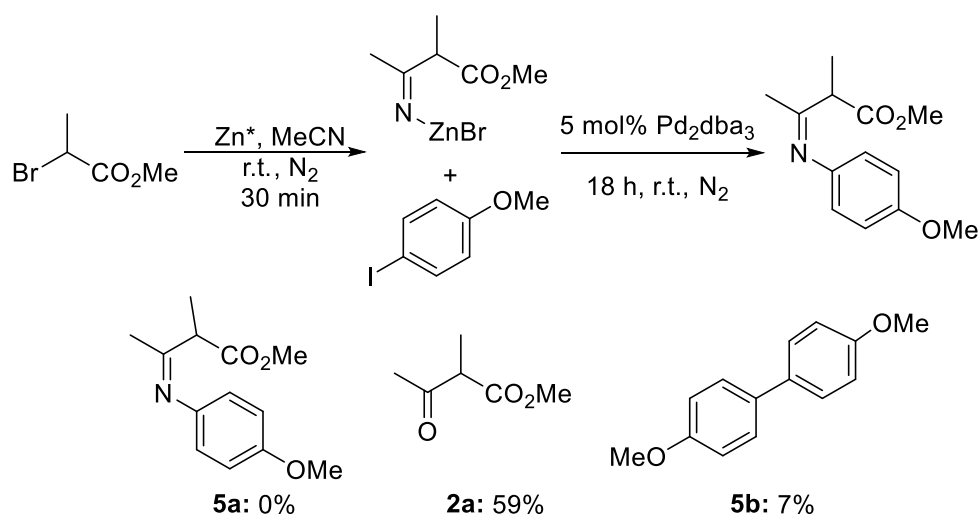
Scheme 3.11 Attempted Negishi-style coupling using palladium and iodoanisole. % yields shown calculated by ^{1}H NMR.

Unfortunately, this reaction did not yield the desired imine **5a**. Instead, the Blaise product **2a** was formed in a moderate yield (59%) which is comparable to previous

reactions, and interestingly the biaryl coupling product **5b** was formed albeit in a low yield (7%). This is likely due to the palladium catalyst facilitating homocoupling. As the desired imine was not formed no further work was done on Negishi couplings

Once it was established that this reaction worked well with the bromoesters, focus was placed on solvent selection to investigate whether alternatives to MeCN could be used to avoid any competition with other electrophiles in the reaction.

3.5   Reaction Monitoring of Blaise Process

During a placement at the AstraZeneca site in Macclesfield the Blaise reaction was studied using the specialised *in situ* reaction monitoring equipment. The reaction set up used was an EasyMax system which allowed for remote monitoring of any temperature changes, additional monitoring such as a conductivity probe and Raman probe, and improved stirring using an overhead stirrer. Once the reaction was replicated using this set-up and the yield was found to be adequate work began on analysing the reaction and its progression.
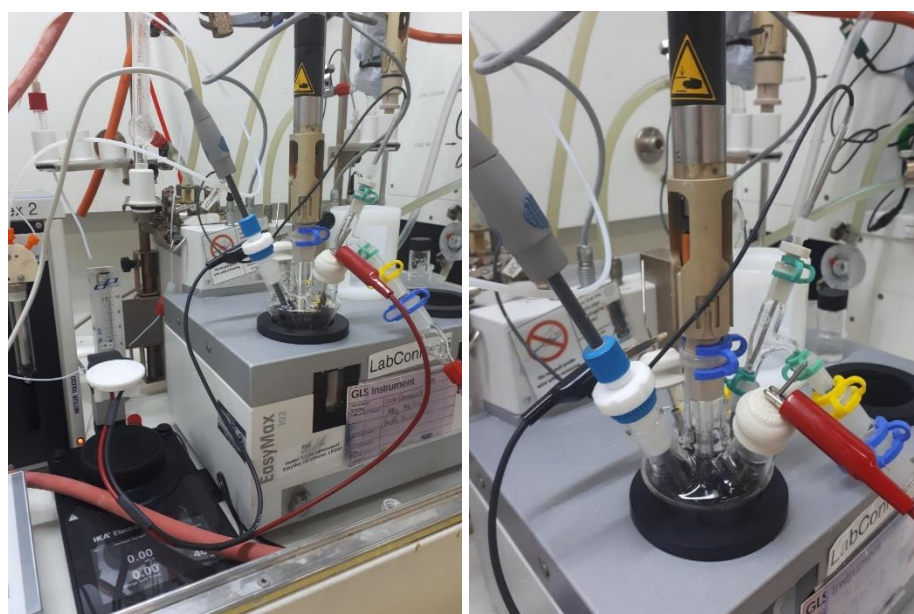
Figure 3.11. Image of the EasyMax reactor set-up (left), a close-up of the additions (right).

A kinetic monitoring reaction was run to deduce whether the reaction had an induction period and to observe the behaviour of the starting material and product over time using HPLC. The methyl phenylbromoacetate substrate was used as it is inherently UV active and gave good yields in the initial substrate scope. Initially, an EasySampler attachment arm was trialled for sampling. However, issues arose once it was realised that zinc electrodeposited onto Hastelloy, the main component of the sampling arm, and when used post electrochemical deposition the arm blocked almost immediately and could not be used despite attempts to add a filter. Therefore, manual sampling was required.

Ultra-Pressure Liquid Chromatography was used to monitor the reaction; a 50 µL aliquot was taken from the reaction mixture, quenched in 50 µL sat. $NH_4Cl_{(aq.)}$ and made up to 1.1 mL with MeCN. The results of this can be seen in Figure 3.12. The starting material and product peaks were identified and referenced against a biphenyl internal standard peak.
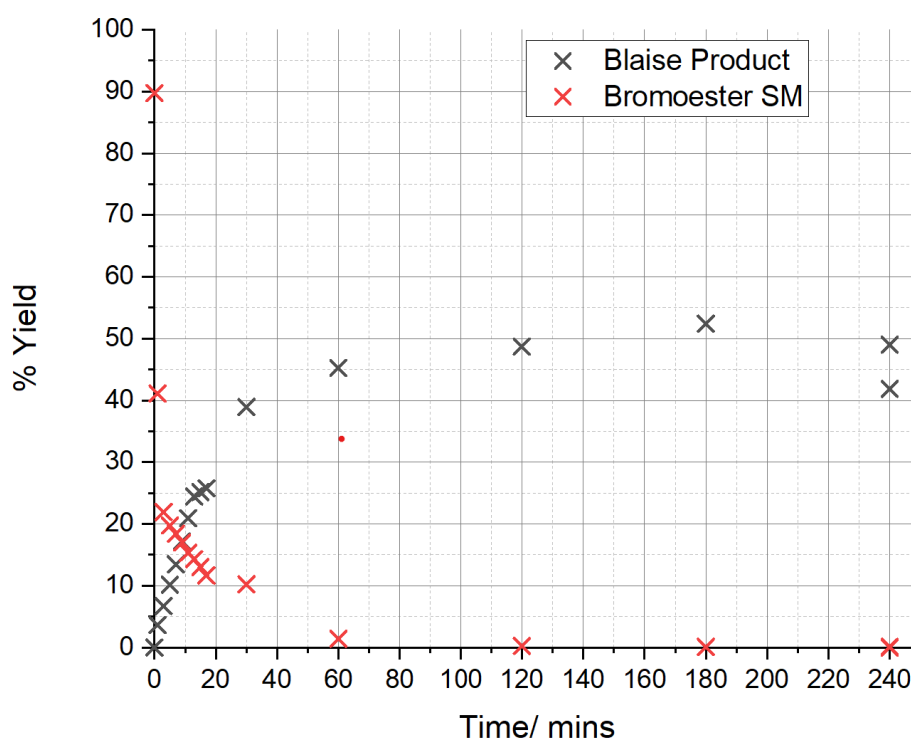
Figure 3.12. Graph depicting starting material and product % yield *vs*. time.

Initially we see a sharp decline of the starting material which is not matched by an immediate increase in product formation. This sharp decrease is likely to be due to zinc insertion into the bromoester's C-Br bond; after 3 minutes there is very little starting material depreciation, likely because the active zinc is already saturated with starting material, and then after 30 minutes there is another drop in starting material to <1 %. However, the decrease in starting material is not matched by product formation; this could be due to product degradation, by-products, or the column or UV detector is affecting the product somehow. In an attempt to shed some light on the reaction as it progressed a non-contact Raman probe was used to monitor the reaction overnight (Figure 3.13).
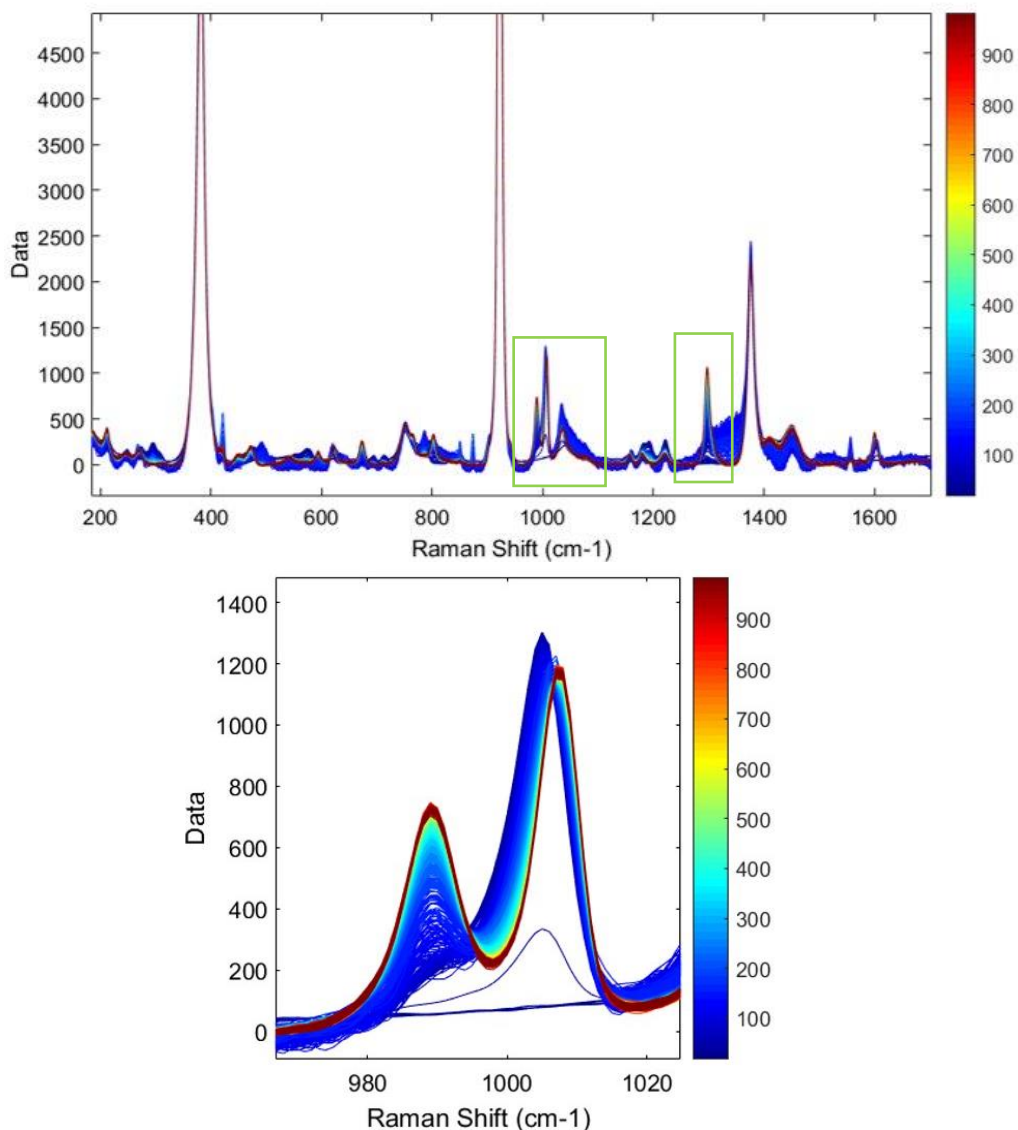
Figure 3.13. Results of overnight Raman probe monitoring of the reaction

The analysis in conjunction with Principal Component Analysis (PCA) analysis of the peaks over time was run by Dr Heidi Fisk. It was proposed that this technique could identify a zinc intermediate as metal-oxygen bonds give strong peaks in the 150-450 cm^{-1} region;[188] unfortunately this was not seen. The three peaks found significant were at 990, 1000-1010, and 1300 cm^{-1}. These peaks can correspond to aliphatic C-C bonds and C-O-C bonds, but unfortunately nothing more comprehensive could be gleaned from the results.

Figure 3.14. Image of the flow cell NMR set-up (left) with a close-up of the reaction vessel and its attachments (right).

The presence of an intermediate was confirmed using Flow Cell NMR set up at AstraZeneca Macclesfield where the step-wise reaction was monitored after addition of the methyl phenylbromoacetate overnight. The NMR monitoring and data analysis was performed by M. Nunn (Figure 3.15).
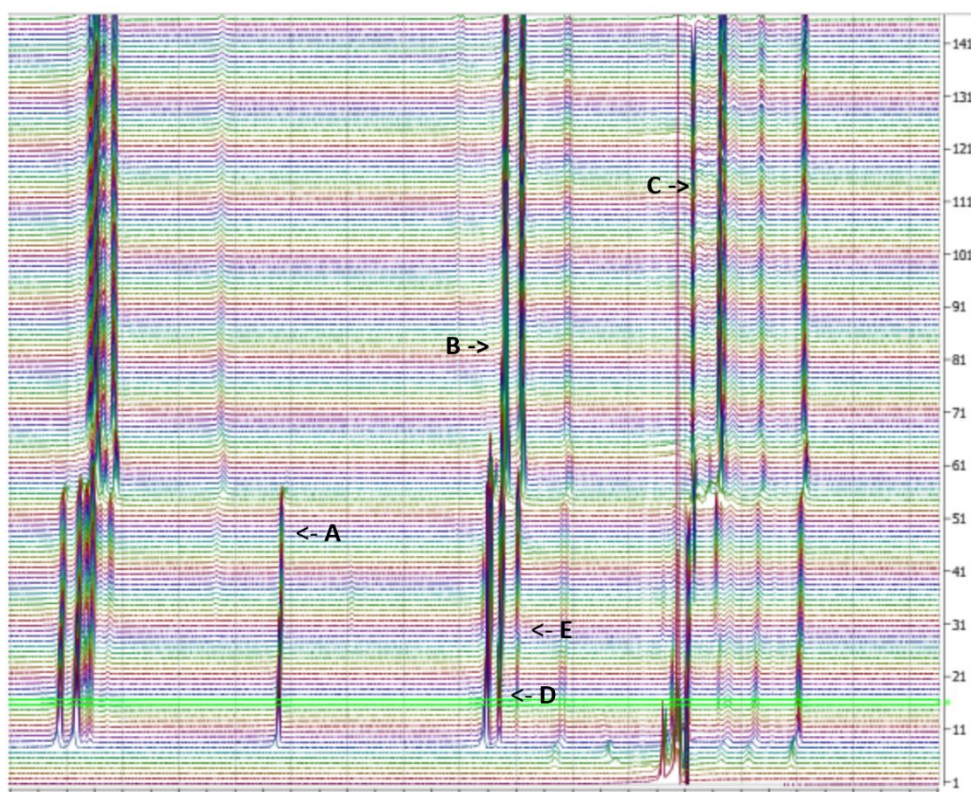
Figure 3.15 Plot of ^{1}H NMR signal (ppm) vs. time (mins) of the Blaise reaction using methyl phenylbromoacetate.

As time goes on an unidentified peak emerges at approximately 3.51 ppm and remains throughout the time period. Its appearance coincides with a second peak at 1.73 ppm suggesting that the two are from the same molecule. Known signals of the starting material (**A**), ketoester (**B**), and enol ester (**C**) products were identified and their intensity over time was plotted relative to the electrolyte TBATBF (3.21 ppm). Two other significant peaks were identified and their intensities plotted, one at 3.51 ppm and 3.65 ppm (Figure 3.16).
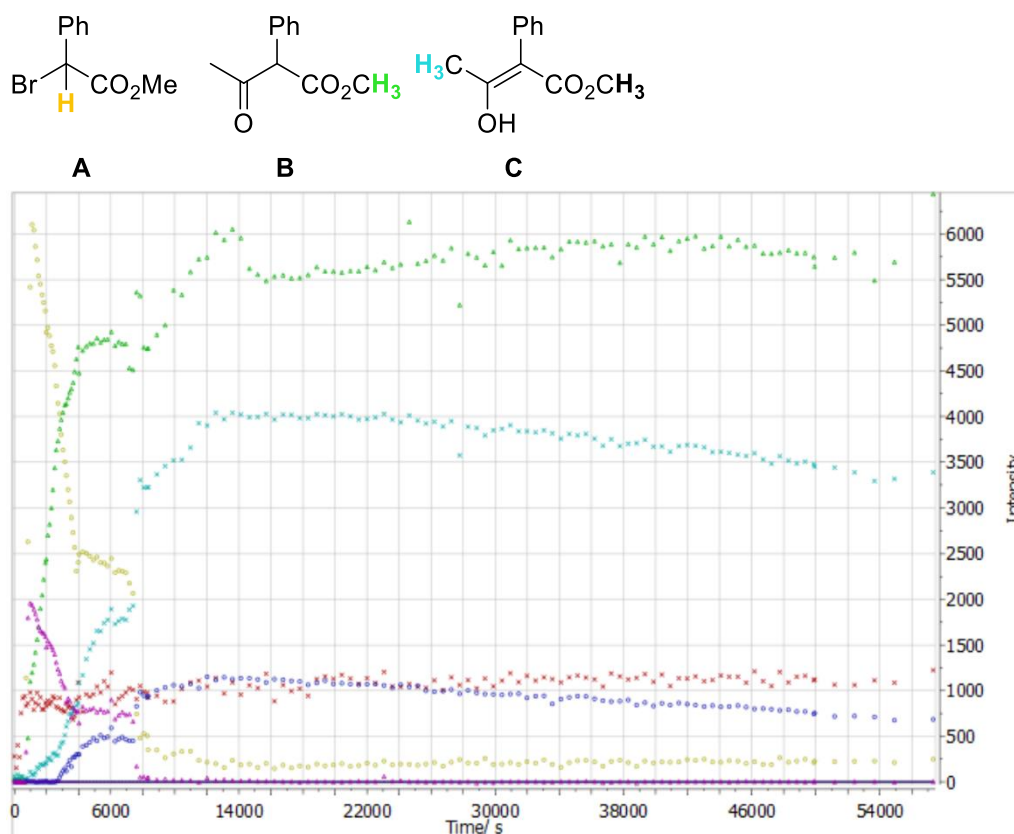
Figure 3.16. Graphical depiction of peak area intensity *vs.* time from the overnight flow NMR Blaise reaction. Yellow – **A**, Green – **B**, Cyan – **C,** Purple – Unknown **D**, Blue – Unknown **E**, Red - Electrolyte.

Within the first hour (t = 4000 s) the starting material drops in concentration to approximately 45%, between t = 1 h and t = 2 h there appears to be a plateau of all signals, then the starting material drops to 4% and remains there for the duration of the experiment. The ketoester (green) product signal appears and remains at approximately 32% after 7.5 h; the enol ester product (cyan) peaks at 3 h at 22% but decreases as time goes on to 19%. This decrease appears to correspond to an increase in ketoester yield so this change is likely to be due to tautomerization. There are two significant peaks which were not identified (blue and purple) but also follow the trend of increase in signal intensity until t = 1 h and a plateau until hour 2. The purple signal drops to 0% after 2 h, suggesting it's an intermediate peak as the green

94

product peak increases immediately after its disappearance by approximately the same intensity. However, the blue peak, as with the enol ester product, peaks at 3 h then slowly depreciates over time.

As the peak at 3.51 and 1.73 ppm is very prevalent both in the flow cell NMR and previous results it was deemed important to identify this unknown species.

3.6   Amine Side Product Identification

Using the data collected when analysing the reaction itself, it became clear that there are unexpected side products which had not been taken into account. Looking back over all previous NMR analysis done of this reaction and the behaviour of the substrates in the literature there were two possibilities which aligned with the unknown peaks seen in the spectra: acac/acnac-style co-ordination with zinc, or enamine/iminoester tautomer intermediate (Figure 3.17).
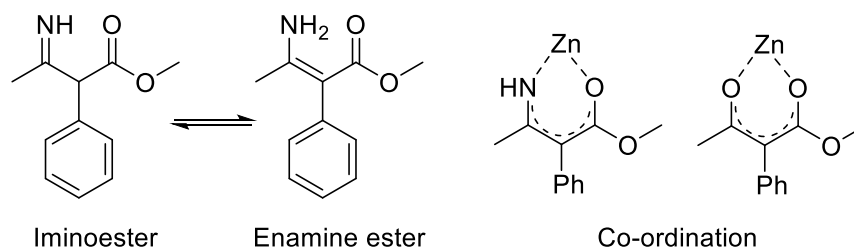
Figure 3.17. Possible Side-Products from the Blaise Reaction.

The enamine product had been reported previously by Zylber,(48) however, it was explained that only by using potassium carbonate solution as a quench and work-up could it be isolated. TLC of the crude mixture did show an unknown species close to the product spot which indicates the species is very similar in polarity to the ketoester. Using column chromatography the aminoester was isolated and identified using ^{1}H NMR, and two different crystal structures were obtained (Figure 3.18 and Figure 3.19). The presence of this amine intermediate shows that the quenching

system used (sat. $NH_4Cl_{(aq.)}$) was not sufficient in hydrolysing the imine intermediate. Including this known peak in the product tables increases mass balance significantly.
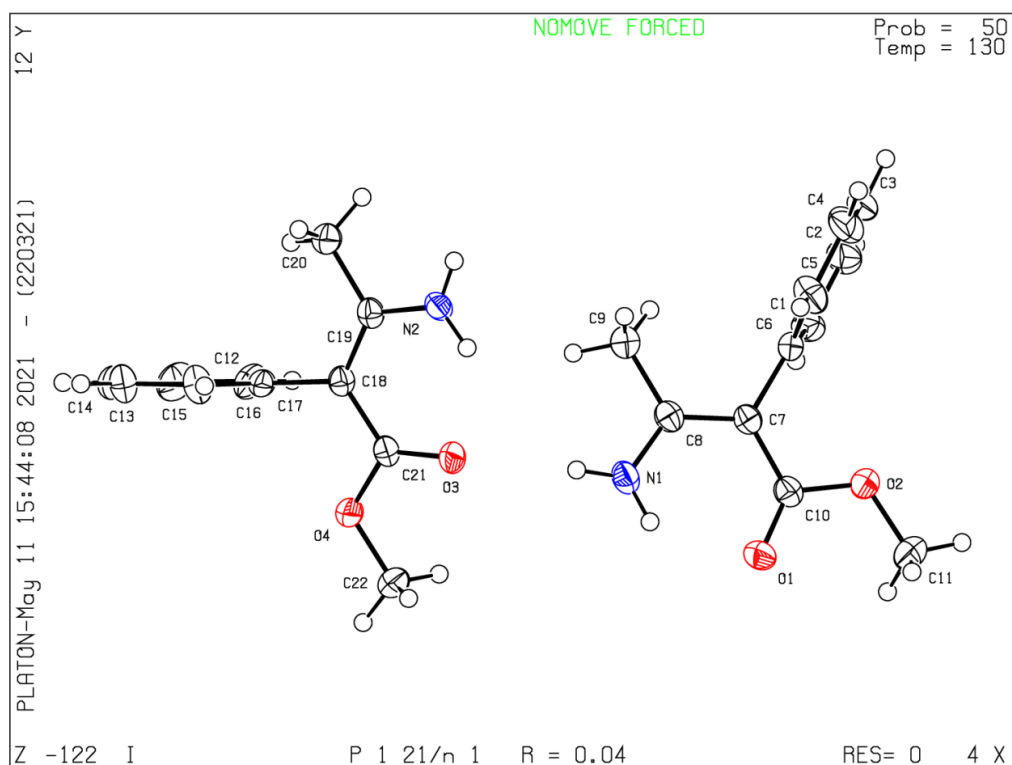
Figure 3.18 Crystal structure of one of the crystal morphologies of the amine by-product (see section 4.2.4.1, RH_100521).
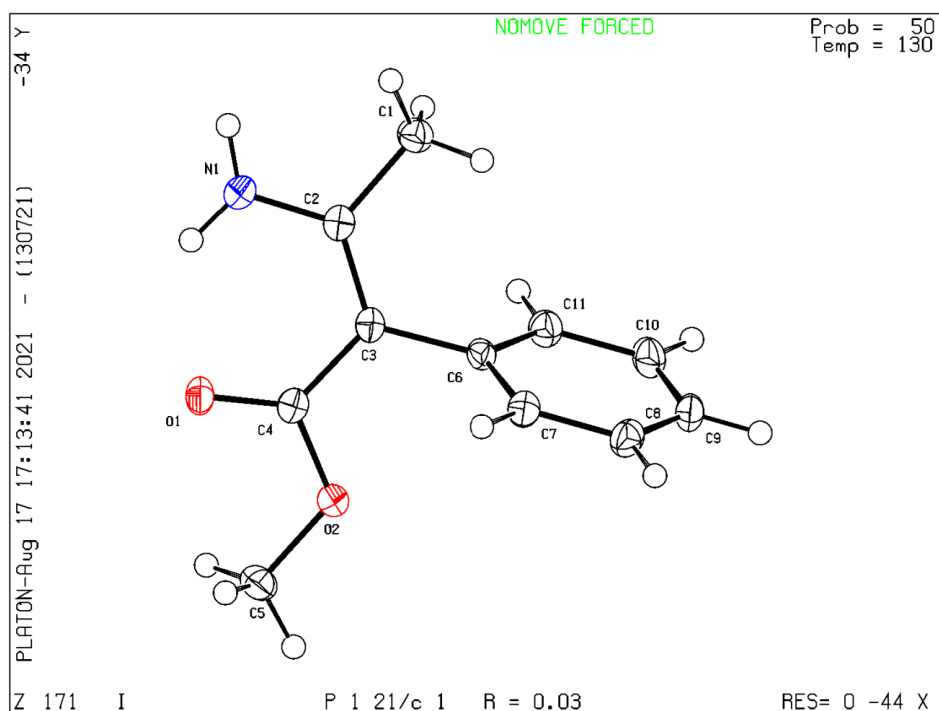
Figure 3.19 Crystal structure of the second found crystal morphologies of the amine by-product (see section 4.2.4.2, RH_170821).

However, it was still suspected that a zinc complex was formed as zinc oxide crystals were found to form over time post work-up; while investigating the unknown intermediate a second by-product was identified by LCMS. Analysis of the species gave a peak at 483.2; this matches the molecular weight of the ketoester dimer (Figure 3.20).

Molecular Weight: 479.84   Molecular Weight: 483.82

Molecular Weight: 481.83
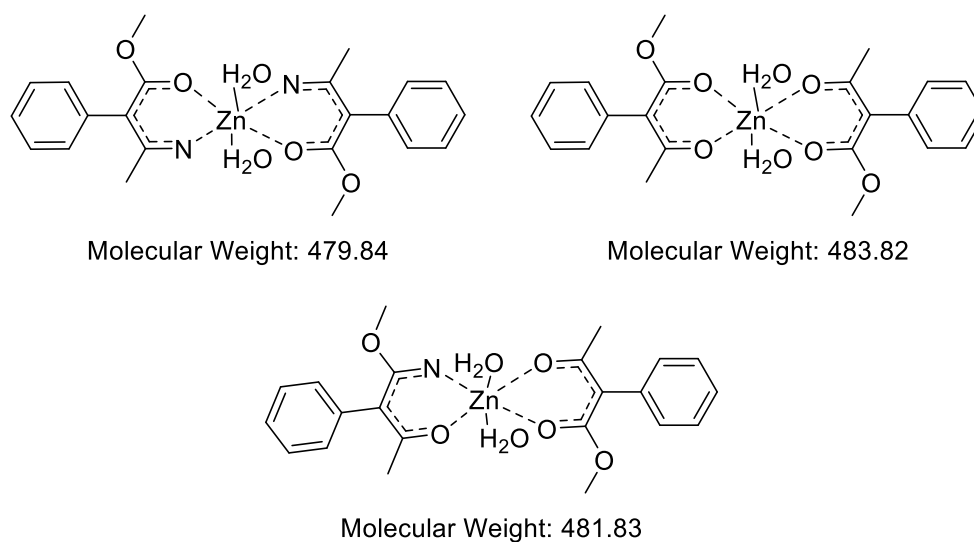
Figure 3.20. Possible dimers and their respective molecular weights.

NMR analysis of previous reactions show the presence of a small shoulder adjacent to some of the ketoester peaks, which M. Howard(189) suggested could be indicative of metal complexation (Figure 3.21).
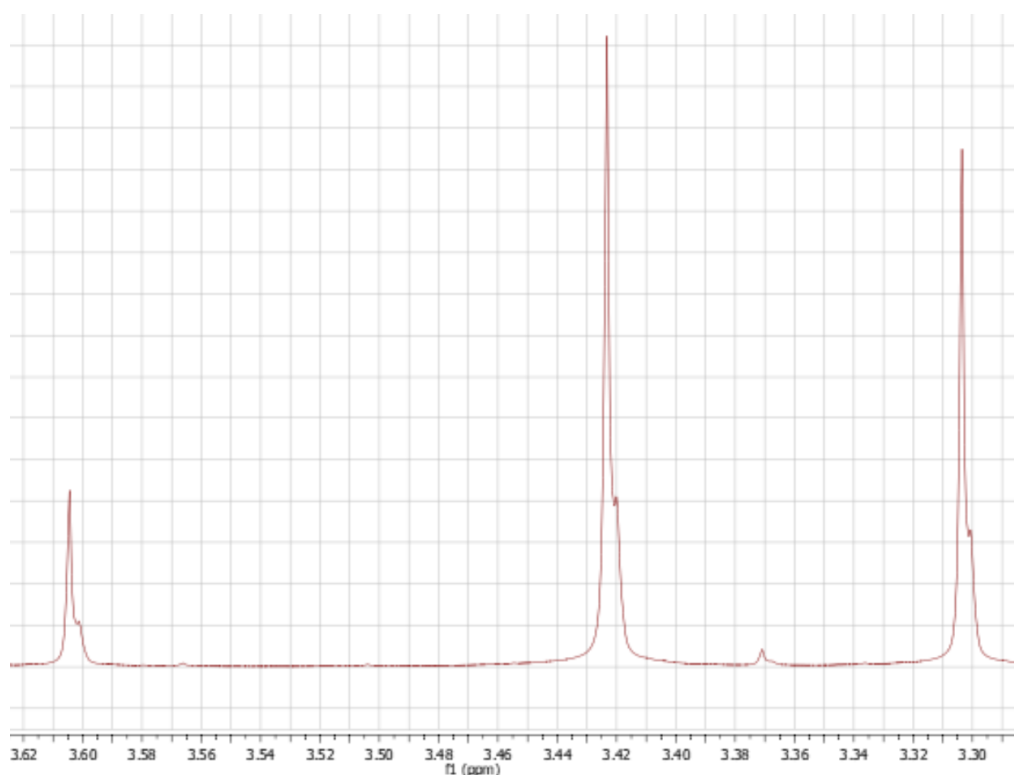
Figure 3.21. Image of ^{1}H NMR peaks from the spectra of the isolated intermediate product with a "shoulder" suggesting metal complexation.

The presence of the zinc was confirmed by addition of 10 µL of 2 M HCl to the NMR vial which formed a cream coloured precipitate, likely to be zinc chloride (Figure 3.22). Unfortunately, as we could not crystallise the zinc dimer or get a conclusive NMR we were unable to confirm its structure.

Figure 3.22. Image of an NMR tube with a visible cream coloured precipitate formed after HCl addition.

3.7 Electrochemical Reactions in the Bottle Reactor

Though the round bottom flask reactor was convenient and easy to set-up and use, the results in section 3.4.4 showed that it does not give reproducible results which is likely to be due to the inconsistency in interelectrode distance from reaction to reaction. In order to solve this issue the reactor type was changed to a Bottle reactor, a standardised reactor pioneered by the Willans group in Leeds (Figure 3.23).(151) This consisted of a 30 mL Durant bottle, GL-32 thread lid with a hole in the middle, PTFE insert with 2 electrode holes, adjustable screws to hold the electrodes in place, inlet hole for addition to the vessel, inert atmosphere inlet, and wiring to connect the electrodes to the power source. The bottle reactor has many advantages: consistent interelectrode distance which greatly affects reproducibility, shorter interelectrode distance which should improve mass transfer of ions between electrodes, fixed electrode docks which avoids painstaking manoeuvring of electrode wires through suba seals.

Figure 3.23 Images of the assembled bottle reactor (left), the assembled lid (top right), and the electrode holders (bottom right). Image from reference (151).

As the reactor volume was 30 mL and the original protocol was for a 40 mL reaction the reaction was scaled down by 75%. For the electrochemical reaction not only was the amount of electricity reduced by 75%, but also the applied current in order to maintain the current density, $j = 9.9$ mA/cm², as the round bottom flask. The calculations can be seen below. Electrodes were attached to the bottle reactor which was filled with 30 mL of solvent and the submerged area of electrode measured (Table 3.8).

$$j = \frac{i}{SA}$$

RBF: $j = 50/4.50 = 9.9 \text{ mA/cm}^2$; Bottle: $9.9 = x/5.05 = 45 \text{ mA}$

$j = current \ density \ (mA/cm^2); \ i = current \ (mA); \ SA = surface \ area \ (cm^2)$

Table 3.8. Values relevant for current density calculations.

Reactor Type	Submerged Surface area/ cm^2	i / mA	j / mA/cm^2
RBF	5.05	50	9.9
Bottle	4.50	45	9.9

3.7.1 Blaise Reaction - Reproducibility Results

The application of the Blaise reaction to the new bottle reactor was initially tested using the methyl α-bromophenylacetate starting material and acetonitrile, as this had previously given the best yield in the round bottom flask reactor. Because of the consistent interelectrode distance its reproducibility was tested to compare its efficacy to the round bottom reactor (Table 3.9).
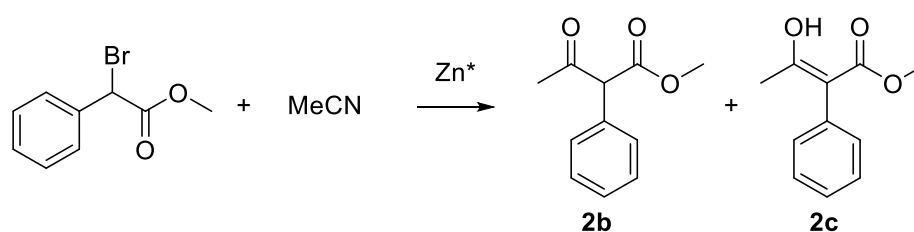
Table 3.9. Bottle reactor Blaise reaction reproducibility experiment results.[a]

Stop time (Min)	SM (%)	2b (%)	2c (%)	By-product (%)	Ar yield/ %	Mass Bal. (%)
15	49	12	5	2	75	68
15	36	8	6	10	71	61
15[b]	42	4	1	24	79	71
30	31	26	21	0	80	78
30	31	15	7	1	65	54
30[b]	31	7	2	34	88	74
60	33	8	6	12	72	58
60	31	9	6	52	105	98

| **60**[c] | 30 | 14 (+5) | 11 (+5) | 36 (-16) | 106 | 91 |
| **60**[b] | 0 | 24 | 14 | 64 | N/A[d] | 102 |

a. 1.75 mmol ZnBr$_2$, 7.5 mmol methyl bromophenylacetate, 30 mL MeCN, 0.1 M TBATBF, 45 mA constant current, 151 C with two zinc electrodes. *b*. High purity zinc electrodes used. *c*. Sample was run 24 h after work-up was completed. *d*. Sample was run in CDCl$_3$ so AR yield was not possible to calculate.

The results from the bottle reactor reproducibility experiments show significant improvement in reproducibility. The table includes an Ar. Yield column, denoting the total yield calculated from the aromatic region; this was not possible for previous results as the CDCl$_3$ NMR solvent used would obscure the results. The yield here shows that there is little to no loss of mass which supported our previous hypothesis of a third (or even fourth) by-product of the reaction. Further exploration into the unknown peaks is discussed in Section 3.6. As with the round bottom reactor, using high purity zinc electrodes did not appear to have a significant impact on yield.

After extensive work into the kinetics and substrate scope of this reaction, the electrophile in the reaction was changed from acetonitrile to various imines to form cyclic β-lactams.

3.7.2   2-Azetidinone Formation

Zinc has been reported as a successful mediator for the formation of 2-azetidinone using either diorganozinc (*e.g.* Et$_2$Zn) or zinc metal.(158,159,190,191) This is thought to proceed *via* a Reformatsky-type intermediate of the zinc metal inserting into the carbon-halogen bond and then the enolate reacts with the imine to form the four-membered ring. As 2-azetidinone is a pharmaceutically relevant structure, this would be an excellent application to the electrodeposited zinc. Initially, N-benzylideneaniline was selected as the imine and methyl bromophenylacetate. The

reaction conditions gave the 2-azetidinone product (**6a**) as the major product and the non-cyclised amine (**7a**) as the main by-product. Traces of the Blaise product (**2c**) and degraded imine product (**8**) were also detected.
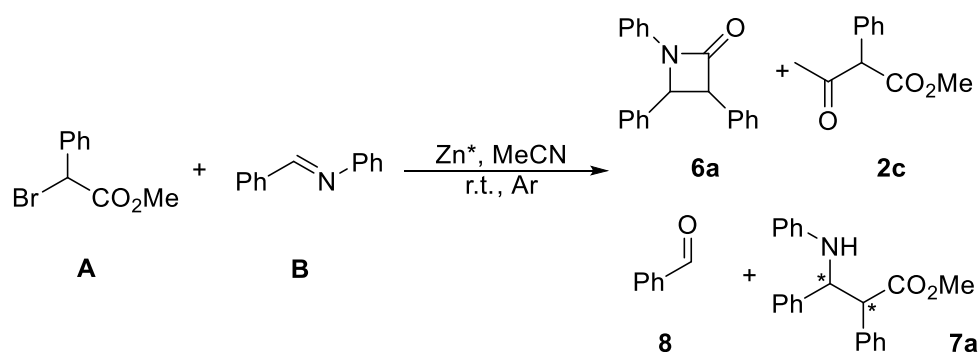
Table 3.10. Initial results for the zinc mediated formation of 2-azetidinone.[a]

Entry	i/ mA	Total Charge/ C[d]	A %	B %	6a %	2c % [e]	8 %	7a %[f]
1[b]	45	77 (0.75)	0	38	37	6 (2:1)	5	9 (5:4)
2[c]	25	77 (0.75)	31	37	32	6 (2:1)	6	7 (3:4)
3[c]	25	154 (1.50)	0	19	44	25 (1:0)	3	13 (7:6)
4[c]	25	231 (2.25)	0	24	21	4 (1:1)	<1	25 (13:12)

a. Electrodeposition: $ZnBr_2$ (1.5 mmol), MeCN (30 mL), TBATBF (0.1 M), zinc electrodes. Methyl bromophenylacetate (5 mmol), *N*-benzylideneaniline (5 mmol), 20 h, r.t., Ar. b. Step-wise reaction. c. One-pot reaction. d. Brackets indicate the mmol of electrons e. Tautomeric ratio of ketoester:enol ester. f. *Syn:Anti* ratio determined by H^1 NMR. **A** and **B** denote residual starting materials present in crude H NMR.

Initially, the conditions used for electrodeposition were identical to that used for the Blaise reaction (Entry 1) which resulted in moderate yields of **6a** (37%) and minor amount of side-product **7a** (9%). After this initial reaction, a swap to a one-pot protocol was trialled (Entry 2-4); this could in theory increase yields as the electrodeposited zinc could react as soon as it was formed.

As imines are known to undergo one-electron processes, the applied current was reduced to 25 mA to mitigate this. Using the same total charge as the previous reaction (77 C) gave a similar (but lower) yield of **6a** (32%) and a lower yield of **7a** (7%). To increase the product yield the total charge was doubled to 154 C. This was successful in improving the yield of **6a**. A further increase in total charge to 2.25 mmol electricity did not lead to greater yields of **6a** but rather a significant drop to 21%. This was not expected as it was thought excess electricity, once all $ZnBr_2$ was electrolysed, would then begin to use the zinc anode in a sacrificial manner and electrodeposit more zinc. It is possible that the excess electricity caused degradation of starting material **B** and product **6a**. Interestingly, the side product **7a** yield did increase with increased total charge; this suggests that **7a** is more electro-stable than its 4-membered ring counterpart or perhaps that the 2-azetidinone ring can be electrolysed into **7a**.

As the conditions for entry 3 gave the best yield, these were continued in the substrate scope reactions. Table 3.11 details the different bromoesters and imines used in the substrate scope, which were successful to various degrees.
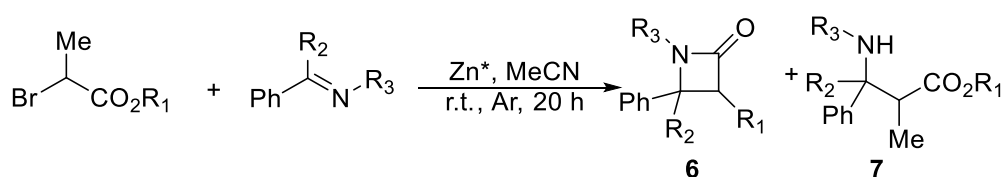
Table 3.11. Substrate scope of zinc-mediated 2-azetidinone formation.[a]

Entry	R_1	R_2	R_3	6 %[b]	7 %[b]
a	Me	H	Ph	40 (27:13)	29 (17:12)
b	Me	H	Me	0	0
c	Me	Ph	H	0	0

d	*t*Bu	H	Ph	0	57

a. One-pot reaction, 25 mA c.c., 20 h, 154 C, r.t., Ar, zinc electrodes. ZnBr$_2$ (1.5 mmol), MeCN (30 mL), TBATBF (0.1 M), bromoester (5 mmol), imine (5 mmol). b. *syn:anti* ratio established by H^1 NMR.

Using benzylideneaniline (entry **a**) showed moderate yields of the cyclised product **6a** and low yields of product **7a**, both comparable to the yield seen in Table 3.10. Entry b did not show any product **6b** yield when using benzylidenemethanimine, the aldehyde hydrolysis product and Blaise product were present in meagre amounts. The yield is not wholly unexpected as the nitrogen in this imine is much less nucleophilic than others in this table. Therefore, it may have not been able to react with the organozinc bromide intermediate formed from the bromoester. However, the low yield of hydrolysis and Blaise product suggests that there may have been some by-products formed. These were not identified in the NMR so likely were lost in the work-up. For entry **c** using benzophenone imine neither product was detected by NMR, this is likely due to the same reasons as in entry b. Furthermore, the benzophenone imine is more prone to hydrolysis than more substituted imines. Using a more sterically hindered ester (entry d) had a marked effect on the yield with 0% of **6d** but 57% of **7d** found. As the cleavage of the ester is part of the reaction mechanism it is understandable that a more sterically hindered ester does not allow for cyclisation and favours product **7d**. It has been reported that propiolactams can undergo *N-N*-dimerization under acidic conditions(192) however no evidence was found of this in the analysis. This work concluded with this substrate scope due to time constraints.

3.8 Summary of Electrodeposition Work

The work described in this chapter has shown the applicability of the electrodeposited zinc to form a range of interesting molecules from relatively simple starting materials. However, these applications are in their relative infancy, therefore, many of the yields reported are not as impressive as seen in the literature. The Substrate scope investigated a range of organohalides, from simple bromoesters to more complex heterocyclic organohalides

What is promising though, is the low-cost methodology of zinc activation which can offer an alternative to the pyrophoric nature of some organozinc reagents. Success was found in home-made and standardised reactors, however, better control over reproducibility was found in the bottle reactor which was not surprising. Any future work described below would be carried out using the bottle reactor or another reactor with standardised interelectrode distances.

3.9 Future Work

This work has shown interesting investigations of the surface morphology of the zinc deposits. Future work would delve further into the behaviour and the nature of the deposits themselves, which would be useful for comparison to commercially available zinc sources (*e.g.* Rieke zinc, zinc dust). Examples of this include: Brunauer-Emmett-Teller (BET) analysis to investigate its porosity as done by Tokuda *et al.* and Atomic Absorption Spectroscopy (AAS) to investigate the change in zinc concentration between the reaction mixture before and after the reaction. The AAS would further highlight the extent to which the electrodes themselves sacrificial, and how much zinc is given from them. To investigate the effect current has on the morphology of the zinc reactions of varying current should be run.

106

Although our initial results of moving to the bottle reactor which had a different interelectrode distance and current to the round bottom reactor did not give significantly different deposits, it is possible that a larger current (*e.g.* 75-100 mA) or significantly smaller current (*e.g.* 5-25 mA) would show a visible change.

In terms of reactors, moving this reaction into continuous flow could increase this reaction's efficacy, energy efficiency, and allow for better product control. The main issue to combat would be the possibility of blockages from the deposited zinc, however, using low currents could avoid this problem.

3.9.1 Blaise Reaction

The Blaise reaction work in both reactors worked to a reasonable degree of success with the best obtained from the standardised reactor. However, there were issues with the work-up as it did not appear to fully hydrolyse the imine intermediate. It would be worth trying the work-up technique used for the 2-azetidinone reactions to see if this rectifies the issue. Furthermore, the NMR and UPLC analysis shows that the product yields peak at around 3 h, therefore shortening the reaction time might also prove beneficial.

3.9.2 Reformatsky Reaction

The *syn-anti* diastereomerism found in the product when using the zinc would be an interesting avenue to explore further. Using a chiral auxiliary to preferentially yield one product over the other is an oft-used practice for the Reformatsky reaction,(193) therefore finding the correct one should not be difficult as there are already publications to reference.

It was found that using a 2:1 ratio of aldehyde to bromoester gave outstanding yields (99%) at ambient temperatures; if this turns out to be a trend for the reaction, the

substrate scope should be expanded to try more difficult aldehydes. The reaction has already been investigated to make industrially relevant compounds,(181) and due to the reaction's functional group tolerance it could be a vital addition to a chemist's toolbox for late-stage functionalisation.

3.9.3   2-Azetidinone

This report has shown that electrodeposited zinc can be used to form β-lactams in up to moderate yields, however this application is in its relative infancy. Further work would be to identify the critical parameters (*e.g.* current, temperature, total charge) and run DoE to optimise formation of the cyclised product. Once the yields are increased to >70 % investigations into substrate scope could continue. While many pharmaceuticals containing 2-azetidinone are now produced on a large scale using fermentation (penicillins, ezetimibe),(194) were this method to be optimised it could be a major player in synthetic labs to reliably produce β-lactams.

Introduction of a chiral auxiliary may help with diastereoselectivity, and there are already examples of this for enolate-imine coupling reactions (*e.g.* chiral ethers, diamines). Furthermore, introduction of bulkier groups such as naphthalene may sterically induce one enantiomer over the other as seen in Table 3.11 where using a bulkier ester was found to only give the non-cyclised product. Selectively protecting the imine nitrogen of the starting material and using a bulky ester could allow for facile formation of unnatural chiral amino acids once the amine protecting group cleaved and ester hydrolysed. Further investigation into the impact the ester has on product yield by changing both the R-oxy and carbonyl-adjacent substituents would greatly benefit the understanding of the reaction and its substrate scope, as there may be a correlation between nature of the ester and product ratios.

4 Experimental Procedures

4.1 C-H Activation/Amination of Benzoxazole Experimental

All solvents and starting materials were obtained from commercial vendors without further purification. All dry solvents were obtained from the University of Leeds Solvent Purification System. Column chromatography was performed using Fisher Chemicals 60A 35-70 micron silica gel. All NMR was run on Bruker 400 MHz spectrometer with $CDCl_3$ as a reference peak at 7.26 ppm. s = singlet, d = doublet, dd = doublet of doublets, t = triplet, dt = doublet of triplets, m = multiplet.

All gas chromatography was run using an Agilent Technologies 7890B System Gas Chromatograph; the method: 15.5 minutes, 50 –300 °C temperature range, 325 °C maximum temperature, 3 minute equilibrium time, 1 µm injection volume, HP-5 column (320 µm diameter, 3 m length). All samples were run in MeCN; a 100 µL aliquot was removed from the starting material, made up to 1 mL with MeCN, and run through celite.

4.1.1 2-Morpholinbenzoxazole Synthesis – Batch

A CSI3005X5 Bench Power Supply battery pack was connected to a DMiotech Smart-C Digital Multimeter and to steel wires attached to crocodile clips which held the electrodes. The steel wires were pushed through suba seals and into two of the three necks of the three necked round bottom flask, the third middle neck is also suba sealed with a nitrogen inlet. Metal electrodes had an electrode surface area of 3.3-3.5 cm^2, glassy carbon electrodes had an electrode surface area of 13.3-13.4 cm^2.

In dry, degassed acetonitrile (100 mL), benzoxazole (600 mg, 5.04 mmol), morpholine (0.88 mL, 10.04 mmol), acetic acid (1.44 mL, 25.1 mmol), and TBAI (187 mg, 0.504 mmol) were combined and stirred for 30 minutes under nitrogen in a

3-necked 250 mL round bottom flask. The electrodes were connected to the power supply and the power turned on; the potential was increased until the desired current was achieved. The current was visually monitored on a potentiostat, and the potential altered accordingly to maintain constant current conditions. After 6 hours the solvent was removed under vacuum, and 25 mL of water was added. The solution was then washed with DCM (3 x 15 mL), the organic layer was separated and washed with saturated sodium carbonate solution. The organic layer was then dried with magnesium sulphate and evaporated under vacuum to give a dark orange-brown oil which was purified using silica chromatography, eluting at 9:1 hexane:acetone. Recrystallization from hexane then gave 2-morpholinbenzoxazole as pale, yellow plates.

4.1.2   2-Morpholinbenzoxazole Synthesis – Flow

The electrochemical flow reactor used for the following experiments was modelled on work previously published by the Nguyen group on copper catalysis.(117) The continuous flow cell consisted of two stainless steel endplates fitted with tubing for input and output, 10 cm x 10 cm metal electrode plates with a 1 cm diameter hole cut out to allow solution to flow, 10 cm x 10 cm PTFE plates with pathways cut out for the solution to flow. The cell was arranged beginning with the inlet/outled PTFE plate, followed by a metal electrode plates sandwiching a PTFE pathway plate, ending in another PTFE inlet/outlet plate, screwed together with stainless steel screws.

The electrodes were connected to a CSI3005X5 Bench Power Supply battery pack and a Tenma 72-1012 Bench Top Digital Multimeter. The syringe pump used in this cell was a Cole-Parmer Four Syringe Pump. The circuit was connected using insulated copper wires with crocodile clips at either end (connecting multimeter to

circuit) or AUX inlets (connecting power pack to multimeter and cell with power pack). The outlet tube feeds into a measuring cylinder as gas production was observed therefore reactor volume was used to monitor progression.

In dry, degassed acetonitrile (100 mL), benzoxazole (600 mg, 5.04 mmol), morpholine (0.88 mL, 10.04 mmol), acetic acid (1.44 mL, 25.1 mmol), and TBAI (187 mg, 0.504 mmol) were combined and stirred for 30 minutes under nitrogen in a 3-necked 250 mL round bottom flask. The electrochemical cell was assembled: stainless steel inlet and outlet plates, six 10 x 10 cm electrodes six 10 x 10 cm PTFE inserts with reaction pathways cut out, stainless steel screws, giving a 12 mL reactor volume system. The electrodes were connected to the power base in alternating
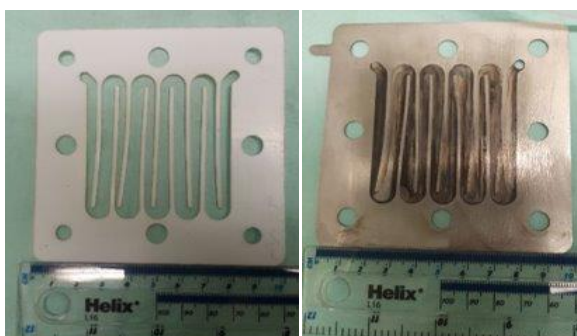
Figure 4.1. Images of the PTFE pathway plate (left) and an electrode (right) from a flow reactor C-H activation/amination of benzoxazole with morpholine.

polarities (anode-cathode-anode-*etc.*). Once the reactor was assembled, dry and degassed MeCN (30 mL) was used to pre-wash the system. A Cole-Palmer C200139 syringe pump was programmed to the desired flow rate and the solution run through the reactor in three syringes (40 mL x 40 mL x 20 mL), then the reactor was washed through with MeCN (40 mL) and nitrogen.

4.1.3 CV Method

Acetonitrile was obtained from the University of Leeds Solvent Purification System and degassed for 30 minutes prior to use. The tetrabutylammonium hexafluorophosphate (TBAPF$_6$) and tetrabutylammonium iodide (TBAI) electrolytes were recrystallised 3 times with MeOH for purification before use. The CV itself was run using a glassy carbon cathode and a platinum wire anode, with Ag/AgCl as a reference electrode. A 0.1 M solution of TBAPF$_6$ was run as a background to check for impurities in the bulk solution before a 0.01 M solution of TBAI, benzoxazole, and benzoxazole with AcOH (0.05 M) were prepared.

4.2 Electrodeposition of Zinc Reactions

All solvents and starting materials were obtained from chemical vendors without further purification. All dry solvents were obtained from the University of Leeds Solvent Purification System. Column chromatography was performed using Fisher Chemicals 60A 35-70 micron silica gel. All yields were determined by H^1 NMR integration against an internal standard from solution NMR.

Figure 4.2. Images of the Electrasyn Adaptor (left) and close-up of underside (right).

The Electrasyn 2.0 from IKA was utilised as a power base to control the current and total charge put into the reaction; an adaptor was designed and created using PTFE and copper wiring to connect the Electrasyn 2.0 to the electrodes in the chemical circuit (Figure 4.2). The electrodes used were held by crocodile clips attached to stainless steel wire which was pushed through a suba-seal.

4.2.1 Round Bottom Flask Reactions

The standard batch reactor used was a 50 mL three-necked round bottom flask with a magnetic stirrer. The flask was prepared by washing with 0.1 M HCl, water, acetone, and ethanol and dried in an 80 $^{\circ}$C oven overnight. The middle neck was attached to the vacuum line, and the left and right necks held the electrodes attached to stainless steel wire with crocodile clips, and the wire pushed through suba seals. The stainless steel wire was connected to the Electrasyn power base using crocodile clips attached to a PTFE adaptor made in-house to expand our reactor possibilities. Average current density of 9.9 mA/cm^2.

ZnBr$_2$ (450 mg, 2 mmol) was vacuum dried for 3 hours at 200 $^{\circ}$C. After drying the flask was placed under nitrogen. A solution of 0.01 M Bu$_4$NBF$_4$ in dry MeCN (40 mL) was added and the stainless steel wiring was attached to the adaptor to connect the circuit. The reaction was run at 50 mA c.c. until 203 C of electricity had passed through. The bromoester (10 mmol) was added to the mixture and the reaction was left stirring for 16 hours until completion. A saturated solution of NH$_4$Cl$_{(aq)}$ (30 mL) was added to quench the reaction. The organic layer was extracted with diethyl ether, dried with MgSO$_4$, concentrated under nitrogen and quantified against an internal standard.

4.2.2 Bottle Reactor Blaise Reaction

Once the zinc bromide was dried the flask was placed under argon and cooled to room temperature. A 30 mL solution of tetrabutylammonium tetrafluoroborate (0.01 M) in dry MeCN was added to the reactor. The reactor was assembled by screwing on the lid, attaching the electrodes to the Electrasyn adaptor using crocodile clips, and resuming the inert atmosphere. Under constant current and stirring the electricity was applied to the solution to form the electrodeposited zinc until a predetermined amount of electricity had passed through. The starting material(s) were added to the reactor and left to stir overnight and were quenched using 30 mL sat. NH_4Cl solution. The mixture was extracted using Et_2O (3 x 30 mL) and dried using $MgSO_4$.

HPLC Sampling: The reaction was allowed to run the allotted time length; at time t = 15, 30, and 60 mins a 200 µL aliquot was removed (Gilson pipette) and injected into a Pasteur pipette celite filter with 200 µL of the TMB internal standard solution and 1 mL MeCN.

Reproducibility reactions full table:
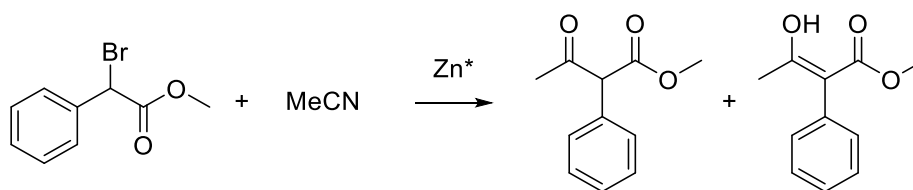
Table 4.1. Bottle reactor reproducibility experiments of an electrochemical Blaise reaction .[a]

Stop time (Min)	SM (%)	Ketone (%)	Enone (%)	By-product (%)	Ar yield/ %	Mass Bal. (%)
15	49	12	5	2	75	68
15	36	8	6	10	71	61
15	31	13	10	3	92	56
15[b]	42	4	1	24	79	71

30	23	20	2	23	75	68
30	31	26	21	0	80	78
30	31	15	7	1	65	54
30[b]	31	7	2	34	88	74
60	34	23	16	39	71	112
60	33	8	6	12	72	58
60	31	9	6	52	105	98
60[c]	30	14 (+5)	11 (+5)	36 (-16)	106	91
60[b]	0	24	14	64	N/A[d]	102

a. 1.75 mmol ZnBr$_2$, 7.5 mmol methyl bromophenylacetate, 30 mL MeCN, 0.1 M TBATBF, 45 mA constant current, 151 C with two zinc electrodes. *b*. High purity zinc electrodes used. *c*. Sample was run 24 h after work-up was completed. *d.* Sample was run in CDCl$_3$ so AR yield was not possible to calculate.

4.2.3 Bottle Reactor Zinc Preparation

The bottle reactor is made up of a 30 mL Durant bottle, GL-32 thread lid with a hole in the middle, PTFE insert with 2 electrode holes, adjustable screws to hold the electrodes in place, inlet hole for addition to the vessel, inert atmosphere inlet, and wiring to connect the electrodes to the power source. A 30 mL Durant bottle was washed with 0.1 M HCl, water, acetone, and alcohol and dried in an 80 °C oven overnight. The zinc electrodes were prepared by sandpapering the surface and edges, washing with acetone and finally alcohol. Once dry, they were then fitted to the bottle reactor lid, a magnetic stirrer and zinc bromide was added to the flask, and the lid screwed on. The ZnBr$_2$ was dried under vacuum ay 180 °C for 3 hours before use. Average current density of 9.9 mA/cm^2.

4.2.4 Bottle Reactor 2-Azetidinone Formation

Once the zinc bromide was dried (see above) the flask was placed under argon and cooled to room temperature.

Stepwise: A 30 mL solution of TBATBF (0.01 M) in dry MeCN was added to the reactor and stirring commenced. Under a constant current of 45 mA a predetermined amount of electricity was applied to the solution to form the electrodeposited zinc. The bromoester (5 mmol) and imine (5 mmol) were added to the reactor and left to stir for 20 h.

One-pot: A 30 mL solution of TBATBF (0.01 M), bromoester (5 mmol) and imine (5 mmol) were added to the dried $ZnBr_2$ with stirring. Under a constant current of 25 mA, electricity was applied to the solution until a predetermined amount of electricity had been passed through; once finished the reactor was left to stir. Total reaction time = 20 h.

The reaction mixture was quenched using 30 mL sat. NH_4Cl solution and stirred for 30 minutes. A 20% solution of $NaOH_{(aq.)}$ (30 mL) was added followed by extraction with DCM (3 x 30 mL). The organic layers were combined and washed with 0.1 M HCl (30 mL), then water (30 mL), and dried using $MgSO_4$. The mixture was dried under nitrogen and the yield quantified using ^1H NMR against an internal standard.

5 NMR Data and Assignments

5.1 C-H Activation Reactions

5.1.1 2-Morpholinbenzoxazole
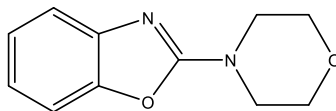
^{1}H NMR (400 MHz, CDCl$_3$) δ 7.37 (d, J = 7.7 Hz, 1H), 7.27 (d, J = 7.2 Hz, 4H), 7.18 (td, J = 7.7, 0.9 Hz, 1H), 7.04 (td, J = 7.8, 1.0 Hz, 1H), 3.83 (d, J = 4.5 Hz, 2H), 3.82 (d, J = 5.1 Hz, 3H), 3.70 (d, J = 5.2 Hz, 3H), 3.69 (d, J = 4.5 Hz, 3H). ^{13}C NMR (101 MHz, CDCl$_3$) δ 162.2, 148.9, 143.0, 124.2, 121.1, 116.6, 109.0, 66.3, 45.9.

Literature values: (195)

^{1}H NMR (400 MHz, CDCl$_3$) δ 7.32 (d, 1H, J = 7.9 Hz); 7.21 (d, 1H, J = 7.9 Hz); 7.13 (t, 1H, J = 7.9 Hz); 6.98 (t, 1H, J = 7.9 Hz); 3.77 (t, 4H, J = 4.5 Hz); 3.64 (t, 4H, J = 4.5 Hz). ^{13}C NMR (101 MHz, CDCl$_3$) δ 161.2, 148.2, 141.1, 124.3, 121.3, 116.0, 108.9, 66.0, 45.8.

5.2 Electrodeposited Zinc-Mediated Reactions

5.2.1 Methyl 2-methyl-3-oxo-butanoate, **2a**
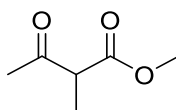
^{1}H NMR (501 MHz, CDCl$_3$) δ 12.58 (s, 1H, enol), 3.82 (s, 3H, enol), 3.73 (s, 3H), 3.58 (s, 3H, enol), 3.51 (q, J = 7.2 Hz, 1H, keto), 2.47 (s, 3H, enol), 2.22 (s, 3H, keto), 1.98 (s, 3H, enol), 1.68 (brs, 3H, enol), 1.33 (d, J = 7.2 Hz, 3H, keto). ^{13}C NMR (126 MHz, CDCl$_3$) δ 203.7, 171.1, 53.5, 52.5, 28.6, 12.9.

Literature values:(84)

δ_H (500 MHz, CDCl$_3$): 3.77 (s, 3H), 3.55 (q, J = 7.2 Hz, 1H), 2.27 (s, 3H), 1.38 (d, J = 7.2 Hz, 3H); δ_C (125 MHz, CDCl$_3$): 203.6, 171.0, 53.4, 52.4, 28.5, 12.8.

5.2.2 Methyl-3-oxo-2-phenyl-butanoate, **2b & 2c**
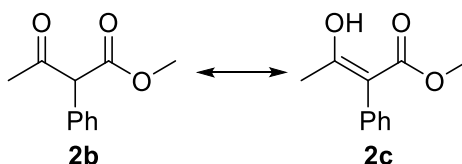
δ_H (400 MHz, CDCl$_3$): 13.04 (s, 1H), 7.21-7.41 (m, 10H), 4.72 (s, 1H, keto), 3.75 (s, 3H, keto), 3.68 (s, 3H, enol), 2.18 (s, 3H, keto), 1.85 (s, 3H, enol); ^{13}C NMR (126 MHz, CDCl$_3$) δ 201.61, 169.14, 132.70, 129.46, 129.10, 128.50, 65.77, 52.75, 28.91.

Literature values:(196)

δ_H (300 MHz, CDCl$_3$): 7.12-7.43 (m, 5H), 4.70 (s, 1H, keto), 3.76 (s, 3H, keto), 3.69 (s, 3H, enol), 2.18 (s, 3H, keto), 1.85 (s, 3H, enol); δ_C (75 MHz, CDCl$_3$): 201.3, 173.9, 172.8, 168.8, 134.9, 132.5, 131.0, 129.2, 128.7, 128.1, 128.0, 126.9, 103.9, 65.4, 52.3, 51.6, 28.6, 19.6.

5.2.3 Methyl 3-hydroxy-2-methyl-3-phenyl-propanoate, **3a**
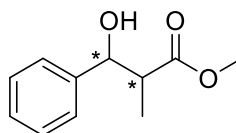
^{1}H NMR (501 MHz, CDCl$_3$) δ 7.41 – 7.20 (m, 10H), 5.11 (d, J = 3.6 Hz, 1H, *syn*), 4.76 (d, J = 8.4 Hz, 1H, *anti*), 3.73 (s, 3H, *anti*), 3.68 (s, 3H, *syn*), 2.98 (s, 1H, *syn*), 2.89 – 2.72 (m, 2H), 2.26 (s, 3H, *anti*), 1.13 (d, J = 7.2 Hz, 3H, *syn*), 1.01 (d, J = 7.2 Hz, 3H, *anti*). δ^{13}C NMR (126 MHz, CDCl$_3$) δ 176.45, 176.39, 141.61, 141.46,

136.53, 134.62, 129.90, 129.14, 128.66, 128.60, 128.41, 128.26, 127.65, 126.81, 126.08, 77.41, 77.16, 76.91, 76.60, 52.11, 52.05, 47.22, 46.46, 14.62, 14.25.

Literature values:(197)

Syn-isomer δ_H (500 MHz, CDCl$_3$): 7.31-7.39 (m, 4H), 7.23-7.30 (m, 1H), 5.10 (d, J = 4.0 Hz, 1H), 3.67 (s, 3H), 2.93-2.98 (brs, 3H), 2.78 (dq, J = 4.1, 7.2 Hz, 1H), 1.12 (d, J = 7.2 Hz, 3H); δ_C (125 MHz, CDCl$_3$): 176.3, 141.5, 128.5, 128.1, 126.6, 76.4, 51.8, 47.1, 14.4.

Anti-isomer δ_H (500 MHz, CDCl$_3$): 7.31-7.42 (m, 4H), 7,25-7.30 (m, 1H), 4.74 (d, J = 8.4 Hz, 1H), 3.72 (s, 3H), 2.90-3.05 (brs, 1H), 2.83 (dq, J = 7.2, 8.4 Hz, 1H), 1.00 (d, J = 7.2 Hz, 3H); δ_C (125 MHz, CDCl$_3$): 176.3, 141.5, 128.5, 128.1, 126.6, 76.4, 51.8, 47.1, 14.4.

5.2.4   1,3,4-Triphenyl-2-azetidinone, **6a**
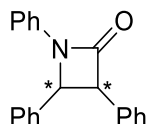
Trans-isomer ^{1}H NMR (501 MHz, CDCl$_3$) δ 7.42 – 7.05 (m, 15H), 4.97 (d, J = 2.6 Hz, 1H), 4.30 (d, J = 2.5 Hz, 1H).

^{13}C NMR (126 MHz, CDCl$_3$) δ 166.4, 138.2, 135.5, 132.2, 129.2, 129.1, 128.4, 128.2, 128.0, 127.6, 127.4, 124.8, 118.0, 65.9, 64.5.

Literature values:(198)

Trans-isomer: ^{1}H NMR (400 MHz, CDCl$_3$) δ 7.42 – 7.22 (m, 14H), 7.09 – 7.03 (m,1H), 4.95 (d, J= 2.6 Hz, 1H), 4.28 (d, J = 2.6 Hz, 1H). 13C NMR (101 MHz,

CDCl$_3$) δ 165.7, 137.6, 137.5, 134.8, 129.4, 129.2, 129.1, 128.7, 128.0, 127.5, 125.9, 124.1, 117.3, 65.2, 63.7.

The non-cyclised product was also identified: methyl 2,3-diphenyl-3-(N-phenylamino)propionate, **7a**
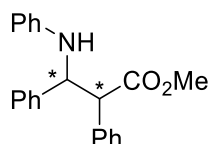
Syn- ^{1}H NMR (501 MHz, CDCl$_3$) δ 7.50 – 7.00 (m, 12H), 6.70 – 6.55 (m, 1H), 6.57 (dd, *J* = 8.6, 1.0 Hz, 2H), 4.94 (m, 2H, 1Hz), 3.96 (d, *J* = 8.2 Hz, 1H), 3.70 (s, 3H).

Anti- ^{1}H NMR (501 MHz, CDCl$_3$) δ 7.50 – 7.00 (m, 12H), 6.70 – 6.55 (m, 1H), 6.38 (dd, *J* = 8.6, 0.9 Hz, 2H), 4.94 (m, 2H, 1Hz), 3.89 (d, *J* = 9.9 Hz, 1H), 3.45 (s, 3H).

^{13}C NMR (101 MHz, CDCl$_3$) δ 172.9, 171.9, 147.1, 146.8, 135.2, 129.4, 129.3, 129.2, 129.1, 128.9, 128.8, 128.7, 128.5, 127.7, 126.3, 126.0, 125.0, 118.2, 118.1, 114.1, 114.0, 60.2, 60.1, 58.8, 55.0, 52.2, 50.8.

Literature values:(199)

^{1}H NMR (400 MHz, CDCl$_3$) δ 7.49 - 7.43 (m, 3H), 7.40 - 7.10 (m, 7H), 7.09 - 6.97 (m, 2H), 6.62 - 6.54 (m, 1H), 6.54 (*syn*, dd, 2H, J=8.6, 1.1 Hz), 6.37 (*anti*, dd, 2H, J=8.6, 0.9 Hz), 4.96 (*anti*, d, 1H, J=9.9 Hz), 4.94 (*syn*, d, 2H, J=7.9 Hz), 3.96 (*syn*, d, 1H, J=7.9 Hz), 3.88 (*anti*, d, 1H, J=9.9 Hz), 3.66 (*syn*, s, 3H), 3.46 (*anti*, s, 3H).^{13}C NMR (125 MHz, CDCl$_3$) δ 172.79, 171.85, 147.00, 146.63, 144.47, 140.54, 135.49,129.74, 129.23, 129.04, 128.99, 128.87, 128.83, 128.71, 128.56,128.40, 127.65, 127.61, 127.23, 126.83, 117.92, 117.72, 113.92,113.86, 61.08, 60.16, 60.01, 56.56, 52.17, 52.00.

5.2.5 3-Methyl-1,4-diphenylazetidin-2-one, 6b
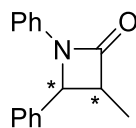
Syn- ^{1}H NMR (501 MHz, CDCl$_3$) δ 7.40 – 7.20 (m, 9H), 7.00 – 7.10 (m, 1H), 5.19 (d, *J* = 5.9 Hz, 1H), 3.71 – 3.66 (m, 1H), 0.88 (d, *J* = 7.6 Hz, 3H).

Anti- ^{1}H NMR (501 MHz, CDCl$_3$) δ 7.40 – 7.00 (m, 10 H), 4.58 (d, *J* = 2.4 Hz, 1H), 3.13 (qd, *J* = 7.4, 2.4 Hz, 1H), 1.48 (d, *J* = 7.4 Hz, 3H).

^{13}C NMR (126 MHz, CDCl$_3$) δ 169.1, 138.3, 135.5, 129.5, 127.3, 127.2, 127.1, 124.0, 115.7, 57.7, 48.6, 7.9.

Literature values:(198)

Syn - 1H NMR (400 MHz, CDCl$_3$) δ: 0.89 (3H, d, J = 8.0 Hz), 3.69 (1H, qd, J = 8.0, 5.6 Hz), 5.20 (1H, d, J = 5.6 Hz), 7.03−7.07 (1H, m), 7.23−7.28 (4H, m), 7.31−7.39 (5H, m); 13C NMR (100 MHz, CDCl3) δ: 9.77, 49.38, 58.47, 117.3, 123.9, 127.1, 128.3, 128.9, 129.2, 135.2, 137.9, 168.7.

Non-cyclised product: methyl 2-methyl-3-diphenyl-3-(N-phenylamino)propionate, **7b**
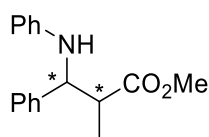
Syn - ¹H NMR (501 MHz, CDCl₃) δ 7.40 – 7.00 (m, 8H), 6.64 (t, *J* = 7.3 Hz, 1H), , 6.52 (dd, *J* = 8.6, 1.0 Hz, 2H), 4.72 (s, 1H), 4.58 (d, *J* = 2.4 Hz, 1H), 4.52 (s, 1H), 3.61 (s, 3H), 2.96 (qd, *J* = 7.1, 5.2 Hz, 1H), 1.35 (d, *J* = 7.2 Hz, 2H), 1.16 (d, *J* = 7.1 Hz, 4H), 1.01 (t, *J* = 7.3 Hz, 4H).

Anti - ¹H NMR (501 MHz, CDCl₃) δ 7.40 – 7.00 (m, 8H), 6.64 (t, *J* = 7.3 Hz, 1H), 6.60 (dd, *J* = 8.6, 0.9 Hz, 1H), 5.19 (d, *J* = 5.9 Hz, 2H), 4.92 (s, 1H), 4.29 (s, 1H), 3.61 (s, 3H), 3.13 (qd, *J* = 7.4, 2.4 Hz, 1H), 1.35 (d, *J* = 7.2 Hz, 3H).

¹³C NMR (126 MHz, CDCl₃) δ 168.60, 168.46, 138.0, 135.1, 129.0 128.9, 128.5, 128.2, 127.0, 126.7, 126.0, 123.8, 117.0, 58.4, 49.3, 9.8.

Literature values:(200)

¹H-NMR (200 MHz, CDCl₃): 1.56 (s, NH), 3.69 (s, 3H), 3.96 (d, 1H, *J* = 8 Hz), 4.95 (d, 1H, *J* = 8 Hz), 6.54-6.65 (m, 5H), 7.00-7.26 (m ,10H); ¹³C-NMR (50 MHz, CDCl₃):- for major *syn* isomer: 52.2, 54.8, 58.9, 114.1, 117.9, 127.0, 127.4, 127.6, 127.7, 128.5, 128.9, 129.2, 135.7, 140.7, 146.9, 173.7; additional signals for minor *anti* isomer: 52.4, 61.3.

5.2.6   *tert*-Butyl 3-anilino-2-methyl-3-phenylpropanoate, **7d**
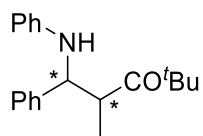
Syn - ¹H NMR (501 MHz, CDCl₃) δ 7.42 – 7.34 (m, 2H), 7.34 – 7.25 (m, 2H), 7.17 – 7.10 (m, 1H), 7.10 – 7.01 (m, 2H), 6.67 (dd, *J* = 8.5, 1.0 Hz, 1H), 6.62 (tt, *J* = 7.4, 1.0 Hz, 1H), 6.59 (dd, *J* = 8.6, 1.0 Hz, 1H), 6.50 (dd, *J* = 8.6, 1.0 Hz, 2H), 4.66 (t, *J* = 5.3 Hz, 1H), 4.24 (d, *J* = 5.7 Hz, 1H), 2.89 – 2.83 (m, 1H), 1.32 (s, 9H), 1.10 (d, *J* = 7.1 Hz, 3H).

^{13}C NMR (126 MHz, CDCl$_3$) δ 173.5, 141.0, 140.0, 129.5, 129.3, 129.2, 128.9, 128.6, 128.5, 127.3, 127.2, 126.3, 126.1, 118.9, 117.5, 113.4, 113.6, 81.1, 56.0, 54.5, 47.1, 28.7, 28.0, 12.2.

Literature values:(198)

syn: A colourless solid; mp 103.5−104.0 °C; 1H NMR (400 MHz, CDCl$_3$) δ: 1.11 (3H, d, J = 6.8 Hz), 1.33 (9H, s), 2.83 (1H, qd, J = 6.8, 6.0 Hz), 4.20 (1H, br), 4.59 (1H, d, J = 6.0 Hz), 6.44− 6.48 (2H, m) 6.65−6.69 (2H, m), 7.19−7.339 (5H, m); 13C NMR (100 MHz, CDCl$_3$) δ: 12.08, 47.14, 55.83, 60.90, 81.10, 114.9, 115.0, 126.9, 127.0, 128.2, 141.0, 141.3, 151.8, 173.3.

6 NMR Spectra

6.1 2-Morpholinbenzoxazole
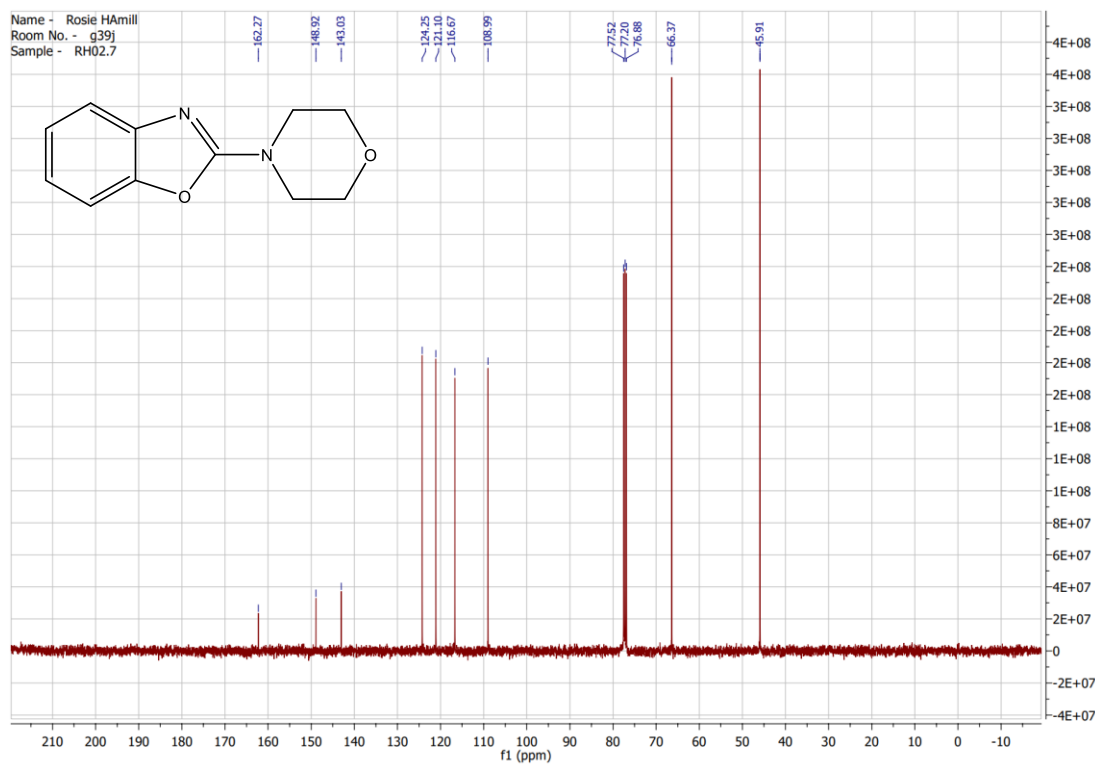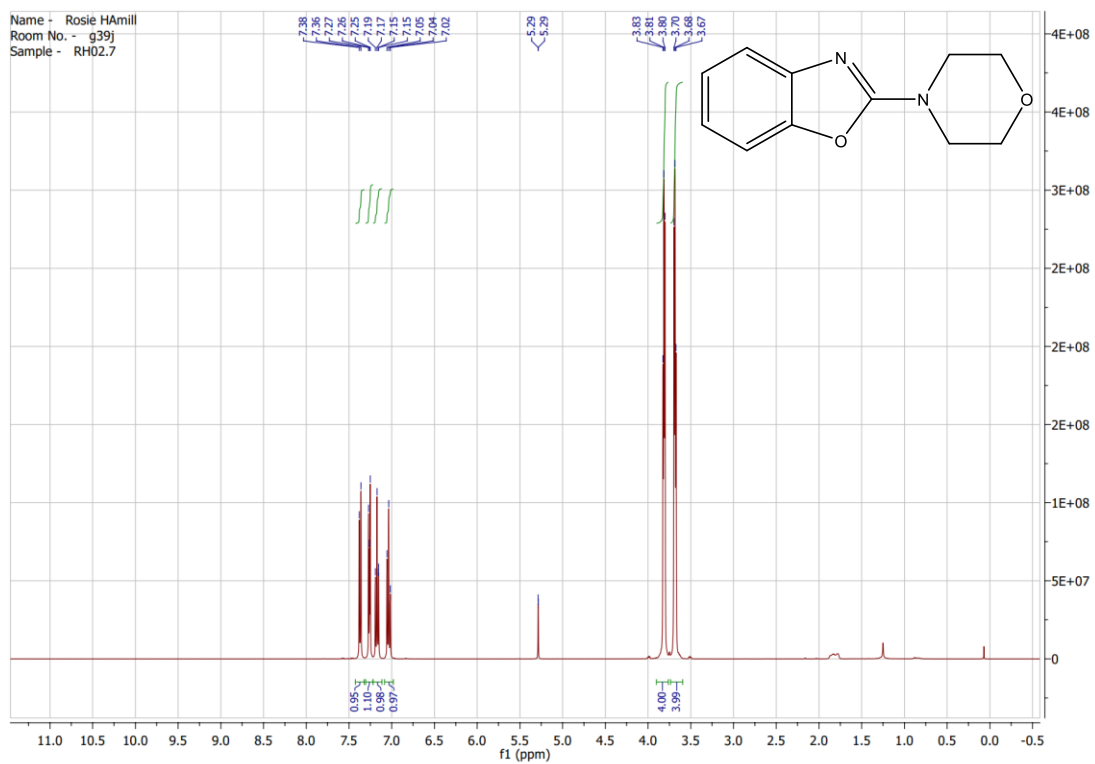
6.2 Electrodeposition of Zinc

6.2.1 Blaise Reaction Flow Cell ^{1}H NMR 2 h
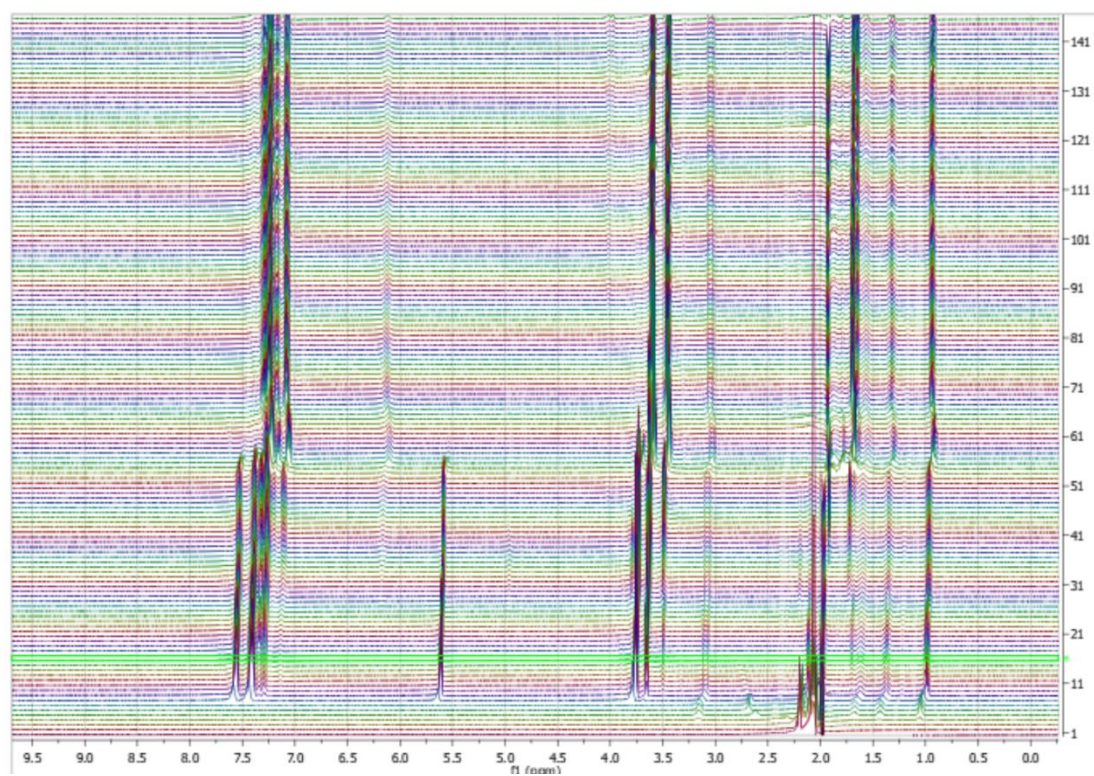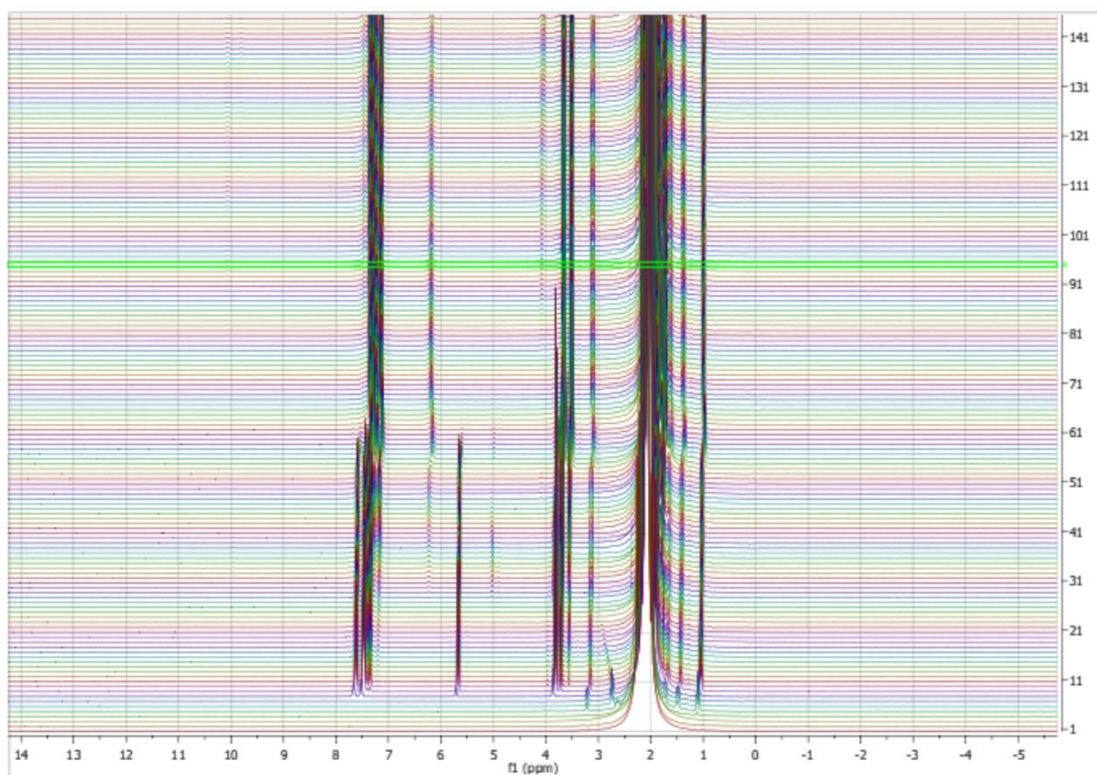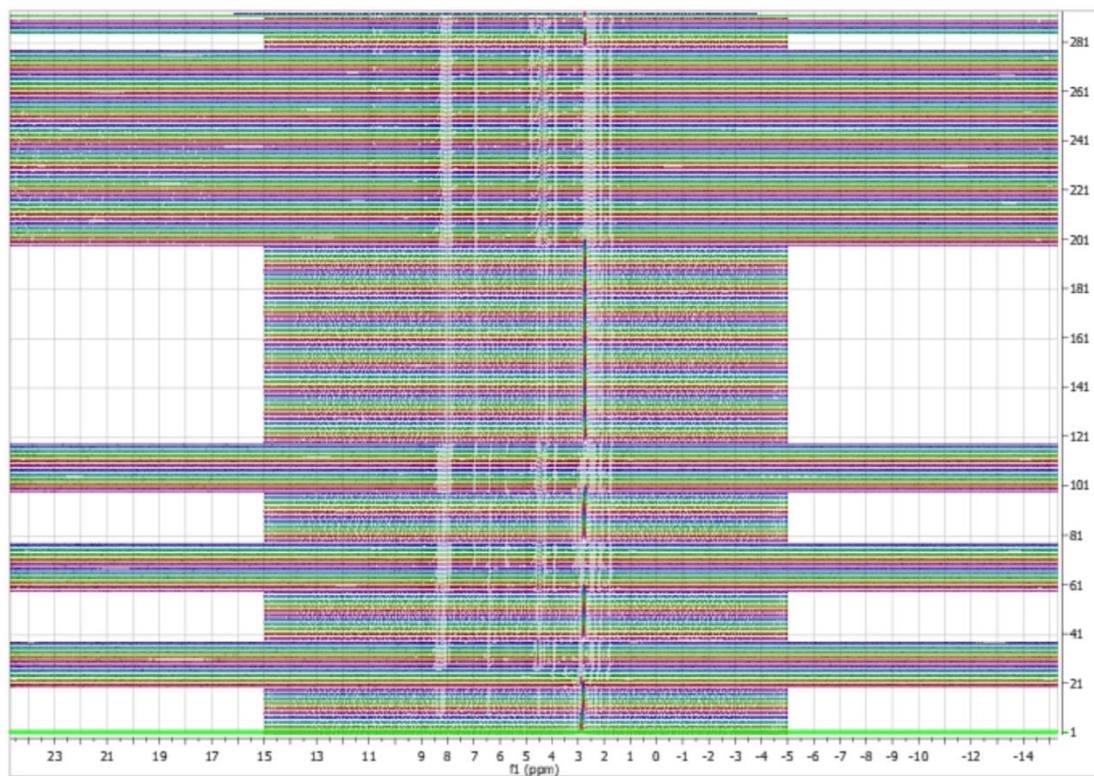
6.2.2   Blaise Reaction Flow Cell ^{1}H NMR 5 h
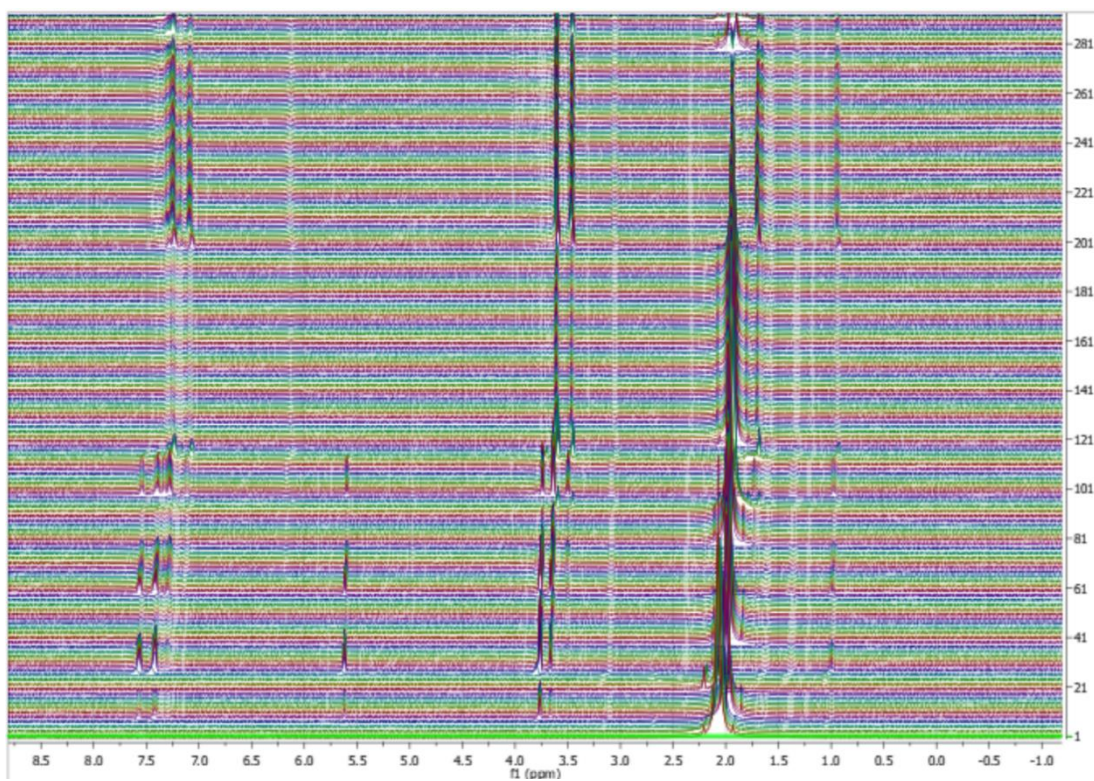
6.2.3 Methyl 2-methyl-3-oxo-butanoate, **2a**
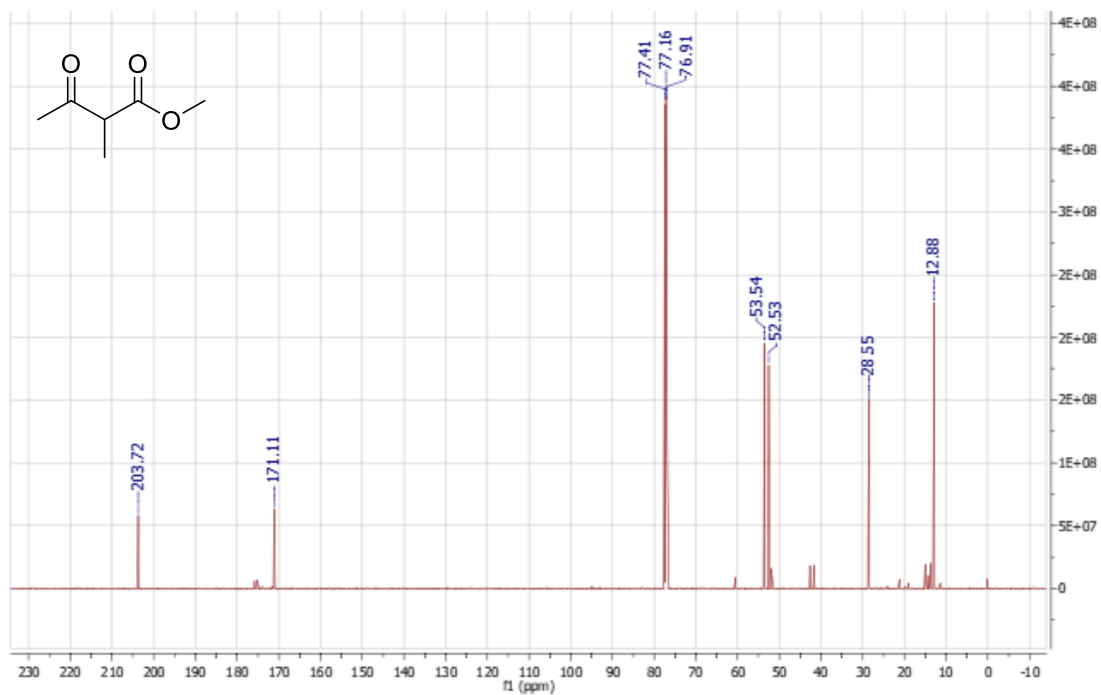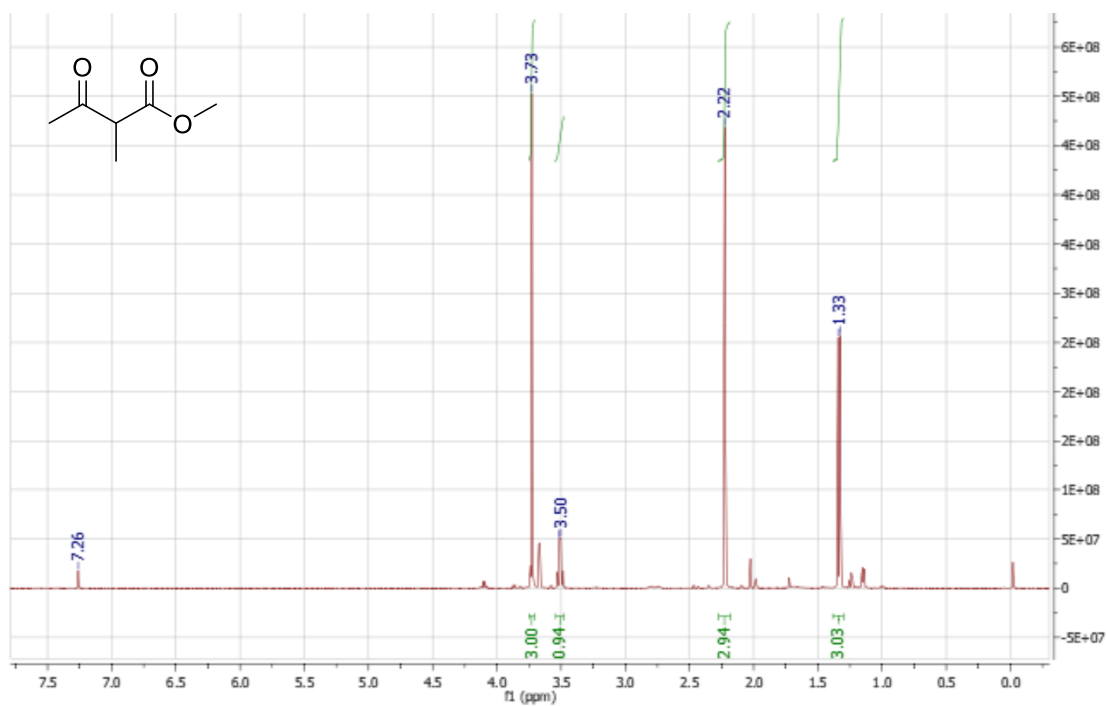
6.2.4   Methyl-3-oxo-2-phenyl-butanoate, **2b & 2c**
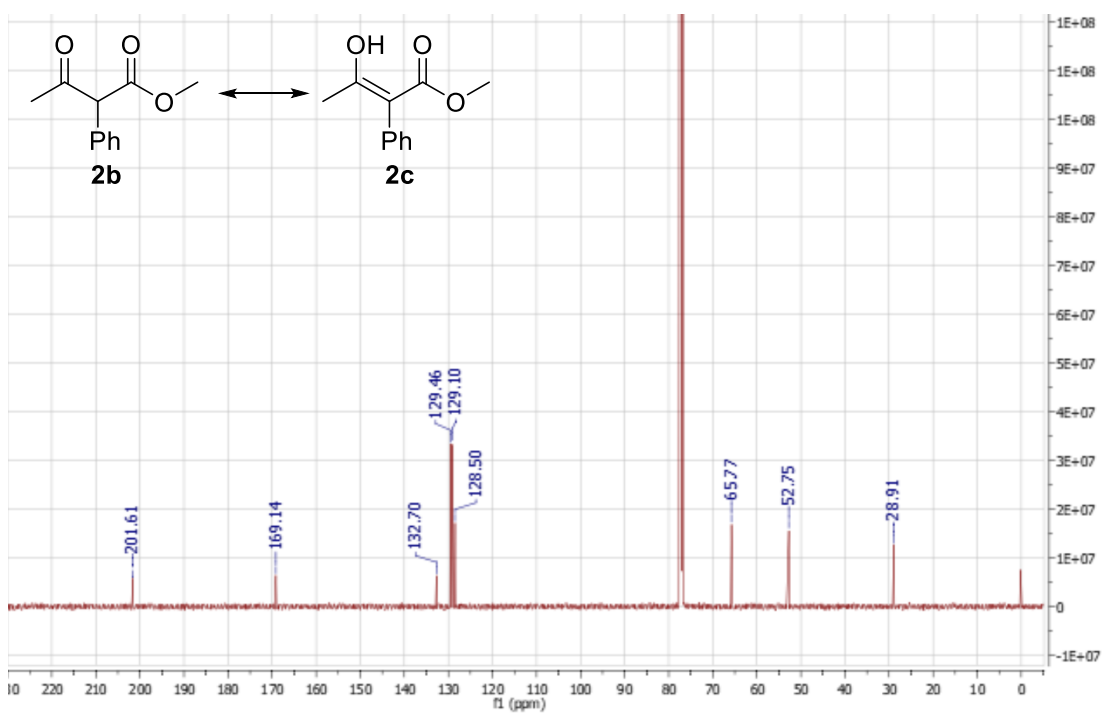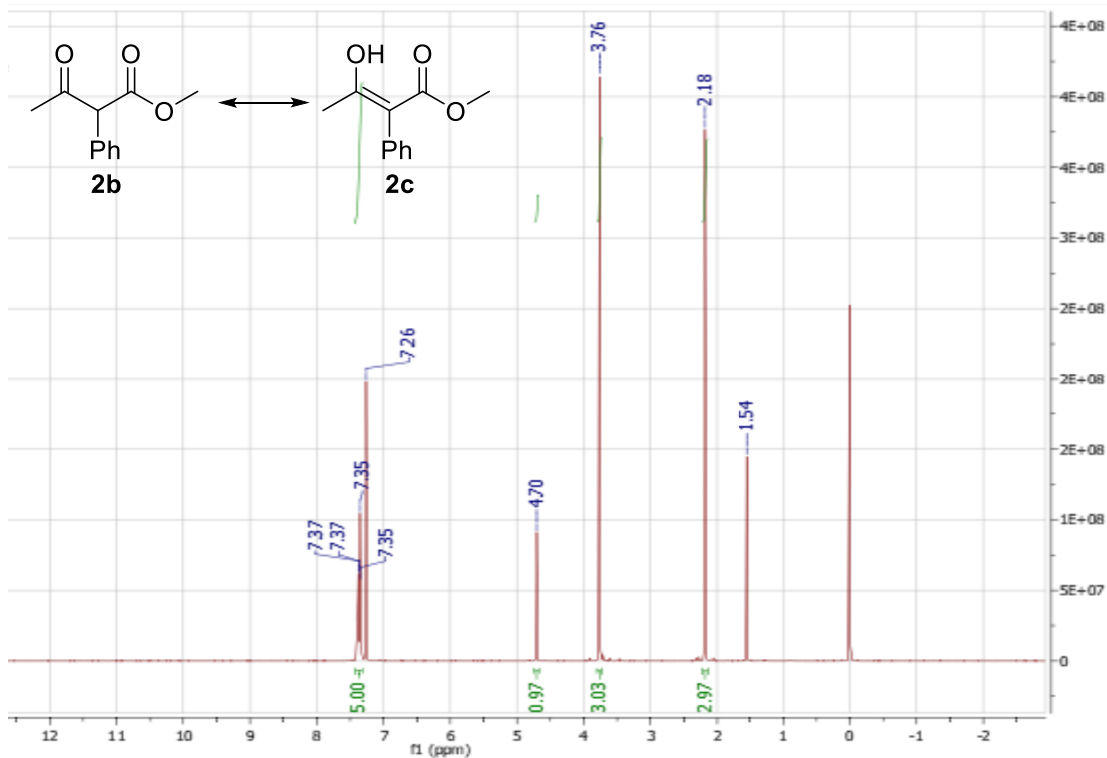
6.2.5 Methyl 3-hydroxy-2-methyl-3-phenyl-propanoate, **3a**
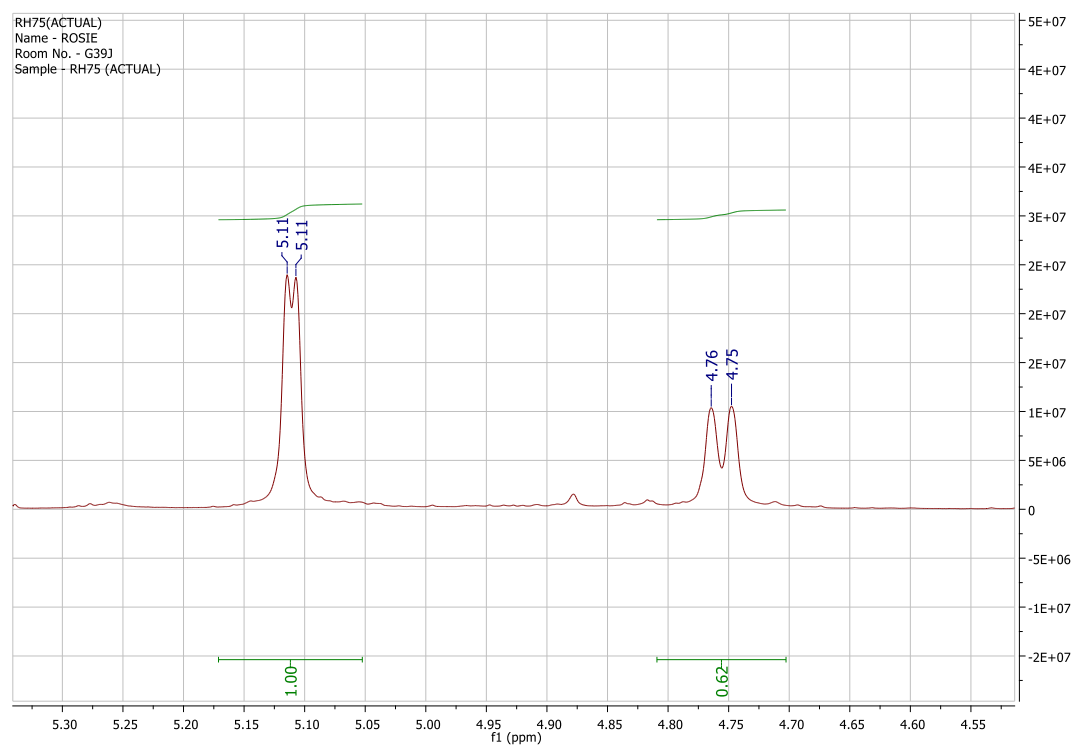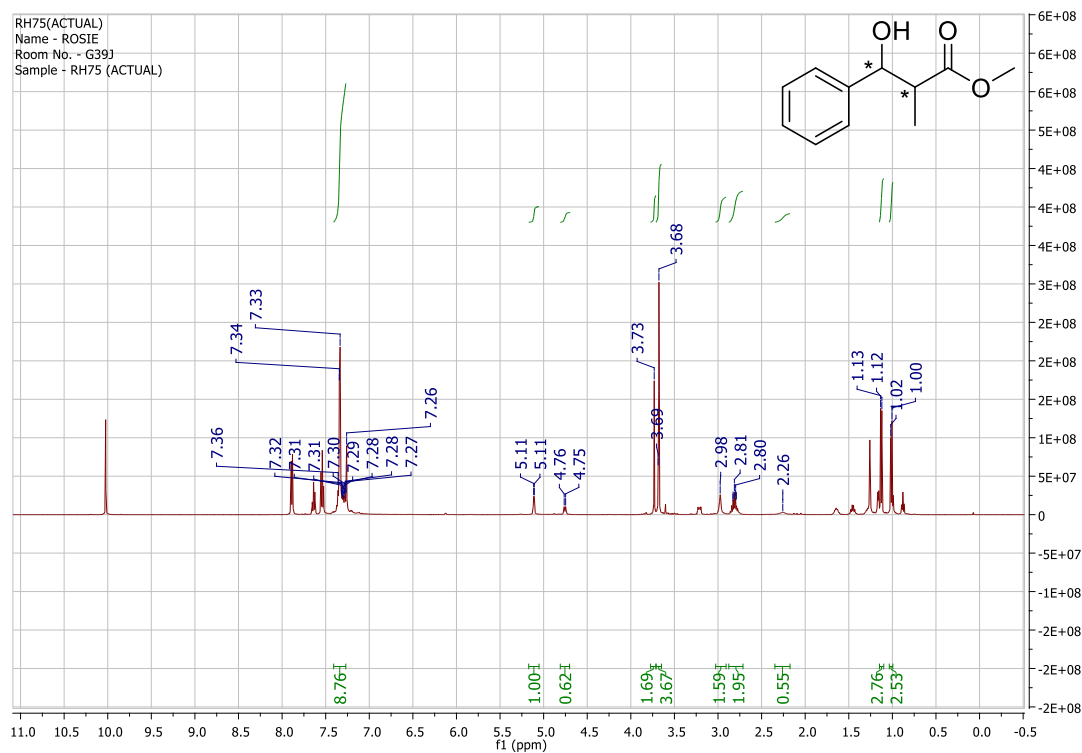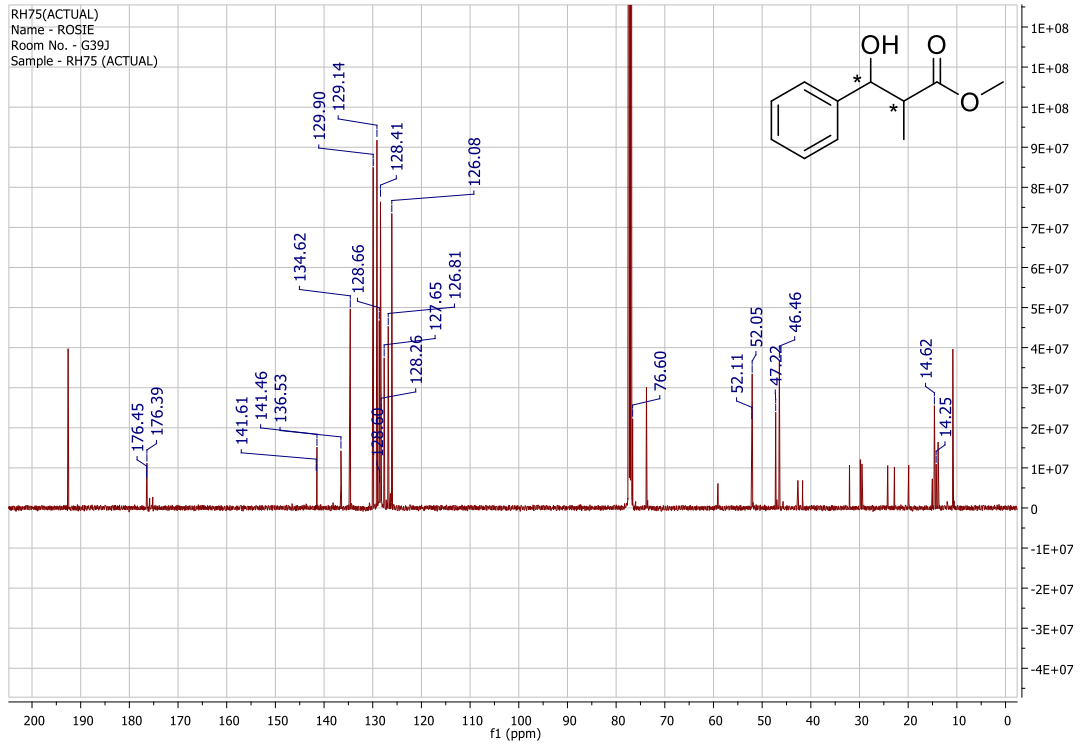
6.2.6   1,3,4-triphenyl-2-azetidinone, **6a**
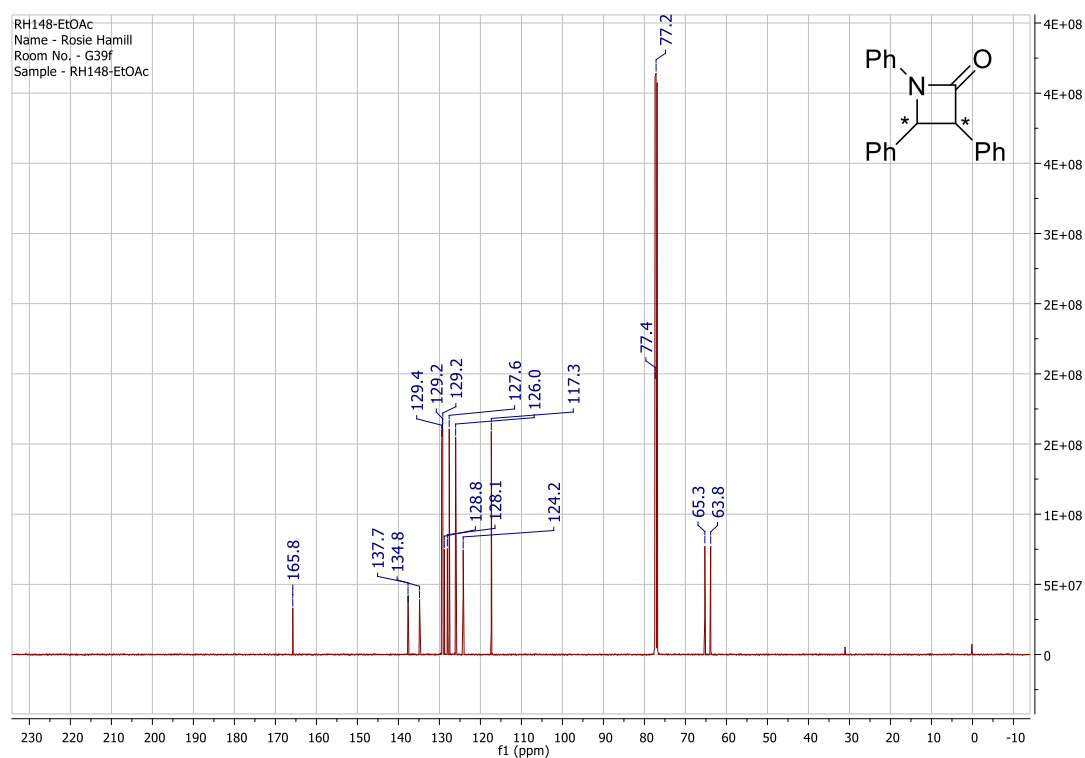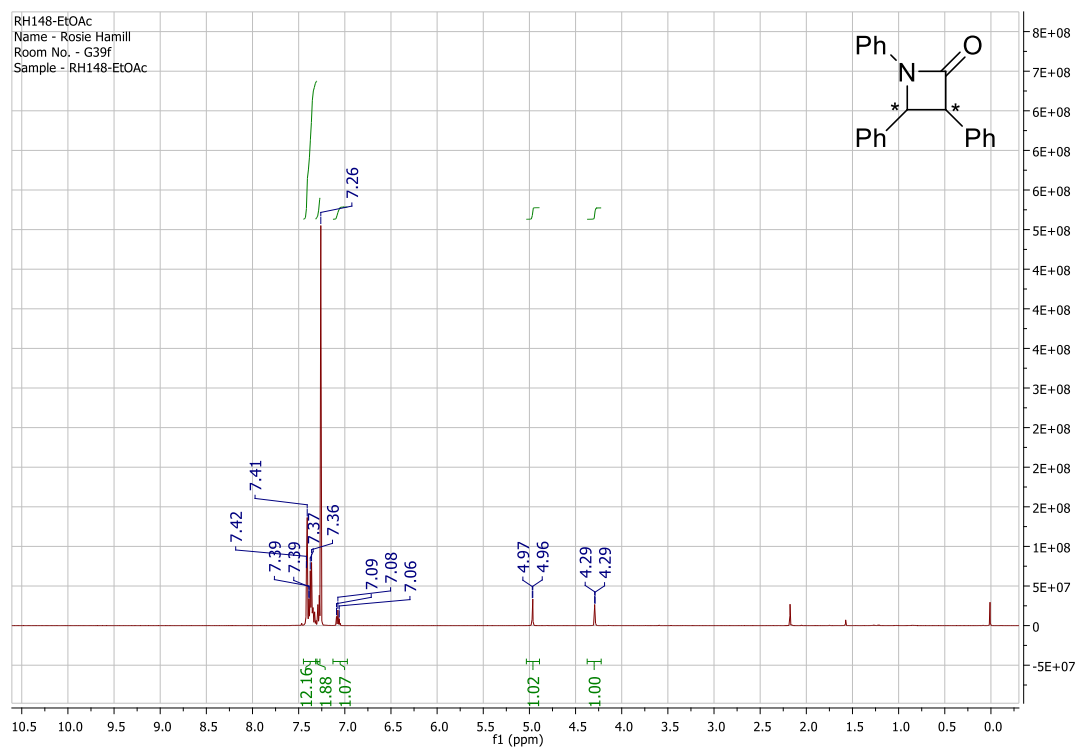
6.2.7   3-Methyl-1,4-diphenylazetidin-2-one, **6b**
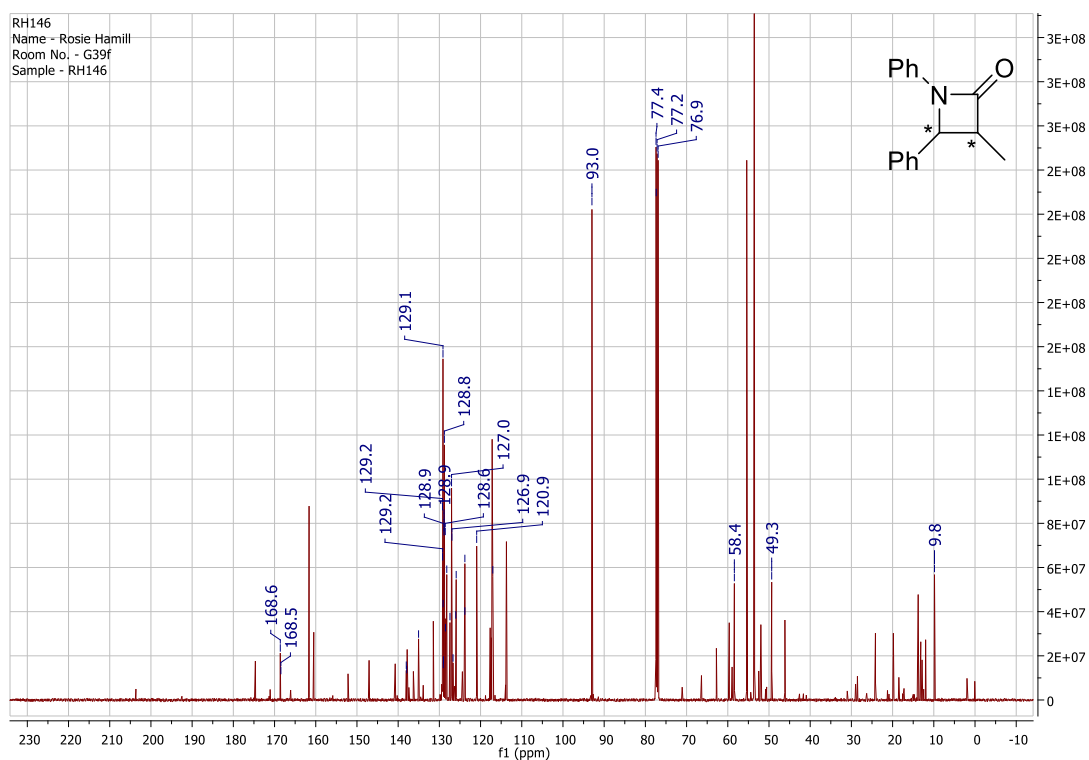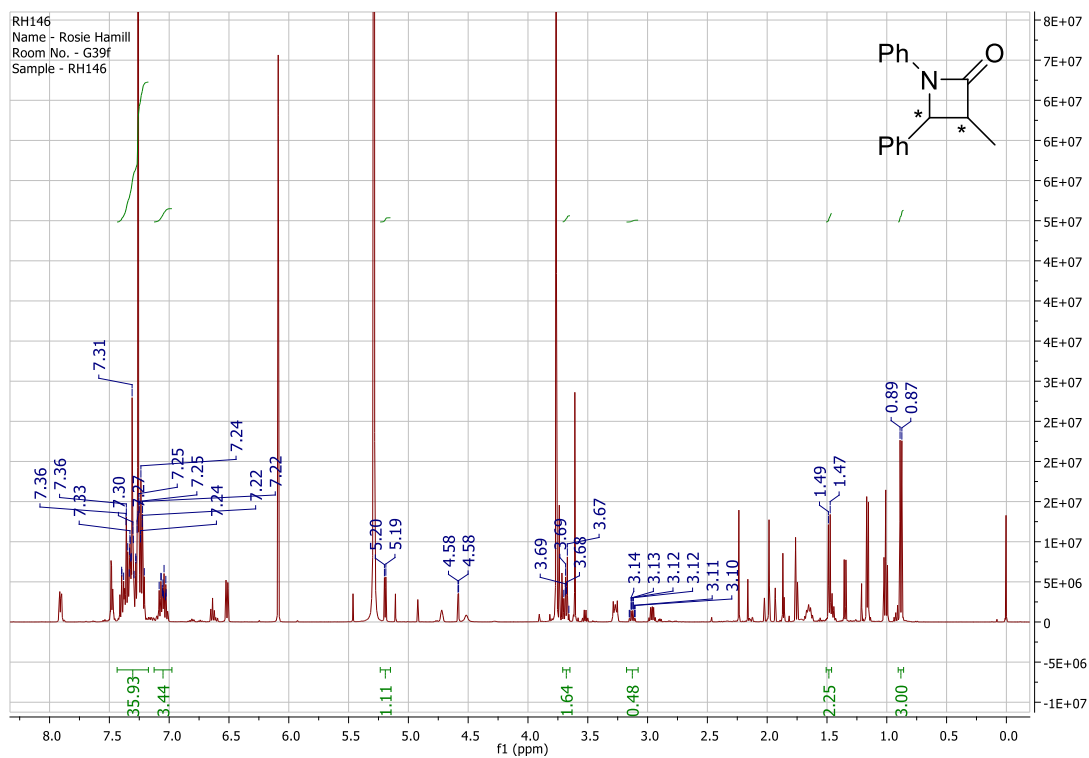
6.2.8   *tert*-Butyl 3-anilino-2-methyl-3-phenylpropanoate
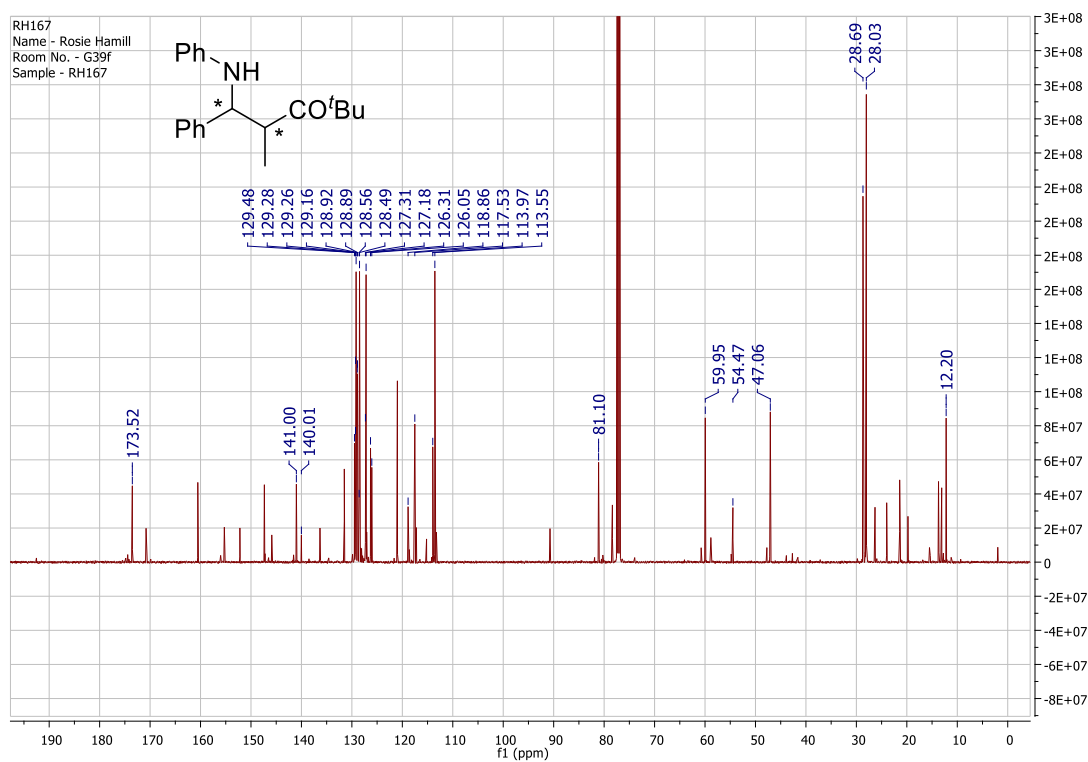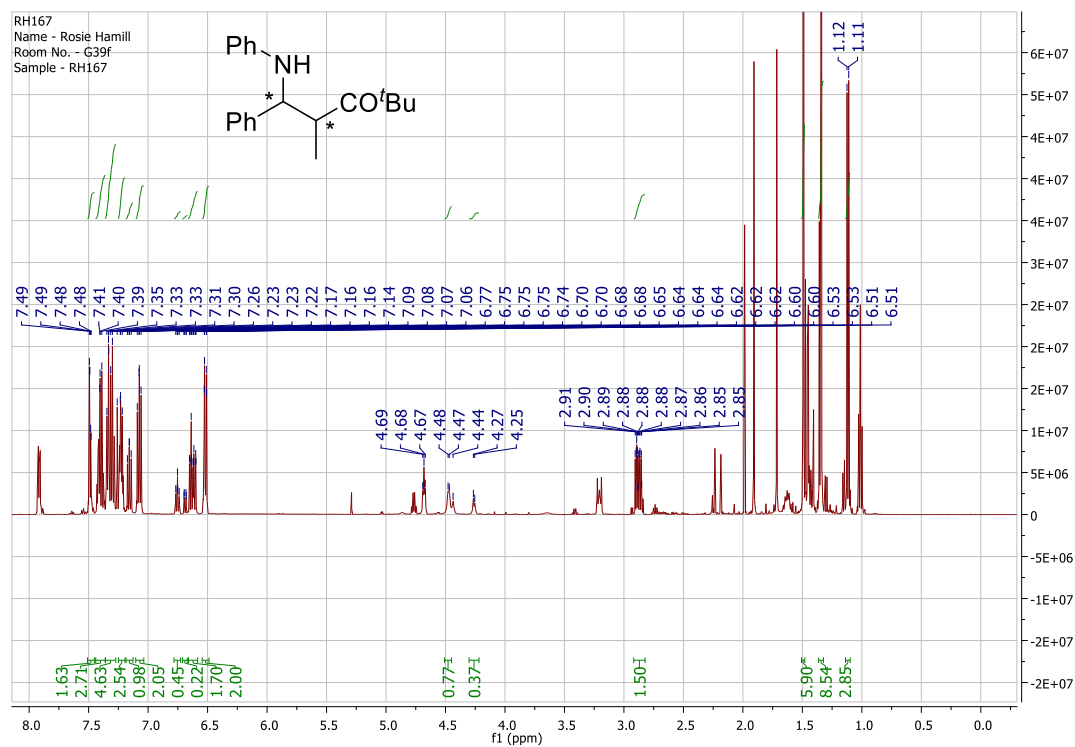
7 References

1. Hoffmann, N. (2015). Electron and hydrogen transfer in organic photochemical reactions. J. Phys. Org. Chem. *28*, 121–136.

2. Pletcher, D., and Walsh, F.C. (1993). Industrial Electrochemistry (Dordrecht: Springer Netherlands).

3. Horn, E.J., Rosen, B.R., and Baran, P.S. (2016). Synthetic organic electrochemistry: An enabling and innately sustainable method. ACS Cent. Sci. *2*, 302–308.

4. Hall Process Production and Commercialization of Aluminum - National Historic Chemical Landmark - American Chemical Society Available at: https://www.acs.org/content/acs/en/education/whatischemistry/landmarks/alu minumprocess.html.

5. O'Brien, T.F.F., Bommaraju, T.V. V, Hine, F., O'Brien, T.F.F., Bommaraju, T.V. V, and Hine, F. (2005). History of the Chlor-Alkali Industry (Springer US).

6. Lipp, A., Selt, M., Ferenc, D., Schollmeyer, D., Waldvogel, S.R., and Opatz, T. (2019). Total Synthesis of (-)-Oxycodone via Anodic Aryl-Aryl Coupling. Org. Lett. *21*, 1828–1831.

7. O-Brien, A.G., Maruyama, A., Inokuma, Y., Fujita, M., Baran, P.S., and Blackmond, D.G. (2014). Radical C-H functionalization of heteroarenes under electrochemical control. Angew. Chemie - Int. Ed. *53*, 11868–11871.

8. Corey, E.J., and Sauers, R.R. (1959). The Synthesis of Pentacyclosqualene (8, 8'-Cycloönocerene) and the α- and β-Onoceradienes. J. Am. Chem. Soc. *81*,

1739–1743.

9. Mihelcic, J., and Moeller, K.D. (2004). Oxidative cyclizations: The asymmetric synthesis of (-)-alliacol A. J. Am. Chem. Soc. *126*, 9106–9111.

10. Kataoka, K., Hagiwara, Y., Midorikawa, K., Suga, S., and Yoshida, J.I. (2008). Practical electrochemical iodination of aromatic compounds. Org. Process Res. Dev. *12*, 1130–1136.

11. Sequeira, C.A.C., and Santos, D.M.F. (2009). Electrochemical Routes for Industrial Synthesis. J. Braz. Chem. Soc *20*, 387–406.

12. Iwasaki, T., and Harada, K. (1974). Electroreductive coupling of Schiff bases with alkyl halides. Synthesis of amino acids. J. Chem. Soc. Chem. Commun., 338–339.

13. Shono, T., and Mitani, M. (1971). Electroorganic Chemistry. VIII. Intramolecular Cycloaddition of Nonconjugate Olefinic Ketones to Form Cyclic Tertiary Alcohols. J. Am. Chem. Soc. *93*, 5284–5286.

14. Eilenberg, W., and Schäfer, H.J. (1984). Anodic intramolecular arylation of enaminones. Tetrahedron Lett. *25*, 5023–5026.

15. Saravanan, K., Selvamani, V., Kulangiappar, K., Velayutham, D., and Suryanarayanan, V. (2013). Regioselective anodic α-methoxylation of 2-oxazolidinone on boron doped diamond in acidic methanol medium. Electrochem. commun. *28*, 31–33.

16. Jiang, Y., Xu, K., and Zeng, C. (2018). Use of Electrochemistry in the Synthesis of Heterocyclic Structures. Chem. Rev. *118*, 4485–4540.

17. Meyer, T.H., Choi, I., Tian, C., and Ackermann, L. (2020). Powering the

Future: How Can Electrochemistry Make a Difference in Organic Synthesis? Chem.

18. Hartle, M.D. (2020). Organic electrosynthesis amps up the potential for synthetic innovation, while technological advances decrease the resistance for entry into this electrifying field. Electrosynthesis Watt's New *4*, 1–9.

19. Frantz, D.E., Fässler, R., Tomooka, C.S., and Carreira, E.M. (2000). The discovery of novel reactivity in the development of C-C bond-forming reactions: In situ generation of zinc acetylides with Zn11/R3N. Acc. Chem. Res. *33*, 373–381.

20. Hilt, G. (2020). Basic Strategies and Types of Applications in Organic Electrochemistry. ChemElectroChem *7*, 395–405.

21. Cardoso, D.S.P., Šljukić, B., Santos, D.M.F., and Sequeira, C.A.C. (2017). Organic Electrosynthesis: From Laboratorial Practice to Industrial Applications. Org. Process Res. Dev. *21*, 1213–1226.

22. Moeller, K.D. (2018). Using Physical Organic Chemistry To Shape the Course of Electrochemical Reactions. Chem. Rev. *118*, 4817–4833.

23. Novaes, L.F.T., Liu, J., Shen, Y., Lu, L., Meinhardt, J.M., and Lin, S. (2021). Electrocatalysis as an enabling technology for organic synthesis. Chem. Soc. Rev.

24. Schotten, C., Nicholls, T.P., Bourne, R.A., Kapur, N., Nguyen, B.N., and Willans, C.E. (2020). Making electrochemistry easily accessible to the synthetic chemist. Green Chem. *22*, 3358–3375.

25. Möhle, S., Zirbes, M., Rodrigo, E., Gieshoff, T., Wiebe, A., and Waldvogel, S.R. (2018). Modern Electrochemical Aspects for the Synthesis of Value-

Added Organic Products. Angew. Chemie - Int. Ed. *57*, 6018–6041.

26. Little, R.D. (2020). A Perspective on Organic Electrochemistry. J. Org. Chem. *85*, 13375–13390.

27. Wiebe, A., Gieshoff, T., Möhle, S., Rodrigo, E., Zirbes, M., and Waldvogel, S.R. (2018). Electrifying Organic Synthesis. Angew. Chemie - Int. Ed. *57*, 5594–5619.

28. Kingston, C., Palkowitz, M.D., Takahira, Y., Vantourout, J.C., Peters, B.K., Kawamata, Y., and Baran, P.S. (2020). A Survival Guide for the "electro-curious." Acc. Chem. Res. *53*, 72–83.

29. Yan, M, Kawamata, Y., and Baran, P.S. (2017). Synthetic Organic Electrochemical Methods since 2000: On the Verge of a Renaissance. Chem. Rev. *117*, 13230–13319.

30. Minteer, S.D., and Baran, P. (2020). Electrifying Synthesis: Recent Advances in the Methods, Materials, and Techniques for Organic Electrosynthesis. Acc. Chem. Res. *53*, 545–546.

31. Yan, M., Kawamata, Y., and Baran, P.S. (2018). Synthetic Organic Electrochemistry: Calling All Engineers. Angew. Chemie Int. Ed. *57*, 4149–4155.

32. Green, R.A., Brown, R.C.D., Pletcher, D., and Harji, B. (2015). A Microflow Electrolysis Cell for Laboratory Synthesis on the Multigram Scale. Org. Process Res. Dev. *19*, 1424–1427.

33. Nicholls, T.P., Schotten, C., and Willans, C.E. (2020). Electrochemistry in continuous systems. Curr. Opin. Green Sustain. Chem. *26*, 100355.

34. Folgueiras-Amador, A.A., Teuten, A.E., Pletcher, D., and Brown, R.C.D. (2020). A design of flow electrolysis cell for "Home" fabrication. React. Chem. Eng. *5*, 712–718.

35. Gütz, C., Stenglein, A., and Waldvogel, S.R. (2017). Highly Modular Flow Cell for Electroorganic Synthesis. Org. Process Res. Dev. *21*, 771–778.

36. Lehmann, M., Scarborough, C.C., Godineau, E., and Battilocchio, C. (2020). An Electrochemical Flow-Through Cell for Rapid Reactions. Ind. Eng. Chem. Res. *59*, 7321–7326.

37. Pletcher, D., Green, R.A., and Brown, R.C.D. (2018). Flow Electrolysis Cells for the Synthetic Organic Chemistry Laboratory. Chem. Rev. *118*, 4573–4591.

38. Folgueiras-Amador, A.A., Philipps, K., Guilbaud, S., Poelakker, J., and Wirth, T. (2017). An Easy-to-Machine Electrochemical Flow Microreactor: Efficient Synthesis of Isoindolinone and Flow Functionalization. Angew. Chemie Int. Ed. *56*, 15446–15450.

39. Noël, T., Cao, Y., and Laudadio, G. (2019). The Fundamentals behind the Use of Flow Reactors in Electrochemistry. Acc. Chem. Res. *52*, 2858–2869.

40. Walsh, F.C., and de León, C.P. (2018). Progress in electrochemical flow reactors for laboratory and pilot scale processing. Electrochim. Acta *280*, 121–148.

41. Maljuric, S., Jud, W., Kappe, C.O., and Cantillo, D. (2020). Translating batch electrochemistry to single-pass continuous flow conditions: an organic chemist's guide. J. Flow Chem. *10*, 181–190.

42. Gao, W.J., Li, W.C., Zeng, C.C., Tian, H.Y., Hu, L.M., and Little, R.D.

(2014). Electrochemically initiated oxidative amination of benzoxazoles using tetraalkylammonium halides as redox catalysts. J. Org. Chem. *79*, 9613–9618.

43. Lide, D.R., Baysinger, G., Berger, L.I., Goldberg, R.N., Kehiaian, H. V, Kuchitsu, K., Roth, D.L., and Zwillinger, D. CRC Handbook of Chemistry and Physics Editor-in-Chief Available at: http://webdelprofesor.ula.ve/ciencias/isolda/libros/handbook.pdf.

44. Chen, H., Cong, G., and Lu, Y.C. (2018). Recent progress in organic redox flow batteries: Active materials, electrolytes and membranes. J. Energy Chem. *27*, 1304–1325.

45. Röckl, J.L., Dörr, M., and Waldvogel, S.R. (2020). Electrosynthesis 2.0 in 1,1,1,3,3,3-Hexafluoroisopropanol/Amine Mixtures. ChemElectroChem *7*, 3686–3694.

46. Kadish, K.M., Wang, L.-L., Thuriere, A., Giribabu, L., Garcia, R., Caemelbecke, E. Van, and Bear, J.L. (2003). Solvent Effects on the Electrochemistry and Spectroelectrochemistry of Diruthenium Complexes. Studies of Ru 2 (L) 4 Cl Where L = 2-CH 3 ap, 2-Fap, and 2,4,6-F 3 ap, and ap Is the 2-Anilinopyridinate Anion. Inorg. Chem. *42*, 8309–8319.

47. Schulz, L., and Waldvogel, S.R. (2019). Solvent Control in Electro-Organic Synthesis. Synlett *30*, 275–285.

48. Zylber, N., Zylber, J., Rollin, Y., Duñach, E., and Perichon, J. (1993). New method of zinc activation by electrochemistry: Synthetic applications to the Blaise reaction. J. Organomet. Chem. *444*, 1–4.

49. Luca, O.R., Gustafson, J.L., Maddox, S.M., Fenwick, A.Q., and Smith, D.C. (2015). Catalysis by electrons and holes: Formal potential scales and

preparative organic electrochemistry. Org. Chem. Front. *2*, 823–848.

50. Maity, A., Frey, B.L., Hoskinson, N.D., and Powers, D.C. (2020). Electrocatalytic C-N Coupling via Anodically Generated Hypervalent Iodine Intermediates. ACS Appl. Mater. Interfaces *142*, 4995.

51. Liu, K., Song, C., and Lei, A. (2018). Recent advances in iodine mediated electrochemical oxidative cross-coupling. Org. Biomol. Chem. *16*, 2375–2387.

52. Tagliatesta, P., Floris, B., and Bellucci, S. (2016). Nanoreactors Based on Porphyrin-Functionalized Carbon Compounds. Org. Nanoreactors From Mol. to Supramol. Org. Compd., 463–518.

53. Cardeña, R., Cercado, B., and Buitrón, G. (2019). Microbial Electrolysis Cell for Biohydrogen Production. Biohydrogen, 159–185.

54. Schmidt-Rohr, K. (2018). How Batteries Store and Release Energy: Explaining Basic Electrochemistry. J. Chem. Educ. *95*, 1801–1810.

55. Pollok, D., and Waldvogel, S.R. (2020). Electro-organic synthesis- a 21st century technique. Chem. Sci. *11*, 12386–12400.

56. Ibanez, J.G., Frontana-Uribe, B.A., and Vasquez-Medrano, R. (2016). Paired electrochemical processes: Overview, systematization, selection criteria, design strategies, and projection. J. Mex. Chem. Soc. *60*, 247–260.

57. Sbei, N., Hardwick, T., and Ahmed, N. (2021). Green Chemistry: Electrochemical Organic Transformations via Paired Electrolysis. ACS Sustain. Chem. Eng. *9*, 6148–6169.

58. Folgueiras-Amador, A.A., and Wirth, T. (2017). Perspectives in flow

electrochemistry. J. Flow Chem. *7*, 94–95.

59.   Tanbouza, N., Ollevier, T., and Lam, K. (2020). Bridging Lab and Industry with Flow Electrochemistry. iScience *23*, 101720.

60.   Ragan, J.A., Raggon, J.W., Hill, P.D., Jones, B.P., McDermott, R.E., Munchhof, M.J., Marx, M.A., Casavant, J.M., Cooper, B.A., Doty, J.L., *et al.* (2003). Cross-coupling methods for the large-scale preparation of an imidazole - Thienopyridine: Synthesis of [2-(3-methyl-3H-imidazol-4-yl)-thieno[3,2-b]pyridin-7-yl] -(2-methyl-1H-indol-5-yl)-amine. Org. Process Res. Dev. *7*, 676–683.

61.   Butters, M., Ebbs, J., Green, S.P., MacRae, J., Morland, M.C., Murtiashaw, C.W., and Pettman, A.J. (2001). Process development of voriconazole: A novel broad-spectrum triazole antifungal agent. Org. Process Res. Dev. *5*, 28–36.

62.   Hardouin, C., Baillard, S., Barière, F., Craquelin, A., Grandjean, M., Janvier, S., Roux, S. Le, Penloup, C., and Russo, O. (2019). Multikilogram Synthesis of a Potent Dual Bcl-2/Bcl-xL Antagonist. 2. Manufacture of the 1,3-Diamine Moiety and Improvement of the Final Coupling Reaction. Org. Process Res. Dev. *24*, 670–685.

63.   Rollin, Y., Gebehenne, C., Derien, S., Duñach, E., and Perichon, J. (1993). Electrochemical activation of zinc in the coupling reaction of α-bromoesters with carbonyl compounds. J. Organomet. Chem. *461*, 9–13.

64.   Cossío, F.P., Arrieta, A., and Sierra, M.A. (2008). The Mechanism of the Ketene−Imine (Staudinger) Reaction in Its Centennial: Still an Unsolved Problem? Acc. Chem. Res. *41*, 925–936.

65. Mandler, M.D.D., Truong, P.M.M., Zavalij, P.Y.Y., and Doyle, M.P.P. (2014). Catalytic Conversion of Diazocarbonyl Compounds to Imines: Applications to the Synthesis of Tetrahydropyrimidines and β-Lactams Scheme 1. Previous Examples of Rhodium Catalyzed Formation of Imines. Org. Lett *16*, 7.

66. Jian, S.Z., Ma, C., and Wang, Y.G. (2005). An efficient and diastereoselective synthesis of trans β-lactams and β-aminocarbonyl compounds. Synthesis (Stuttg)., 725–730.

67. Jian, S.Z., Yuan, Q., and Wang, Y.G. (2006). Diastereoselective Synthesis of trans β-lactams on soluble polymer support. Synthesis (Stuttg)., 1829–1835.

68. Townes, J.A., Evans, M.A., Queffelec, J., Taylor, S.J., and Morken, J.P. (2002). Stereoselective synthesis of trans β-lactams through iridium-catalyzed reductive coupling of imines and acrylates. Org. Lett. *4*, 2537–2540.

69. Blanksby, S.J., and Ellison, G.B. (2003). Bond dissociation energies of organic molecules. Acc. Chem. Res. *36*, 255–263.

70. Verschueren, R.H., and Borggraeve, W.M. De (2019). Electrochemistry and Photoredox Catalysis: A Comparative Evaluation in Organic Synthesis. Molecules *24*, 2122.

71. Liu, J., Lu, L., Wood, D., and Lin, S. (2020). New Redox Strategies in Organic Synthesis by Means of Electrochemistry and Photochemistry. ACS Cent. Sci. *6*, 1317–1340.

72. Oliva, M., Coppola, G.A., der Eycken, E.V. Van, and Sharma, U.K. (2021). Photochemical and Electrochemical Strategies towards Benzylic C−H Functionalization: A Recent Update. Adv. Synth. Catal. *363*, 1810–1834.

73. Barrett, S.M., Stratakes, B.M., Chambers, M.B., Kurtz, D.A., Pitman, C.L., Dempsey, J.L., and Miller, A.J.M. (2020). Mechanistic basis for tuning iridium hydride photochemistry from H 2 evolution to hydride transfer hydrodechlorination. Chem. Sci. *11*, 6442–6449.

74. Romero, N.A., Margrey, K.A., Tay, N.E., and Nicewicz, D.A. (2015). Site-selective arene C-H amination via photoredox catalysis. Science (80-.). *349*, 1326–1330.

75. Rossberg, M., Lendle, W., Pfleiderer, G., Tögel, A., Dreher, E.-L., Langer, E., Rassaerts, H., Kleinschmidt, P., Strack, H., Cook, R., *et al.* (2006). Chlorinated Hydrocarbons. Ullmann's Encycl. Ind. Chem.

76. Labinger, J.A. (2012). Alkane Functionalization via Electrophilic Activation. Alkane Funct. via Electrophilic Act., 17–71.

77. Horn, E.J., Rosen, B.R., Chen, Y., Tang, J., Chen, K., Eastgate, M.D., and Baran, P.S. (2016). Scalable and sustainable electrochemical allylic C-H oxidation. Nature *533*, 77–81.

78. Kawamata, Y., Yan, M., Liu, Z., Bao, D.-H., Chen, J., Starr, J.T., and Baran, P.S. (2017). Scalable, Electrochemical Oxidation of Unactivated C–H Bonds. J. Am. Chem. Soc. *139*, 7448–7451.

79. Waterman, R. (2013). σ-Bond Metathesis: A 30-Year Retrospective. Organometallics *32*, 7249–7263.

80. Qi, X., Li, Y., Bai, R., and Lan, Y. (2017). Mechanism of Rhodium-Catalyzed C–H Functionalization: Advances in Theoretical Investigation. Acc. Chem. Res. *50*, 2799–2808.

81. Fernández, D.F., Gulías, M., Mascareñas, J.L., and López, F. (2017).

Iridium(I)-Catalyzed Intramolecular Hydrocarbonation of Alkenes: Efficient Access to Cyclic Systems Bearing Quaternary Stereocenters. Angew. Chemie Int. Ed. *56*, 9541–9545.

82. Labinger, J.A., and Bercaw, J.E. (2015). Mechanistic studies on the Shilov system: A retrospective. J. Organomet. Chem. *793*, 47–53.

83. Abdellaoui, F., Youssef, C., Ammar, H. Ben, Roisnel, T., Soulé, J.F., and Doucet, H. (2016). Palladium-Catalyzed Regioselective C-H Bond Arylations of Benzoxazoles and Benzothiazoles at the C7 Position. ACS Catal. *6*, 4248–4252.

84. Arredondo, V., Hiew, S.C., Gutman, E.S., Premachandra, I.D.U.A., and Van Vranken, D.L. (2017). Enantioselective Palladium-Catalyzed Carbene Insertion into the N−H Bonds of Aromatic Heterocycles. Angew. Chemie Int. Ed. *56*, 4156–4159.

85. Littke, A.F., and Fu, G.C. (2002). Palladium-Catalyzed Coupling Reactions of Aryl Chlorides. Angew. Chemie Int. Ed. *41*, 4176–4211.

86. Iglesias, Á., Álvarez, R., De-Lera, Á.R., and Muñiz, K. (2012). Palladium-catalyzed intermolecular C(sp 3)-H amidation. Angew. Chemie - Int. Ed. *51*, 2225–2228.

87. Heck, R.F. (2002). Palladium-catalyzed reactions of organic halides with olefins. Acc. Chem. Res. *12*, 146–151. Available at: https://pubs.acs.org/doi/pdf/10.1021/ar50136a006.

88. Kazmierski, I., Gosmini, C., Paris, J.M., and Périchon, J. (2003). New progress in the cobalt-catalysed synthesis of aromatic organozinc compounds by reduction of aromatic halides by zinc dust. Tetrahedron Lett. *44*, 6417–

6420.

89.   Moselage, M., Li, J., and Ackermann, L. (2015). Cobalt-Catalyzed C–H Activation. ACS Catal. *6*, 498–525.

90.   Huang, M.G., Shi, S., Li, M., Liu, Y.J., and Liu, Y.J. (2021). Salicylaldehyde-Promoted Cobalt-Catalyzed C-H/N-H Annulation of Indolyl Amides with Alkynes: Direct Synthesis of a 5-HT3 Receptor Antagonist Analogue. Org. Lett. *23*, 7094–7099.

91.   Zhang, R.K., Chen, K., Huang, X., Wohlschlager, L., Renata, H., and Arnold, F.H. (2018). Enzymatic assembly of carbon–carbon bonds via iron-catalysed sp3 C–H functionalization. Nat. 2018 5657737 *565*, 67–72.

92.   Doba, T., Ilies, L., Sato, W., Shang, R., and Nakamura, E. (2021). Iron-catalysed regioselective thienyl C–H/C–H coupling. Nat. Catal. 2021 47 *4*, 631–638.

93.   Doba, T., Matsubara, T., Ilies, L., Shang, R., and Nakamura, E. (2019). Homocoupling-free iron-catalysed twofold C–H activation/cross-couplings of aromatics via transient connection of reactants. Nat. Catal. 2019 25 *2*, 400–406.

94.   Mo, J., Messinis, A.M., Oliveira, J.C.A., Demeshko, S., Meyer, F., and Ackermann, L. (2021). Iron-Catalyzed Triazole-Enabled C–H Activation with Bicyclopropylidenes. ACS Catal. *11*, 1053–1064.

95.   Shang, R., Ilies, L., and Nakamura, E. (2017). Iron-Catalyzed C–H Bond Activation. Chem. Rev. *117*, 9086–9139.

96.   Wang, H., Pesciaioli, F., Oliveira, J.C.A., Warratz, S., and Ackermann, L. (2017). Synergistic Manganese(I) C−H Activation Catalysis in Continuous

Flow: Chemoselective Hydroarylation. Angew. Chemie *129*, 15259–15263.

97.   Liu, W., and Ackermann, L. (2016). Manganese-Catalyzed C–H Activation. ACS Catal. *6*, 3743–3752.

98.   Yahaya, N.P., Appleby, K.M., Teh, M., Wagner, C., Troschke, E., Bray, J.T.W., Duckett, S.B., Hammarback, L.A., Ward, J.S., Milani, J., *et al.* (2016). Manganese(I)-Catalyzed C−H Activation: The Key Role of a 7-Membered Manganacycle in H-Transfer and Reductive Elimination. Angew. Chemie *128*, 12643–12647.

99.   Capaldo, L., Ravelli, D., and Fagnoni, M. (2022). Direct Photocatalyzed Hydrogen Atom Transfer (HAT) for Aliphatic C-H Bonds Elaboration. Chem. Rev. *122*, 1875–1924.

100.   Singh, M., Yadav, A.K., Yadav, L.D.S., and Singh, R.K.P. (2017). Visible light photocatalysis with benzophenone for radical thiol-ene reactions. Tetrahedron Lett. *58*, 2206–2208.

101.   Nguyen, T.H., Chau, N.T.T., Castanet, A.S., Nguyen, K.P.P., and Mortier, J. (2007). First general, direct, and regioselective synthesis of substituted methoxybenzoic acids by ortho metalation. J. Org. Chem. *72*, 3419–3429.

102.   Murphy, J.M., Liao, X., and Hartwig, J.F. (2007). Meta halogenation of 1,3-disubstituted arenes via iridium-catalyzed arene borylation. J. Am. Chem. Soc. *129*, 15434–15435.

103.   Wang, D.-H., Mei, T.-S., and Yu, J.-Q. (2008). Versatile Pd(II)-Catalyzed C−H Activation/Aryl−Aryl Coupling of Benzoic and Phenyl Acetic Acids. J. Am. Chem. Soc. *130*, 17676–17677.

104.   Onda, K., Shiraki, R., Ogiyama, T., Yokoyama, K., Momose, K., Katayama,

N., Orita, M., Yamaguchi, T., Furutani, M., Hamada, N., *et al.* (2008). Design, synthesis, and pharmacological evaluation of N-bicyclo-5-chloro-1H-indole-2-carboxamide derivatives as potent glycogen phosphorylase inhibitors. Bioorg. Med. Chem. *16*, 10001–10012.

105. Leonard, F., Wajngurt, A., Tschannen, W., and Block, F.B. (2002). Unnatural Amino Acids. I. 3-Carboxytyrosine Derivatives. J. Med. Chem. *8*, 812–815.

106. Brückl, T., Baxter, R.D., Ishihara, Y., and Baran, P.S. (2012). Innate and guided C-H functionalization logic. Acc. Chem. Res. *45*, 826–839.

107. Ghoshal, T., Nagar, V., Vutla, A., Kotturi, S., and Kuttappan, S. (2019). Synthesis of aminobenzoxazoles via simple, clean and efficient electrochemical redox reactions. Tetrahedron Lett. *60*, 358–361.

108. Demmer, C.S., and Bunch, L. (2015). Benzoxazoles and oxazolopyridines in medicinal chemistry studies. Eur. J. Med. Chem. *97*, 778–785.

109. Alvesalo, J., Vuorela, H., Tammela, P., Leinonen, M., Saikku, P., and Vuorela, P. (2006). Inhibitory effect of dietary phenolic compounds on Chlamydia pneumoniae in cell cultures. Biochem. Pharmacol. *71*, 735–741.

110. Wells, G., Berry, J.M., Bradshaw, T.D., Burger, A.M., Seaton, A., Wang, B., Westwell, A.D., and Stevens, M.F.G. (2003). 4-Substituted 4-hydroxycyclohexa-2,5-dien-1-ones with selective activities against colon and renal cancer cell lines. J. Med. Chem. *46*, 532–541.

111. Sheldon, R.A. E-factor. Available at: https://www.sheldon.nl/roger/efactor.html [Accessed May 25, 2022].

112. Sheldon, R.A. (2017). The: E factor 25 years on: The rise of green chemistry and sustainability. Green Chem. *19*, 18–43.

113. Koleda, O., Broese, T., Noetzel, J., Roemelt, M., Suna, E., and Francke, R. (2017). Synthesis of Benzoxazoles Using Electrochemically Generated Hypervalent Iodine. J. Org. Chem. *82*, 11669–11681.

114. Gieshoff, T., Kehl, A., Schollmeyer, D., Moeller, K.D., and Waldvogel, S.R. (2017). Electrochemical synthesis of benzoxazoles from anilides-a new approach to employ amidyl radical intermediates. Chem. Commun. *53*, 2974–2977.

115. Froehr, T., Sindlinger, C.P., Kloeckner, U., Finkbeiner, P., and Nachtsheim, B.J. (2011). A metal-free amination of benzoxazoles - The first example of an iodide-catalyzed oxidative amination of heteroarenes. Org. Lett. *13*, 3754–3757.

116. Lamani, M., and Prabhu, K.R. (2011). Iodine-catalyzed amination of benzoxazoles: A metal-free route to 2-aminobenzoxazoles under mild conditions. J. Org. Chem. *76*, 7938–7944.

117. Chapman, M.R., Shafi, Y.M., Kapur, N., Nguyen, B.N., and Willans, C.E. (2015). Electrochemical flow-reactor for expedient synthesis of copper-N-heterocyclic carbene complexes. Chem. Commun. *51*, 1282–1284.

118. El-Hallag, I.S. (2010). Electrochemical oxidation of iodide at a glassy carbon electrode in methylene chloride at various temperatures. J. Chil. Chem. Soc. *55*, 67–73.

119. Pei, Z., Zhu, Z., Sun, D., Cai, J., Mosallanezhad, A., Chen, M., and Wang, G. (2021). Review of the I−/I3− redox chemistry in Zn-iodine redox flow batteries. Mater. Res. Bull. *141*, 111347.

120. Qiu, Y., Struwe, J., Meyer, T.H., Oliveira, J.C.A., and Ackermann, L. (2018).

Catalyst- and Reagent-Free Electrochemical Azole C−H Amination. Chem. - A Eur. J. *24*, 12784–12789.

121. Seyferth, D. (2001). Zinc Alkyls, Edward Frankland, and the Beginnings of Main-Group Organometallic Chemistry. Organometallics *20*, 2940–2955.

122. Enthaler, S. (2013). Rise of the zinc age in homogeneous catalysis? ACS Catal. *3*, 150–158.

123. Reformatsky, S. (1887). Neue Synthese zweiatomiger einbasischer Säuren aus den Ketonen. Berichte der Dtsch. Chem. Gesellschaft *20*, 1210–1211.

124. Rathke, M.W. (2011). The Reformatsky Reaction. Org. React., 423–460.

125. Rao, H.S.P., Rafi, S., and Padmavathy, K. (2008). The Blaise reaction. Tetrahedron *64*, 8037–8043.

126. Simmons, H.E., and Smith, R.D. (1958). A new synthesis of cyclopropanes from olefins. J. Am. Chem. Soc. *80*, 5323–5324.

127. King, A.O., Okukado, N., and Negishi, E.I. (1977). Highly general stereo-, regio-, and chemo-selective synthesis of terminal and internal conjugated enynes by the Pd-catalysed reaction of alkynylzinc reagents with alkenyl halides. J. Chem. Soc. Chem. Commun., 683–684.

128. Krasovskiy, A., Duplais, C., and Lipshutz, B.H. (2009). Zn-mediated, Pd-catalyzed cross-couplings in water at room temperature without prior formation of organozinc reagents. J. Am. Chem. Soc. *131*, 15592–15593.

129. Ross, A.J., Dreiocker, F., Schä Fer, M., Oomens, J., Meijer, A.J.H.M., Pickup, B.T., and Jackson, R.F.W. (2011). Evidence for the role of tetramethylethylenediamine in aqueous negishi cross-coupling: Synthesis of

nonproteinogenic phenylalanine derivatives on water. J. Org. Chem. *76*, 1727–1734.

130. Knochel, P., and Diène, C. (2011). Preparation of functionalized Zn and Mg-organometallics. Application to the performance of diastereoselective cross-couplings. Comptes Rendus Chim. *14*, 842–850.

131. Balkenhohl, M., Ziegler, D.S., Desaintjean, A., Bole, L.J., Kennedy, A.R., Hevia, E., and Knochel, P. (2019). Preparation of Polyfunctional Arylzinc Organometallics in Toluene by Halogen/Zinc Exchange Reactions. Angew. Chemie Int. Ed. *58*, 12898–12902.

132. Knochel, P., Millot, N., Rodriguez, A.L., and Tucker, C.E. (2001). Preparation and Applications of Functionalized Organozinc Compounds. Org. React., 417–759.

133. Fujiwara, M., Ichikawa, J., Okauchi, T., and Minami, T. (1999). Vinylic C-F bond activation with low-valent zirconocene: The generation and cross-coupling reactions of 1-fluorovinylzirconocene. Tetrahedron Lett. *40*, 7261–7265.

134. Han, B.H., and Boudjouk, P. (1982). Organic Sonochemistry. Sonic Acceleration of the Reformatsky Reaction. J. Org. Chem. *47*, 5030–5032.

135. Rieke, R.D., Hanson, M. V, Brown, J.D., and Niu, Q.J. (1996). Direct formation of secondary and tertiary alkylzinc bromides and subsequent Cu(I)-mediated couplings. J. Org. Chem. *61*, 2726–2730.

136. Y. Rollin J. Perichon, C.G. (1999). Organozinc ReagentsA Practical Approach Edited by P. Knochel and P. Jones. Oxford University Press: Oxford, UK. 1999. 354 pp. £75.00. ISBN 0 19 850121 8. Org. Process Res. Dev. *3*, 292.

Available at: https://pubs.acs.org/doi/10.1021/op9900232.

137. Cao, Q., Howard, J.L., Wheatley, E., and Browne, D.L. (2018). Mechanochemical Activation of Zinc and Application to Negishi Cross-Coupling. Angew. Chemie Int. Ed. *57*, 11339–11343.

138. Schlenk, W., and Schlenk, W. (1929). Über die Konstitution der Grignardschen Magnesiumverbindungen. Berichte der Dtsch. Chem. Gesellschaft (A B Ser. *62*, 920–924.

139. Abraham, M.H., and Rolfe, P.H. (1967). Organometallic compounds 4. The constitution of the ethylzinc halides. J. Organomet. Chem. *7*, 35–43.

140. Evans, D.F., and Fazakerley, G. V (1971). Proton resonance studies of the Schlenk equilibria for methyl- and ethyl-zinc iodide in tetrahydrofuran. J. Chem. Soc. A Inorganic, Phys. Theor. Chem., 182–183.

141. Blake, A.J., Shannon, J., Stephens, J.C., and Woodward, S. (2007). Demonstration of Promoted Zinc Schlenk Equilibria, their Equilibrium Values and Derived Reactivity. Chem. - A Eur. J. *13*, 2462–2472.

142. Chen, T.A., Wu, X., and Rieke, R.D. (1995). Regiocontrolled Synthesis of Poly(3-alkylthiophenes) Mediated by Rieke Zinc: Their Characterization and Solid-State Properties. J. Am. Chem. Soc. *117*, 233–244.

143. Rieke, R.D. (1989). Preparation of organometallic compounds from highly reactive metal powders. Science (80-.). *246*, 1260–1264.

144. Zhu, L., Wehmeyer, R.M., and Rieke, R.D. (1991). The Direct Formation of Functionalized Alkyl (aryl) zinc Halides by Oxidative Addition of Highly Reactive Zinc with Organic Halides and Their Reactions with Acid Chlorides, α, β-Unsaturated Ketones, and Allylic, Aryl, and Vinyl Halides. J. Org. Chem.

56, 1445–1453.

145. Erdik, E. (1987). Use of activation methods for organozinc reagents. Tetrahedron *43*, 2203–2212.

146. Cao, Q., Stark, R.T., Fallis, I.A., and Browne, D.L. (2019). A Ball-Milling-Enabled Reformatsky Reaction. ChemSusChem *12*, 2554–2557.

147. Yin, J.X., Stark, R.T., Fallis, I.A., and Browne, D.L. (2020). A Mechanochemical Zinc-Mediated Barbier-Type Allylation Reaction under Ball-Milling Conditions. J. Org. Chem. *85*, 2347–2354.

148. Tokuda, M., Kurono, N., and Mimura, N. (1996). New Electrochemical Preparation of Reactive Zinc with a Large Surface Area. Chem. Lett. *25*, 1091–1092.

149. Takai, K., Kakiuchi, T., and Utimoto, K. (1994). A Dramatic Effect of a Catalytic Amount of Lead on the Simmons-Smith Reaction and Formation of Alkylzinc Compounds from Iodoalkanes. Reactivity of Zinc Metal: Activation and Deactivation. J. Org. Chem. *59*, 2671–2673.

150. Tokuda, M., Mimura, N., Karasawa, T., Fujita, H., and Suginome, H. (1993). New preparation of reactive zinc metal by electrolysis and its use for a facile isoprenylation of aldehydes and ketones. Tetrahedron Lett. *34*, 7607–7610.

151. Stephen, H.R., Schotten, C., Nicholls, T.P., Woodward, M., Bourne, R.A., Kapur, N., and Willans, C.E. (2020). A Versatile Electrochemical Batch Reactor for Synthetic Organic and Inorganic Transformations and Analytical Electrochemistry. Org. Process Res. Dev.

152. Dekker, J., Budzelaar, P.H.M., Boersma, J., van der Ker, G.J.M., and Spek, A.L. (1984). The Nature of the Reformatsky Reagent. Crystal Structure of

(BrZnCH2COO-t-Bu·THF)2. Organometallics *3*, 1403–1407.

153. Blaise, E.E. (1901). No. Comptes Rendus Chim. *132*, 478.

154. Pospíšil, J., and Markó, I.E. (2007). Total synthesis of jerangolid D. J. Am. Chem. Soc. *129*, 3516–3517. Available at: http://pubs.acs.org.

155. Bush, K., and Bradford, P.A. (2016). β-lactams and β-lactamase inhibitors: An overview. Cold Spring Harb. Perspect. Med. *6*.

156. Elander, R.P. (2003). Industrial production of β-lactam antibiotics. Appl. Microbiol. Biotechnol. *61*, 385–392.

157. Mehta, P.D., Sengar, N.P.S., and Pathak, A.K. (2010). 2-Azetidinone – A new profile of various pharmacological activities. Eur. J. Med. Chem. *45*, 5541–5560.

158. Deep, A., Kumar, P., Narasimhan, B., Lim, S.M., Ramasamy, K., Mishra, R.K., and Mani, V. (2016). 2-azetidinone derivatives: Synthesis, antimicrobial, anticancer evaluation and QSAR studies. Acta Pol. Pharm. - Drug Res. *73*, 65–78.

159. Brandi, A., Cicchi, S., and Cordero, F.M. (2008). Novel syntheses of azetidines and azetidinones. Chem. Rev. *108*, 3988–4035.

160. Corey, E.J., and Felix, A.M. (2002). A New Synthetic Approach to the Penicillins. J. Am. Chem. Soc. *87*, 2518–2519.

161. Doyle, M.P., Protopopova, M.N., Winchester, W.R., and Daniel, K.L. (1992). Enantiocontrol and regiocontrol in lactam syntheses by intramolecular carbon-hydrogen insertion reactions of diazoacetamides catalyzed by chiral rhodium(II) carboxamides. Tetrahedron Lett. *33*, 7819–7822.

162. Doyle, M.P., and Kalinin, A. V (1995). Highly Enantioselective Route to β-Lactams via Intramolecular C-H Insertion Reactions of Diazoacetylazacycloalkanes Catalyzed by Chiral Dirhodium(II) Carboxamidates. Synlett *1995*, 1075–1076.

163. Staudinger, H. (1907). Zur Kenntniss der Ketene. Diphenylketen. Justus Liebig's Ann. der Chemie *356*, 51–123.

164. Taggi, A.E.E., Hafez, A.M.M., Wack, H., Young, B., Drury, W.J.J., and Lectka, T. (2000). Catalytic, asymmetric synthesis of β-lactams [11]. J. Am. Chem. Soc. *122*, 7831–7832.

165. Méndez, L., and Mata, E.G. (2010). Synthesis of multicyclic β-Lactam derivatives via solid-phase- generated ketenes. J. Comb. Chem. *12*, 810–813.

166. Vaske, Y.S.M., Mahoney, M.E., Konopelski, J.P., Rogow, D.L., and McDonald, W.J. (2010). Enantiomerically pure trans -β-lactams from α-amino acids via compact fluorescent light (CFL) continuous-flow photolysis. J. Am. Chem. Soc. *132*, 11379–11385.

167. Gilman, H., and Speeter, M. (1943). The Reformatsky Reaction with Benzalaniline. J. Am. Chem. Soc. *65*, 2255–2256.

168. Takahashi, E., Fujisawa, H., Yanai, T., and Mukaiyama, T. (2005). Highly trans-selective synthesis of β-lactams by tandem phenoxide anion-catalyzed Mannich-type addition and cyclization. Chem. Lett. *34*, 994–995.

169. Kanai, K., Wakabayashi, H., and Honda, T. (2002). Selective synthesis of β-amino esters and β-lactams by rhodium-catalyzed reformatsky-type reaction. Heterocycles *58*, 47–51.

170. Gong, Y., and Kato, K. (2001). Nucleophilic reactions with α-trifluoromethyl

imine and N,O-disubstituted aminal: synthesis of β-trifluoromethyl β-anilino esters. J. Fluor. Chem. *111*, 77–80.

171. Kinugasa, M., and Hashimoto, S. (1972). The reactions of copper(I) phenylacetylide with nitrones. J. Chem. Soc. Chem. Commun., 466–467.

172. Tufariello, J.J., and Tegeler, J.J. (1976). Nitrone cycloaddition. A route to the lupin class of alkaloids. Tetrahedron Lett. *17*, 4037–4040.

173. Dagne, E., and Castagnoli, N. (1972). Structure of hydroxycotinine, a nicotine methobolite. J. Med. Chem. *15*, 356–360.

174. Gössinger, E. (1980). Stereoselektive synthese von (±)-porantheridin. Tetrahedron Lett. *21*, 2229–2232.

175. Stecko, S., Furman, B., and Chmielewski, M. (2014). Kinugasa reaction: an 'ugly duckling' of β-lactam chemistry. Tetrahedron *70*, 7817–7844.

176. Ardura, D., López, R., and Sordo, T.L. (2006). A Theoretical Study of Rhodium(I) Catalyzed Carbonylative Ring Expansion of Aziridines to β-Lactams: Crucial Activation of the Breaking C−N Bond by Hyperconjugation. J. Org. Chem. *71*, 7315–7321.

177. Khumtaveeporn, K., and Alper, H. (1995). Transition Metal Mediated Carbonylative Ring Expansion of Heterocyclic Compounds. Acc. Chem. Res. *28*, 414–422.

178. Diethelm, S., and Carreira, E.M. (2013). Total Synthesis of (±)-Gelsemoxonine. J. Am. Chem. Soc. *135*, 8500–8503.

179. Lvov, A.G., Yadykov, A. V, Lyssenko, K.A., Heinemann, F.W., Shirinian, V.Z., and Khusniyarov, M.M. (2020). Reversible shifting of a chemical

equilibrium by light: The case of keto-enol tautomerism of a β-ketoester. Org. Lett. *22*, 604–609.

180. Bunting, J.W., and Kanter, J.P. (1993). Acidity and Tautomerism of β-Keto Esters and Amides in Aqueous Solution. J. Am. Chem. Soc. *115*, 11705–11715.

181. Huck, L., Berton, M., Hoz, A.D. La, Díaz-Ortiz, A., and Alcázar, J. (2017). Reformatsky and Blaise reactions in flow as a tool for drug discovery. One pot diversity oriented synthesis of valuable intermediates and heterocycles. Green Chem. *19*, 1420–1424.

182. Byrne, F.P., Jin, S., Paggiola, G., Petchey, T.H.M., Clark, J.H., Farmer, T.J., Hunt, A.J., Robert McElroy, C., and Sherwood, J. (2016). Tools and techniques for solvent selection: green solvent selection guides. Sustain. Chem. Process. *4*, 7.

183. Murray, P.M., Bellany, F., Benhamou, L., Bučar, D.K., Tabor, A.B., and Sheppard, T.D. (2016). The application of design of experiments (DoE) reaction optimisation and solvent selection in the development of new synthetic chemistry. Org. Biomol. Chem. *14*, 2373–2384.

184. House, H.O., Feng, E., and Peet, N.P. (1971). A Comparison of Various Tetraalkylammonium Salts as Supporting Electrolytes in Organic Electrochemical Reactions. J. Org. Chem. *36*, 2371–2375.

185. Hammerich, O., and Lund, H. eds. (2000). Organic Electrochemistry (CRC Press) Available at: https://www.taylorfrancis.com/books/9781420029659.

186. Figueiredo, M.C., Trieu, V., Eiden, S., and Koper, M.T.M. (2017). Spectro-Electrochemical Examination of the Formation of Dimethyl Carbonate from

CO and Methanol at Different Electrode Materials. J. Am. Chem. Soc. *139*, 14693–14698.

187. Rohani, S., Horne, S., and Murthy, K. (2005). Control of Product Quality in Batch Crystallization of Pharmaceuticals and Fine Chemicals. Part 1: Design of the Crystallization Process and the Effect of Solvent. Org. Process Res. Dev. *9*, 858–872.

188. Bands, R. RAMAN DATA AND ANALYSIS Raman Spectroscopy for Analysis and Monitoring. Available at: www.jobinyvon.fr.

189. Mark J. Howard, former NMR Technician at the University of Leeds.

190. van der Steen, F.H., Kleijn, H., Jastrzebski, J.T.B.H., and van Koten, G. (1991). A New and Efficient Route to 3-Amino-2-azetidinones via Zinc Enolates of N,N-Disubstituted Glycine Esters. J. Org. Chem. *56*, 5147–5158.

191. Troisi, L., Granito, C., and Pindinelli, E. (2010). Novel and Recent Synthesis and Applications of β-Lactams. Top Heterocycl Chem *22*, 101–209.

192. Imming, P., Klar, B., and Dix, D. (2000). Hydrolytic stability versus ring size in lactams: Implications for the development of lactam antibiotics and other serine protease inhibitors. J. Med. Chem. *43*, 4328–4331.

193. Charette, A.B., and Roy, M.N. (2012). 3.25 Stoichiometric Auxiliary Ligands for Metals and Main Group Elements: Ligands for Zinc. Compr. Chirality *3*, 780–806.

194. Huisman, G.W. (2014). 9.16 Enzyme Evolution as a Tool for Creating Improved Catalysts for Large-Scale Organic Synthesis. Compr. Org. Synth. Second Ed. *9*, 421–437.

195. Murty, M.S.R., Ram, K.R., Rao, R.V., Yadav, J.S., Murty, U.S.N., and Kumar, K.P. (2011). CsF-Celite catalyzed facile N-alkylation of 2(3H)-benzoxazolones and antimicrobial properties of 2-substituted benzoxazole and 3-substituted-2(3H)- benzoxazolone derivatives. Med. Chem. Res. *20*, 626–636.

196. Ashida, Y., Sato, Y., Suzuki, T., Ueno, K., Kai, K.I., Nakatsuji, H., and Tanabe, Y. (2015). (E)-,(Z)-parallel preparative methods for stereodefined β,β-diaryl- and α,β-diaryl-α,β-unsaturated esters: Application to the stereocomplementary concise synthesis of zimelidine. Chem. - A Eur. J. *21*, 5934–5945.

197. Matsukawa, S., Fukazawa, K., and Kimura, J. (2014). Polymer-supported PPh3 as a reusable organocatalyst for the Mukaiyama aldol and Mannich reaction. RSC Adv. *4*, 27780–27786.

198. Isoda, M., Sato, K., Funakoshi, M., Omura, K., Tarui, A., Omote, M., and Ando, A. (2015). Diastereoselective Synthesis of syn-β-Lactams Using Rh-Catalyzed Reductive Mannich-Type Reaction of α,β-Unsaturated Esters. J. Org. Chem. *80*, 8398–8405.

199. Akiyama, T., Takaya, J., and Kagoshima, H. (2002). Brønsted Acid-Catalyzed Mannich-Type Reactions in Aqueous Media. Adv. Synth. Catal. *344*, 338–347.

200. Periasamy, M., Suresh, S., and Subramaniapillai, S.G. (2005). Stereoselective synthesis of syn-β-amino esters using the TiCl4/R3N reagent system. Tetrahedron Lett. *46*, 5521–5524.

201. Sheldrick, G.M. (2015). SHELXT – Integrated space-group and crystal-

structure determination. Acta Crystallogr. Sect. A Found. Adv. *71*, 3–8.

202.   Sheldrick, G.M. (2015). Crystal structure refinement with SHELXL. Acta Crystallogr. Sect. C Struct. Chem. *71*, 3–8.

8 Appendix

8.1 C-H Activation of Benzoxazole

8.1.1 CV Diagrams

TBAI

Scan rate: 0.1 V/s 5 scans

Scan rate: 1.0 V/s 10 scans

Scan rate: 10 V/s 20 scans

Benzoxazole

Scan rate: 0.1 V/s   5 scans

Scan rate: 1.0 V/s   10 scans

Scan rate: 10 V/s   20 scans

Benzoxazole + AcOH

Scan rate: 0.1 V/s   5 scans

Scan rate: 1.0 V/s   10 scans

Scan rate: 10 V/s   20 scans

8.1.2 GC Graphs

Benzoxazole Calibration

$y = 4.24E\text{-}02x + 9.94E\text{-}05$
$R^2 = 1.00E\text{+}00$

Concentration/ M (y-axis)
Signal Area/IS Area (x-axis)

2-morpholinbenzoxazole Calibration

$y = 2.66E\text{-}02x + 1.12E\text{-}04$
$R^2 = 9.99E\text{-}01$

Concentration/ M (y-axis)
Signal Area/IS Area (x-axis)

8.1.3 EDX Work

Images from iron anode – iron cathode pairing.

Iron anode:
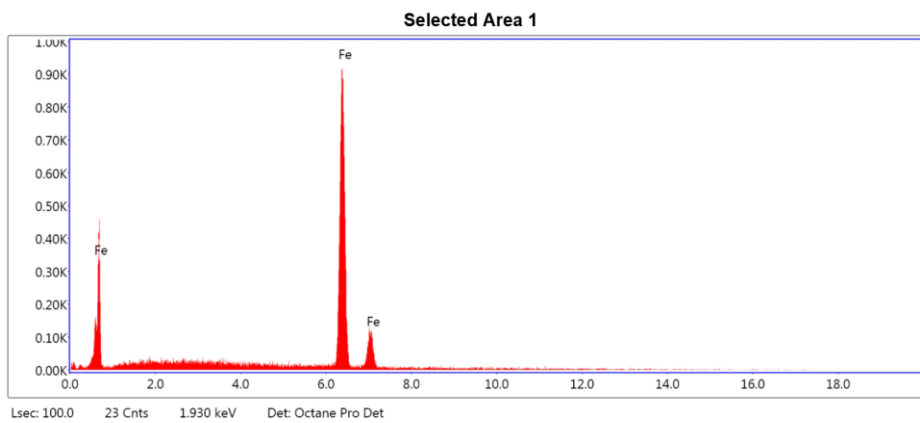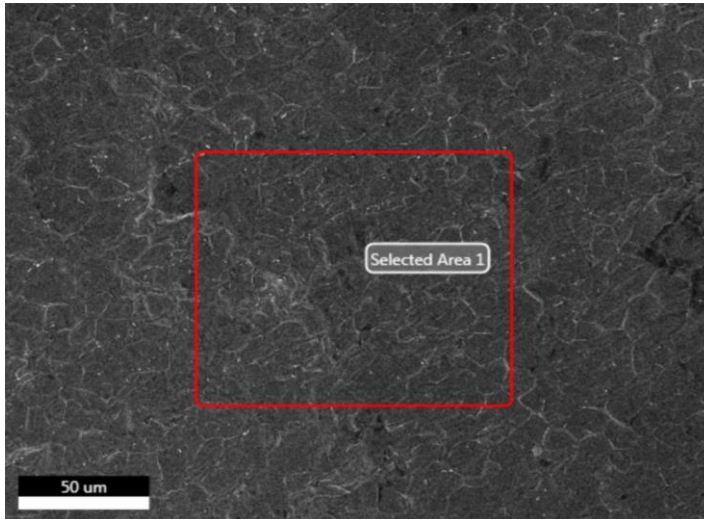
eZAF Smart Quant Results

Element	Weight %	Atomic %	Net Int.	Error %	Kratio	Z	R	A	F
FeK	100.00	100.00	125.13	2.64	1.0000 0.0000	1.0000	1.0000	1.0000	1.0000

Area analysed shows only iron present on the sample surface.

Iron cathode:
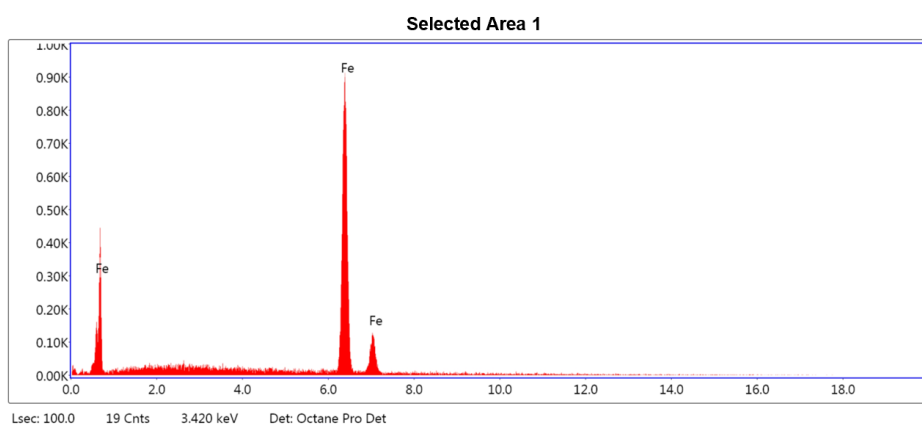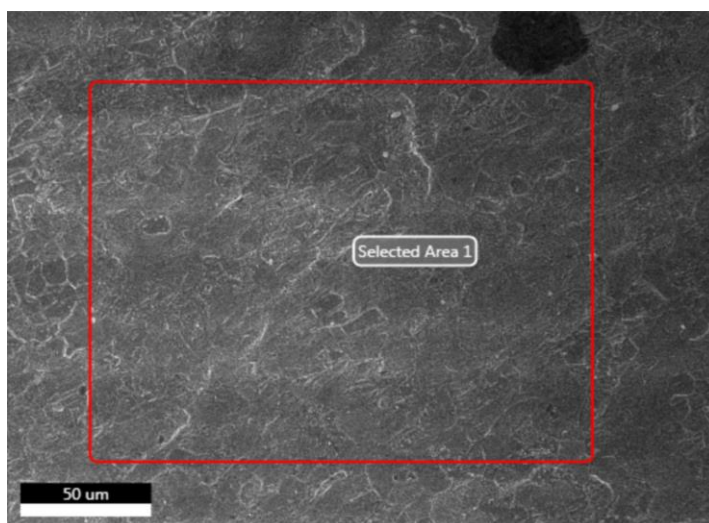
Selected Area 1

Lsec: 100.0   19 Cnts   3.420 keV   Det: Octane Pro Det

eZAF Smart Quant Results

Element	Weight %	Atomic %	Net Int.	Error %	Kratio	Z	R	A	F
FeK	100.00	100.00	121.26	2.66	1.0000 0.0000	1.0000	1.0000	1.0000	1.0000

Both iron electrodes did not have any other metals detected post electrosynthesis, therefore we can conclude that the methodology and substrates do not cause any change in the metal surface's elemental constitution.

Images from stainless steel anode – iron cathode pairing.

Iron Cathode:

Selected Area 1

Lsec: 100.0   1 Cnts   10.680 keV   Det: Octane Pro Det
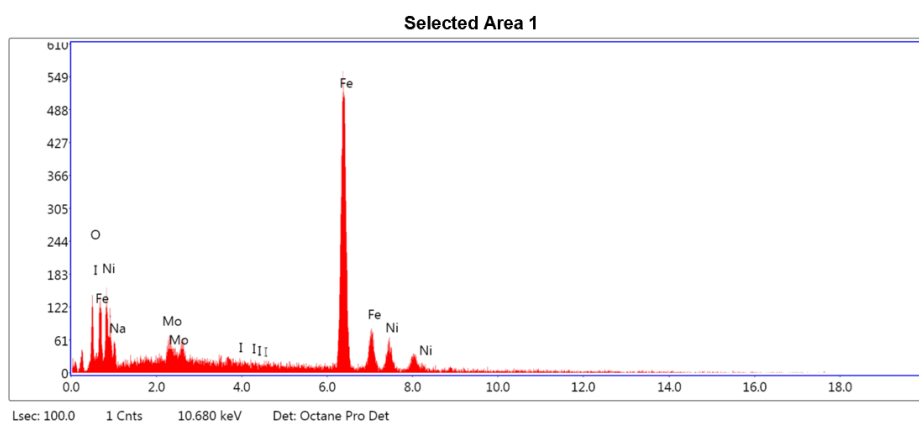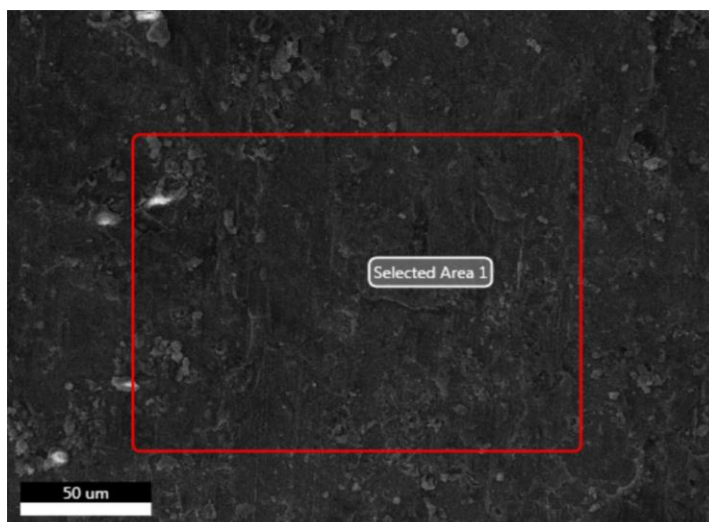
eZAF Smart Quant Results

Element	Weight %	Atomic %	Net Int.	Error %	Kratio	Z	R	A	F
O K	3.99	12.04	5.99	12.89	0.0228 0.0228	1.2578	0.8691	0.4532	1.0000
NaK	5.43	11.38	3.74	17.78	0.0105 0.0105	1.1468	0.9002	0.1689	1.0014
MoL	2.28	1.15	3.26	17.60	0.0177 0.0177	0.8758	1.1120	0.8607	1.0279
I L	0.75	0.29	0.72	57.48	0.0074 0.0074	0.8084	1.1543	1.0580	1.1473
FeK	76.74	66.27	74.71	3.34	0.7800 0.7804	0.9805	1.0062	0.9973	1.0400
NiK	10.81	8.88	7.10	8.75	0.1028 0.1028	0.9920	1.0140	0.9231	1.0386

Analysis of the iron cathode surface post-electrochemical reaction shows a significant increase in the number of metals detected on the surface.

Stainless steel anode:

Selected Area 1
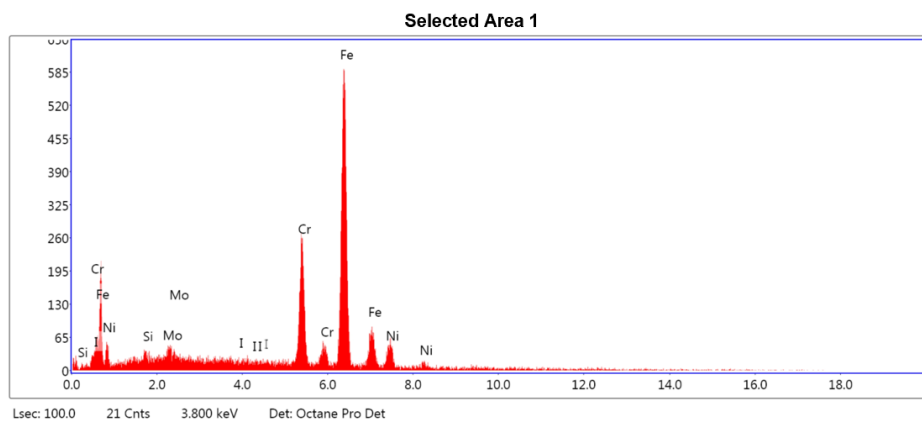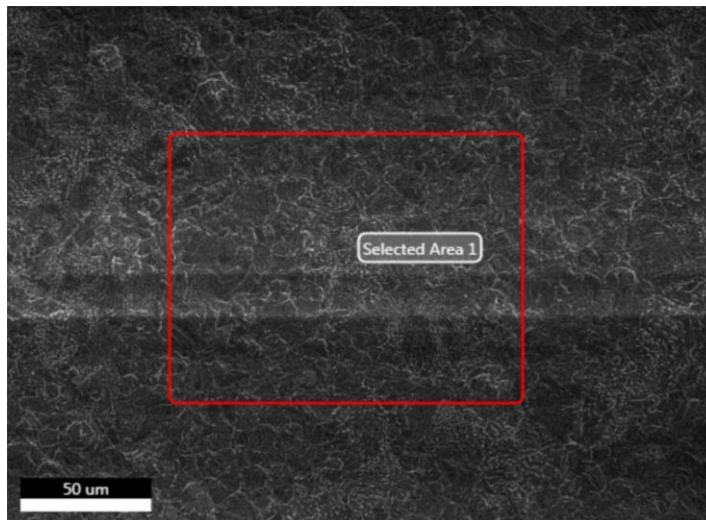
eZAF Smart Quant Results

Element	Weight %	Atomic %	Net Int.	Error %	Kratio	Z	R	A	F
SiK	0.41	0.80	1.19	51.10	0.0024	1.1727	0.9191	0.4999	1.0069
MoL	1.23	0.71	2.09	38.57	0.0097	0.8919	1.1027	0.8627	1.0279
I L	0.32	0.14	0.37	59.13	0.0032	0.8236	1.1459	1.0618	1.1461
CrK	17.13	18.30	31.89	5.53	0.2079	1.0030	0.9896	0.9886	1.2238
FeK	71.43	71.06	80.46	3.49	0.7192	0.9995	1.0001	0.9716	1.0367
NiK	9.49	8.98	7.34	13.01	0.0910	1.0118	1.0086	0.9134	1.0379

The EDX analysis here shows clear elemental change in the iron cathode which is likely to be due to the stainless steel anode, as the new metals identified on the cathode are present in the stainless steel surface analysis.

8.2 Electrodeposition of Zinc

8.2.1 Mass Spectrometry Data

8.2.1.1 DMF Reaction Solvent
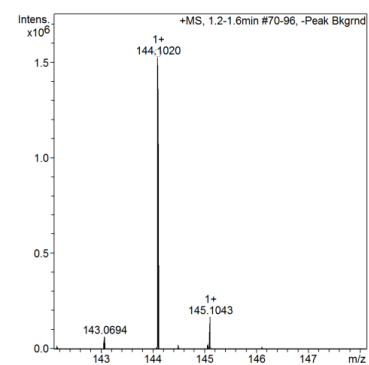
Confirm/Find Formula Results

The section below shows the results of formula calculation. If an expected formula was provided and found these are the results that are listed. If no formula was provided or no matches were found the system has attempted to determine the formula constrained by the parameters listed to the left

Concentration too high. Dilute sample!

Meas. m/z	Ion Formula	z	m/z	err [mDa]	err [ppm]	mSigma	Score	Sum Formula	Adduct
144.101952	C7H14NO2	1+	144.101905	-0.0	-0.3	16.1	100.00	C7H13NO2	M+H
	C7H14NO2	1+	144.101905	-0.0	-0.3	16.1	100.00	C7H10O2	M+NH4
200.127940	C10H18NO3	1+	200.128120	0.2	0.9	10.7	100.00	C10H17NO3	M+H
	C10H18NO3	1+	200.128120	0.2	0.9	10.7	100.00	C10H14O3	M+NH4

Smart Formula Parameter	Value
Expected Formula	
Adducts Considered	
Smart Formula Search Parameters	
CHNO and adducts considered implicitly	
Formula Search Minimum	
Formula Search Maximum	C 10 H 20 N 3 O 3
Algorithm Parameters	
Tolerance	4 ppm
Match to Isotope Pattern(mSigma)	40
Electron Configuration	even
Estimate No of Carbons	yes
Filter by H/C Ratio	0< H/C < 3
Number of Double Bonds & Rings	0< rings&DB < 80

8.2.1.2 Analysis of possible zinc dimer

School of Chemistry Mass Spectrometry Service

SampleID	RH Biotage		**Submitter**	Rosie Hamill
Sample Descriptio				
Analysis Name	C:\Data\srisridharan\cm13rh\RH		**Supervisor**	Sri Sridharan
Method	Biotage_113273_GB1906390639.D		**Acquisition Dat**	20/04/2021 16:19:52
Instrument	amaZon speed **n/a** n/a	**Ion Polarity** Positive	**n/a** n/a	**n/a** n/a

Summary of Results

BPC 60.00-1300.00 +All MS, Smoothed (0.21,1,GA)

EIC C10H11O2 [M+H, M+NH4, M+Na]1+-2+ 164.08; 82.55; 181.11; 99.5

UV Chromatogram, 200-340 nm

Analog Only

Cmpd 1, 0.5 min

+MS, 0.4-0.6min #105-140, -Peak Bkgrnd

1+
483.17

224.23

Cmpd 2, 0.6 min

+MS, 0.6-0.6min #140-166, -Peak Bkgrnd

1+
464.11

240.86
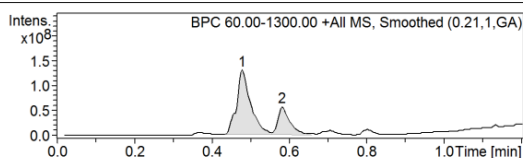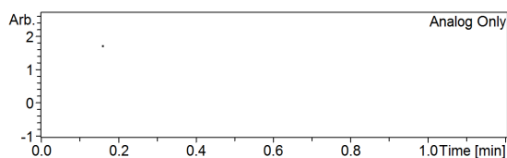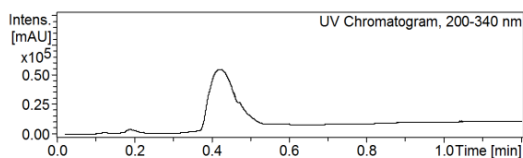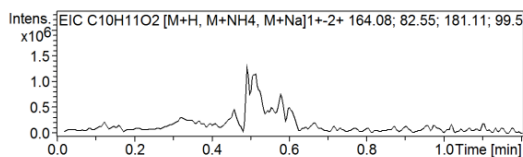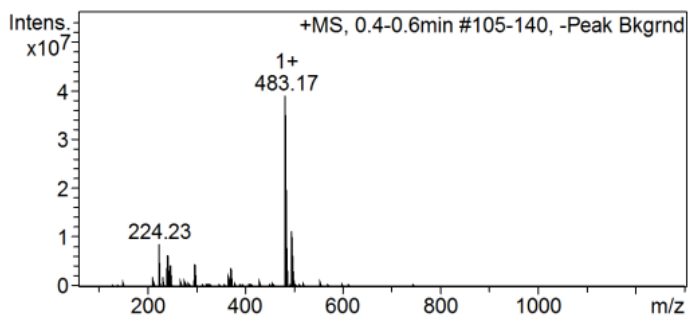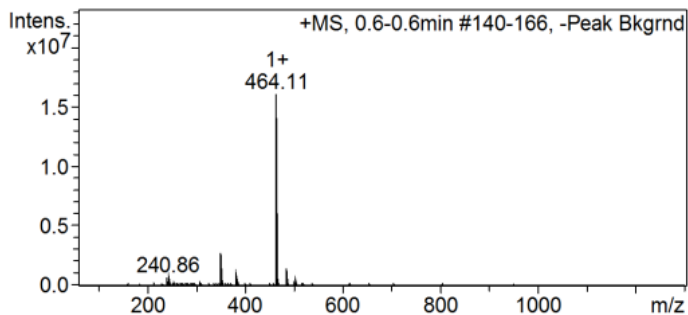
8.2.2 Zinc Electrode Surface Analysis – Round bottom flask reactor

The images below are of each electrode at varying magnifications.

8.2.2.1 Pre Blaise reaction Anode
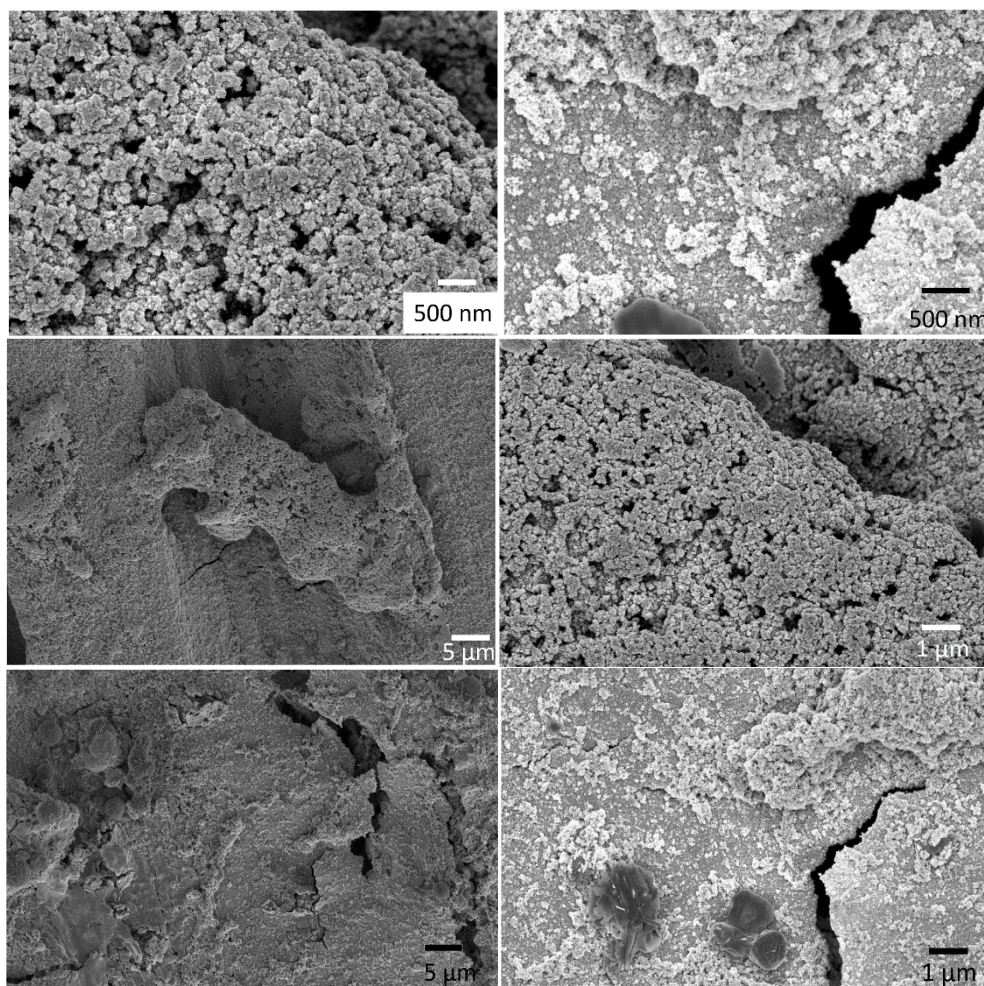
Before the starting materials are added, clear changes can be observed on the anode surface. The cracks and chasms are indicative of electrode leeching, which also explains the surface appearance of the cathode.

8.2.2.2 Pre Blaise reaction Cathode
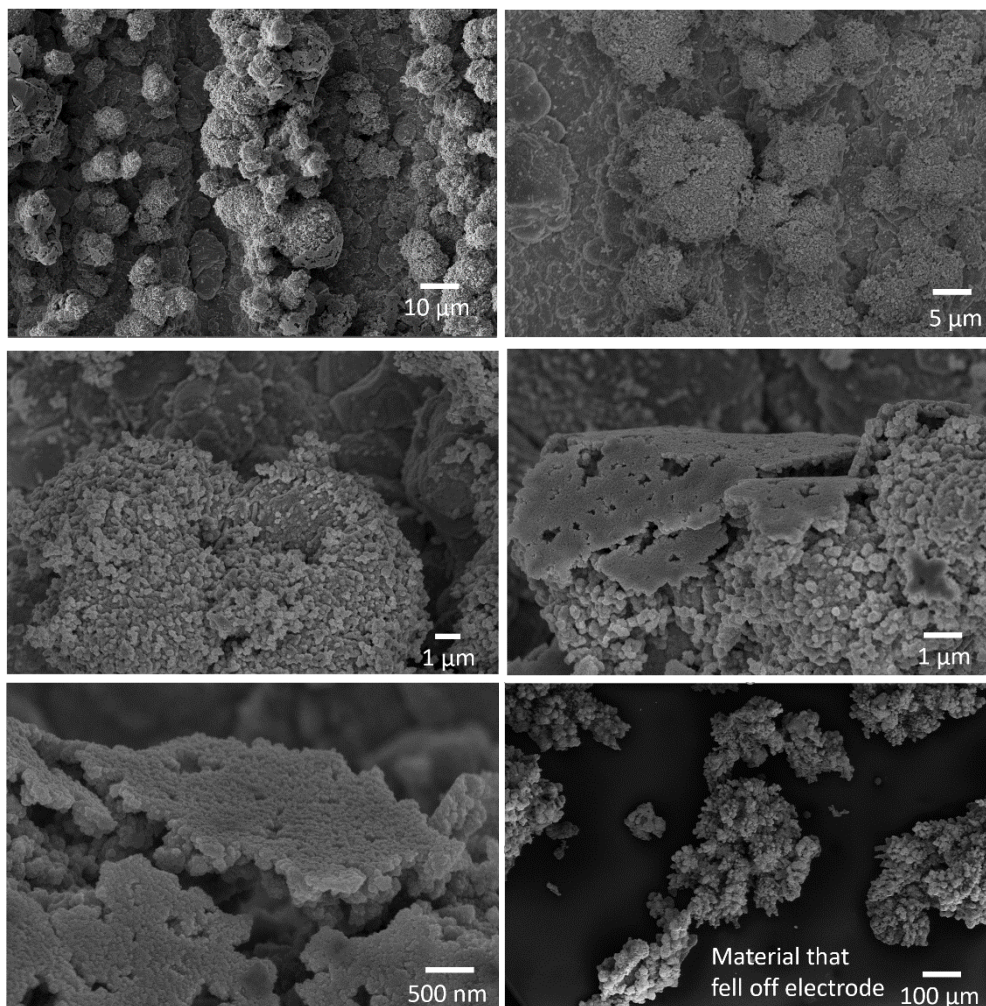
On the cathode there is clear, nanoscale electrodeposition appearing in clusters of high surface area deposits.

8.2.2.3 Post Blaise reaction Anode
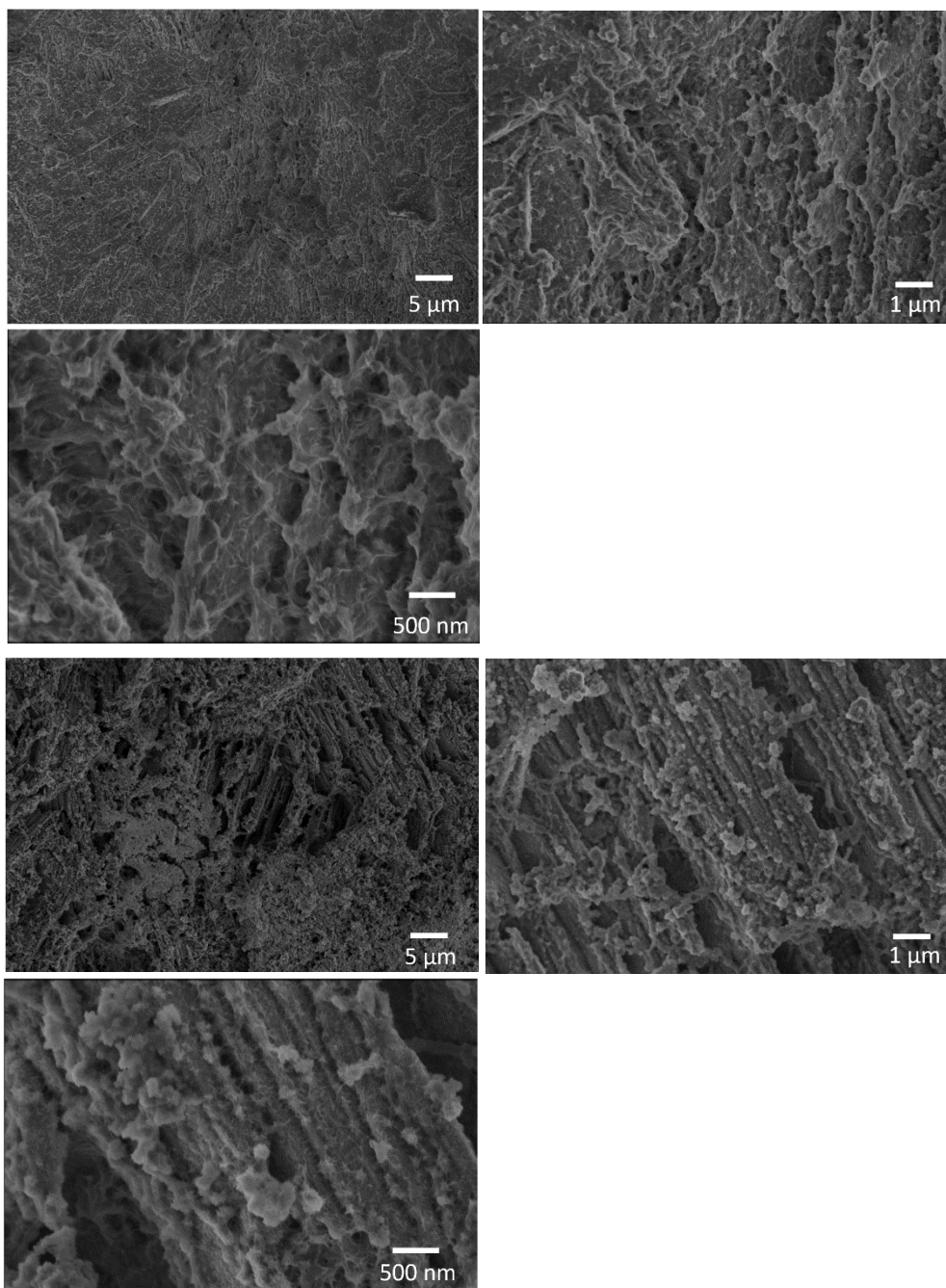
The two sections of this electrode which were analysed were found to have chasms, indicating electrode leeching, leaving in some places an almost fibrous topography.

8.2.2.4 Post Blaise reaction Cathode
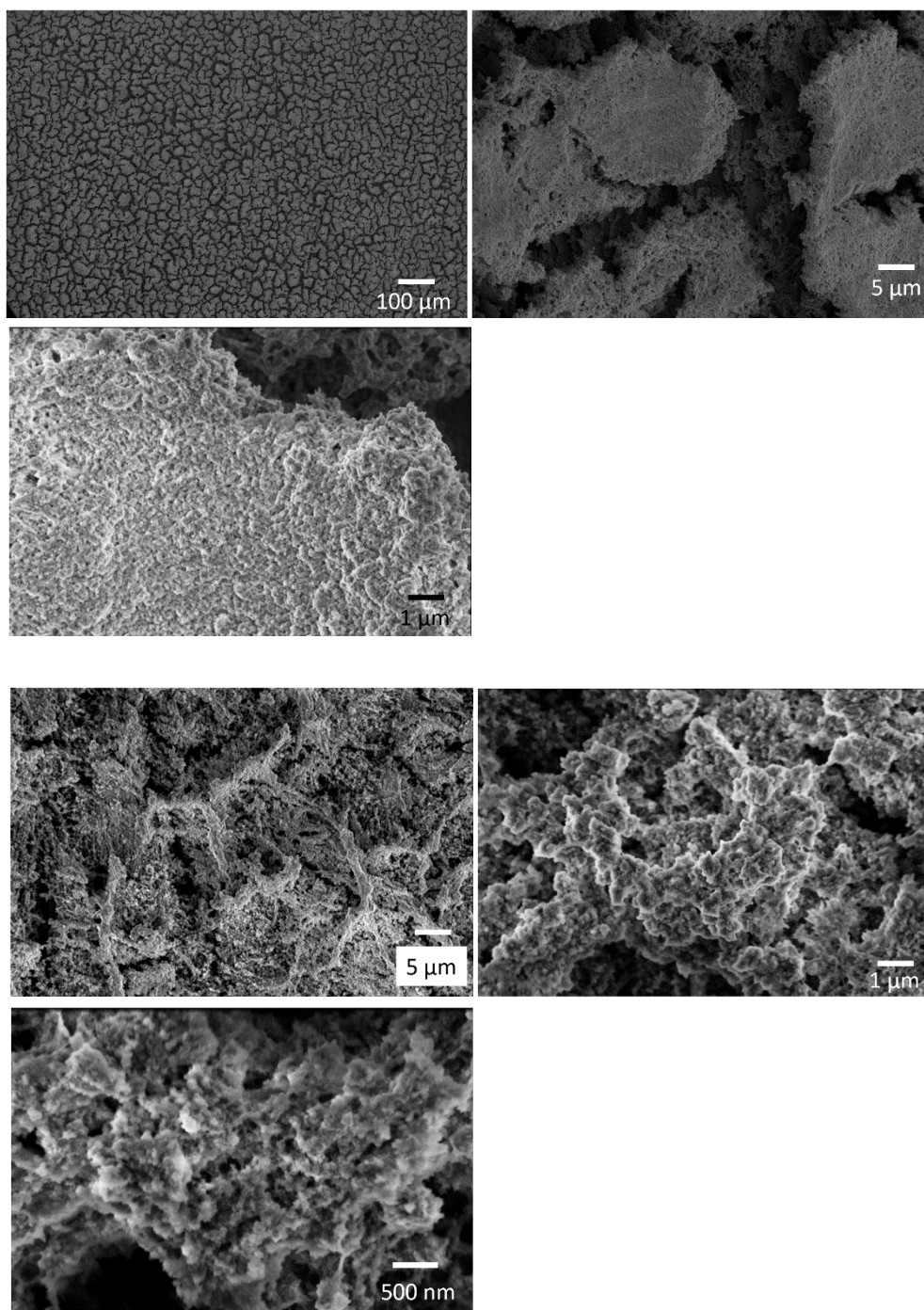
Both sections of the cathode analysed show clear electrodeposition; the first area the deposition appears as a layer on the surface, the second an amorphous agglomeration of zinc metal.

8.2.3 Zinc Electrode Surface Analysis – Bottle Reactor

8.2.3.1 Pre Blaise reaction Anode
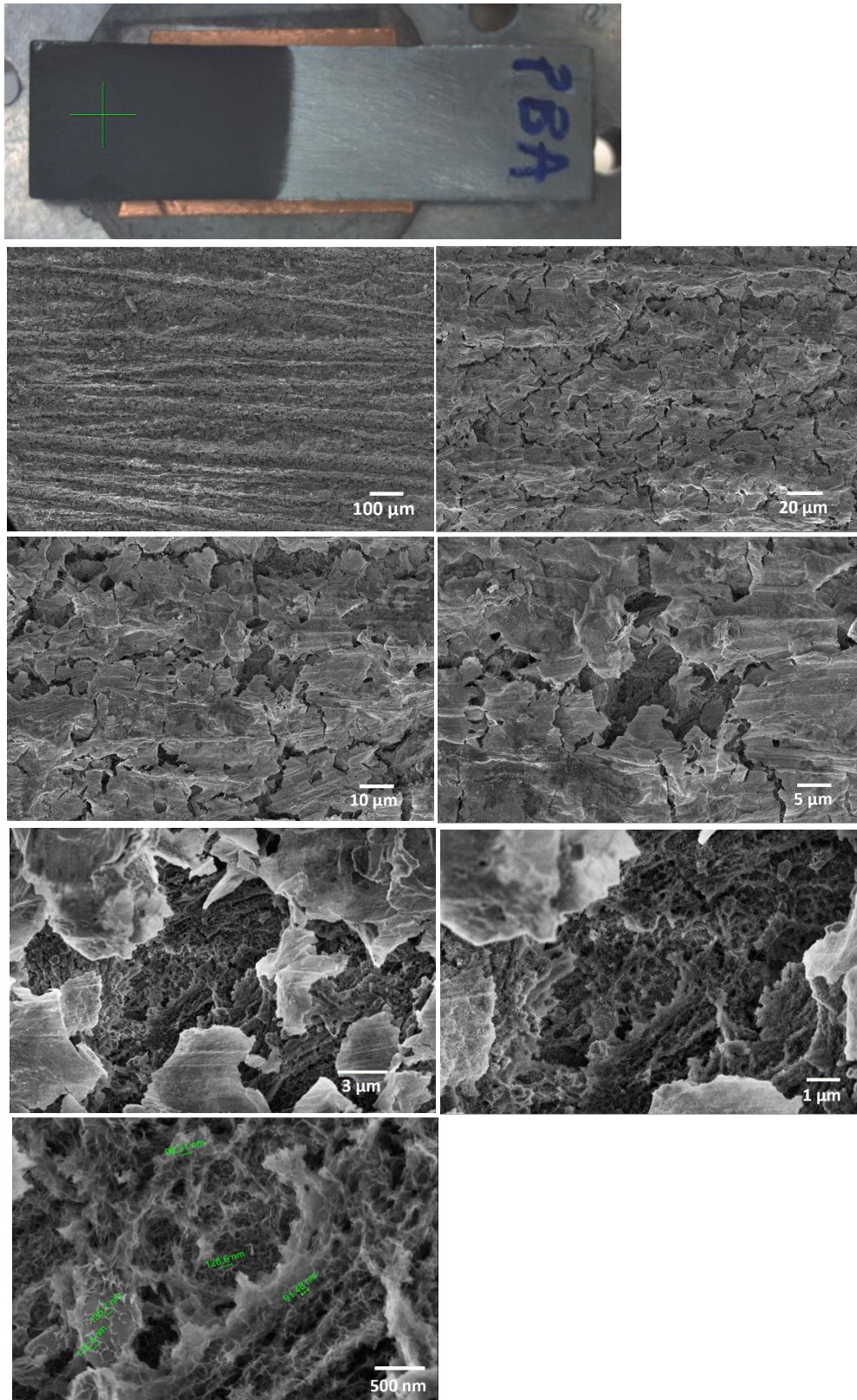
8.2.3.2 Pre Blaise reaction Cathode:
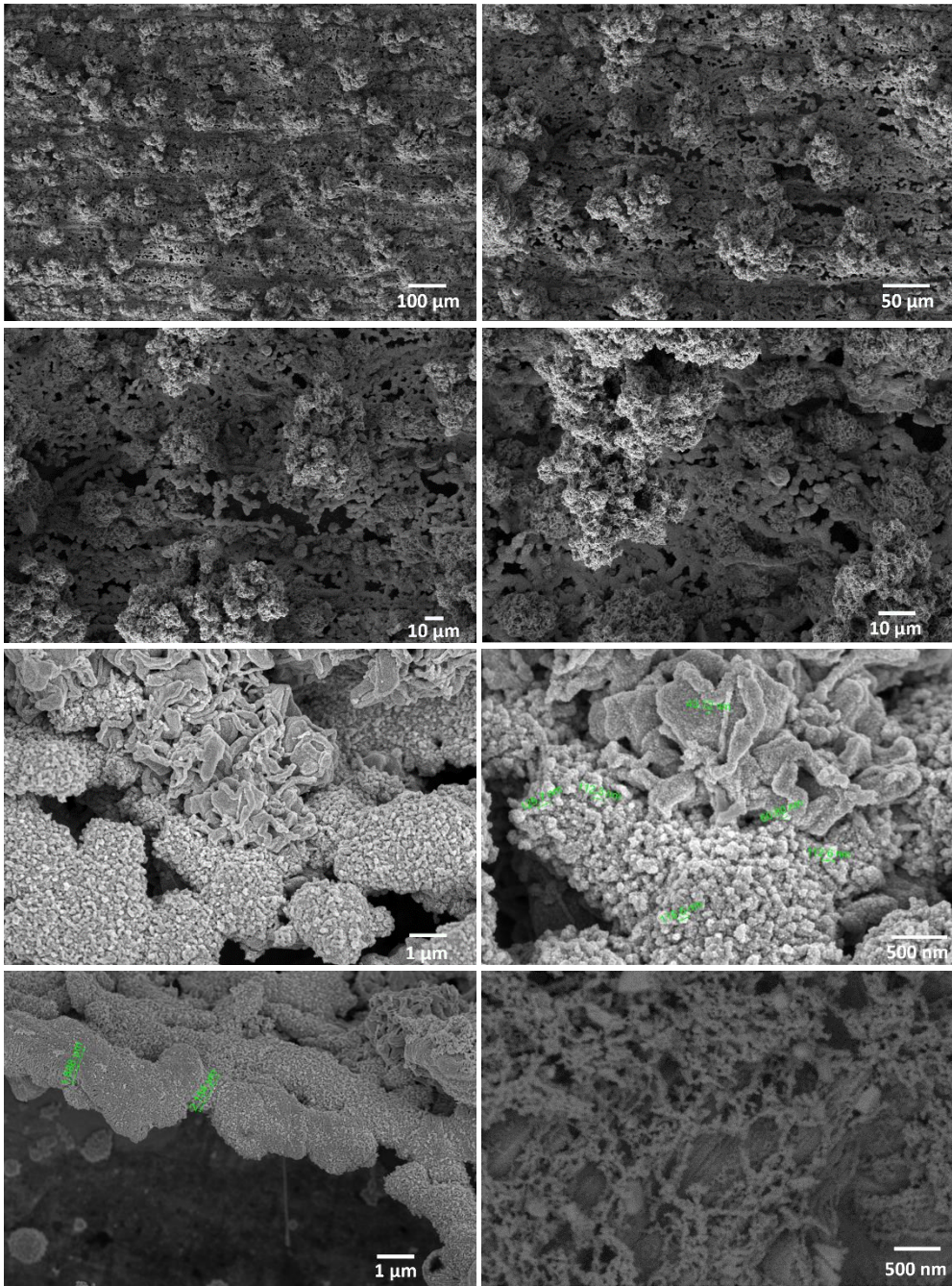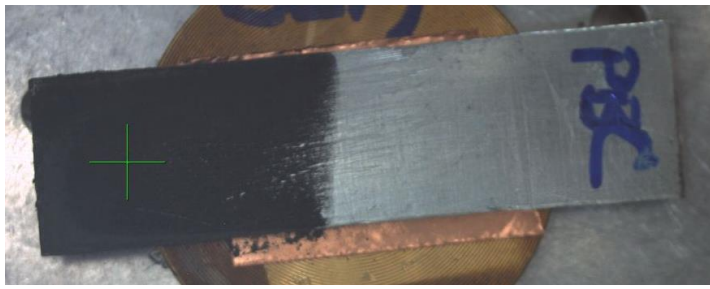
8.2.3.3 Post Blaise reaction Anode:
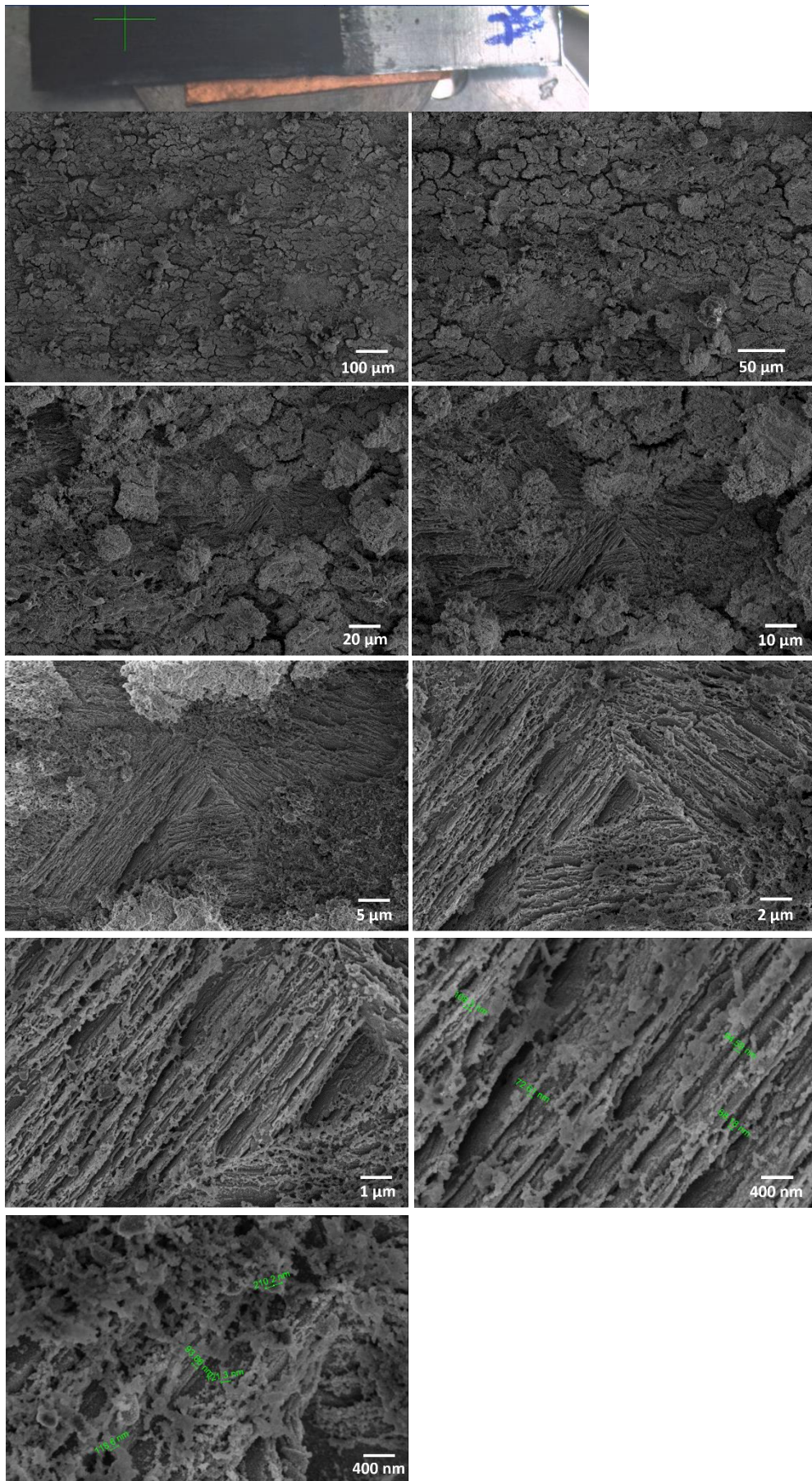
8.2.3.4 Post Blaise reaction Cathode
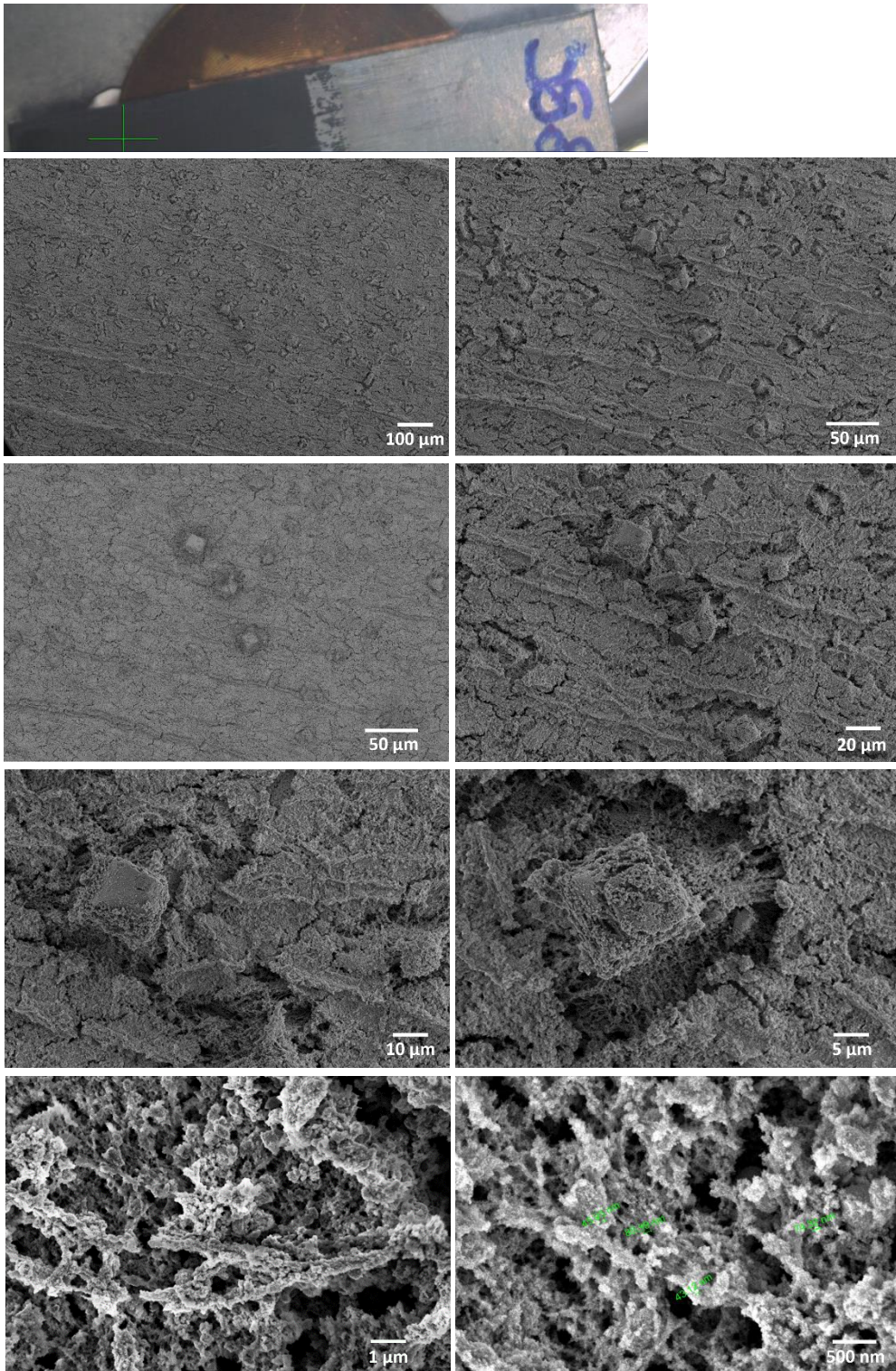
8.2.4 X-Ray Crystallography

Measurements were carried out at 130K on an Agilent SuperNova diffractometer equipped with an Atlas CCD detector and connected to an Oxford Cryostream low temperature device using mirror monochromated Cu K$_\alpha$ radiation (λ = 1.54184 Å) from a Microfocus X-ray source. The structure was solved by intrinsic phasing using SHELXT(201) and refined by a full matrix least squares technique based on F^2 using SHELXL2014.(202) All non-hydrogen atoms were located in the Fourier Map and refined anisotropically. All carbon-bound hydrogen atoms were placed in calculated positions and refined isotropically using a "riding model". Nitrogen-bound hydrogen atoms were located in the Fourier Map and refined isotropically. Pictures are presented with non-hydrogen atoms displayed as displacement ellipsoids, which are set at the 50% probability level.

8.2.4.1 *Acnac* Crystal Configuration 1

The compound crystallised as colourless blocks. The compound crystallised in a monoclinic cell and was solved in the *P*2$_1$/*n* space group, with *X* molecules in the asymmetric unit.
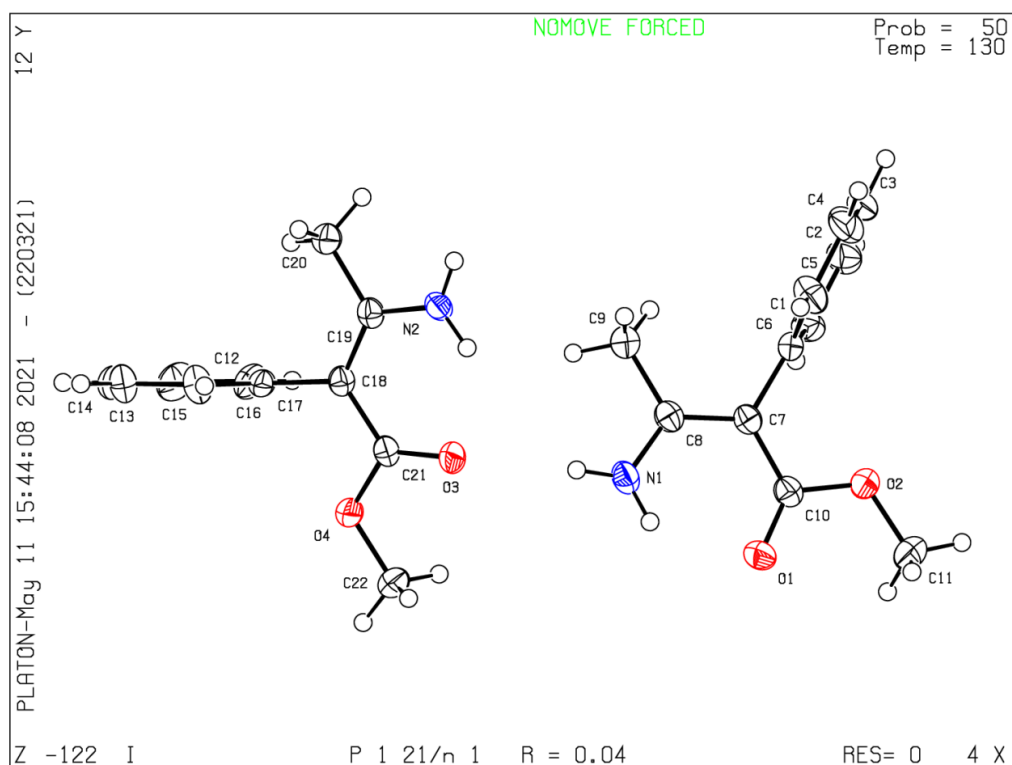
Table 8.1. Crystal data and structure refinement for RH_100521.

Identification code	RH_100521	Volume/Å^3	2080.09(5)
Empirical formula	$C_{11}H_{13}NO_2$	Z	8
Formula weight	191.22	$\rho_{calc}g/cm^3$	1.221
Temperature/K	130.01(10)	μ/mm^{-1}	0.684
Crystal system	monoclinic	F(000)	816.0
Space group	$P2_1/n$	Crystal size/mm^3	$0.38 \times 0.31 \times 0.24$
a/Å	8.62640(10)	Radiation	CuKα (λ = 1.54184)
b/Å	13.3257(2)	2Θ range for data collection/°	8.24 to 144.626
c/Å	18.2000(2)	Index ranges	$-10 \le h \le 10, -16 \le k \le 16, -21 \le l \le 22$

			Reflections collected	16478
α/°	90			

β/°	96.1530(10)	Independent reflections	4075 [R_{int} = 0.0336, R_{sigma} = 0.0260]

γ/°	90	Data/restraints/parameters	4075/0/273
		Goodness-of-fit on F^2	1.042

Final R indexes [I>=2σ (I)]	R_1 = 0.0396, wR_2 = 0.1073
Final R indexes [all data]	R_1 = 0.0446, wR_2 = 0.1117
Largest diff. peak/hole / e Å^{-3}	0.21/-0.17

Table 8.2. Fractional Atomic Coordinates ($\times 10^4$) and Equivalent Isotropic Displacement Parameters (Å$^2 \times 10^3$) for RH_100521. U_{eq} is defined as 1/3 of the trace of the orthogonalised U_{IJ} tensor.

Atom	x	y	z	U(eq)
O1	-406.6(10)	2873.1(6)	4400.4(5)	33.9(2)
N1	2308.0(13)	3822.4(7)	4265.8(6)	30.4(2)
C1	2041.0(15)	890.0(9)	2889.9(7)	32.4(3)
O2	-516.9(10)	1249.5(6)	4053.7(6)	38.3(2)
C2	2681.9(17)	36.2(10)	2602.5(8)	41.5(3)
C3	3686.7(17)	-563.8(9)	3045.7(9)	43.9(4)
C4	4036.3(18)	-319.5(10)	3780.9(10)	48.1(4)

C5	3387.1(17)	528.7(9)	4070.2(8)	39.4(3)
C6	2388.5(13)	1151.8(8)	3623.7(7)	25.7(2)
C7	1779.5(13)	2103.3(8)	3924.6(6)	25.0(2)
C8	2718.7(14)	2943.6(8)	3986.5(6)	27.5(3)
C9	4321.9(16)	2933.3(10)	3740.1(10)	44.3(4)
C10	230.3(14)	2138.7(8)	4147.2(6)	27.5(2)
C11	-2086.2(19)	1216.1(12)	4253.8(13)	61.9(5)
N2	7368.8(13)	4691.0(7)	4325.8(6)	27.6(2)
O3	4554.7(10)	5596.2(6)	4306.0(5)	31.4(2)
O4	4372.8(9)	7156.0(6)	3834.3(5)	30.3(2)
C12	8275.0(16)	7930.8(9)	3873.7(8)	36.2(3)
C13	8864.9(17)	8775.0(10)	3546.9(9)	44.4(3)
C14	8486.0(16)	8955.9(10)	2805.0(9)	44.2(4)
C15	7536.3(17)	8293.9(11)	2388.9(8)	44.3(3)
C16	6960.8(14)	7444.2(10)	2710.1(7)	33.9(3)
C17	7320.8(13)	7255.0(8)	3457.8(6)	24.7(2)
C18	6746.3(13)	6327.9(8)	3810.9(6)	23.8(2)
C19	7723.5(13)	5520.0(8)	3952.7(6)	24.6(2)
C20	9330.1(14)	5511.1(9)	3710.0(7)	32.8(3)

C21	5173.5(13)	6303.2(8)	4010.6(6)	24.8(2)
C22	2756.3(15)	7145.6(10)	3964.6(8)	39.1(3)

Table 8.3. Anisotropic Displacement Parameters ($Å^2 \times 10^3$) for RH_100521. The Anisotropic displacement factor exponent takes the form: $-2\pi^2[h^2a^{*2}U_{11}+2hka^*b^*U_{12}+\ldots]$.

Atom	U_{11}	U_{22}	U_{33}	U_{23}	U_{13}	U_{12}
O1	36.6(5)	27.9(4)	38.9(5)	-4.0(3)	11.4(4)	3.4(3)
N1	37.2(6)	22.3(5)	32.0(5)	-3.5(4)	4.7(4)	-3.4(4)
C1	33.8(6)	32.5(6)	31.6(6)	-3.8(5)	7.2(5)	3.0(5)
O2	31.9(5)	30.0(4)	55.8(6)	-9.4(4)	16.8(4)	-5.5(3)
C2	51.1(8)	35.8(7)	40.8(8)	-9.5(6)	19.5(6)	-1.4(6)
C3	43.6(8)	23.8(6)	68.5(10)	-4.9(6)	25.8(7)	1.8(5)
C4	45.5(8)	27.1(6)	70.0(11)	5.1(6)	-1.4(7)	7.2(6)
C5	46.3(8)	27.8(6)	41.9(7)	-0.4(5)	-5.1(6)	2.1(5)
C6	24.5(5)	21.8(5)	31.4(6)	-0.3(4)	5.7(4)	-3.0(4)
C7	29.2(6)	23.4(5)	22.1(5)	-0.9(4)	1.5(4)	-0.2(4)
C8	31.6(6)	24.8(5)	25.4(6)	0.7(4)	0.2(4)	0.3(4)
C9	34.8(7)	29.0(6)	71.0(10)	-7.3(6)	14.6(7)	-4.6(5)
C10	32.4(6)	24.6(5)	25.7(6)	-0.8(4)	3.5(5)	-0.1(4)

C11	41.6(8)	44.5(8)	106.1(15)	-18.2(9)	37.9(9)	-10.9(7)
N2	33.8(5)	19.4(5)	31.1(5)	0.9(4)	10.9(4)	1.7(4)
O3	34.9(4)	24.1(4)	37.4(5)	4.2(3)	13.7(4)	-3.8(3)
O4	27.4(4)	25.1(4)	39.9(5)	5.4(3)	10.3(3)	-0.1(3)
C12	44.1(7)	27.2(6)	36.4(7)	1.7(5)	0.9(5)	-6.2(5)
C13	43.0(8)	26.2(6)	64.2(10)	0.0(6)	7.4(7)	-8.1(5)
C14	38.4(7)	29.8(6)	67.7(10)	20.5(6)	21.0(7)	1.2(5)
C15	40.5(7)	52.2(8)	41.9(8)	24.2(6)	11.5(6)	1.9(6)
C16	28.8(6)	42.0(7)	31.0(6)	8.6(5)	3.9(5)	-4.4(5)
C17	23.5(5)	23.6(5)	27.8(6)	4.1(4)	6.3(4)	0.1(4)
C18	28.8(6)	23.0(5)	19.9(5)	0.3(4)	4.2(4)	-3.2(4)
C19	31.1(6)	23.0(5)	20.1(5)	-2.7(4)	4.2(4)	-3.6(4)
C20	31.4(6)	28.6(6)	39.8(7)	5.0(5)	9.5(5)	0.4(5)
C21	31.4(6)	20.8(5)	22.6(5)	-0.7(4)	4.5(4)	-3.1(4)
C22	29.9(6)	34.3(6)	55.6(8)	6.0(6)	16.4(6)	0.8(5)

Table 8.4. Bond Lengths for RH_100521

Atom	Atom	Length/Å		Atom	Atom	Length/Å
O1	C10	1.2355(14)		N2	C19	1.3489(15)

183

N1	C8	1.3394(15)		O3	C21	1.2340(14)
C1	C2	1.3913(18)		O4	C21	1.3506(14)
C1	C6	1.3820(17)		O4	C22	1.4394(14)
O2	C10	1.3509(14)		C12	C13	1.3939(18)
O2	C11	1.4397(16)		C12	C17	1.3885(17)
C2	C3	1.375(2)		C13	C14	1.376(2)
C3	C4	1.379(2)		C14	C15	1.375(2)
C4	C5	1.390(2)		C15	C16	1.3901(18)
C5	C6	1.3935(18)		C16	C17	1.3861(17)
C6	C7	1.4984(15)		C17	C18	1.5011(14)
C7	C8	1.3795(16)		C18	C19	1.3747(16)
C7	C10	1.4382(16)		C18	C21	1.4421(16)
C8	C9	1.4990(18)		C19	C20	1.4991(16)

Table 8.5. Bond Angles for RH_100521.

Atom	Atom	Atom	Angle/°		Atom	Atom	Atom	Angle/°
C6	C1	C2	121.07(12)		C21	O4	C22	115.64(9)
C10	O2	C11	116.37(10)		C17	C12	C13	120.87(13)

C3	C2	C1	120.38(13)	C14	C13	C12	120.06(13)
C2	C3	C4	119.37(12)	C15	C14	C13	119.53(12)
C3	C4	C5	120.31(13)	C14	C15	C16	120.64(13)
C4	C5	C6	120.85(13)	C17	C16	C15	120.56(13)
C1	C6	C5	118.01(11)	C12	C17	C18	120.27(10)
C1	C6	C7	121.24(10)	C16	C17	C12	118.33(11)
C5	C6	C7	120.68(11)	C16	C17	C18	121.36(10)
C8	C7	C6	119.39(10)	C19	C18	C17	120.07(10)
C8	C7	C10	120.38(10)	C19	C18	C21	120.62(10)
C10	C7	C6	120.23(9)	C21	C18	C17	119.30(9)
N1	C8	C7	124.31(11)	N2	C19	C18	124.64(11)
N1	C8	C9	114.30(10)	N2	C19	C20	114.12(10)
C7	C8	C9	121.38(10)	C18	C19	C20	121.23(10)
O1	C10	O2	121.10(11)	O3	C21	O4	120.78(10)
O1	C10	C7	126.50(10)	O3	C21	C18	126.15(10)
O2	C10	C7	112.40(9)	O4	C21	C18	113.07(9)

185

Table 8.6. Hydrogen Atom Coordinates (Å×10^4) and Isotropic Displacement Parameters (Å^2×10^3) for RH_100521.

Atom	x	y	z	U(eq)	Atom	x	y	z	U(eq)
H1	1368	1291	2583	39	H14	8870	9522	2587	53
H2	2429	-130	2108	50	H15	7276	8416	1888	53
H3	4126	-1129	2851	53	H16	6329	6999	2421	41
H4	4710	-724	4085	58	H20A	10072	5714	4114	49
H5	3622	682	4568	47	H20B	9371	5967	3304	49
H9A	4584	3595	3585	66	H20C	9576	4846	3556	49
H9B	4347	2475	3335	66	H22A	2284	7775	3814	59
H9C	5061	2724	4143	66	H22B	2679	7043	4481	59
H11A	-2679	1759	4018	93	H22C	2228	6612	3686	59
H11B	-2067	1278	4780	93	H2A	8008(18)	4202(12)	4342(8)	31(4)
H11C	-2560	589	4097	93	H2B	6454(19)	4650(11)	4496(9)	37(4)
H12	8524	7819	4377	43	H1A	1400(20)	3845(13)	4453(10)	46(4)
H13	9515	9216	3831	53	H1B	2994(19)	4304(12)	4304(9)	38(4)

8.2.4.2 *Acnac* Crystal Configuration 2

The compound crystallised as colourless plates. The compound crystallised in a monoclinic cell and was solved in the $P2_1/c$ space group, with one molecule in the asymmetric unit.
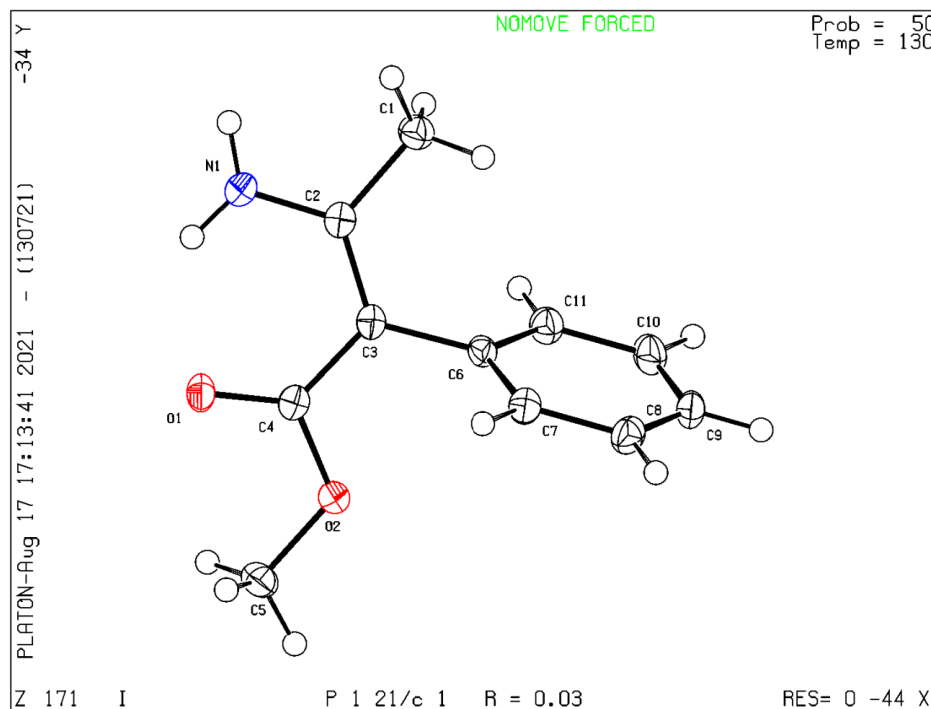
Table 8.7 Crystal data and structure refinement for RH_170821.

Identification code	RH_170821	Volume/Å^3	978.49(3)
Empirical formula	$C_{11}H_{13}NO_2$	Z	4
Formula weight	191.22	$\rho_{calc}g/cm^3$	1.298
Temperature/K	130.01(10)	μ/mm^{-1}	0.727
Crystal system	Monoclinic	F(000)	408.0
Space group	$P2_1/n$	Crystal size/mm^3	$0.55 \times 0.31 \times 0.1$

187

		Radiation	CuKα ($\lambda = 1.54184$)
a/Å	13.8919(3)	Radiation	CuKα ($\lambda = 1.54184$)
b/Å	6.02420(10)	2Θ range for data collection/°	16.026 to 145.71
c/Å	11.7225(2)	Index ranges	$-16 \le h \le 16$, $-7 \le k \le 6$, $-14 \le l \le 9$
α/°	90	Reflections collected	3681
β/°	94.118(2)	Independent reflections	1883 [R_{int} = 0.0174, R_{sigma} = 0.0219]
γ/°	90	Data/restraints/parameters	1883/0/137
		Goodness-of-fit on F^2	1.054
Final R indexes [I>=2σ (I)]		$R_1 = 0.0348$, $wR_2 = 0.0900$	
Final R indexes [all data]		$R_1 = 0.0381$, $wR_2 = 0.0935$	
Largest diff. peak/hole / e Å^{-3}		0.28/-0.19	

Table 8.8. Fractional Atomic Coordinates ($\times 10^4$) and Equivalent Isotropic Displacement Parameters (Å$^2 \times 10^3$) for RH_170821. Ueq is defined as 1/3 of the trace of the orthogonalised U_{IJ} tensor.

Atom	x	y	z	U(eq)
O1	9278.5(5)	5635.6(14)	4007.1(7)	21.9(2)
O2	8485.3(5)	6110.8(13)	2283.1(6)	20.9(2)
N1	8823.6(7)	1974.5(18)	5156.4(8)	22.8(2)

Atom	x	y	z	U(eq)
C1	7393.0(8)	-35.1(19)	4551.7(10)	22.5(3)
C2	8070.1(8)	1864.8(19)	4372.4(9)	17.9(2)
C3	7928.6(7)	3304.9(18)	3457.2(9)	17.4(2)
C4	8615.3(7)	5069.8(18)	3320.4(9)	17.5(2)
C5	9174.3(8)	7835(2)	2087.6(11)	25.6(3)
C6	7072.4(7)	3102.7(19)	2613.6(9)	17.6(2)
C7	6372.2(8)	4770(2)	2539.6(9)	20.8(3)
C8	5572.9(8)	4641(2)	1756.5(10)	24.2(3)
C9	5460.8(8)	2828(2)	1033.2(10)	25.9(3)
C10	6141.9(9)	1148(2)	1100.5(10)	27.1(3)
C11	6942.0(8)	1284(2)	1883.3(10)	22.5(3)

Table 8.9. Anisotropic Displacement Parameters ($\text{Å}^2 \times 10^3$) for RH_170821. The Anisotropic displacement factor exponent takes the form: $-2\pi^2[h^2a^{*2}U_{11}+2hka^*b^*U_{12}+\ldots]$.

Atom	U_{11}	U_{22}	U_{33}	U_{23}	U_{13}	U_{12}
O1	17.7(4)	24.2(4)	23.0(4)	-1.6(3)	-3.9(3)	-2.8(3)
O2	20.5(4)	21.9(4)	20.1(4)	2.5(3)	-1.0(3)	-4.3(3)
N1	22.4(5)	25.9(5)	19.5(5)	3.9(4)	-3.4(4)	-2.9(4)

Atom	U$_{11}$	U$_{22}$	U$_{33}$	U$_{23}$	U$_{13}$	U$_{12}$
C1	23.7(6)	23.0(6)	20.8(6)	0.7(4)	2.2(4)	-2.8(5)
C2	16.5(5)	20.3(5)	17.0(5)	-3.3(4)	2.0(4)	1.5(4)
C3	15.2(5)	20.3(5)	16.6(5)	-2.7(4)	0.6(4)	0.0(4)
C4	15.8(5)	18.9(5)	17.7(5)	-2.7(4)	1.3(4)	3.1(4)
C5	21.5(6)	23.3(6)	32.2(6)	5.0(5)	2.2(5)	-3.6(5)
C6	16.0(5)	21.3(6)	15.7(5)	1.0(4)	1.6(4)	-3.5(4)
C7	18.8(5)	23.9(6)	19.5(5)	-1.1(4)	0.7(4)	-0.4(4)
C8	17.5(5)	31.1(6)	23.8(6)	3.7(5)	0.0(4)	1.6(5)
C9	20.3(6)	35.2(7)	21.2(5)	3.9(5)	-5.2(4)	-8.5(5)
C10	30.3(6)	27.2(6)	23.0(6)	-4.4(5)	-3.4(5)	-9.0(5)
C11	22.3(6)	22.2(6)	22.7(5)	-1.8(5)	0.0(4)	-1.3(4)

Table 8.10. Bond Lengths for RH_170821.

Atom	Atom	Length/Å	Atom	Atom	Length/Å
O1	C4	1.2274(13)	C3	C6	1.4962(14)
O2	C4	1.3685(13)	C6	C7	1.3964(16)
O2	C5	1.4417(14)	C6	C11	1.3941(16)
N1	C2	1.3442(14)	C7	C8	1.3911(15)

Atom	Atom	Length/Å	Atom	Atom	Length/Å
C1	C2	1.5057(15)	C8	C9	1.3848(18)
C2	C3	1.3827(16)	C9	C10	1.3841(19)
C3	C4	1.4450(15)	C10	C11	1.3921(16)

Table 8.11. Bond Angles for RH_170821.

Atom	Atom	Atom	Angle/°	Atom	Atom	Atom	Angle/°
C4	O2	C5	115.13(9)	O2	C4	C3	112.94(9)
N1	C2	C1	113.93(10)	C7	C6	C3	119.98(10)
N1	C2	C3	124.05(10)	C11	C6	C3	122.13(10)
C3	C2	C1	122.00(10)	C11	C6	C7	117.89(10)
C2	C3	C4	119.31(10)	C8	C7	C6	121.37(11)
C2	C3	C6	121.58(10)	C9	C8	C7	119.81(11)
C4	C3	C6	119.10(9)	C10	C9	C8	119.72(10)
O1	C4	O2	120.03(10)	C9	C10	C11	120.30(11)
O1	C4	C3	127.01(10)	C10	C11	C6	120.90(11)

Table 8.12. Torsion Angles for RH_170821.

A	B	C	D	Angle/°	A	B	C	D	Angle/°

191

A	B	C	D	Angle/°	A	B	C	D	Angle/°
N1	C2	C3	C4	-0.76(16)	C4	C3	C6	C11	114.69(12)
N1	C2	C3	C6	-179.80(10)	C5	O2	C4	O1	0.42(14)
C1	C2	C3	C4	-178.78(9)	C5	O2	C4	C3	-177.90(9)
C1	C2	C3	C6	2.19(16)	C6	C3	C4	O1	169.94(10)
C2	C3	C4	O1	-9.12(17)	C6	C3	C4	O2	-11.89(13)
C2	C3	C4	O2	169.05(9)	C6	C7	C8	C9	0.16(17)
C2	C3	C6	C7	113.75(12)	C7	C6	C11	C10	0.47(16)
C2	C3	C6	C11	-66.27(14)	C7	C8	C9	C10	0.46(17)
C3	C6	C7	C8	179.35(10)	C8	C9	C10	C11	-0.62(18)
C3	C6	C11	C10	-179.51(10)	C9	C10	C11	C6	0.15(18)
C4	C3	C6	C7	-65.28(13)	C11	C6	C7	C8	-0.62(16)

Table 8.13. Hydrogen Atom Coordinates ($Å×10^4$) and Isotropic Displacement Parameters

($Å^2×10^3$) for RH_170821.

Atom	x	y	z	U(eq)
H1C	7654	-1399	4239	34
H1D	6761	284	4161	34
H1E	7323	-227	5372	34

Atom	x	y	z	U(eq)
H5A	9044	8437	1315	38
H5B	9828	7216	2164	38
H5C	9119	9022	2651	38
H7	6443	6017	3034	25
H8	5105	5795	1718	29
H9	4919	2738	493	31
H10	6063	-105	610	32
H11	7406	122	1920	27
H1A	9251(11)	3050(30)	5101(12)	28(4)
H1B	8826(11)	1040(30)	5741(15)	36(4)

8.2.5 PCA Solvent Analysis

PCA mapping was run by B. N. Nguyen.

Table 8.14. Solvents and their calculated PCA values from reference (183).

| Solvent	CAS	PC1	PC2	PC3	PC4	Distance
MeCN	75-05-8	-2.18069	-1.48531	-0.24727	-2.24492	0
EtCN	107-12-0	-1.14806	-1.10032	-0.77095	-1.78471	1.304064
MeCOMe	67-64-1	-0.55297	-1.91748	-1.04346	-1.69659	1.941867
EtO$_2$CH	109-94-4	-0.32966	-1.48624	-0.51899	-1.57999	1.98552
HCO$_2$Me	107-31-3	-0.51451	-2.49657	-0.00131	-1.92678	1.990102
PrCN	109-74-0	-0.4547	-0.7202	-0.96234	-1.24958	2.250879
MeNO$_2$	75-52-5	-2.71732	0.086056	1.42703	-2.80464	2.423576
MeCOEt	78-93-3	-0.10952	-1.14461	-1.18802	-1.1745	2.537055
Ac$_2$O	108-24-7	-0.97294	0.442237	0.277486	-1.02003	2.636252
DMF	68-12-2	-2.67998	0.527336	-1.58183	-0.77524	2.870724
MeOAc	79-20-9	0.595777	-2.0205	-0.66796	-1.35945	2.992697
THF	109-99-9	0.424405	-1.34983	-1.44861	-1.35114	3.007814
MeCOPr	107-87-9	-0.07949	-0.42876	-1.23595	-0.48517	3.099279
Dioxane	123-91-1	0.55908	-0.19863	0.074978	-1.43489	3.1499
EtCOEt	96-22-0	0.416783	-0.37744	-0.98319	-0.5587	3.370333
DMC	616-38-6	0.760087	-1.30966	0.303787	-0.70228	3.37082
CH2Cl2	75-09-2	0.544955	-0.42223	1.45303	-2.76417	3.423437
EtOH	64-17-5	-2.84452	-3.95306	-0.28267	0.140398	3.49592
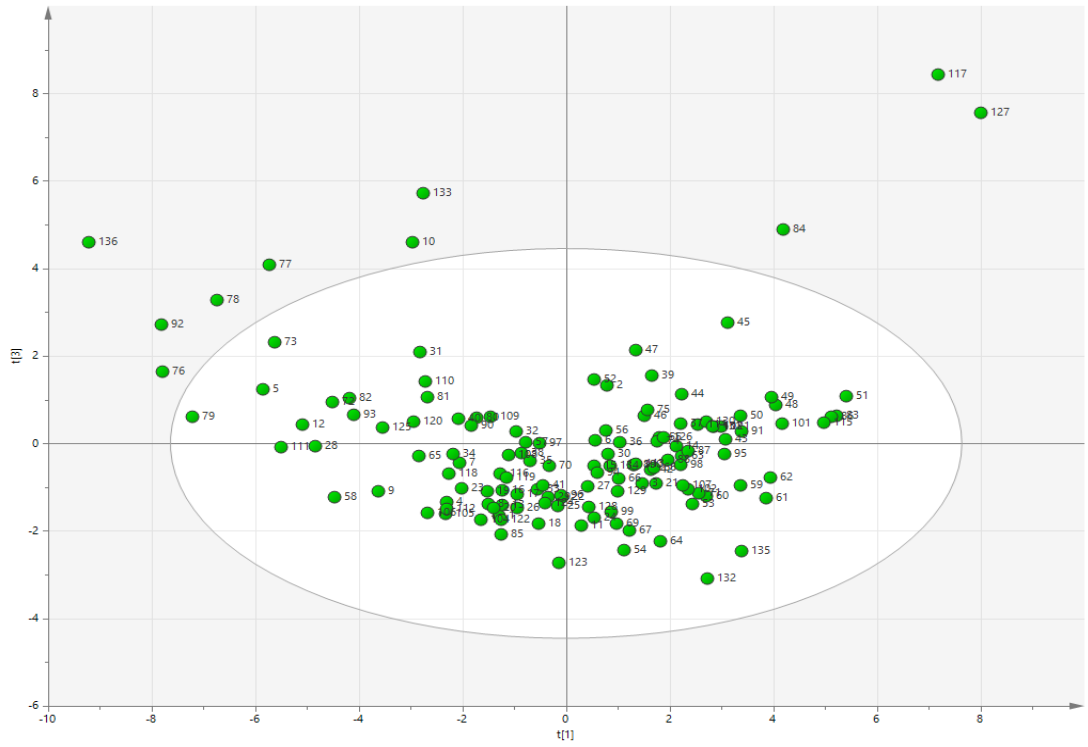
Figure 8.1. PCA map generated by B. N. Nguyen.